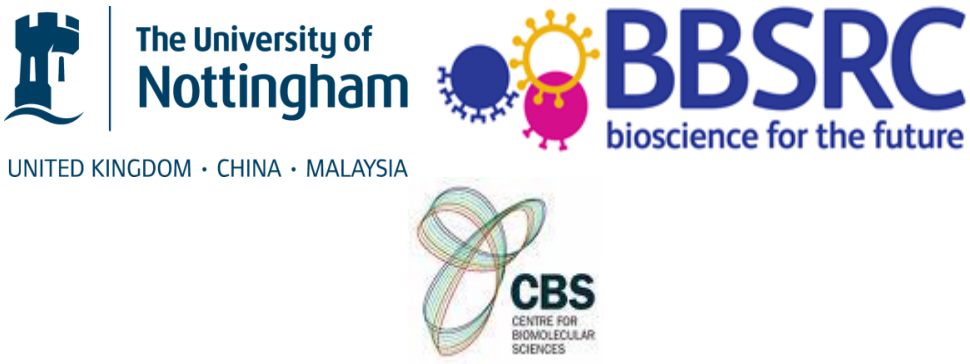

Design, synthesis and evaluation of MRI agents for *in vivo* imaging of protease activity.

James Lee Krupa, MChem. (Hons)

Thesis submitted to the University of Nottingham for the degree of

Doctor of Philosophy

September 2015

Abstract

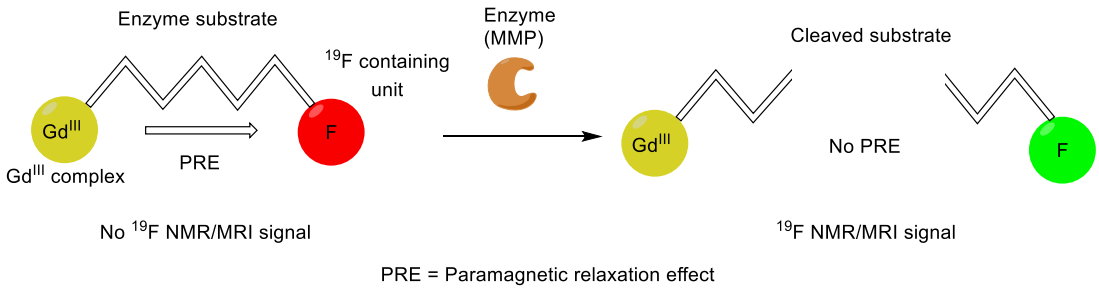

Scheme 1: Generic structure of an MMP activated contrast agent

This thesis details the design and synthesis of a small library of ^{19}F MRI MMP probes containing an MMP substrate bound to a paramagnetic agent (gadolinium contrast agent) with a fluorine containing group at the opposite terminus. The largest obstacle in the synthesis of the probe was the conjugation of the paramagnetic agent. Multiple different modifications to the Gd^{III} chelators AAZTA (6-amino-6-methylperhydro-1,4-diazepinetetraacetic acid) and DOTA (1,4,7,10-tetraazacyclododecane-1,4,7,10-tetraacetic acid) are detailed, as well as methods for the conjugation.

Once a successful method was achieved the probes were carried forward for *in vitro* testing. Whilst the agent was whole or non-cleaved the paramagnetic relaxation effect (a distance dependent effect) of the Gd^{III} eliminated the ^{19}F NMR/MRI signal. The introduction of an MMP to the probe caused the probe to be cleaved. This cleavage then resulted in the increased distance between the Gd^{III} complex and the ^{19}F containing group, which in turn reduced the PRE, resulting in the emergence of a ^{19}F NMR/MRI signal. This enzymatic activity was visualised using high field NMR (600 MHz AV(III)400) by the increase in signal peak height with ^{19}F NMR, as well as the changes in the T_1 and T_2^* (observed as a change in linewidth) values observed before

and after cleavage of the probe showed a diagnostic change in the magnetic properties of the probe.

Reaction rates were ascertained whilst altering the solvent (H_2O vs D_2O), and the temperature of the reaction. A reduction in the rate of cleavage was noticed as the D_2O concentration was increased as expected, however, the change in temperature did not always follow an expected reaction profile change.

Acknowledgements

Firstly, I would like to thank Profs Neil Thomas and Simon Johnson for giving me the opportunity to undertake this project, and The University of Nottingham and the BBSRC for turning my lights on with money.

Secondly, I would like to thank all the past and present members of the Thomas group who have/do work on A and C floor, especially Will Drewe, Indi Thaker (nee Sehmi), Terry May, Alex Wichlacz and Francesco Zamberlan for guidance, proof reading and people to bounce ideas off.

All the technicians that keep everything working in chemistry and the CBS, Dane and Lee who can literally fix anything. Shaz in chemistry keeps a good set of NMR spectrometers, and Graham, Mick and Ben for the mass spec.

Alex Taylor and Huw Williams for their help with the MR imaging and NMR time courses and calculations.

My best mates, Greg and Mike for the last 15 years and Jon and Sam for the good times all the way through uni, from start to end.

The project students we've had during my time in Nottingham in the Thomas group for providing a large amount of entertainment, especially Heather, Emma and Freya.

The fantasy football lads, especially Terry, Alex and Matt for constantly keeping football alive at work.

Finally I'd like to thank Mum and Dad for a kick in the right direction and Ash for putting up with me.

Declaration

I declare that the substance of this thesis has not been submitted, nor is concurrently being submitted for any other degree. I also declare that the work embodied in this thesis is the result of my own investigations. Where the work of other investigators has been used, this has been fully acknowledged in the text.

Contents

List of Equations

List of Figures

List of Schemes

List of Spectra

List of Tables

Abbreviations

AA	Amino acid
AAc	azide alkyne cycloaddition
AAZTA	(6-Amino-6-methylperhydro-1,4-diazepinetetraacetic acid)
AIDs	Acquired Immunodeficiency Syndrome
atm	atmopshere
ATP	Adenosine tri-phosphate
AU	Arbitrary units
b	Broad IR signal
bFGF	Basic fibroblast growth factor
bs	broad singlet (NMR), broad signal (IR)
Bn	Benzyl
Boc	*tert*-butoxycarbonyl
BOP	(Benzotriazol-1-yloxy)tris(dimethyl amino)phosphonium hexafluorophosphate
Bu	Butyl
Bz	Benzoyl
CA	contrast agent
CDI	Carbodiimidazole
Cbz	Carboxybenzyl
CEST	Chemical Exchange Saturation Transfer
COMU	(1-Cyano-2-ethoxy-2-oxoethylidenaminooxy) dimethylamino-morpholino- carbenium hexafluorophosphate
CT	Computer Tomography
d	Doublet
dd	Doublet of doublets
Da	Daltons (1Da = 1 amu)
DCC	*N,N'*-Dicyclohexylcarbodiimide

DCU	*N,N'*-Dicyclohexylurea
DCM	Dichloromethane
DIPEA	*N,N*-Diisopropylethylamine
DMTMM	4-(4,6-dimethoxy-1,3,5-triazin-2-yl)-4-methylmorpholin-4-ium chloride
DMF	*N,N*-Dimethylformamide
DMS	Dimethyl sulphide
DMSO	Dimethyl sulphoxide
DOTA	1,4,7,10-Tetraazacyclododecane-1,4,7,10-tetraacetic acid
DO2A	1,4,7,10-Tetraazacyclododecane-1,7-diacetic acid
DO3A	1,4,7,10-Tetraazacyclododecane-1,4,7-triacetic acid
EDC	1-Ethyl-3-(3-dimethylaminopropyl) carbodiimide
ECM	Extracellular matrix
EDTA	Ethylenediaminetetraacetic acid
EGFR	Epidermal growth factor receptor ligands
ESI	Electro spray ionisation
ESI-MS	Electro spray ionisation mass spectroscopy
Et	Ethyl
FAA	Fluorinated amino acid
FAD	Flavin adenine dinucleotide (oxidised form)
Fmoc	Fluorenylmethyloxycarbonyl
GAGs	Glycosaminoglycans
GSH	Glutathione
h	hour(s)
HATU	*O*-(7-Azabenzotriazol-1-yl)-*N,N,N',N'*-tetramethyluronium hexafluorophosphate
HBTU	*O*-Benzotriazole-*N,N,N',N'*-tetramethyl-uronium-hexafluoro-phosphate
HIV	Human Immunodeficiency Virus
HMBC	Heteronuclear multiple bond correlation
HMQC	Heteronuclear multiple-quantum correlation

HOBt	1-Hydroxybenzotriazole
HPLC	High performance liquid chromatography
HRMS	High resolution mass spectroscopy
IGF	Insulin like growth factor
IR	Infrared spectroscopy
IS	inner sphere
K_d	dissociation constant
K_i	inhibitor binding affinity
LCMS	Liquid chromatography mass spectrometery
Lit.	literature
J	Joule(s)
m/z	mass to charge ratio
m	Multiplet
MALDI	matrix assisted laser desorption ionisation
Me	Methyl
MeCN	Acetonitrile
mins	minute(s)
Mol	Mole
MMP	Matrix metalloproteinase
MRI	Magnetic resonance imaging
MRS	Magnetic resonance spectrometry
MS	Mass spectrometry
MW	molecular weight
NAD	Nicotinamide adenine dinucleotide (oxidised form)
NADH	Nicotinamide adenine dinucleotide (reduced form)
NFTB	Nonafluoro-*tert*-butanol
NaNFTB	Sodium nonafluoro-*tert*-butoxide
NMM	*N*-methylmorpholine
NMR	Nuclear magnetic resonance
NOESY	Nuclear Overhauser effect spectroscopy
OS	outer sphere
Pbf	2,2,5,7,8-Pentamethyl-chroman-6-sulphonyl

PEG	Poly ethylene glycol
PET	Positron Emission Tomography
PG	Protecting group
pH	potential hydronium ($-\log_{10}[H^+]$)
PMB	*para*-methoxy benzyl
ppm	parts per million
PRE	Paramagnetic Relaxation Effects
PyBOP	Benzotriazol-1-yl-oxytripyrrolidinophosphonium hexafluorophosphate
PyOxim	[Ethyl cyano(hydroxyimino)acetato-O2) tri-1-pyrrolidinylphosphonium hexafluorophosphate
$\mathbf{r_f}$	retention factor
RF	radio frequency
RT	room temperature
s	singlet (NMR), sharp (IR)
$\mathbf{S_N1}$	Nucleophilic substitution unimolecular
$\mathbf{S_N2}$	Nucleophilic substitution bimolecular
SPECT	Single photon emission computed tomography
SPPS	Solid phase peptide synthesis
T	temperature
TBTU	O-(Benzotriazol-1-yl)-N,N,N',N'-tetramethyluronium tetrafluoroborate
Tert	Tertiary
TFA	Trifluoroacetic acid
TFFH	Tetramethylfluoroformamidinium hexafluorophosphate
THF	tetrahydrofuran
THPTA	3,3',3''-(4,4',4''-(Nitrilotris(methylene))tris(1*H*-1,2,3-triazole-4,1-diyl))tris(propan-1-ol)
TIPS	triisopropyl silane
TLC	thin layer chromatography
Tos	Tosyl
Trt	Triphenylmethyl

T_1	Longitudinal relaxation or spin-lattice relaxation
T_2	Transverse relaxation or spin-spin relaxation
UV	ultra violet
VEGF	vascular endothelial growth factor

Amino acid abbreviations

Ala	Alanine
Arg	Arginine
Asn	Asparagine
Asp	Aspartic acid
Cys	Cysteine
Gly	Glycine
Gln	Glutamine
Glu	Glutamic acid
His	Histidine
Ile	Isoleucine
Leu	Leucine
Lys	Lysine
Met	Methionine
Phe	Phenylalanine
Pro	Proline
Sec	Selenocysteine
Ser	Serine
Thr	Threonine
Trp	Tryptophan
Tyr	Tyrosine
Val	Valine

Chapter 1 - Introduction

1.1 Brief overview of the introduction

Matrix metalloproteinases (MMPs) are implicated in various diseases, as well as non-disease based physiological processes within humans, therefore detailed knowledge of both which MMPs are active and the extracellular concentration is valuable information from a health perspective. The intended approach to study this is by using NMR/MRI; to this end an NMR/MRI probe was designed utilising the paramagnetic properties of Gd^{III}. The synthesis of this probe included extensive utilisation of solid phase peptide synthesis (SPPS), as well as standard chemical laboratory methods. As such the introduction covers MMPs, NMR and MRI, MRI smart contrast agents, SPPS and different coupling agents.

1.2 MMPs

1.2.1 Introduction to matrix metalloproteinases (MMPs)

Cancer is a leading cause of death throughout the world;[1] because of this there is a large amount of research into cancer and cancerous processes within the biochemical community. Matrix metalloproteases (MMPs) belong to a family of extracellular zinc-dependent endopeptidases[2] involved in the remodelling of the extracellular matrix (ECM).[3] Each MMP has multiple substrates with varying lengths of recognition site on the peptide, these include collagen and cadherin, structural

proteins found within the ECM, as well as integrin. In humans there are 24 genes which code for 23 different MMPs with the first and last gene coding for the same MMP.[4] MMPs are categorised by their structure, all of which contain the following: a catalytic domain of approximately 170 amino acids, a pro-peptide region of approximately 80 amino acids, and a hemopexin-like C-terminal of around 200

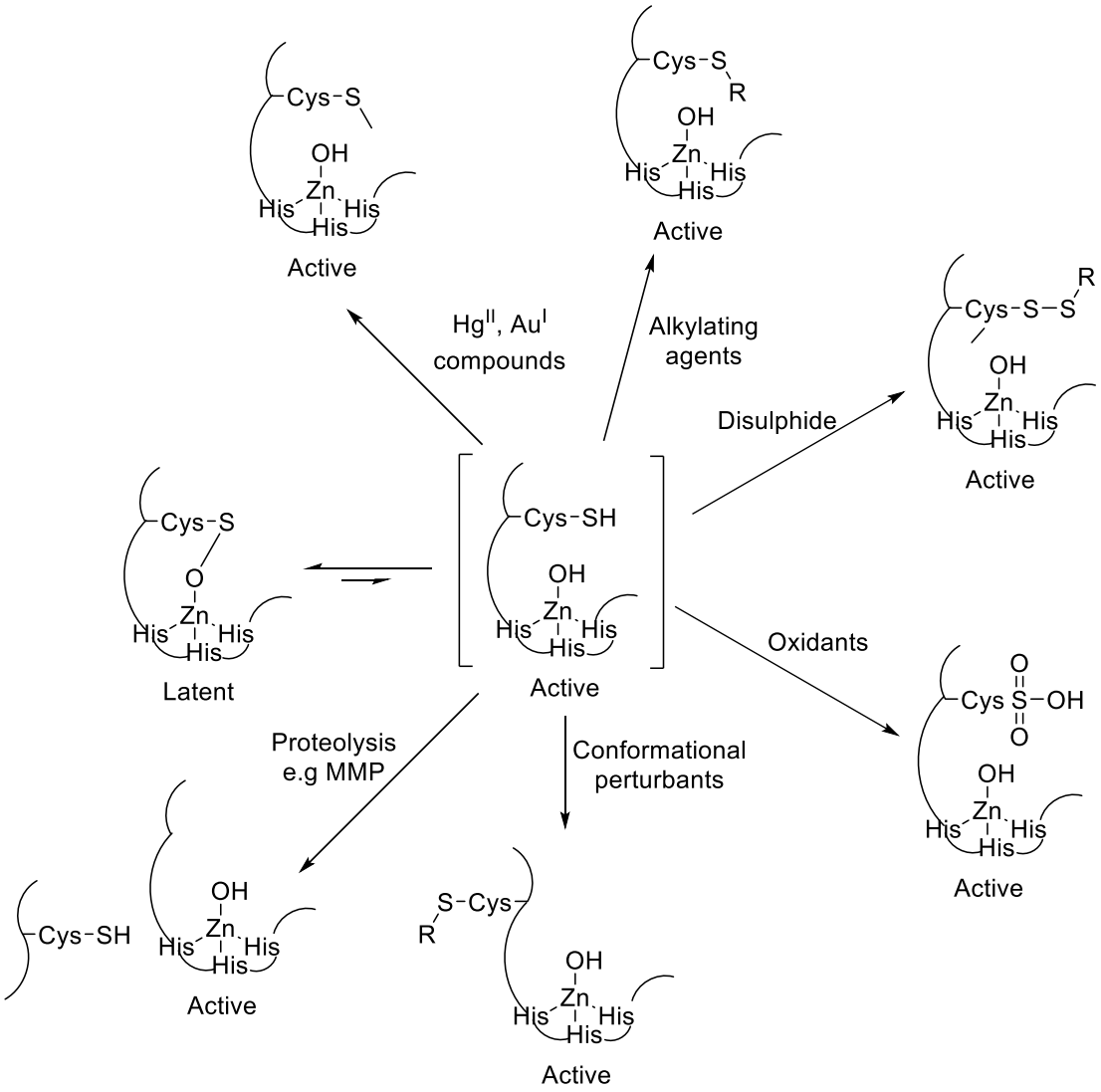

amino acids, which is connected to the catalytic region *via* a flexible hinge region; some MMPs may also include other domains.[5] Produced as a latent pro-MMP, MMPs are activated when required.[3] The pro-MMP region of latent MMPs, contains

multiple cysteines, however, one of these is responsible for maintaining the inactivity of the enzyme by chelating to the zinc at the catalytic site. Once this cysteine-zinc bond is broken the MMP becomes active, this is known as the "cysteine switch" mechanism, see Scheme 2.[6] The selective activation of MMPs is important to regulate their roles in physiological processes, such as wound healing, uterine involution, organogenesis and pathological processes, such as inflammation, auto immune and vascular disorders, and carcinogenesis. MMP levels can be used as potential diagnostic and prognostic biomarkers for determining types and stages of cancer.[7] This link was first made in 1980 when it was shown that the levels of MMPs were correlated to the metastatic potential of cancerous cells.[8] It is important to note however, that MMPs can have both a positive or negative affect towards cancer growth, and also that they are required for general cellular growth remodelling and repair.

1.2.2 MMPs and their roles in metastasis

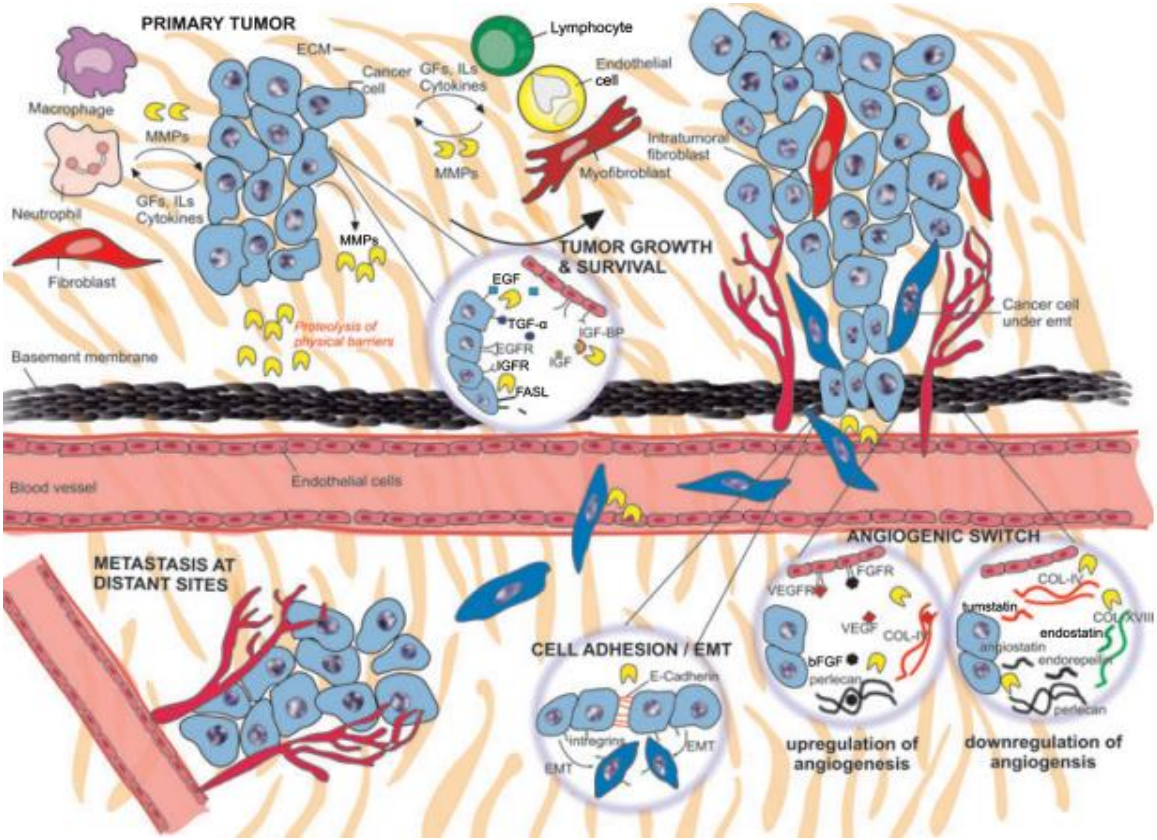

MMPs are expressed on the outside of the cellular membrane in both healthy and cancerous cells. They are then able to interact with a tumour's microenvironment and begin the breakdown of the ECM in order to allow cancerous cells to enter and leave tissue. This process was shown as a whole by Gialeli *et al.* (Figure 1) and involves multiple stages.[7]

1.2.3 Invasion

The invasion begins with the proteolytic breakdown of the ECM, this breakdown is essential to provide space to facilitate growth. This is then followed by intravasation at nearby blood vessels (entering of blood vessels), extravasation, and then invasion

into new tissues within the body. During this process MMPs localise to the site of the invasion on surface structures. These structures are called invadopodia, and mark the area of active ECM degradation.[9]

1.2.4 Growth

MMPs can liberate precursors to growth factors from the ECM, such as: insulin-like growth factor (IGF), epidermal growth factor receptor ligands (EGFR), vascular endothelial growth factor (VEGF) and basic fibroblast growth factor (bFGF). This increase, in the growth factors, further elevates the number of MMPs present. High levels of EGFR ligands are directly responsible for cell growth and proliferation,[10] and EGFR ligands are expressed in over a third of tumours. This increase is caused by the cleavage of membrane-anchored ligands by MMPs-3 and -7.[11] MMP-3 can then activate Pro-MMP-1 and -7, generating a positive feedback loop, which constantly promotes growth.[3]

Glycosaminoglycans (GAGs) are polysaccharides which are made up of a repeating unit of disaccharides (usually an amino and uronic sugar). GAGs can recruit MMPs, causing a release of growth factor from cell surfaces. This GAG-MMP interaction is a positive control for the activation of pro-MMPs, for example MMP-7 has a high affinity for heparan sulphate chains (a form of GAG) and when MMP-7 anchors heparan sulphate to cells, free epidermal growth factor (EGF) is released.[12] These growth factors not only encourage growth of the tumour, but also factors such as

VEGF stimulate angiogenesis, which is essential for the tumour to continue its high metabolic activity and to metastasize.

1.2.5 Angiogenesis

In order for any tissue to survive it needs a source of oxygen and nutrients; cancer cells are no different. To do this they need to stimulate the production of new blood vessels, through a process known as angiogenesis.

The main MMPs involved in angiogenesis are MMP-2, -9 and -14, although MMP-1 and -7 also play a part.[13] The first step is the remodelling of the ECM, which leads to the release of angiogenic growth factors. MMP-9 increases the bioavailability of VEGF, the most potent angiogenic promoter used by cancer cells. Bergers *et al.* showed that tumours with inhibited MMP-9 displayed a dramatic reduction in angiogenic growth.[14] MMPs can also down-regulate angiogenesis through the formation of statins, such as angiostatin, which is produced from plasminogen by MMP-2.[15] Once the tumour has a blood supply, it can begin the next stage of its life: migration.

1.2.6 Migration

The migration of cancerous cells from one tissue to another involves the breakdown of both ECM-cell and cell-cell interactions in order to 'free' a cancer cell. Integrins are receptors involved in cell-cell and cell-ECM communications, and more

importantly, the physical link between cell-cell and cell-ECM. Due to this they are also involved in cell migration, as they can act as MMP substrates.[16]

Epithelial – mesenchymal transition (EMT) is a process whereby the ability of a cell to migrate is increased by reducing cell-cell interactions, this is achieved *via* cleavage of cadherin by MMP-1 and -7. As the cadherin breaks down, the cell loses its shape and acquires a mesenchymal phenotype, so is shapeless with no connective tissue to hold it together. Once mesenchymal, the cell can then enter the blood stream and migrate to another tissue.[17]

1.3 Imaging

1.3.1 Imaging introduction

Molecular imaging of patients has become one of the most rapidly developing techniques in biomedical science. The intention behind imaging is to increase the understanding of *in vivo* systems in a non-invasive manner. There are a multitude of different clinical non-invasive imaging techniques, including magnetic resonance imaging (MRI), single photon emission computed tomography (SPECT), positron emission tomography (PET), X-ray, computed tomography (CT), and ultrasound. All of these techniques have an array of advantages, but in this project the main focus will be on the use of MRI, specifically ^{19}F MRI, which is modulated by intrinsic enzymatic activity. This will be achieved by taking advantage of the paramagnetic relaxation effect of a Gd^{III} ion.

Table 1: Medical imaging techniques comparison[18]

Technique	Clinical resolution and time scale	Animal resolution and time scale	Application	Main characteristics
SPECT	6-8 mm; s	1-2 mm; min	Functional	The emission is initiated by harmful gamma rays. Cheaper technique than PET.
PET	4 mm; s	1-2 mm; min	Metabolic, functional, molecular	Ionising radiation from radioisotope, also requires injection of an agent, more expensive than SPECT, but very sensitive.
CT	0.5 mm; s	50-100 µm; min	Anatomical, functional	A quick technique which uses multiple X-rays to build an image, high exposure to ionising X-rays. Poor contrast for soft tissues.
Ultrasound	0.3-0.5 mm; s	50 µm; min	Anatomical, functional	Painless and safe. Low quality images, dependant on the skill of the operator, images easily perturbed by calcified objects.

MRI	1 mm; s to min	80-100 µm; s to h	Anatomical, functional, molecular	No harmful radiation is used. Patient must remain still, can be noisy.
Bioluminescence	NA	1-10 mm; s to min	Molecular	Low penetration of interested area.
Optical imaging	NA	1-3 mm; s to min	Molecular	Low penetration of interested area.
X-ray		min	Anatomical	A quick technique that uses ionising radiation, can't be used to image soft tissue.

1.3.2 Magnetic resonance imaging

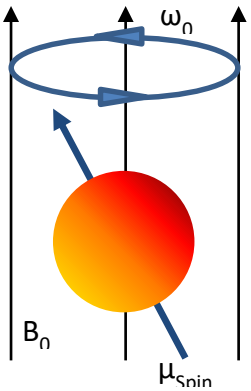

The basic principles of MRI are identical to nuclear magnetic resonance (NMR) spectroscopy. A hydrogen atom consists of a singly, positively charged proton, constantly precessing about its axis, shown in Figure 2. All nuclei have a magnetic field called a magnetic moment or μ_{spin}, and with regards to a nucleus, this is known as spin. The idea behind NMR is to expose the nucleus to an external magnetic field generating torque on the nuclear spin. When exposed to the field the nucleus is forced to align to the external field, and once aligned, the nucleus will adopt one of two possible spin states. The precession that the proton displays will now align with the magnetic field and is directly proportional to the magnetic field strength (B_0) and described by the Larmor frequency. The difference in energy (ΔE) between the two spins states is given by the following equation:

$$\Delta E = \frac{h\gamma B_0}{2\pi}$$

Equation 1: Spin state energy difference[19]

Where h is Plank's constant, γ is the magnetogyric ratio, the magnetic strength of the nucleus and finally B_0 is the strength of the applied magnetic field. The distribution of these spins states is given by the Boltzmann equation below.[19]

$$\frac{N_\alpha}{N_\beta} = e^{-\frac{\Delta E}{kT}}$$

Equation 2: Boltzmann equation[19]

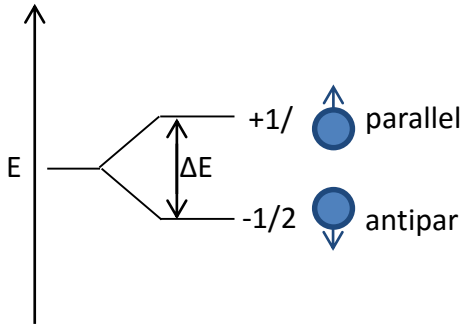

Spin–up or parallel (N_α), denotes alignment of the magnetic pulse (+1/2) and is lower in energy. Alternatively a spin-down, or antiparallel (N_β), with respect to the magnetic field (-1/2) can be adopted; however, this is a higher energy configuration, therefore spin-up is preferred, see Figure 3. Once the nuclei have aligned to the magnetic field, an RF pulse (radio frequency) is applied which rotates to 90° in the x,y plane of the magnetic field. This rotation is essential. The magnetic field of the sample of interest may be of the order of microtesla (μT), therefore when compared to the B_0 it is not detectable, however in the x,y plane this small field is detectable,

as a result detectors are placed here. Once this RF pulse is removed the nuclear spins begin the process of returning to the starting position, in alignment with B_0. The main processes behind relaxation are a dephasing of the spins from the pulse and a re-alignment of the nuclear spins with the z axis with B_0.

There are two different types of relaxation: spin-lattice or longitudinal relaxation and spin-spin or transverse relaxation. Typically in MRI, the hydrogens in water are used due to the high availability of water in the human body, which can be between 55% and 78% dependent on the tissue imaged.[20]

The T_1 is inversely dependent on the field strength of the instrument used. The T_1 is the time taken after the RF pulse has been applied, for the nuclear spin states of the imaged nuclei to return to their equilibrium state (which is then used in order to create an image, for T_1 weighted images). The greater the difference in T_1 between two regions of tissue, the better the contrast resolution of the image, for example in Figure 4 two different relaxation curves are shown, the black curve shows a faster relaxing nuclei than the red curve, upon observation of the nuclei at 1000 ms a large difference in signal is observed. Using a CA enhances the relaxation, increasing the difference between neighbouring tissues. Fast relaxation corresponds to a short T_1 and shows up on the image as a lighter colour, while the darker region on an MRI corresponds to the slow relaxation of a longer T_1, depending on the colour weighting of the image.

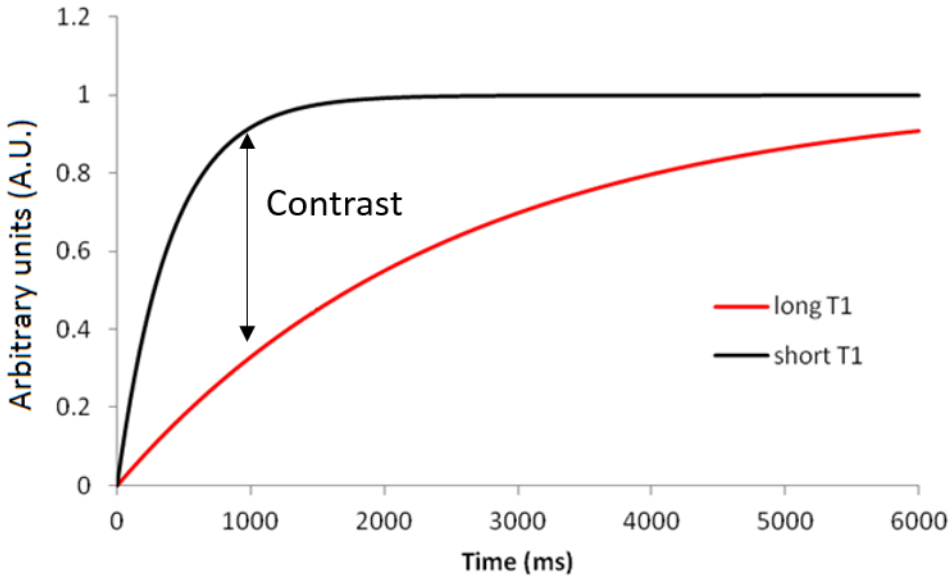

Figure 4: Example comparison of arbitrary long and short T_1 values

T_2 relaxation conversely involves two separate pulses; as with T_1 imaging the nuclei align with the external magnetic field, which is then followed by an RF pulse to push the magnetic moment of the nuclei to 90˚ of the magnetic field. The nuclei will relax at different rates, so some faster than others; a second RF pulse is then applied after a set time, which flips the moment through 180˚. This second RF pulse means that the faster relaxing nuclei are now "behind" the more slowly relaxing nuclei. Then the sample is allowed to relax and the time this takes is recorded.

1.3.3 ^{19}F MRI

^{1}H and ^{19}F are the most and second most sensitive NMR active elements respectively, with ^{19}F being 83.4% as sensitive as ^{1}H.[21] Both nuclei have a spin of a ½ and are 100% abundant. ^{19}F MRI is not a new concept; four years after the development of ^{1}H MRI in 1973, Holland *et al.* described imaging NaF.[22] Eight years

later in 1985 McFarland presented ^{19}F *in vivo* images of a rat abdomen.[23] Whilst ^{19}F MRI is only four years younger than ^{1}H MRI, there has been substantially fewer advances in the field, due to a lack of suitable fluorinated agents.[24] A major advantage ^{19}F MRI has over standard ^{1}H MRI is the lack of background noise, as the high ^{1}H content of the human body, 10% by weight, leads to background noise on scans. Whereas ^{19}F makes up only 0.7% of the human body by weight.[25] This means that a fluorinated agent introduced into the body can be imaged more easily and clearly. In order to lower the required dosage that needs to be administered to patients, the fluorinated agent should contain as many equivalent ^{19}F nuclei as possible, and ideally they should not couple to any neighbouring NMR active nuclei, so as to obtain a strong single signal. Equivalent fluorines within a ^{19}F MRI agent make the imaging process easier due to the different resonance of the fluorines. The fluorines will couple to the carbon they are bound to, however, due to the low abundance of active ^{13}C (1.1%), this is minimal.

1.3.4 Contrast agents

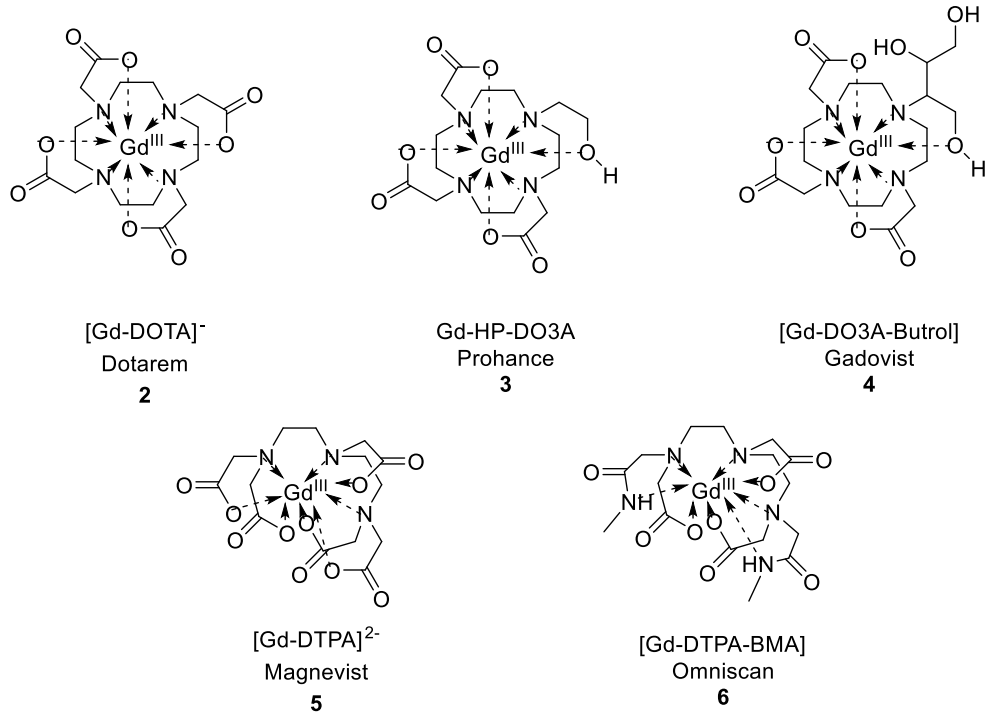

Figure 5: Modern contrast agents

Contrast agents (CA) are widely used in imaging to further enhance a difference in T_1 times; they do this by increasing the relaxation rate ($R_1 = 1/ T_1$). The increase in the relaxation rate comes from the paramagnetic nature of the metal centre. This paramagnetic nature is determined by the outer shell of electrons; a paramagnetic atom will have at least one unpaired electron, whereas a diamagnetic atom will only have paired electrons. Paramagnetic metals in contrast agents are used in their oxidised forms, meaning that they are positively charged due to a loss of electrons, and the number of electrons reflects the oxidation state of the metal. The most common paramagnetic ion used is Gd^{III} which has 7 unpaired electrons ([Xe] $4f^7$). Gd^{III} is not the only possible choice of metal, as Mn^{II} and super paramagnetic iron oxide (for T_2 imaging) can also be used and are areas currently being researched.[26, 27]

Figure 5 shows five different Gd^{III} based CAs split into two types, macrocyclic and linear ligands. Dotarem **2**, ProHance **3** and Gadovist **4** all contain a macrocyclic nitrogen ring with acetate arms coordinated to the Gd^{III} centre, whilst Magnevist **5** and Omniscan **6** have a linear heterocyclic conformation. All of these CA are administered intravenously (0.1 mmol/Kg) and are excreted by the kidneys within 24 hours of administration. Non-chelated Gd^{III} is highly toxic at the doses administered due to its similar size to Ca^{II}, and it tends to build up in the liver and kidneys.[28] The standard imaging dose of a Gd^{III} CA contains a potentially fatal amount of Gd^{III}, therefore the chelate bound to Gd^{III} has to be both thermodynamically and kinetically stable *in vivo*.

1.3.5 Inner/ Outer sphere binding of water

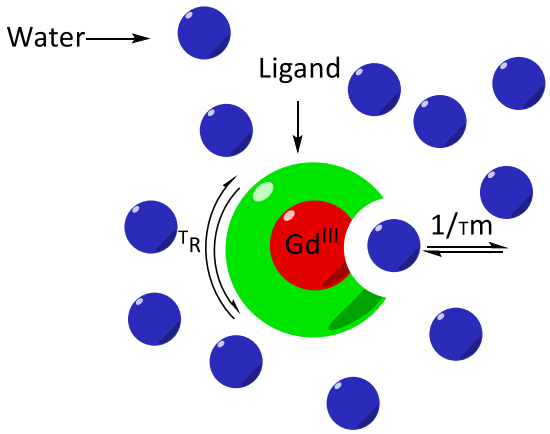

Scheme 3: Relaxation of water

The Lanthanide most commonly used for MRI CA purposes is Gd^{III}, which contains seven unpaired electrons. Lanthanides in their +3 oxidation state are 8 or 9 coordinate metals, whereas standard CA ligands are usually hepta or octa dentate. This allows for one or two free binding site(s) for water molecules. Without at least one free site the contrast agent would be less efficient for ^1H MRI. In theory by increasing the number of available binding sites for water, the relaxation effect can be increased, however, a ligand which has less than 7 donor groups gives a more labile complex, and therefore unsuitable. The free sites on the Gd^{III} centre are crucial. Scheme 3 shows the dissociative mechanism which leads to the relaxation, where τ_m is the water exchange lifetime, τ_R is the rotational correlation time and T_{1M} is the longitudinal relaxation time of bound water protons. The inner sphere contains water molecules directly bound to the Gd^{III}, which are free to exchange with the surrounding water, enhancing relaxation, due to their proximity to the paramagnetic Gd^{III}. These molecules generate the greatest effect. The second sphere consists of

water molecules hydrogen-bonded to the CA chelate, and these molecules are not so strongly relaxed simply due to their increased distance from the Gd^{III}. The outer sphere of water molecules are the bulk of the water surrounding the CA, and also contribute to the overall relaxation. Whilst aquated, Gd^{III} alone is sufficient for this process, the toxicity of Gd^{III} is so great that it must be bound by a thermodynamically stable chelate.[29]

1.3.6 Nephrogenic systemic fibrosis (NSF)

After the introduction of CAs, a new disease was diagnosed, called nephrogenic systemic fibrosis (NSF). This is where tissues, firstly skin, begin to produce an excessive amount of connective tissue. NSF can then spread to other organs such as the heart, lungs and liver. NSF was first described in 2000, however, it was then a further six years until NSF was attributed to CAs. Patients administered with Omniscan **6** were shown to be most at risk of NSF. Sufferers of NSF were almost exclusively patients with kidney failure who had been given excess CA to improve imaging; the CA localises in the kidneys.[28]

The neutral ligand of Omniscan is highly stable at physiological pH (7.6), however in the acidic environment of the kidney, the ligand is more labile, thus releasing Gd^{III}. Since 2008, CAs have been withheld from renal patients with a glomerular filtration of <30mL min^{-1}, which has eradicated the disease.[30]

1.3.7 Smart MRI agents

As mentioned previously, ^{1}H MRI contrast agents have been under development for a number of years, as a result, alternative agents to the standard CA are also under development. Smart agents can be divided into a two main categories:

- Responsive CA
- Enzymatically activated CA

1.3.8 Responsive CA

Responsive CAs can be activated by an endogenous or exogenous stimulus. Aime and coworkers.[31] demonstrated that biological copper (Cu^{I} and Cu^{II}) can be used as an activator for the conformation change in the DO3A (three arm binding analogue of DOTAREM **2**) CA below. Once the CA **7** is exposed to copper, the pyridine which was coordinated at the Gd^{III} centre instead binds to the copper along with the tertiary aniline. This then exposed the Gd^{III} centre **8**, allowing water to occupy a binding site enhancing the water relaxation, as shown in Scheme 4.

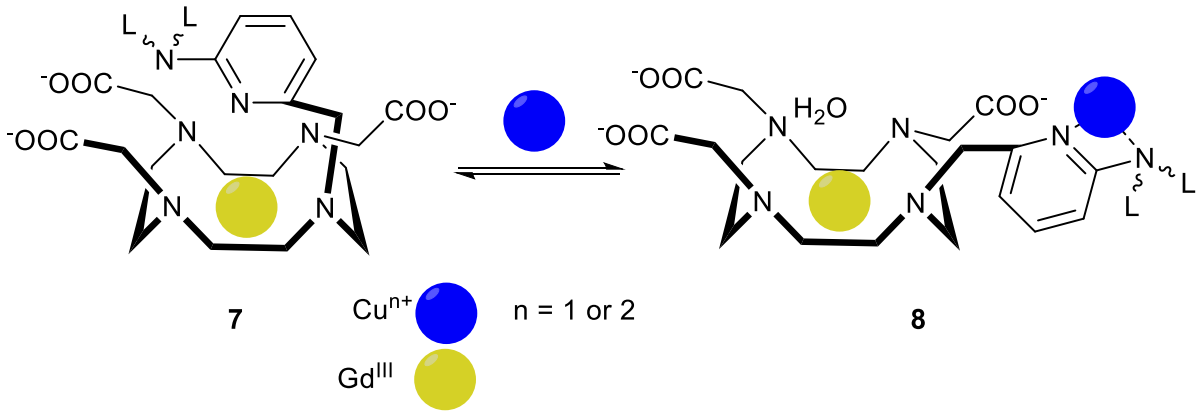

Scheme 4: Cu sensitive contrast agent developed by Aime and coworkers.

Esqueda *et al.*[32] in 2009 demonstrated a DO2A (two-binding arm analogue) CA **9** selective for Zn^{II} over other biological ions, as shown in Figure 6, that could be used to enhance the relaxation rate of Gd^{III}. Whilst the pyridine moieties bind to biological zinc the relaxation effect is increased due to availability of the Gd^{III}, without the zinc the pyridines shield the Gd^{III}. Zinc is the second most abundant metal in the body after iron and is found solely as Zn^{II}.[33] Zn^{II} plays a major part in controlling gene transcription and is found in metalloenzymes, including MMPs.

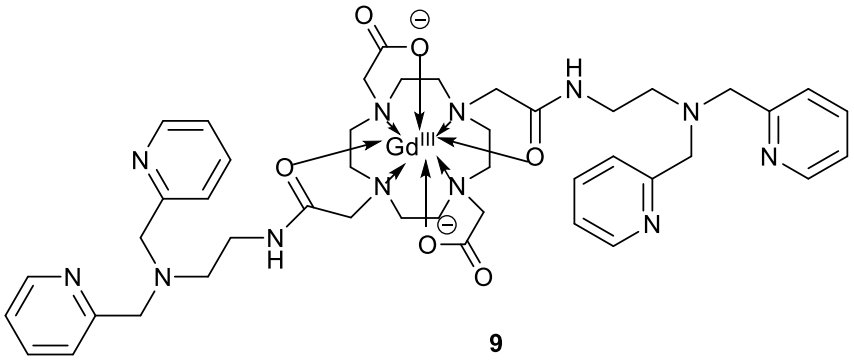

9

Figure 6: Esqueda *et al.* Zn^{II} sensitive contrast agent

1.3.9 Enzymatically activated CAs

Enzymatically activated CAs are those which require an enzyme to enact a chemical alteration to the CA in order to alter its relaxation properties. In 2000 Meade and coworkers.[34] published work on using β-galactosidase, a common marker for gene expression, to cleave the galactopyranosyl blocking group attached to a DO3A **10**, to activate the CA **11**, as shown in Scheme 5.

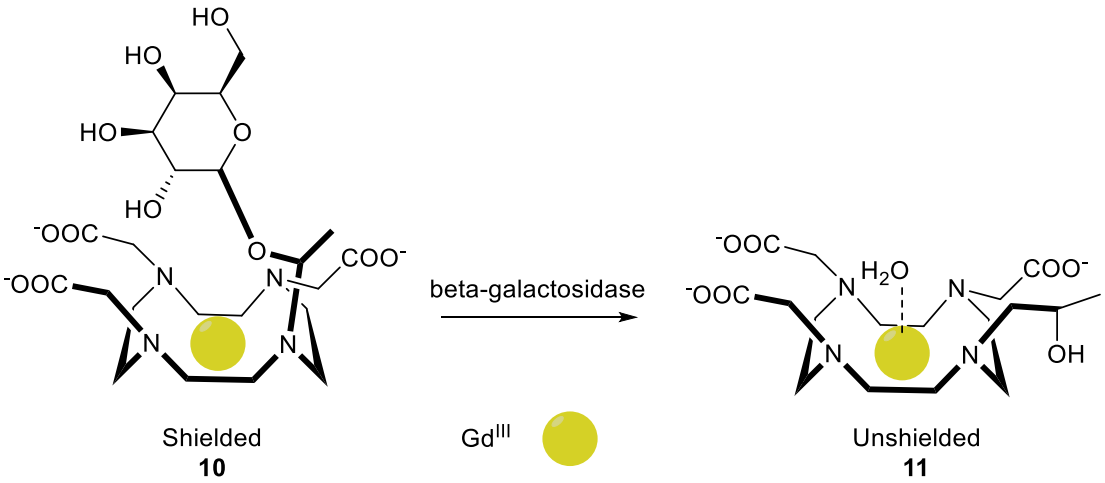

Scheme 5: Meade and coworkers. β-galactosidase activated contrast agent

In 2007 Kikuchi *et al.*[35] demonstrated the use of an enzymatically activated agent **12** specific for caspase-3, Figure 7. The agent **12** consists of a DOTA complex attached to a β-alanine, bound to a caspase-3 substrate, with an amino acid containing a CF_3 group. The fluorine atoms are relaxed whilst in close proximity to the Gd^{III} centre due to the paramagnetic relaxation effect (PRE), but once the substrate is cleaved (at the benzyl amide), the ^{19}F nuclei are no longer relaxed by the Gd^{III} and generate a signal. Due to the low levels of ^{19}F within the tissue, the 'new' CF_3 signal is then imaged, without any background noise.

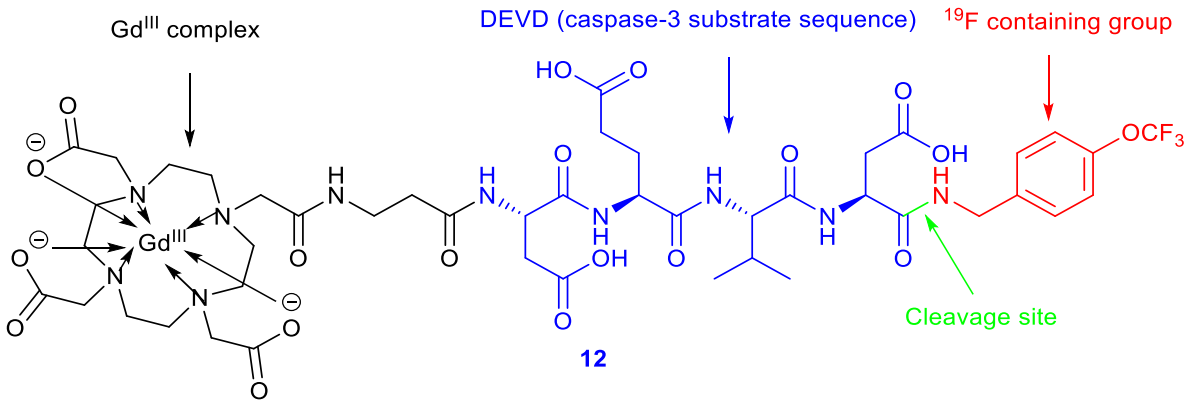

Figure 7: Kikuchi *et al.* caspase-3 activated contrast agent

More recently in 2014, Chen *et al.* described the synthesis of an MMP-2 activated ^{19}F MRI probe **13**.[36] The probe, shown Figure 8, contained nine equivalent fluorine atoms attached to the protease substrate *via* a short PEG linker. The probe **13** displayed a similar reaction profile to the probe **12** described by Kikuchi *et al.*[37] in 2007.

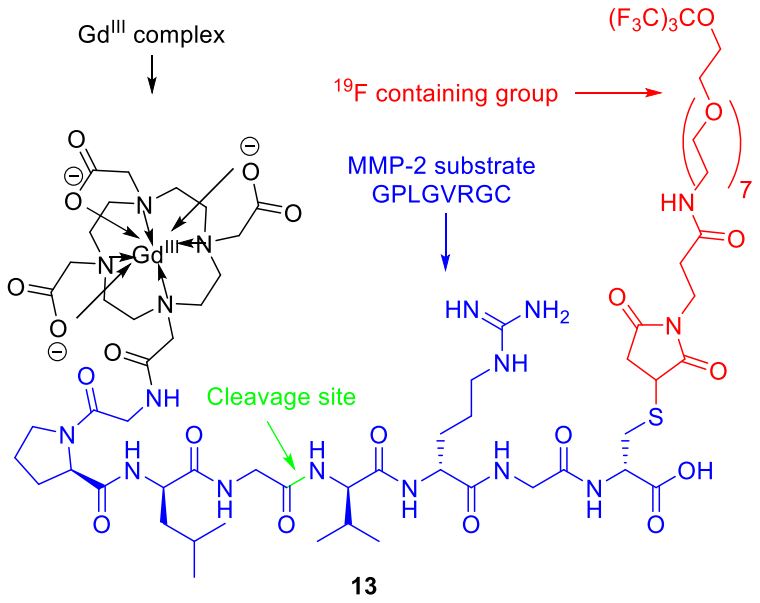

1.3.10 Brief recent history of smart agents

Year	Sensing	Group	Notes
2005	Zinc	Sherry *et al.*[38]	Europium based agent which coordinates Zn^{II}, Sherry also shows the agent to be unaffected by Ca^{II} and Mg^{II}.
2006	Fe, Ni, Mn	Desreux *et al.*[39]	A Gd^{III}-DO3A based agent which aggregates around a transition metal centre, resulting in three Gd^{III}-DO3A based agents around either Fe, Ni, or Mn, during aggregation relaxation is enhanced by up to 90%.
2006	Fe^{III}	Binnemans *et al.*[40]	A Gd^{III}-DTPA based probe with similar activity to the above Desreux probe. Binnemans *et al.* used this probe as a "blood pool agent".
2006	Lipase and cell function	Hoehn *et al.*[41]	Gd^{III}-DTPA based probe activated by lipase activity, insoluble precursor doesn't affect relaxation, once activated the probe is soluble enhancing relaxation effects.
2006	Cu^{II}	Chang *et al.*[42]	Gd^{III}-DO3A based copper chelator, copper alters the conformation of the probe altering

			relaxation properties by up to 41%.
2007	Zn^{II}	Meade *et al.*[43]	Gd^{III} DO3A probe, very similar to the above Chang probe.
2007	β-galactosidase	Wang *et al.*[44]	A ^{1}H MRI contrast agent containing a β-galactosidase labile linker, cleavage results in a reactive phenolate which can further react with proteins labelling them, once the Gd^{III}-DOTA based unit is bound the tumbling of the agent lowering T_1 constants of the surroundings.
2007	Esterase and cell labelling	Lowe *et al.*[45]	Membrane permeable Eu^{III}-DO3A based probe, activated by esterases.
2007	MMP-7	McIntyre *et al.*[46]	Gd^{III}-DOTA proteolytic probe that when activated becomes hydrophobic,
2007	β-galactosidase	Bogdanov *et al.*[47]	A ^{1}H MRI contrast agent containing a β-galactosidase labile linker, cleavage results in a naked tyrosine residue which is then polymerised by tyrosinase, once the Gd^{III}-DOTA based unit has polymerised the tumbling of the agent reduces again lowering T_1 constants of the surroundings.
2007	Ca^{II}	Logothetis *et*	Bis Gd^{III}-DO3A based probe, metal coordination alters relaxometry but by only 15%.

		al.[48]	
2008	β-galactosidase	Toth *et al.*[49]	A ^{1}H MRI Yb^{III}-DOTA based contrast agent containing a β-galactosidase labile linker, cleavage results in a labile electron rich carbamate, upon loss and formation of the amine a CEST agent is generated naked tyrosine residue which is then polymerised by tyrosinase, once the Gd^{III}-DOTA based unit has polymerised the tumbling of the agent reduces again lowering T_1 constants of the surroundings.
2008	MMP-9	Schnorr *et al.*[50]	MMP-9 substrate which when cleaved results in aggregation of the cleavage products into nanoparticles.
2008	Ca^{II}	Logothetis *et al.*[51]	Based on the previously reported probe, a new range of Gd^{III}-DO3A probes were designed with relaxation enhancements up to 100%.
2009	Carbonic anhydase	Chambers *et al.*[52]	A ^{129}Xe based agent which a ligand which is able to noncovalently bind to the target enzyme, generating a shift in the ^{129}Xe signal position.
2009	Cu^{II}	Chang *et al.*[31]	Chang reports enhancements upon the probe of 2006, relaxation effects improved dramatically from 41% to 360%, as well as high specificity towards Cu^{II}.

2009	Urokinase plasminogen activator	Pagel et al.[53]	Ln^{III}-DOTA based agent for the target enzyme. Papers shows a new methodology for loading a SPPS resin with an Fmoc-DOTA
2009	MMP-2	Lepage *et al.*[54]	Gd^{III}-DOTA based agent which functions as a solubility agent, pre-cleaved the agent is soluble and expected characteristics, post-cleavage the Gd^{III}-DOTA section becomes insoluble.
2009	Zn^{II}	Leon-Rodriguez *et al.*[32]	Gd^{III}-DOTA agent containing two Zn^{II} chelators, once a Zn^{II} was chelated an increase in relaxation was observe, upon chelation of a second a 165% change was observed.
2009	Light or NADH	Louie *et al.*[55]	Gd^{III}-DO3A based agent which reversibly isomerised under light altering relaxation. A similar change is also observed by irreversible NADH activation.
2010	Cathepsin D	Hudson *et al.*[56]	Tm^{III}-DOTA based probe proteolytically activated and then taken into cell, the probe was also tagged with a fluorescent probe for visual confirmation of cellular uptake.
2010	Design principles for ^{19}F agents	Parker *et al.*[57]	Whilst not a smart contrast agent, Parker and co-workers presented an in depth analysis of relaxation rate enhancement based on changing the lanthanide (Tb, Ho, Dm, Er, Tm etc),

			the distance effects of the ^{19}F nuclei and lanthanide, as well as the enhancement effects in different magnetic fields.
2010	Ca^{II}, Mg^{II} and Zn^{II}	Peters *et al.*[58]	Gd^{III}-DO3A with a bisphosphonate chelator for di-cations. Unfortunately whilst the probe reports up to 500% relaxometry effects, the concentration of biological ions isn't low enough to achieve this.
2011	Liposome activated trypsin	Aime *et al.*[59]	Liposomes filled with Gd^{III}-DO3A based compound, the surface of the liposomes aggregate due to anionic effects stabilised by the cationic protein protamine, trypsin cleaves the protamine resulting in disassemble and increases water access to the liposomes.
2011	Tyrosinase	Botta *et al.*[60]	Mn^{II} based probe, various metal ligands are shown, polymerisation of the MnII results in the probes relaxometry effects
2011	Nanomolar imaging	Parker et al.[61]	An alternative application to imaging with lanthanides, instead of knocking out a signal so that it cannot be imaged, instead take advantage of the relaxation to rapidly image the target enabling very low (to nanomolar) concentrations to be imaged.
2011	Dextrinase	Shapiro *et al.*[62]	Iron oxide nanoparticles coated in a polymer which is degraded by an enzyme, releasing the

			nanoparticles.
2011	MMP-2	Matsumura *et al.*[63]	Iron oxide nanoparticles labelled with an MMP-2 substrate once cleaved the nanoparticles aggregate.
2011	Zn^{II}	Sherry *et al.*[64]	A Gd^{III}-DOTA based probe capable of showing Zn^{II} presence, which was used to image the pancreas of mice.
2012	β-galactosidase	Engelmann *et al.*[65]	A ^{19}F MRI agent which contained a unit cleavable by β-galactosidase, once the agent was cleaved a ^{19}F MRI signal emerges.
2012	In vivo redox state of brain	Saga *et al.*[66]	Presented a nitroxy radical labelled compound which in the brain would be reduced or oxidised depending on the health of the brain, oxidising conditions oxidised and activate the hydroxy to the radical (lowering T_1) indicating a brain tumour.
2012	β-galactosidase	Engelmann *et al.*[65]	A Gd^{III}-DO3A agent with dual ^{1}H and ^{19}F MRI applications with a self immolative linker, in the initial state no ^{19}F signal is detect and the ^{1}H MRI is.
2013	Transglutaminase	Pagel *et al.*[67]	Tm^{III}-DO3A based which once cleaved forms a covalent bond with the target enzyme, creating a shift in the ppm of certain signals on the enzyme.

2013	Glutamate decarboxylase	Aime *et al.*[68]	Gd^{III}-DO3A based agent targeted towards neural imaging. The agent contained terminal glutamate residues which are accepted by the target enzyme, decarboxylation results in the increase in the inner sphere hydration number.
2013	Techniques for rapid imaging	Parker *et al.*[69]	Work presented showed the effect of changing the paramagnetic source (lanthanide) with a view for rapid imaging, to increase the signal to noise achieved in MRI.
2013	Cu^{II}	Hong *et al.*[70]	Gd^{III}-DTTA based Cu^{II} chelator than once in the presence of Cu^{II} the agent coordinates altering the q number.
2014	Urokinase plasminogen activator	Pagel *et al.*[71]	Tm^{III}-DOTA based agent which once part is cleaved by the target results in a coordination site for water.
2014	Lipase and cell function	Deng *et al.*[72]	Similar to the Hoehn probe of reported in 2006, however Gd^{III}-DTPA nanoparticles were used for an in vivo study of the pancreas.
2015	^{129}Xe agent	Thomas *et al.*[73]	The Thomas group reported a novel proof of principle detailing a hyperpolarised ^{129}Xe modulated by a Gd^{III}-DOTA based compound.

2015	MMP-9	Thomas *et al.* (Submitted)[74]	The Thomas group reported the design and synthesis of two Gd^{III}-DOTA based ^{19}F MRI probes for proteolytic activity.

1.3.11 Alternative paramagnetic sources

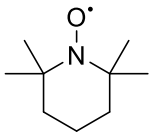

TEMPO

Figure 9: TEMPO

By definition an atom is paramagnetic if it has unpaired electrons in its outer shell; therefore there are many different examples of paramagnetic atoms. Within the MRI community the most commonly exploited atoms for relaxation purposes are gadolinium, manganese and iron, however, other paramagnetic sources such as stabilised free radicals can also be used. TEMPO radicals for example, Figure 9, contain an oxygen radical, with a single electron making it paramagnetic. Due to these characteristics, TEMPO and similar radicals have been used to modulate NMR signals for enzymatic studies.

1.3.12 Alternative nuclei for the NMR/MRI signal

There are a large number of NMR active nuclei, and a nucleus which has garnered increasing amounts of interest over the last few years is ^{129}Xe. Xenon has multiple different stable isotopes, however, the main isotope of interest is ^{129}Xe (26.4% abundant), which is ½ spin active and also the most common isotope, xenon can also be purchased as enriched ^{129}Xe. The sensitivity with regards to ^{129}Xe compared to ^{1}H is several orders of magnitude weaker. A technique called hyperpolarisation is used to force all of the nuclei into a higher energy state and align in the desired field, this

then caused a dramatic increase in the signal achieved, becoming several orders of magnitude better in favour of ^{129}Xe than ^{1}H NMR.[75, 76] Typically, ^{129}Xe is temporarily encaged within structures called cryptophanes. This temporary encapsulation gives the observer the ability to observe changes based upon the environmental fluctuations in the cryptophane's environment.[73]

1.3.13 ^{129}Xe MRI agent

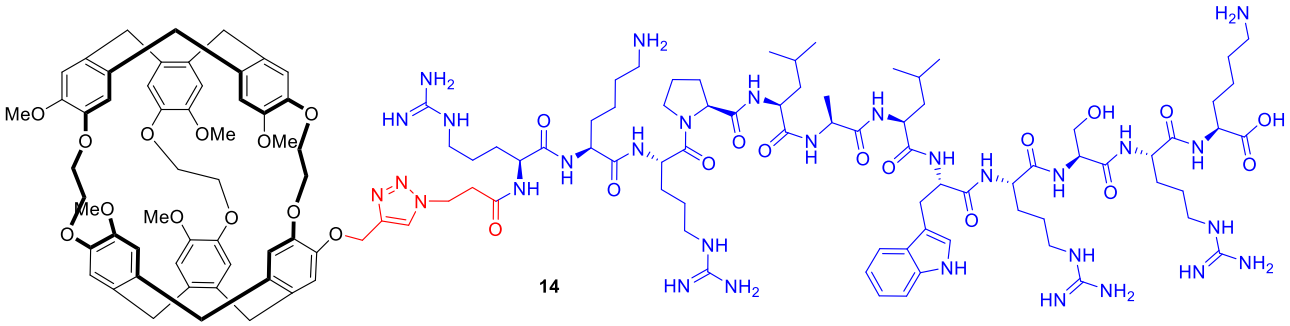

Figure 10: Wei *et al.* MMP-7 Xe Probe

In 2006 Wei *et al.* described an MMP-7 probe, see Figure 10, which contained three units: a cryptophane (black), a triazole linker (red), and a MMP-7 peptide sequence (blue),. The conjugation of cryptophane was achieved by including an alkyne moiety for “click” chemistry onto the azide of the MMP-7 substrate.[77]

1.3.14 Förster Resonance Energy Transfer (FRET)

The PRE of Gd^{III} on surrounding NMR active atoms is a distance dependent process, and is based upon the same distance dependences as Förster resonance energy transfer (FRET). FRET is a distance dependent transfer of energy from an excited state compound or donor to an acceptor compound. The energy is transferred non-radiatively and transfer can only occur up to a short distance of approximately 10 nm.[78]

Förster derived an expression for the rate constant of the energy transfer k_T see Equation 3.[79]

$$k_T(R) = (1 / \tau_D) (R_0 / r)^6$$

Equation 3

The Förster theory of energy transfer states that the transfer is determined by three major factors. Firstly, as mentioned, the physical distance between the donor and acceptor, the spectral overlap of the donor emission spectrum and the acceptor absorption spectrum, and finally the physical orientation of the donor and acceptor compounds.

The efficiency (E_{FRET}) of energy transfer is based on the physical distance between donor and acceptor, which can be shown to have an inverse sixth power relationship, as shown in Equation 4 and Equation 5.[80]

$$E_{FRET} = 1 / 1 + (r / R_0)^6$$

Equation 4

$$R = R_0 ((1 / E_{FRET}) – 1)^{1/6}$$

Equation 5

The Förster radius (R_0) is the distance where the efficiency of the transfer is 50%. R_0 defines the length scale of interaction, i.e. the effective range of interaction, which is

approximately between 3 - 8 nm depending on the acceptor/ donor pairing, and corresponds to between 5 – 95% of the E_{FRET} allowing for sufficient sensitivity.

FRET is dependent on the overlap of the donor emission and acceptor absorption spectrum. EDANS and Dabcyl are a classic donor and acceptor pair commonly used for imaging protease activity.[81] The overlap of the emission spectra, as shown in Spectra 1,[82] shows the ideal overlap of the donor (EDANS) and acceptor (Dabcyl) emission and absorption ranges.

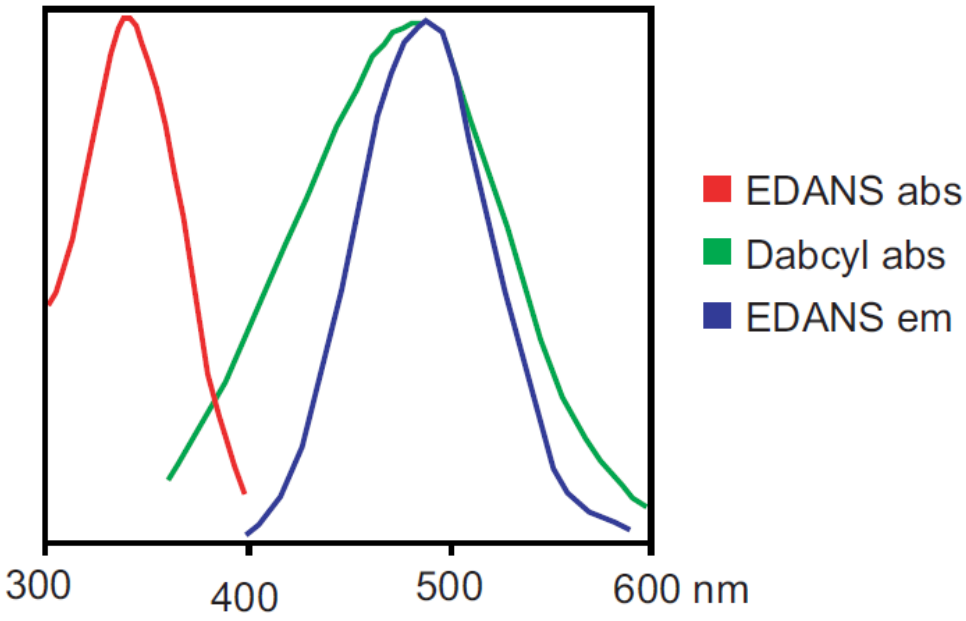

Spectra 1: EDANS emission and absorbance vs. Dabcyl absorption[82]

Finally, the dipole overlap of the fluorochromes needs to be considered. If donor and acceptor are aligned parallel to each other, near maximum E_{FRET} can be achieved; if however, they align perpendicularly, the E_{FRET} is dramatically reduced to near zero. This relationship can be seen mathematically in Equation 6, where κ^2 defines the level of alignment.[83]

$$\kappa^2 = [\cos\theta_T - 3\cos\theta_D \cos\theta_A]^2 = [\sin\theta_D \sin\theta_A \cos\phi - 2\cos\theta_D \cos\theta_A]^2$$

Equation 6: FRET alignment relationship[83]

κ^2 varies between 0 and 4, although it is assumed to be 2/3, which is the average value of all possible angles the FRET agents can occupy with respect to one another. These angles are possible due to the degrees of freedom of the fluorochromes.

1.4 Solid phase peptide synthesis (SPPS)

Solid phase peptide synthesis (SPPS) was first performed by Merrifield in 1963.[84] The introduction of SPPS completely revolutionised the way in which peptides could be synthetically produced. In this technique the first amino acid in the sequence was *N*-carboxybenzyl (Cbz)-protected, which was chemically bound to an insoluble solid support (resin) **14** *via* a cleavable benzyl ester **15**. The amino protecting group was then removed using a hydrogen bromide / acetic acid mix resulting in **16**, and the next amino acid was attached with the diimide of the desired amino acid in a two-fold excess giving **17**, using *N,N'*-dicyclohexylcarbodiimide (DCC) to activate the acid and all subsequent acids. Once coupled, the peptide was exposed to acetic anhydride and triethylamine (TEA) in order to acetylate any unreacted amines. This process was followed until the desired amino acids had been coupled, the peptides **18** were then cleaved from the resin using sodium hydroxide. This process is shown in Scheme 6.

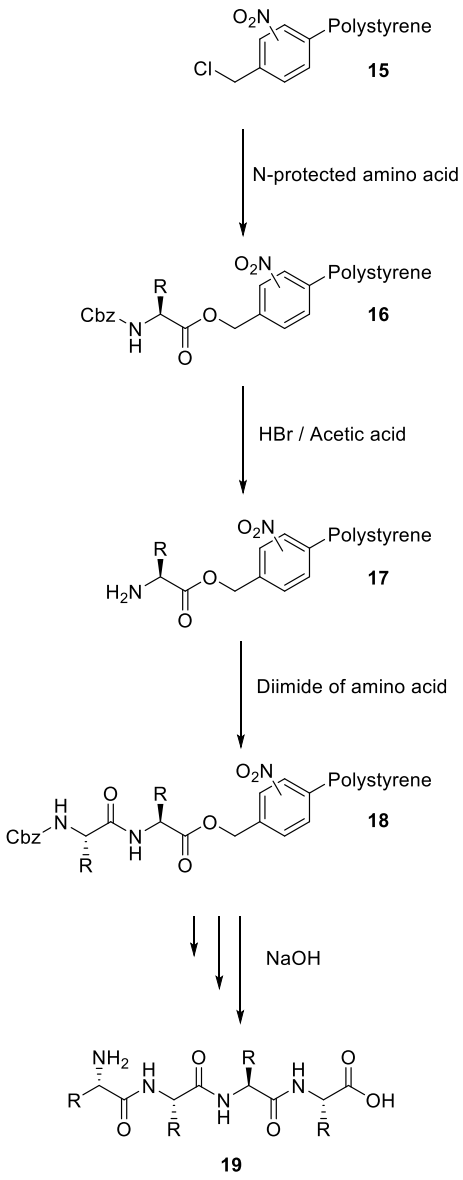

Scheme 6: Merrifield's original SPPS

Whilst SPPS has changed since its inception in 1963, the basic principles have remained the same. SPPS and common solution-based chemistry vary in a few key ways. SPPS-based synthesis has the advantage of washing away any excess reagent used, because the peptide is bound to an insoluble support, hence simple filtration and excess washings are an effective form of purification. This results in a second

advantage, as large excesses of reagents can be used in a coupling and washed away giving near 100% yields. Thirdly, with new protecting strategies and excess reagents, high-yielding coupling can be achieved in 1-2 minutes.[85]

SPPS has one main advantage over standard solution chemistry, which also constitutes its greatest weakness. The amino acids are attached to a resin, which allows for a more facile purification, however, because of this, in the eventuality that one amino acid is missed in the sequence, it would not be detected until the final stage, which over the course of the process wastes large amounts of expensive reagents. It is also not possible to produce peptides using SPPS on the same scale as standard solution phase chemistry.

1.4.1 Solid supports in SPPS

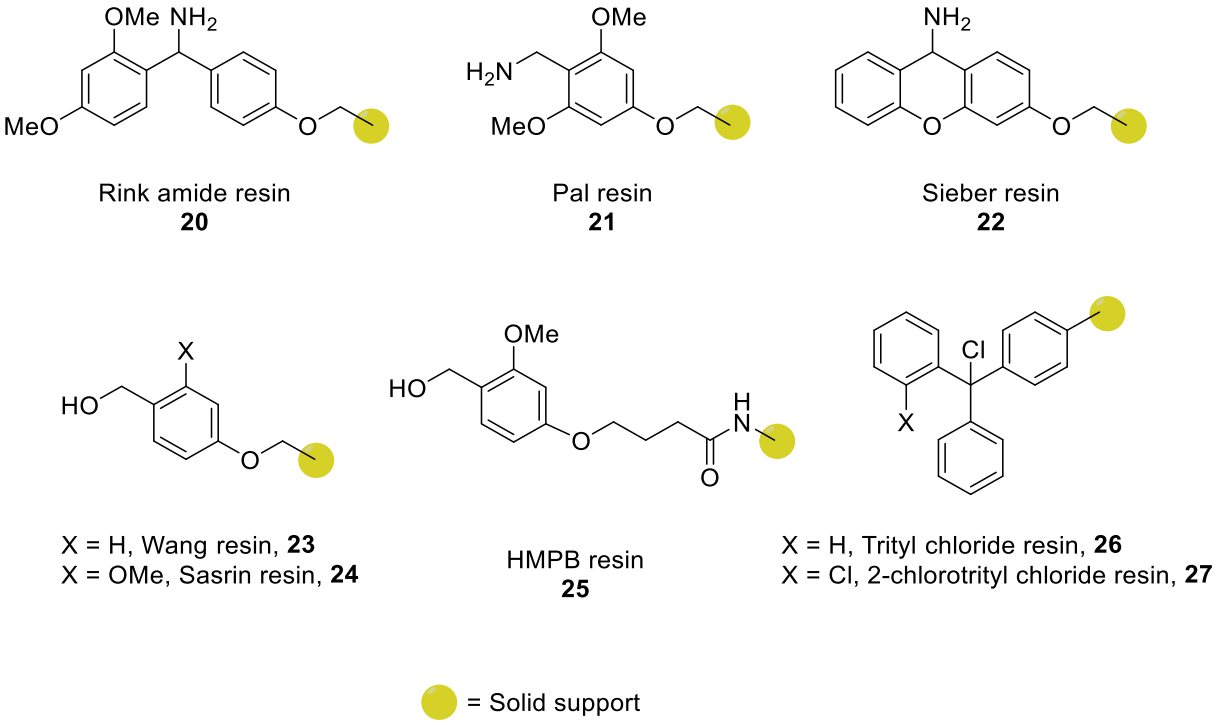

Figure 11: Resin supports

Figure 11 shows some of the most commonly used solid supports within SPPS. Rink **20**,[86] Pal **21**[87] and Sieber **22**[88] resins are used to synthesise peptides with a terminal amide instead of an acid. With these resins the first amino acid is coupled to the resin using coupling agents. Wang **23**,[89] Sasrin **24**,[90] HMPB **25**,[91] trityl chloride **26** and 2-chlorotrityl chloride **27** resins[92] are used when the free acid is required. When using the Wang **23**, Sasrin **24** and HMPB **25** resins, the first amino acid is coupled to form the ester. With the trityl based resins **26** and **27**, the cation is produced *in situ* and then the deprotonated amino acid attacks to form the ester in an E_1 reaction, as shown in Scheme 7.

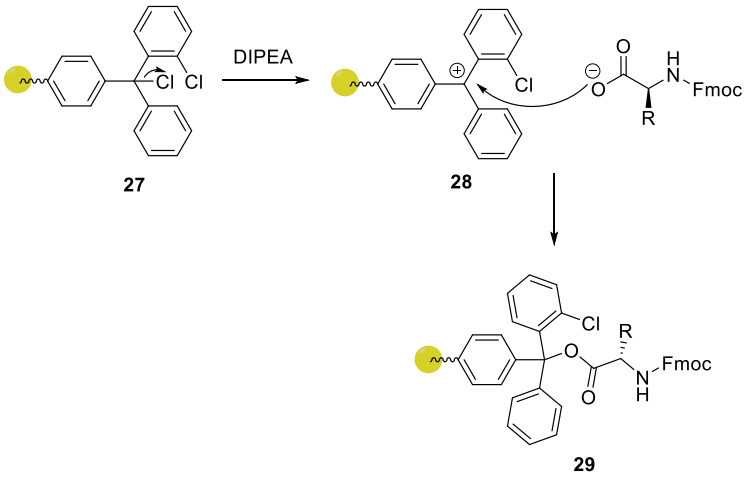

Scheme 7: Formation of resin amino acid ester linkage

1.4.2 Types of SPPS, Boc vs. Fmoc

N-protected amino acids are still used, but instead of the original Cbz strategy used by Merrifield, Boc or Fmoc groups are typically now utilised instead.

Boc SPPS uses trifluoroacetic acid (TFA) in dichloromethane (DCM) to remove the Boc groups, and resin cleavage is achieved using anhydrous HF, therefore requiring very specialist equipment and therefore not usually performed in research.

Fmoc SPPS is a technique which uses basic conditions, usually piperidine to cleave the protecting group. The piperidine used then reacts further with the cleaved fluorenyl methylene, avoiding alkylation of the peptide. Fmoc SPPS does not require

equipment as expensive as Boc SPPS and is therefore used more frequently in research.

1.4.3 The process of SPPS with trityl based resins

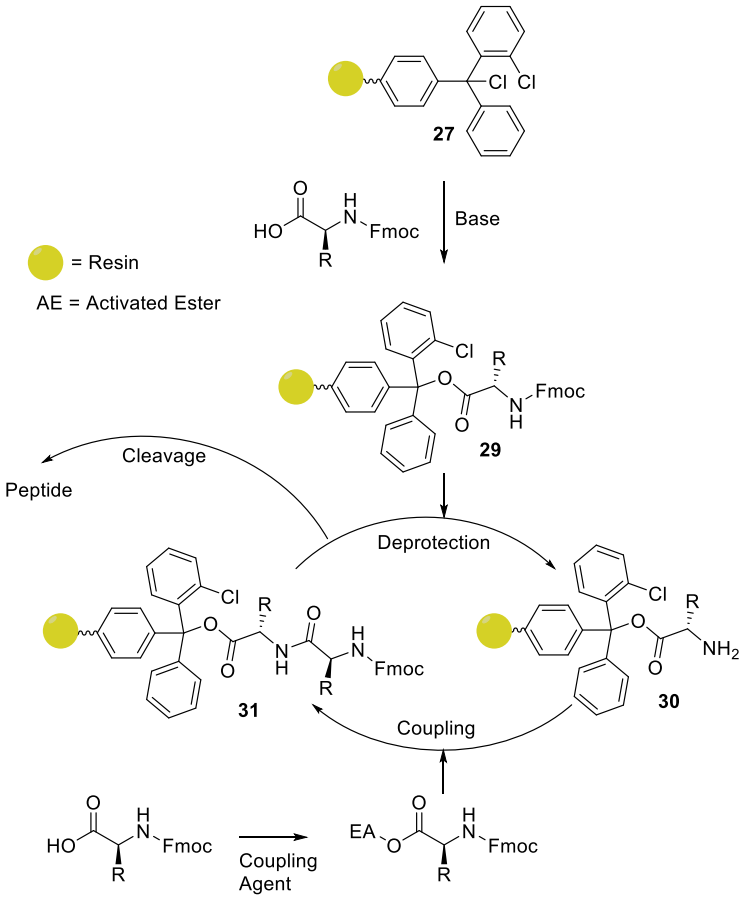

Scheme 8: The cycle of SPPS

SPPS is a powerful technique regularly used to synthesise peptides. The desired peptides for this project are between 6-10 amino acids long and are synthesised using Fmoc SPPS. Plastic resin beads **27** with a binding site for the carboxyl end of amino acids (shown in Scheme 8) are placed into a standard reaction vessel, along

with the first Fmoc-amino acid of the desired sequence in the absence of base, usually diisopropylethylamine (DIPEA) in DCM, which allows the resin to swell resulting in **29**. Once the reaction is completed, methanol is added to form the methyl ether with any unreacted trityl **27**. The resin is then washed with DMF to remove any impurities, followed by sequential DCM and hexane washes. The DCM swells the resin **29**, whilst the hexane shrinks the resin **29**, ensuring any unreacted material is removed. The resin **29** is then transferred to a SPPS column where it sits between two pieces of high grade filter paper, preventing it from being transferred to the solvent or waste lines. The resin **29** is washed with DMF for approximately ten minutes to remove any unreacted amino acid and then washed with a DMF-piperidine mix to deprotect the terminal amine, giving **30**. This deprotection can be monitored under UV due to the chromophoric nature of the cleaved Fmoc, or *via* ninhydrin staining to monitor amine formation. The next amino acid in the sequence is then loaded into the column with a coupling agent and a base, and very slowly stirred between 30 minutes and three hours giving **31**. Additional agents such as hydroxybenzotriazole (HOBt) or *N*-methylmorpholine are also added with some coupling agents to avoid side reactions and epimerisation, as well as to increase the coupling rate. The resin **31** is slowly stirred to avoid grinding of the fragile bead. After this, the column is rewashed with DMF, removing excess reagents, and the amino acid deprotected, all these steps are then repeated until the sequence is complete. When the final amino acid has been coupled, deprotected and washed, the resin is exposed to a cleavage mixture, hydrolysing the peptide-resin ester bond. The cleavage mixture is dependent on the peptide and protecting groups used, although commonly TFA, triisopropylsilane (TIPS) and H_2O are used in various ratios.

The cleavage mixture is then collected, dried, washed with diethyl ether, and the filtrate collected as the TFA salt and purified *via* HPLC (high performance liquid chromatography).

1.4.4 Coupling Agents

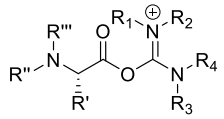

Activated Uronium
32

Figure 12: Acyl uronium

A carboxylic acid and an amine at high temperatures will form an amide bond, however, this is not suitable for synthesis. Coupling agents are used as activating agents, substantially lowering the activation energy required for the amide bond to form, enabling ambient temperature couplings. Coupling agents all follow the same basic idea, with the amine attacking an activated carboxyl group. Whilst the basic concepts of activated carboxyl groups are the same, they come in various different types; either activated esters or acyl halides, azides, mixed or symmetrical acid anhydrides, or deciduous intermediates. Some of these can be isolated, such as certain activated esters; others cannot and are formed *in situ*, and may or may not even be detectable, for example acyl uroniums **32**, see Figure 12.

1.4.5 Couplings *via* carbodiimides

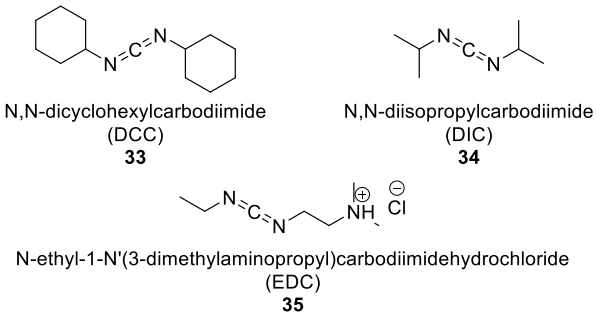

Figure 13: Common diimide coupling agents

Figure 13 shows three of the most commonly used diimides. All the diimides have

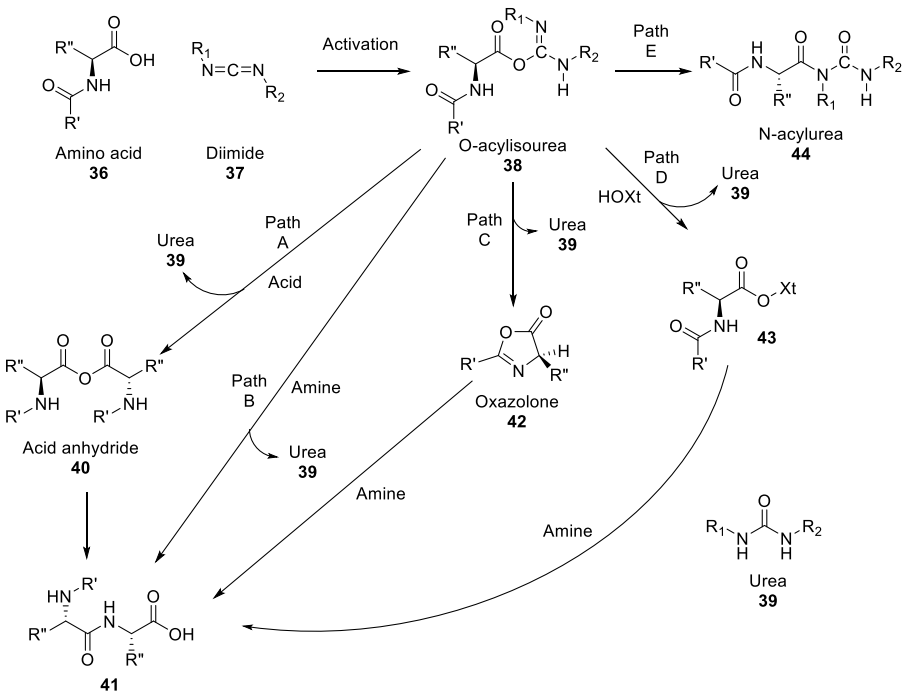

Scheme 9: Potential reaction pathways of diimides

similar mechanisms of action, as shown in Scheme 9, and are normally used with additives to form more stable activated esters, less prone to epimerisation. Upon addition of the acid to the coupling mixture, the acid becomes deprotonated by the diimide, and is followed by the nucleophilic attack of the acid onto the protonated

diimide, forming an *O*-acylisourea **38**. The *O*-acylisourea **38** is very reactive and can react in several different ways.

The *O*-acylisourea **38** can react with another amino acid **36**, thereby generating the acid anhydride **40**, which can then be attacked by an amine forming the desired product (Path A, Scheme 9). The *O*-acylisourea **38** can also react with an amine directly to produce the desired amide **41** (Path B, Scheme 9). The *O*-acylisourea **38** contains two basic nitrogens which can deprotonate the carbamates of the amino acid to be coupled; forming an imidate that can then attack and form an oxazolone **42**, which can then be attacked by the incoming amine to form the desired amide **41** (Path C, Scheme 9). The final route to the product includes the addition of an additive; these additives form a more stable, yet still reactive ester **43** (Path D, Scheme 9). These additives (referred to as HOXt in Scheme 9) not only prevent side reactions such as the formation of *N*-acylurea **44** (Path E, Scheme 9), but they also prevent the formation of acid anhydrides **40** and oxazolones **42**, which can epimerise. They also react with the *O*-acylisourea **38** rapidly, which is crucial as this can also epimerise.

In the original example of SPPS, Merrifield used DCC **33**. DCC **33** was originally developed by Sheehan *et al.*[93] in 1955 and is a very popular method for forming an amide bond. The main disadvantage with DCC **33** is that the urea by-product (DCU) of the reaction is insoluble in all solvents except TFA (it is slightly soluble in ethyl acetate and water), making DCC **33** only compatible with Boc SPPS. EDC **35** and DIC **34**, shown in Figure 13, provide Fmoc-SPPS-compatible alternatives to DCC **33**, as the

urea by-product **39** for both agents is DCM soluble.[94] EDC **35** also has the added advantage that both the urea by-product **39** and EDC **35** itself are water soluble, making their removal from organic soluble compounds in standard syntheses very easy.

1.4.6 Couplings *via* anhydrides

As mentioned previously, acid anhydrides can be used to form amide bonds. Acid anhydrides can be synthesised using DCC **33** or other diimides mentioned previously, or they can be made by reacting an acyl chloride and acid moiety to produce symmetrical anhydrides. Alternatively acyl chlorides can also be used to create unsymmetrical anhydrides as originally shown by Vaughan *et al.*[95] This method has the obvious draw backs of unselective amide formation, but was one of the original methods of forming amides. However, Vaughan then went on to produce a similar method where the desired acid reacts with a chloroformate to form a carbonic anhydride, which is then cleaved by an amine to form the desired amide.[96]

1.4.7 Couplings *via* active esters

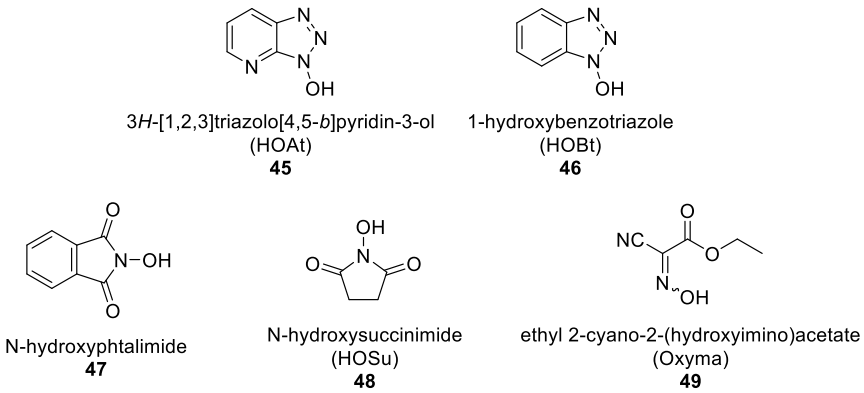

Figure 14: Coupling additives

In the diimide method of coupling, additives were mentioned and above of the generic form HOXt (Scheme 9). Commonly used additives HOAt **45** (developed by Sheehan) and HOBt **46** are shown in Figure 14.[93, 97] Sheehan developed *N*-hydroxysuccinimide (HOSu) **48**, which can also be used to form the hydroxamic acid and then be stored.[98] *N*-hydroxypthalimide **47** was developed at a later date by Fujino *et al.* and is also a common activating agent used today.[99] Very recently Albericio *et al.* presented ethyl 2-cyano-2-(hydroxyimino)acetate (Oxyma) **49** as an additive to replace HOAt **45** and HOBt **46**.[100]

HOAt **45**, but predominantly HOBt **46**, are an integral part to coupling agents and are still used today. HOAt **45** is used far less frequently due to its high cost and explosive nature and the fact it is only available as a solution. HOBt **46** is relatively cheap (approximately £1/g, Sigma), yet it is also becoming less available due to its explosive

nature and shipping restrictions. Nonetheless, these components along with Oxyma **49** have now been included into the structure of many coupling agents.

1.4.8 Couplings *via* phosphonium salts

The next step forward for coupling agents came in 1969, when Kenner *et al.* described the first use of a phosphonium based coupling agent.[101] Kenner's approach used large excesses of the highly toxic hexamethylphosphoramide (HMPA), as both reagent and solvent, with tosic anhydride to make a phosphoxane. This phosphoxane then readily reacts with an incoming acid, forming an active ester with HMPA, which can then react with an amine. Whilst Kenner *et al.* did report low levels of racemisation, they also reported that this method was incompatible with hydroxy containing amino acids and histidine.

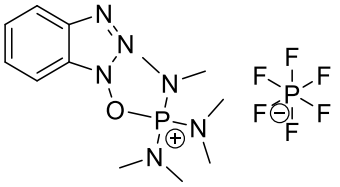

(Benzotriazol-1-yloxy)tris(dimethylamino)phosphonium hexafluorophosphate
(BOP)
50

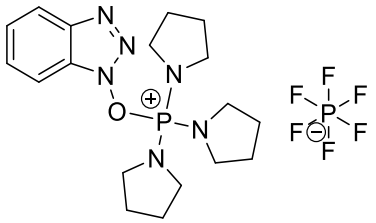

Benzotriazol-1-yl-oxytripyrrolidinophosphonium hexafluorophosphate
(PyBOP)
51

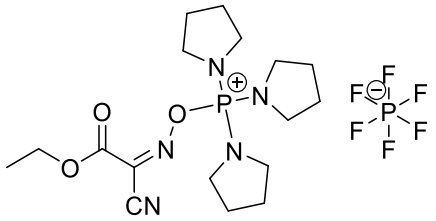

[Ethyl cyano(hydroxyimino)acetato-O2]tri-1-pyrrolidinylphosphonium hexafluorophosphate
(PyOxim)
52

Figure 15: Common phosponium coupling agents

Phosphonium salts (Figure 15) were not regularly used as coupling agents until the introduction of the new agent, (benzotriazol-1-yloxy)tris(dimethylamino) phosphonium hexafluorophosphate (BOP) **50**, by Castro *et al.* in 1975.[102] BOP **50** was based on the work produced by Kenner and the additive HOBt **46**. The combination of these ideas produced a highly active agent with low levels of racemisation. BOP **50** was later modified in 1990 into PyBOP **51** by Castro, who replaced the dimethyl amines of the HMPA unit with pyrrolidine groups, thereby preventing the release of HMPA post coupling.[103]

In 2010 Albericio *et al.* replaced the HOBt **46** unit of PyBOP **51** with Oxyma **49**, to produce two agents, PyOxP and PyOxB, differing only in the counter ion.[104] PyOxP is now known as PyOxim **52** (Figure 15) and offers highly efficient couplings, with very

low levels of racemisation, as well as an effective means of coupling highly hindered units. PyOxim **52** also possesses very low levels of toxicity when compared to other coupling agents.

1.4.9 Couplings *via* aminium/ uronium salts

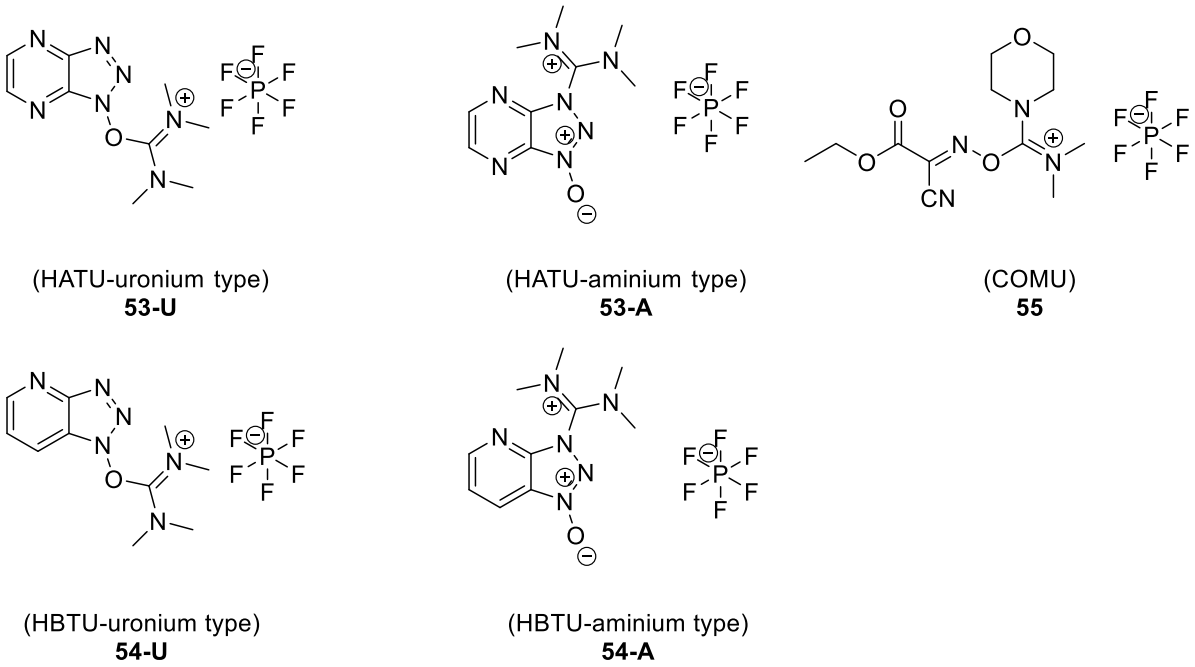

Figure 16: Aminium and uronium coupling agents

HATU **53** and HBTU **54** are amongst the best known peptide coupling agents. HBTU **54** was first reported in 1978 by Dourtoglou *et al*.[105] HATU **53** and HBTU **54** were based on the coupling agent BOP **50** and the corresponding benzotriazoles, HOAt **45** and HOBt **46** respectively. Both agents were believed to be the corresponding uronium salt of the BOP **50** phosphonium, but after X-ray crystal analysis, they were

shown to actually be the guanidinium salt, more commonly known as the aminium salt, see Figure 16.[106]

Currently the newest coupling agent of this type to gain popularity is the agent COMU **55**, which was introduced in 2009 by Albericio.[107] COMU **55**, like PyOxim **52**, boasts very low levels of epimerisation, but with a faster coupling rate, COMU **56** is also the least toxic coupling agent to date and is one of the few that is not explosive at high temperatures. Due to the Oxyma **49** leaving group, COMU **55** is also very efficient with sterically difficult couplings.

Cost efficiency is a major drawback to SPPS; Fmoc protected amino acids are very cheap (~£0.5-2/g, Sigma), but the coupling agents involved, however, are significantly more expensive. HBTU **54**, COMU **55**, BOP **50** and PyOxim **52** all cost a similar amount (~£9/g, Sigma), with PyBOP **51** being slightly more expensive and HATU **53** being the most expensive (~£20/g, Sigma). When taking into consideration that four equivalents of Fmoc-protected amino acid and coupling agent are used per cycle, this in effect increases the cost per coupling by four-fold.

Chapter 2 - Aims

The aim of this project is to design and evaluate a smart ^{19}F MRI contrast agent based on four substrate sequences for different MMPs, which are capable of showing MMP activity by MRI, thereby providing insight into disease in the region of interest by showing unusual levels of MMP activity. In order to do this *in vitro* initially, to optimise the probe as required, and possibly *in vivo* the target compound consists of three sub units. The first is similar to a standard CA consisting of a Gd^{III} ion bound by a DOTA based complex to cause the initial paramagnetic relaxation effect of ^{19}F within the agent. The Dotarem **2** like chelator is then bound to the second unit, an amino acid sequence which is a substrate to specific individual MMPs. The third and final part of the agent is a fluorinated compound which generates the ^{19}F MRI signal. The general intended structure of the MMP ^{19}F MRI CA is shown in Figure 17.

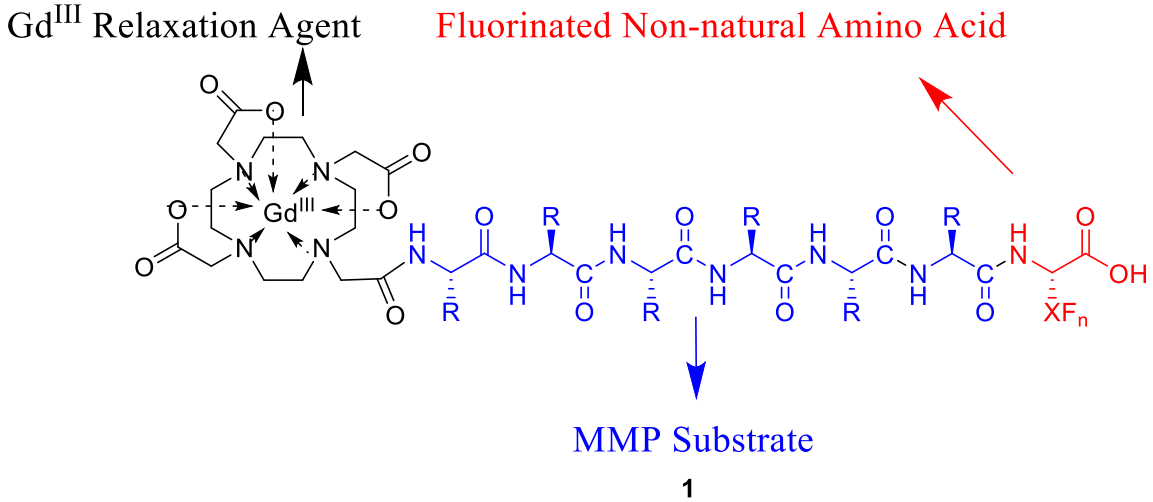

Figure 17: Generic structure of a MMP activated contrast agent

The probe takes advantage of the fact that ^{19}F is NMR active and of the strong paramagnetic nature of Gd^{III}. Initially the Gd^{III} relaxes the fluorine resulting in no ^{19}F

MRI signal, once the probe is introduced into an MMP containing environment, the targeted MMP(s) are intended to cleave the peptide region of the agent, thereby removing the PRE of the Gd^{III} on the fluorine giving rise to the ^{19}F NMR/MRI signal.

Initially the focus was towards using a peptide sequence with a broad-range of activity to measure overall MMP activity; once this was achieved other challenges could then be tackled, such as selectively targeting individual classes of MMP. As MMPs are involved in many disease processes, the ability to study the *in vivo* activity of these enzymes is paramount in order to gain further insight into how these modifications are achieved, as well as when they occur. Therefore a small library of probes was synthesised based upon literature precedent of sequences known to be cleaved selectively by individual types of MMP.

Chapter 3 - Results and discussion

3.1 Target MRI compound

The target agent was down into three different sections:

1. Fluorinated unnatural amino acid (FAA)
2. MMP peptide substrate
3. Gd^{III} containing relaxation agent

Peptides are frequently synthesised using SPPS, therefore it is logical to implement this technique into the synthesis of the entire agent. Once the Fmoc-FAA was synthesised it was then attached to a solid phase resin and using Fmoc chemistry, the MMP substrate was synthesised. Once the substrate synthesis was completed, the terminal amine of the resin-bound peptide could be deprotected and coupled to the DO3A-based complex as detailed in proceeding sections.

3.2 Fluorinated compounds

Kikuchi and co-workers[35] in 2008 were the first to publish the design of a ^{19}F MRI probe **12** capable of being used as an "OFF/ON" type of agent, indicating proteolytic activity.[35] This enzymatically activated agent was used to monitor caspase-3 activity utilizing the PRE. In Kikuchi's agent **12** (see Figure 7, page 23) there are three magnetically equivalent fluorines which give the resultant signal once the peptide is cleaved. Expanding from this, one aim for this set of fluorinated compounds was two-fold, firstly to develop an agent with more than three equivalent fluorines, and

secondly to develop a compound easily incorporated into standard Fmoc solid phase peptide synthesis. The final agent must contain equivalent fluorines for the imaging process; with more equivalent fluorines producing a greater single signal to noise ratio just as with NMR, making the 3D images easier to resolve. Multiple ^{19}F environments cause difficulty with regards to resolving the images, as the ^{19}F are imaged separately and then not spatially resolved correctly with regards to each other.

3.2.1 Synthesis of trifluorinated Fmoc-FAA synthesis

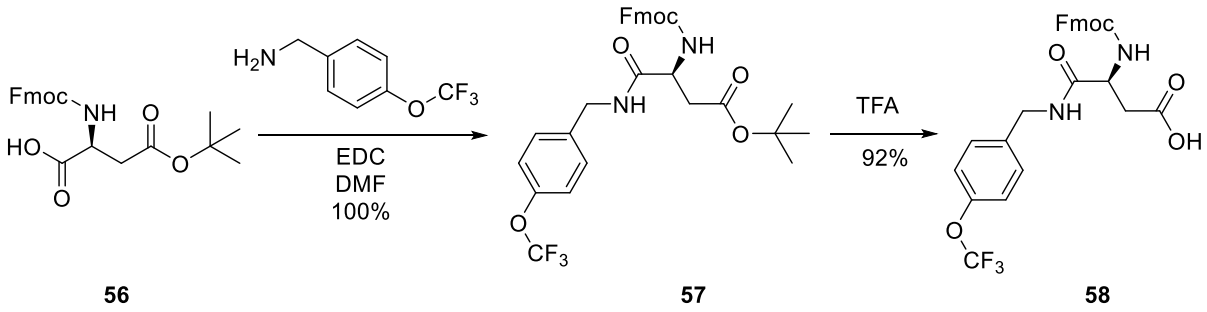

56 **57** **58**

Scheme 10: Kikuchi et al. trifluorinated amino acid synthesis

Initially the fluorinated acid **58** reported by Kikuchi *et al.* was synthesised which utilised the above synthesis.[35] Therefore, based on this literature precedent, the FAA **58** was synthesised using EDC **35** with Fmoc-Asp-^{t}Bu **56** under argon. An argon atmosphere was observed to give the best yield for this reaction; argon is heavier than nitrogen and is better for maintaining an anhydrous environment. The reaction was performed at 0 ˚C due to the temperature sensitive nature of EDC **35**.

In ethyl acetate, an aqueous basic wash removes unreacted amino acid (AA) **56**, followed by an aqueous acid wash to remove unreacted benzylamine. Finally brine was used to wash any EDC **35** remaining as well as to dry the ethyl acetate, furnishing the protected FAA **57** in excellent yield.

The hydrolytic deprotection of the *tert*-butyl ester **57** was performed using TFA. The reaction slowly changed from a colourless to a bright yellow colour; concentration of the mixture removed the TFA and *tert*-butyl alcohol by-product. This was then purified *via* recrystallisation from ethyl acetate and *n*-hexane yielding **58**.

3.2.2 Retrosynthetic analysis of Fmoc-serine nonafluoroether

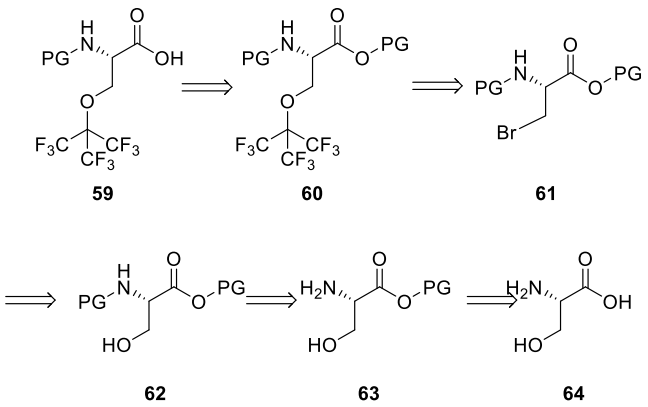

Scheme 11: Retrosynthesis of F_9-Serine *tert*-butyl ether

A screening of the commercially available fluorinated compounds was performed. At the time of the search, the compound with the most magnetically equivalent fluorines was a perfluorinated *tert*-butanol **65**, bearing nine fluorines, see Scheme 11. As shown previously Kikuchi's method[35] utilised an aspartic acid to incorporate three fluorines into the MRI agent *via* an amide bond, which would not be suitable

for an alcohol, as the resultant ester may be labile to biologically endogenous esterases. As such, a modification for the amino acid serine was planned. The nonafluoro-serine analogue **59** containing a perfluorinated tertbutanol was predicted to have low water solubility, a soluble linker could have been included at the acid terminus to address this. The retrosynthesis for this modification of the amino acid L-serine is shown in Scheme 11. It was envisaged that an *N*-protected serine nonafluoroether **59** could be synthesised from the acid protected derivative **60**. Acid protection would be needed to avoid competing reactions during the Williamson ether synthesis of **60**, where a halide is required to form the ether linkage from the bromide **61** with nonafluoro-*tert*-butanol (NFTB) **65** or sodium nonafluoro-*tert*-butoxide (NaNFTB) **66**. To generate a suitable leaving group, Appel bromination was suggested to brominate the hydroxyl moiety of appropriately protected serine **59**. The protection groups on the serine need to be orthogonal to each other, so as not to be globally deprotected in one step. In order to incorporate the final product **59** into solid phase synthesis, the amine protection group would ideally need to be Fmoc, although this could be altered depending on the resin used.

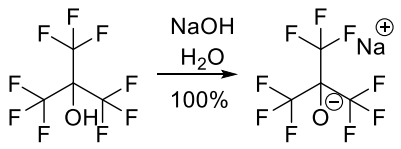

65 **66**

Scheme 12: Sodium salt of nonafluorotertbutanol

The NFTB **65** provided nine equivalent fluorines and therefore offered an excellent starting material for the fluorination of serine.

3.2.3 Sttempted synthesis of L-serine fluorinated ether analogue

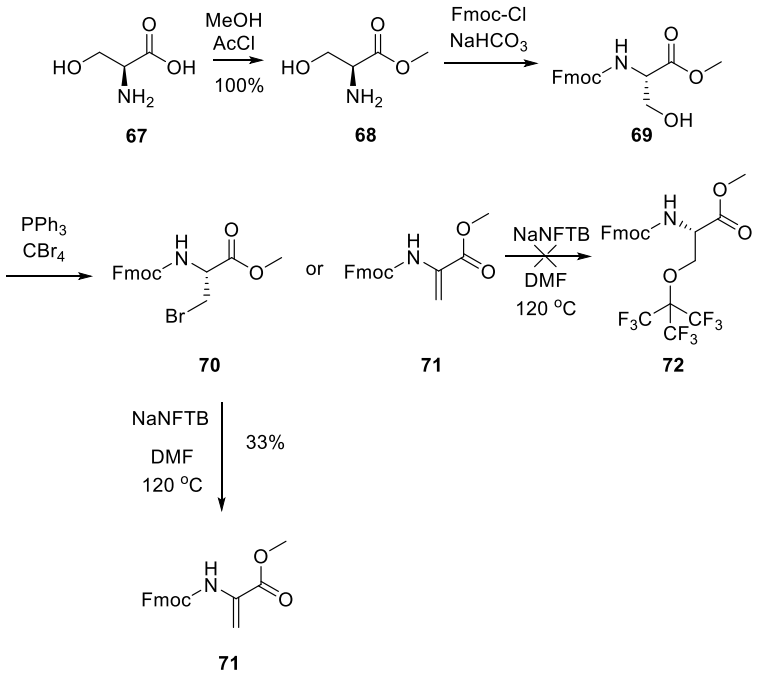

Scheme 13: Planned synthesis of L-serine fluorinated analogue

Originally the acid group was to be benzyl-protected, however, due to very low yields (≤ 5%) methyl protection was preferred. Benzyl protection was attempted using benzyl bromide and lithium bromide as reported by Hughes,[108] and also using an acid catalysed method with *para*-toluene sulfonic acid (PTSA) and benzyl alcohol, both under normal and Dean-Stark conditions, but both methods failed.

Methyl ester protected serine **68** was synthesised quantitatively the acetyl chloride forms an acid anhydride with the L-serine **67**, which is then rapidly attacked by the MeOH. The reaction was performed at low temperatures to avoid the formation of an *N*-acetyl derivative. The acetyl chloride was also slowly added to avoid instant formation of methyl acetate, which is due to the MeOH being a better nucleophile than the acid moiety of serine.

Fmoc protection of **68** was achieved using Fmoc-Cl and sodium hydrogen carbonate as a base. The fully protected serine is base sensitive, however, as studies have previously shown, it can eliminate water to form the protected dehydroalanine.

The bromination of the protected serine **69** was attempted under standard Appel (bromination) conditions, yielding the desired product **70** and the dehydroalanine **71**. Unfortunately, a clean sample was not isolated, even after column chromatography, due to contamination of triphenyl phosphine and triphenyl phosphine oxide. Nonetheless the mixture of products of **70** and **71** were used in the next step.

NaNFTB **66** at 120 ˚C in DMF has previously been shown to be an efficient method for the formation of the desired ether from an alkyl halide, however, in the case of the brominated substrate **70** the high temperature leads to an elimination reaction forming protected dehydroalanine **71**, as shown in Scheme 13. The potential mechanism for this is shown in Scheme 14; the proton alpha to the ester is acidic, once deprotonated, the enolate produced can then reform to the ester eliminating the bromine, or in the case of serine the hydroxyl *via* an E1cB reaction.

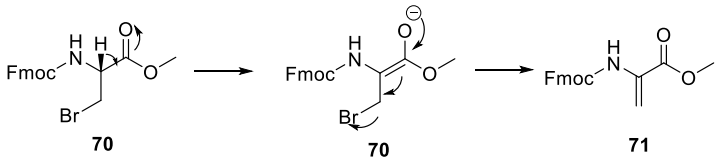

Scheme 14: Possible mechanism for dehydroalanine formation

3.2.4 Sodium nonafluoro-*tert*-butoxide (NaNFTB) (66)

NaNFTB **66** was easily synthesised from NFTB **65** using NaOH. The fluorinated alcohol has a lower pKa (9.2) than non-fluorinated alcohols (e.g. vs. ^{t}BuOH which has a pKa of 16.5), the lower pK_a and lower nucleophilicity are due to the withdrawing effect of the nine fluorines making deprotonation facile, and formation of the sodium oxide salt **66** rapid. Formation of the salt **66** was confirmed by IR spectroscopy, with the absence of the O-H peak. NaNFTB **66** was synthesised due to the volatility of the parent alcohol **65**, thereby making it easier to handle, and potentially a superior nucleophile, due to the formal negative charge.

After the unsuccessful attempts of the Williamson ether synthesis, NaNFTB **66** and NFTB **65** were used in an attempted nucleophilic on methyl 2-bromoacetate. If successful, after a deprotection this would give the free acid, which could be used for coupling. However, all attempts yielded less than 7% product which could not be cleanly isolated, suggesting that both NaNFTB **66** and NFTB **65** are not suitable for such chemistries.

3.2.5 Dehydroalanine formation

A multitude of conditions and protecting agents were trialled in order to protect L-serine. Serine has been shown by Ferreira *et al.*[109] to degrade to the dehydroalanine **71** product when exposed to bases such as DMAP and triethylamine, a few examples of these eliminations are shown below in Scheme 15 and Table 2.

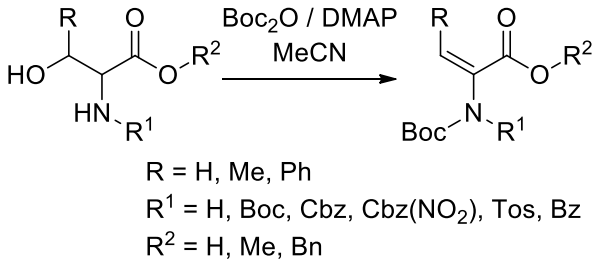

Scheme 15: Ferreira conditions of dehydroalanine formation (Where Cbz(NO_2) is *p*-nitrobenzyloxycarbonyl, and Tos is tosyl, Bz is benzoyl and Bn is benzyl)

Table 2: Dehydroalanine analogue formation[109]

Reagent	Product	Yield (%)
Boc-Ser-OMe	Boc-ΔAla(*N*-Boc)-OMe,	92
Tos-Ser-OMe	Tos-ΔAla(*N*-Boc)-OMe	99
H-Ser-OMe	Boc-ΔAla(*N*-Boc)-OMe,	82
Boc-Thr-OH	Boc-ΔAbu(*N*-Boc)-O^{t}Bu,	73

In the presence of mild bases the elimination is possible; with stronger bases such as LiOH/NaOH, which are required for methyl ester deprotection, elimination of the oxide of NFTB would be facile. Due to these ease by which hydroxide, a poor leaving group, is eliminated, ether **59** which would have a superior leaving group, making an E1cB more likely, less stable hence this synthesis was abandoned.

3.2.6 Synthesis of glycine trifluoroacetamide

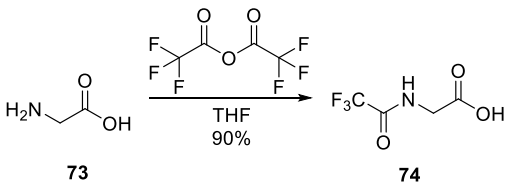

73 74

Scheme 16: Trifluoroacetamide of glycine

Acid anhydrides are very reactive compounds often formed *in situ* when used on industrial scale with the appropriate acid and acid chloride. Trifluoroacetic anhydride's (TFAA) reactivity is increased by the presence of the fluorines, which causes an increase in electron withdrawal generating a more electrophilic centre at the anhydride's carbonyls; because of this, the amine of glycine **73** attacks to form acetamide **74** and TFA, without requiring base in a yield of 90%. This fluorination method previously reported by *Peng et al.,*[110] could potentially be used on other materials to achieve high numbers of equivalent fluorine.

TFAA could also potentially be used to react with the terminal amine of a peptide on a solid support to introduce a fluorinated substituent, and under basic conditions, to avoid hydrolysis from the solid support caused by the TFA by-product.

3.2.7 Synthesis of hexafluorinated Fmoc-FAA

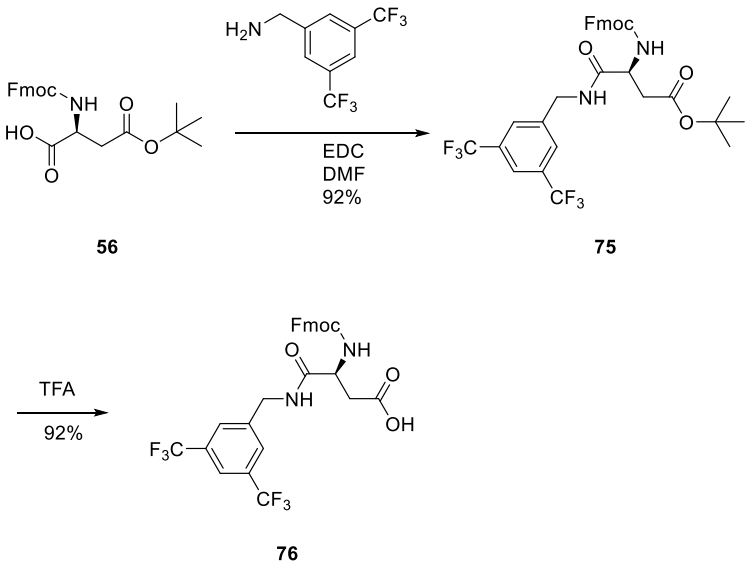

Scheme 17: Hexafluorinated amino acid

Owing to the difficulties encountered in the previous sections, an alternative amine was sought. Based on the previous synthesis of a fluorinated protected aspartic acid, it is possible to increase the number of equivalent fluorines by using perfluoromethyls, *meta* to each other on a benzylamine ring. This FAA **76** was synthesised using the same conditions as for FAA **58**. Once synthesised, SPPS could be undertaken using the FAA **76**.

The *meta*-substituted benzylamine provided three extra equivalent fluorines in comparison to the previously synthesised FAA **58**, resulting in six equivalent fluorines. Whilst not as highly fluorinated as the original FAA target **59**, six equivalent fluorines was still an improvement on those described in the literature at the time. This FAA **76** was then used for all of the ^{19}F NMR MMP probes within this thesis.

3.2.8 Retrosynthetic analysis of an amino acid bearing 27 equivalent fluorines

In order to maximise the ^{19}F NMR signal another FAA **77** was designed; this target contains 27 equivalent fluorines dramatically increasing the achievable signal, subject to its aqueous solubility.

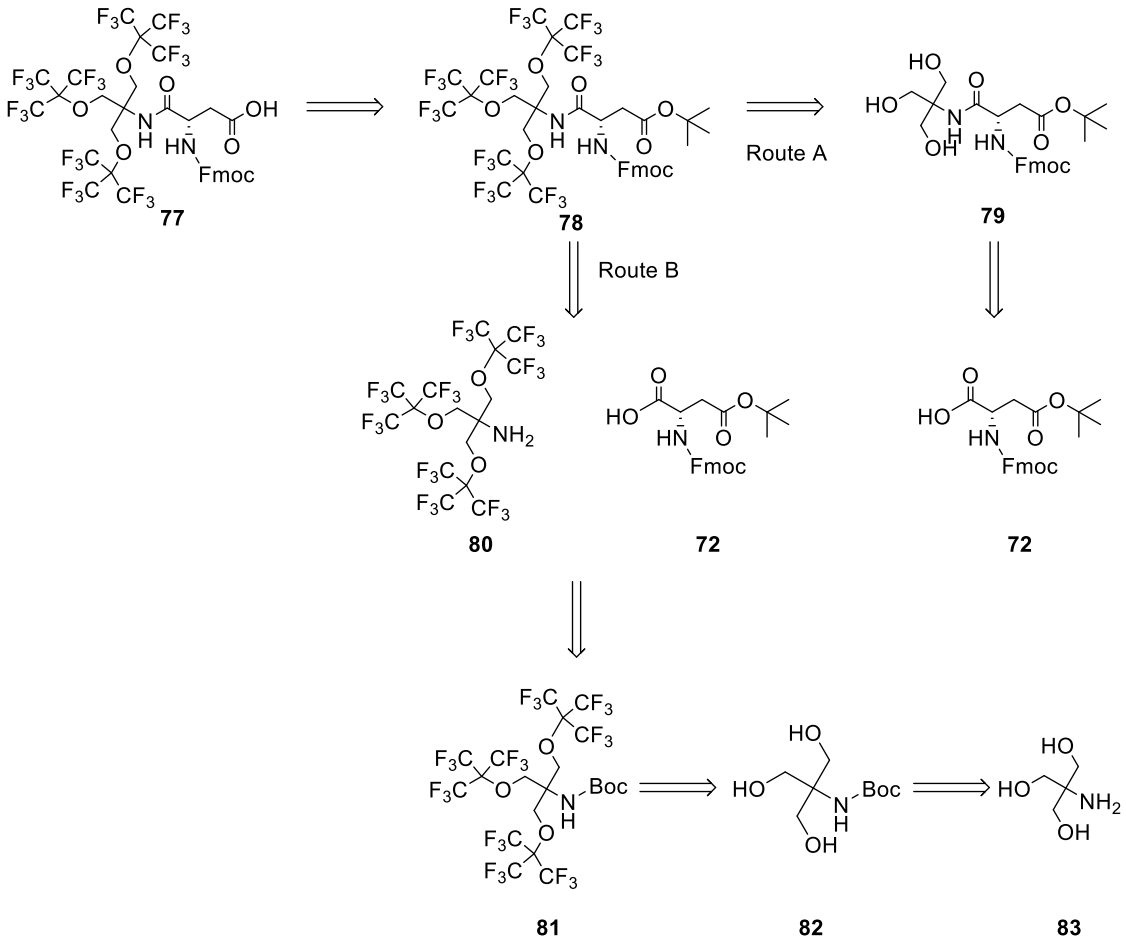

Scheme 18: Retrosynthetic analysis of 27-FAA

Deprotection of ester **78** would result in acid **78.** It was postulated that ester **78** could be made from two separate routes, see Scheme 18. Route A involves a Mitsunobu etherification to form the tri-ether **78** from tri-ol **77**. The amide of **79** being prepared from a direct coupling of Trizma® **83** with Fmoc-Asp(O^{t}Bu)-OH **72**.

Alternatively in route B, **78** could be prepared from the amidation of **80** and **72.** The amine **80** being deprotected, with protection required for a successful tri-etherifaction of tri-ol **82**. **82** would be prepared by protecting Trizma® **82**. Exposing Trizma® **82** to the etherification conditions is unlikely to produce the desired ether, it would most likely form the aziridine, and as such, this was not attempted, shown in Scheme 19.

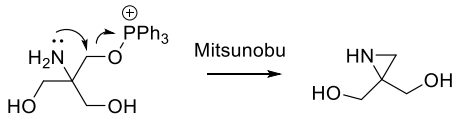

84 **85**

3.2.9 Attempted synthesis of the 27-fluorinated amino acid via direct coupling

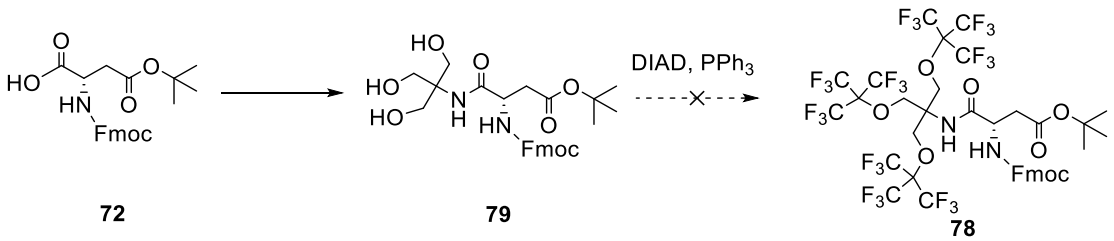

72 **79** **78**

Scheme 20: Route A

The synthesis began with the coupling between Trizma® **83** and Fmoc-Asp(O^{t}Bu)-OH **72**, which was achieved using EDC **34**, and an aqueous organic work up to purify. The following step was a Mitsunobu etherification, which could not be achieved regardless of the conditions, or order of addition. The Mitsunobu reaction was not successful; it was trialled at ambient temperature, 0 ˚C, and -78 ˚C. Pre-activation of the triol **79** was attempted with DIAD and triphenyl phosphine before addition of the

fluoric alcohol, as well as conducting the reaction with all reagents added at the start, prior to the solvent, all of which were unsuccessful.

3.2.10 Attempted synthesis of the 27-fluorinated amino acid via protection

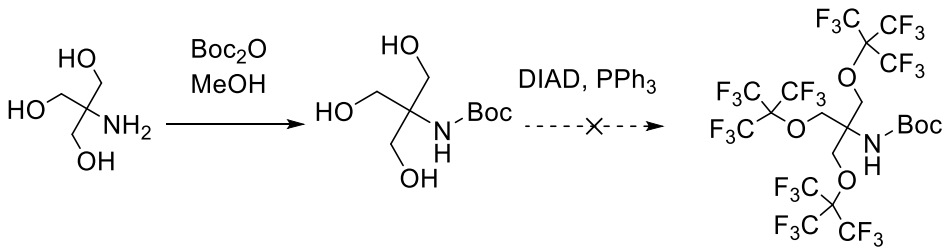

83 **82** **81**

Scheme 21: Route B

The alternative approach initially involved the Boc protection of Trizma® **83**, which was best achieved with Trizma® **83** and Boc anhydride in methanol. A similar approach to the Mitsunobu etherification in the previous section was attempted, however as previously described, it was unsuccessful.

3.3 Solid phase peptide synthesis

3.3.1 Resin loading

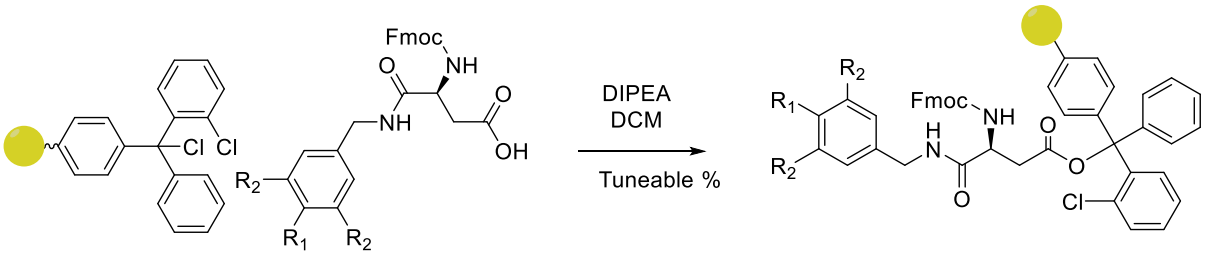

26

$R_1 = OCF_3$, $R_2 = H$, **74**
$R_1 = H$, $R_2 = CF_3$, **76**

$R_1 = OCF_3$, $R_2 = H$, **86**
$R_1 = H$, $R_2 = CF_3$, **87**

Scheme 22: Loading of a 2-chlorotrityl chloride resin

The first step in the Fmoc SPPS approach is the loading of the resin, as shown in Scheme 22. For the synthesis of the probes 2-chlorotritylchloride resin **26** was used. The resin was suspended in DCM, which allows the resin to swell this is crucial; as the polystyrene swells, it exposes all of the surface trityl groups to the DCM. The desired FAAs were then added in DCM, with DIPEA. The basic conditions caused the formation of the cation, which can be seen as the by-product, and HCl, which is given off as a gas. Adding the DIPEA until no more gas evolved, gave a reasonable indication that all the trityl groups had formed the cation, and all the AA present had been deprotonated. The reaction was stirred very slowly so as not to damage or grind the resin. Once complete, the suspension was diluted with MeOH, which caps any unreacted resin. This methyl ether then prevents any loading of the subsequent AA in the sequence, which would result in an AA deletion. The resin was then washed with DMF, DCM and hexane; these washes swell and force the resin to

shrink. This method of expansion and reduction forced any unreacted material off the resin, which left only the desired resin bound AA trityl ester.

3.3.2 Calculating the potential loading and actual loading of the resin

Once the loading procedure was complete, the next step was to prove how much AA has actually been bound to the resin. Firstly the theoretical molar loading was calculated using Equation 7.

$$Max\ loading\ = \frac{1.22 \text{ x } 1000}{1000 + 1.22\ (\mathrm{MW}_{AA} - \mathrm{MW}_{HCl})}$$

Equation 7: Theoretical maximum resin loading

Where 1.22 is the maximum loading for the resin used in the NRT group (Sigma Aldrich) in mmol / gram of resin (this value varies depending on the resin), MW_{AA} is the molecular weight of the AA and MW_{HCl} is the molecular weight of HCl. Even though the resin manufacturers will indicate an estimated maximum loading.

Once calculated, the next step was to determine the actual resin loading. In order to do this a small sample of the loaded resin was taken and then gently stirred in a 20% piperidine/DMF mixture. The piperidine removed the Fmoc group, forming the fluorenyl methylene and the alkylated piperidine adduct. Once completed a small amount of the solution from the cleavage was removed and placed into a UV spectrometer, recording the absorbance at 290 nm against a blank piperidine / DMF vial. The loading was then calculated using the Beer-Lambert equation, Equation 8.

$$A = \varepsilon\, c\, l$$

Equation 8: Beer-Lambert Law

Where A is the absorbance, ε the molar extinction coefficient constant for the considered species (1.75 for Fmoc), c is the concentration, finally l is the path length (cm). The value for c is then placed into Equation 9.

$$Calculated\ loading = \frac{\mathrm{c\ df}}{\mathrm{r}}$$

Equation 9

Where df is the dilution factor (of the sample compared to the neat deprotection mixture), and r is the amount of resin that was used in the cleavage. The calculated loading gave the amount of AA loaded. In order to then determine a yield for the process, Equation 10 was used.

$$Loading\ (\%) = \frac{Calculated\ loading}{\mathrm{Theoretical\ loading}} * 100$$

Equation 10

More details on loading calculations and general SPPS can be found in Fmoc Solid Phase Peptide Synthesis: A Practical Approach by Chan and White.[111]

3.3.3 Amino acid sequences of MMP substrates

Amino acid sequence	Substrate for MMP
Pro-Leu-Gly-Leu-Trp-Ala-Arg[112]	Broad-range
Pro-Leu-Ala-Leu-Trp-Ala-Arg[113]	MMP-1
Pro-Leu-Gly-Met-Trp-Ser-Arg[114]	MMP-2/-9
Pro-Tyr-Ala-Tyr-Trp-Met-Arg	MMP-3
Arg-Pro-Leu-Ala-Leu-Trp-Arg-Ser[115]	MMP-7
Pro-Leu-Ala-Tyr-Trp-Ala-Arg	MMP-8

Table 3: MMP substrate peptide sequence

The proposed model for a protease probe can be broken down into three sections, two of which do not vary from probe to probe, namely the paramagnetic and signal inducing units; the final unit will vary depending on the protease to be studied. Originally four different sequences of interest were identified for synthesis. A broad-range probe was targeted to allow for work with any human MMP, an MMP-1 sequence, which was the first MMP to be identified and purified. An MMP-2/-9 sequence was identified due to roles in connective tissue diseases (both MMP-2 and MMP-9), as well as cancer and cardiovascular disease (MMP-9). An MMP-7 sequence was decided upon due to its various roles in cancer. An additional two sequences were decided upon later in the project. All of these sequences were identified from a literature based search; the sequences were selected to be as short as possible to avoid complications during synthesis. The sequences for the selected MMPs can be found in Table 3.

3.3.4 Synthesis of the peptides

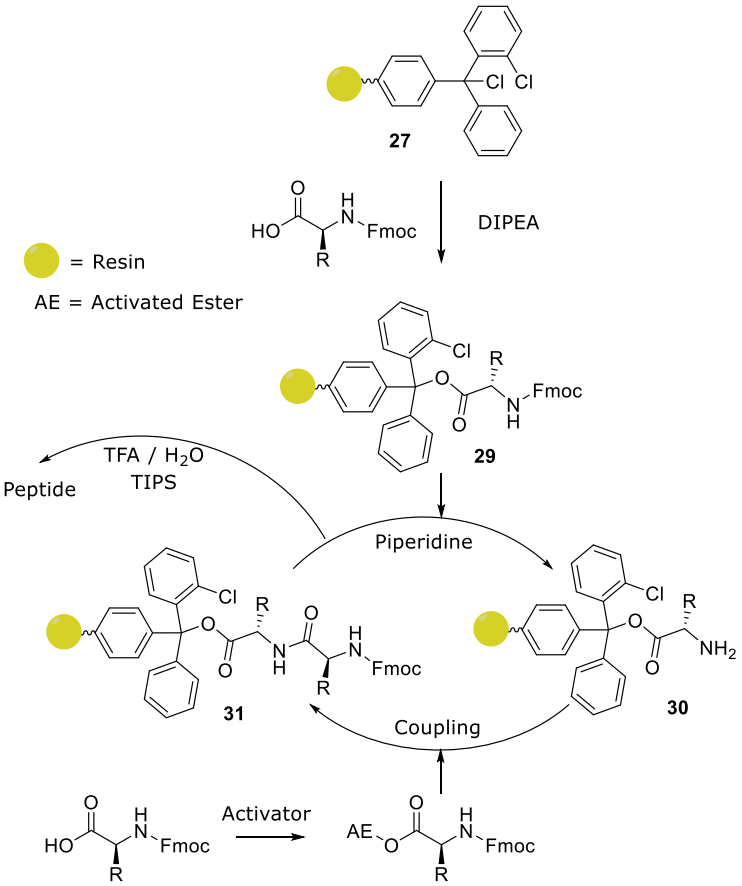

All peptides for ^{19}F NMR were synthesised using the same procedure. Following the loading of the first AA, Fmoc deprotection was achieved using a steady flow of 20% piperidine in DMF (by volume). The continuous flow prevents a build-up of the deprotected Fmoc group, which then prevents side reactions with the peptide, such as terminal amine alkylation. During the synthesis, due to the labile nature of Fmoc, the resin bound peptide was stored overnight with the Fmoc removed, preventing possible Fmoc based side reactions.

The 2-chlorotrityl chloride resin approach to SPPS incorporates a trityl ester as the linking group, which is extremely labile under acidic conditions rapidly hydrolysing to form terminal carboxyl acid. Protection of certain side chains is necessary to avoid undesirable side reactions. Arg, Ser and Trp all require protection using acid labile protecting groups, see Table 4.

Amino acid	Protecting group	Structure
Arginine	Pbf (2,2,5,7,8-Pentamethyl-chroman-6-sulphonyl)	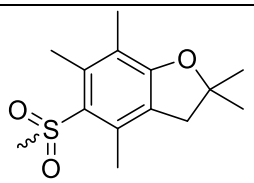
Serine	*tert*-Butyl	
Tryptophan	Boc	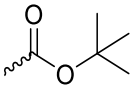

Table 4: Amino acid protecting groups

Using these protecting strategies the peptides in Table 5 were synthesised. An investigation into a variety of methods to attempt to attach a paramagnetic compound began. The syntheses of these paramagnetic chelator compounds are detailed in the following sections.

Sequence	Substrate for MMP
Arg-Ser-Trp-Met-Gly-Leu-Pro-FAA(**74**)	None
Pro-Leu-Gly-Leu-Trp-Ala-Arg^{112}-FAA(**74**)	Broad-range
Pro-Leu-Gly-Leu-Trp-Ala-Arg-FAA(**76**)	Broad-range
Pro-Leu-Ala-Leu-Trp-Ala-Arg^{113}-FAA(**74**)	MMP-1
Pro-Leu-Ala-Leu-Trp-Ala-Arg-FAA(**76**)	MMP-1
Pro-Leu-Gly-Met-Trp-Ser-Arg^{114}-FAA(**74**)	MMP-2/-9
β-Ala-Pro-Leu-Gly-Met-Trp-Ser-Arg-FAA(**74**)	MMP-2/-9
Pro-Leu-Gly-Met-Trp-Ser-Arg-FAA(**76**)	MMP-2/-9
Pro-Tyr-Ala-Tyr-Trp-Met-Arg-FAA (**76)**	MMP-3
Arg-Pro-Leu-Ala-Leu-Trp-Arg-Ser^{115}-FAA(**74**)	MMP-7
Arg-Pro-Leu-Ala-Leu-Trp-Arg-Ser-FAA(**76**)	MMP-7
Pro-Leu-Ala-Tyr-Trp-Ala-Arg-FAA(**76**)	MMP-8

Table 5: Synthesised peptide sequences for ^{19}F NMR

3.4 Design and synthesis of the paramagnetic moiety of the probe

The final unit of the ^{19}F MMP probe consists of the signal modulating paramagnetic moiety. The paramagnetic unit needs to contain a paramagnetic element/ion. During this course of work two potential paramagnetic modalities were studied: Gd^{III} and stabilised free radicals. As mentioned previously, when the Gd^{III} ion is utilised within a compound for biological applications it must be encased within a suitably thermodynamically and kinetically stable chelator.

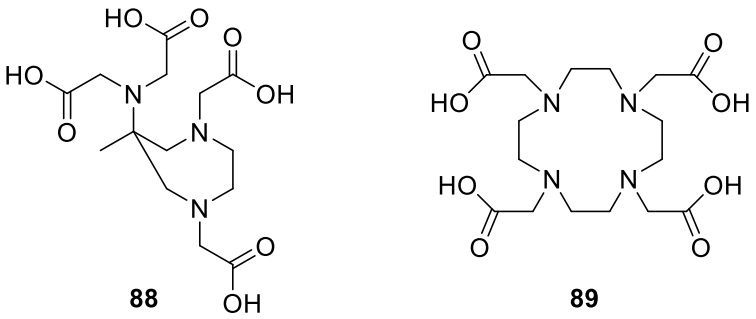

Figure 18: The Gd^{III} chelators AAZTA and DOTA

Gd^{III} contains the most unpaired electrons possible on a single element, with a $^8S_{7/2}$ ground state and a long electron-spin relaxation time similar to the frequency of protons and fluorine therefore making it the ideal paramagnetic ion. Due to the reduced number of synthetic steps by which a stabilised free radical can theoretically be attached to a peptide, as well as synthetic challenges discussed in following sections, stabilised free radicals were explored. A multidimensional approach then began with work on stabilised free radicals (TEMPO **90** and PROXYL **92** based) as well as two classes of Gd^{III} chelators, AAZTA **88** and DOTA **89**.

3.5 Stabilised free radicals

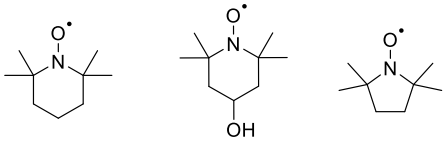

Figure 19: Stabilised free radicals

Stabilised radicals offer a relatively long-lived, single electron paramagnetic source. Stabilised free radicals such as TEMPO **90** and PROXYL **92** (see Figure 19) and their analogues are readily available and have been used to probe enzymatic activity previously.[116] It is important to note that stabilised free radicals are nontoxic; TEMPO and TEMPOL **91** have been shown to protect against alopecia.[117, 118] TEMPOL **91** was in phase I clinical trials in cancer patients undergoing whole brain radiotherapy.[119]

3.5.1 Attaching the free radicals

Two methods for the attachment of the radicals were identified: using an acid moiety with coupling agents, or using an α-halocarbonyl, both directly binding to the terminal amine of the desired peptide substrate. As such, two stabilised free radicals were purchased, 3-carboxy-PROXYL and 4-amino-TEMPO **93**.

3.5.2 Couplings with 3-carboxy-PROXYL

3-Carboxy-PROXYL was coupled to the broad-range peptide sequence and the MMP-2/-9 peptide sequence, with PyOxim **52** as an activator. Unfortunately the cleavage process from the SPPS resin involves TFA, which resulted in the reduction of the nitroxy radical to the hydroxylamine for both peptides. Hydroxylamines can be oxidised back to the nitroxide using sensitizers such as Cu^{II} salts. However, re-activations of radicals are reported to be inefficient reactions.

3.5.3 Synthesis and substitutions with free radical containing compounds

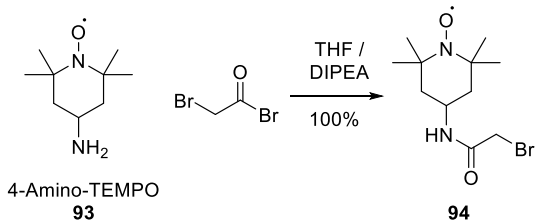

Scheme 24: Acetylation of amino-TEMPO

Based on the previous literature precedent establish by Knipp *et al.*, who used an α -

iodoamide of PROXYL to introduce a stabilised free radical as a probe *via* reaction with a thiol, a modified method was devised to alkylate an amine instead of forming a thio-ether.[116]

In order to produce the radical labelled alkylator, 4-amino-TEMPO **93** was acylated using bromo-acetlybromide. THF was used as solvent to avoid any solvent-based reaction with the radical, and DIPEA was used so the base could be removed *in vacuo*. This yielded a salmon orange radical, and this radical was used as produced when attempting to couple to the peptide to avoid deactivation. The reaction was monitored by ESI-MS until all the starting material had been consumed. The reaction was performed protected from light and under argon to avoid deactivation from oxygen radicals.

Following this, attempts were then made to substitute on to the terminal amine of three resin free peptides. Labelling was attempted with β-Ala-Pro-Leu-Gly-Met-Trp-Ser-Arg-FAA(**12**), β-Ala-Pro-Leu-Gly-Leu-Trp-Ala-Arg-FAA(**15**) and Pro-Leu-Gly-Leu-Trp-Ala-Arg-FAA(**15**), however in all three cases the desired products were not formed.

A TEMPO functionalise with an alkyne amenable to the "Click" reaction was also synthesised but upon labelling of the peptide the radical was deactivated in the same manner as the PROXYL radicals.

Following these unsuccessful labelling experiments, efforts towards using Gd^{III}

chelators became the focus of this work.

3.6 AAZTA analogues

AAZTA **88**, shown below in Figure 20, was first synthesised in 2004 by Aime *et al.*; AAZTA **88** is an septa-dentate chelator designed for Gd^{III} chelation.[120]

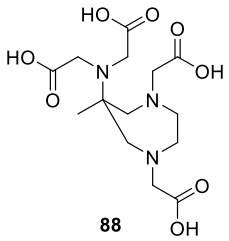

88

In comparison to other chelators such as DOTA **89**, the major benefit is that by functionalising the methyl group, the pocket where the metal ion would be bound is unaffected.[121] Additionally modification at the methyl substituent angles the chelator away from the peptide, thereby reducing peptide-chelator steric and electronic clashes.

3.6.1 Proposed retrosynthesis of AAZTA-Cl

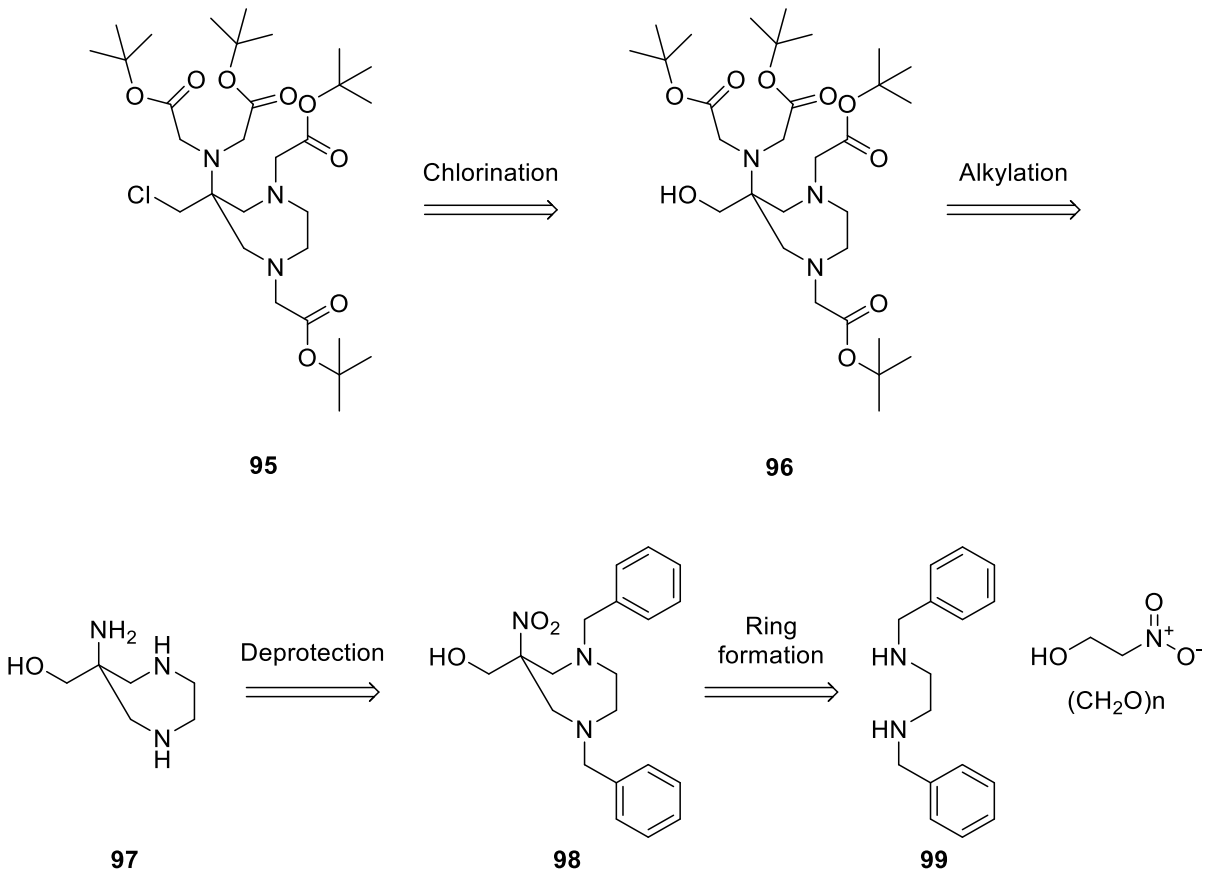

Scheme 25: Retrosynthesis of AAZTA-Cl

The AAZTA-Cl **95** was initially planned as an alternative to DO3A analogues, discussed in the following section, and the synthetic work was performed concurrently. By synthesising an AAZTA-Cl **95**, an electrophilic centre was produced within the compound to allow further functionalization, in this case alkylation. The synthesis of AAZTA-Cl **95** was based on the previously reported synthesis by Tei *et al*.[121]

3.6.2 Synthesis of AAZTA-Cl (51)

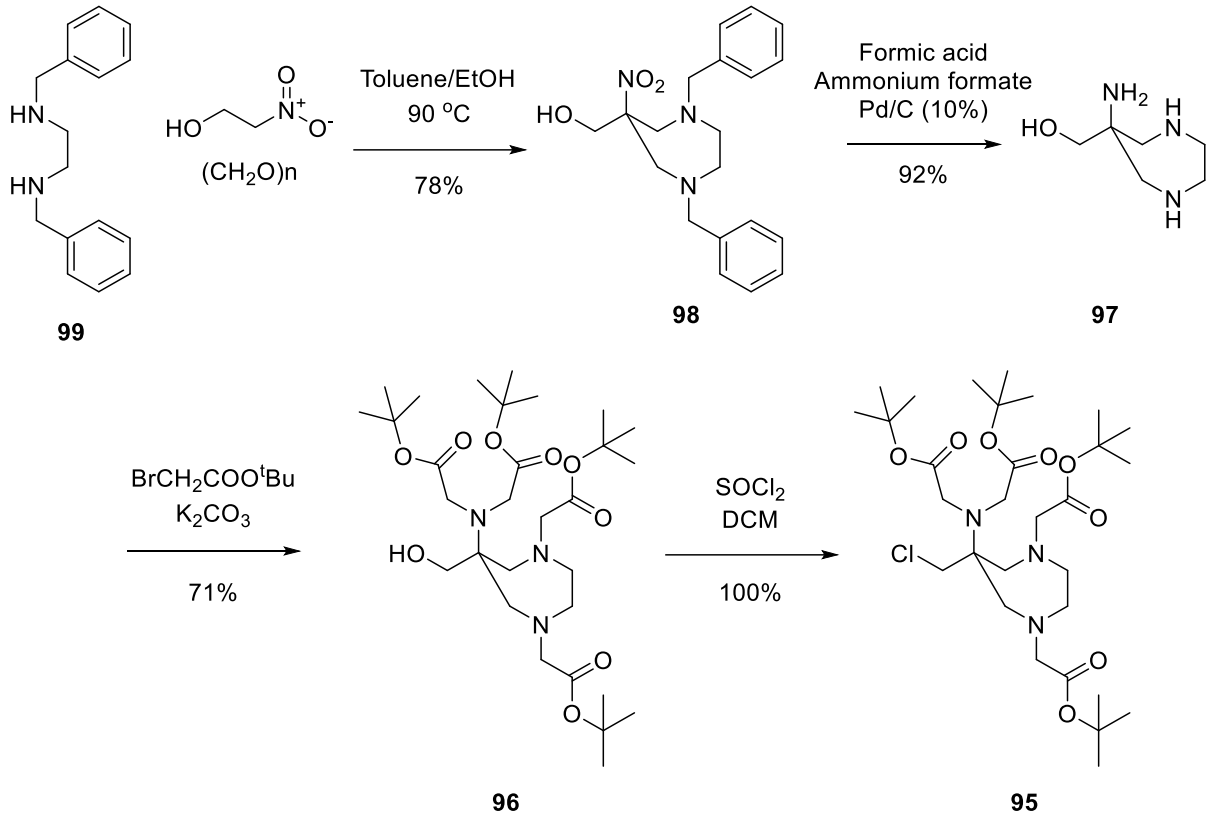

Scheme 26: Synthesis of AAZTA-Cl 95

The nitrodiazepene **98** was formed by a double nitro-Mannich reaction with *N,N'*-dibenzyl ethylenediamine, paraformaldehyde and 2-nitroethanol in high yield, and easily purified using column chromatography. The nitrodiazepene **98** was then reduced and deprotected in one step using Pd/C with formic acid/ ammonium formate as the hydrogen source to give triamine **97**. Triamine **97** was then alkylated forming the protected product **96**. It was observed that triamine **96** was very sensitive under basic conditions, and readily undergoes a cyclisation to form the oxomorpholine **100** with the neighbouring *tert*-butyl protected ester, see Scheme

27. This cyclisation was avoided by reducing the number of equivalents of base used within the reaction (1.2 equivalents of K_2CO_3) as opposed to (seven equivalents) that is reported within the literature.[121]

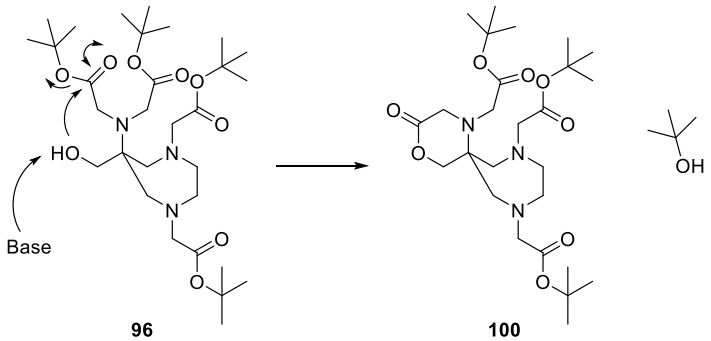

Scheme 27: Intramolecular oxomorpholine formation

Once the protected AAZTA (**96**) was formed, it was chlorinated with thionyl chloride to form the reactive chloro-methylene product (**95**), the formation of this chloro product was only achieved on very small scale (< 10 mg). This chloro-methylene product (**95**) then readily undergoes substitution reactions with nucleophilic amines. This method was not scaled up due to issues synthesising enough of the AAZTA-Cl **95**, the stability of the final compound and scale up issues.

3.6.3 Manipulations of AAZTA

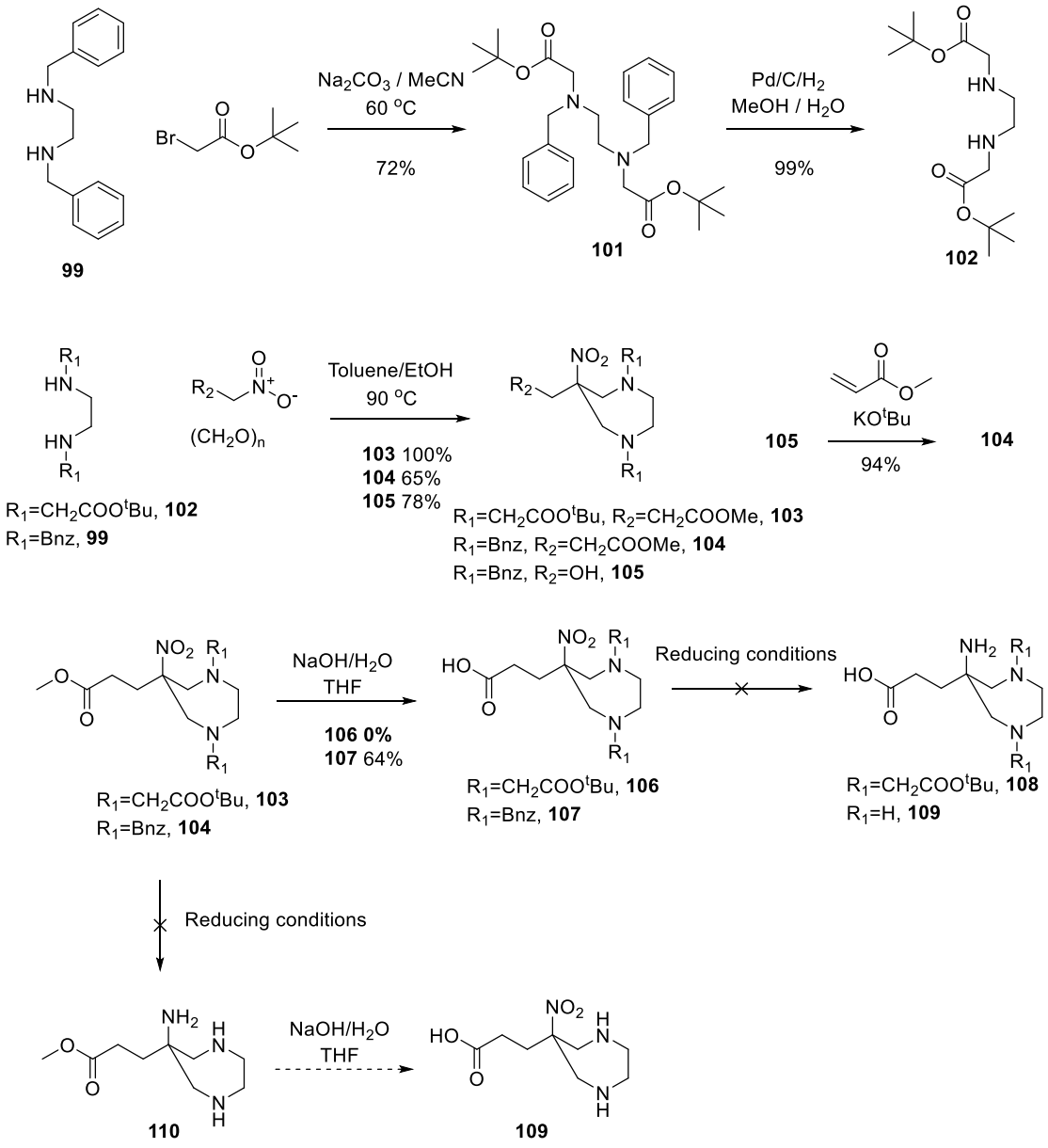

Scheme 28: Attempted AAZTA-acid syntheses

Two alternative syntheses for an AAZTA-acid product were explored; the synthesis was based on the chemistry that had proved successful with regards to AAZTA-Cl **95**, as summarised in Scheme 28.

N,N'-dibenzyl ethylenediamine **99** was alkylated using *tert*-butyl bromoacetate in the presence of sodium carbonate. This was achieved in high yield to give the pure protected diamine **101** (after column chromatography). Following the alkylation, diamine **102** was formed *via* the hydrogenolysis of the benzyl groups using palladium on carbon and purified. This diamino compound **102** or *N,N'*-dibenzyl ethylenediamine **99** was then used in a double nitro-Mannich reaction with paraformaldehyde and either 2-nitroenthanol or methyl 4-nitrobutanoate, to form one of **103**, **104**, **105** in good to excellent yields. Alcohol **105** then underwent a retro-Henry reaction, deprotonated *in situ* with potassium *tert*-butoxide to form the azinate, this was followed by a nitro-Mannich reaction onto the Michael acceptor, methyl acrylate, to form the protected ester **104**, and purified using column chromatography in an excellent yield. This was the original method for the synthesis of **104**, however the shorter method detailed previously was then employed in future work. After the formation of the methyl esters **103** and **104**, two routes were taken, the first involved the cleavage of the esters **103** and **104** to the free carboxylic acids **106** and **107** using aqueous sodium hydroxide in reasonable yields. The following reduction of **106**, and reduction and hydrogenolysis of **107** were unsuccessful. Alternatively the reduction of **103**, and reduction and hydrogenolysis of **104**, were attempted and were also unsuccessful.

3.7 Synthesis of cyclen based complexes

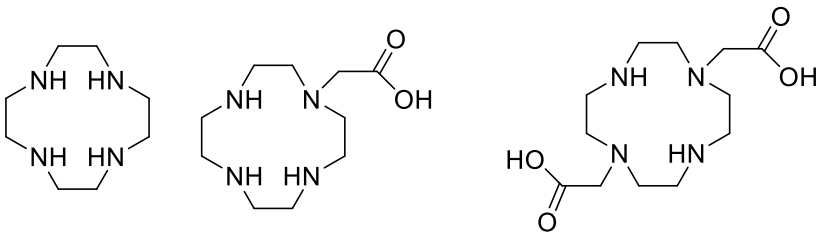

Cyclen **111** DO1A **112** DO2A **113**

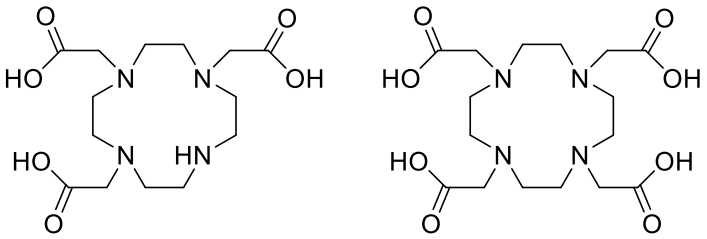

DO3A **114** DOTA **89**

The naming convention for chelators derived from cyclen can be seen in Figure 21.

3.7.1 Synthesis of DOTA-acid (117)

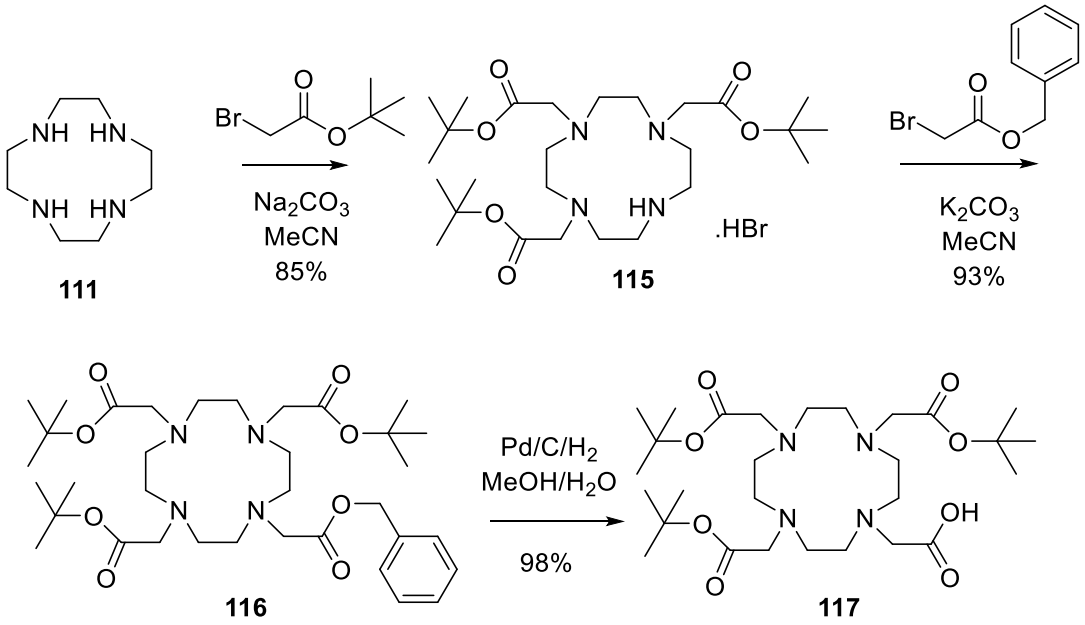

Scheme 29: Synthesis of DOTA-acid 118

Previous literature precedent was followed in the synthesis of the tri-*tert*-butyl-DO3A **115** from cyclen **111**,[122] the reaction was left overnight and stirred at 80 ˚C. The reaction gave high yields in acetonitrile, and the product was best recrystallised from toluene, giving **115** as the HBr salt. Alternatively, flash chromatography could have been used, however, purification by silica lowered the yield substantially, by up to 30%, as the tri-*tert*-butyl-DO3A **115** was unstable on silica, as also shown by Waengler *et al*, an issue which affects all the DOTA based compounds studied here.[123] Altering the number of equivalents of *tert*-butyl bromoacetate gave the corresponding protected DO1A **112**, DO2A **113**, DO3A **114**, or DOTA **89** based protected compounds, depending on the number of equivalents of the alkylating agent additional reaction time was needed, the reaction was most efficient at 80 ˚C. The concentration of this reaction was critical; if the suspension was too concentrated, the four-arm cyclen (protected DOTA) was formed. The ideal

concentration for this reaction was 1 mg/mL of cyclen in acetonitrile. The reaction was monitored by ESI-MS; after one to two hours the one-arm cyclen (DO1A) was produced, after approximately four hours large amounts of the two arm cyclen (DO2A) were observed, and the three arm cyclen (DO3A) was formed after ten hours, whilst total conversion to the product was observed after 16 hours.

Previous literature precedent demonstrated that synthesis of benzyl ester **116** was best performed in acetonitrile to give excellent yields (~98%),[37] but it could also be performed in DMF to give reasonable yields (~65%). The pure compound was obtained by DCM work-up with aqueous washing, methyl ester protection was also performed however the deprotection was far less efficient for the benzyl ester.

The hydrogenolysis of the benzyl ester **116** to the free carboxylic acid **117** was easily achieved under standard Pd-catalysed hydrogenolysis conditions, as shown previously by Kikuchi *et al.*[122] Purification of the target molecule **117** was carried out *via* organic aqueous work up. It is interesting to note that the acid **117** remained insoluble in an aqueous medium even under basic conditions, which was most likely due to the lipophilic nature of the *tert*-butyl protecting groups. An acid wash to attempt to protonate the tertiary amines and to force this compound into the aqueous was also unsuccessful.

A special mention about all of the cyclen-based compounds in this section and the entire report is the unusual NMR. Due to the highly flexible macrocycle, at ambient temperature the methylene units are highly fluxional generating very broad ^{1}H-NMR

signals. Figure 22 shows a zoomed region of ^{1}H NMR of three different DO3A/DOTA based compounds, where A is protected DO3A **115**, and B and C are DOTA based compounds with increasing complexity.

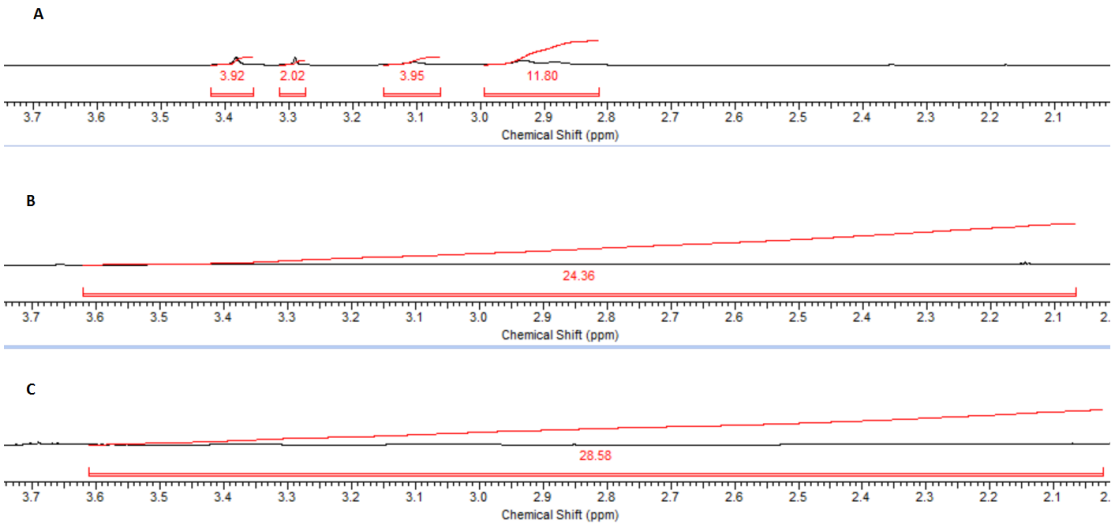

Figure 22: Comparison of different DO3A/DOTA NMR spectra

3.7.2 Direct coupling of tris-DOTA-acid (117) to the peptides

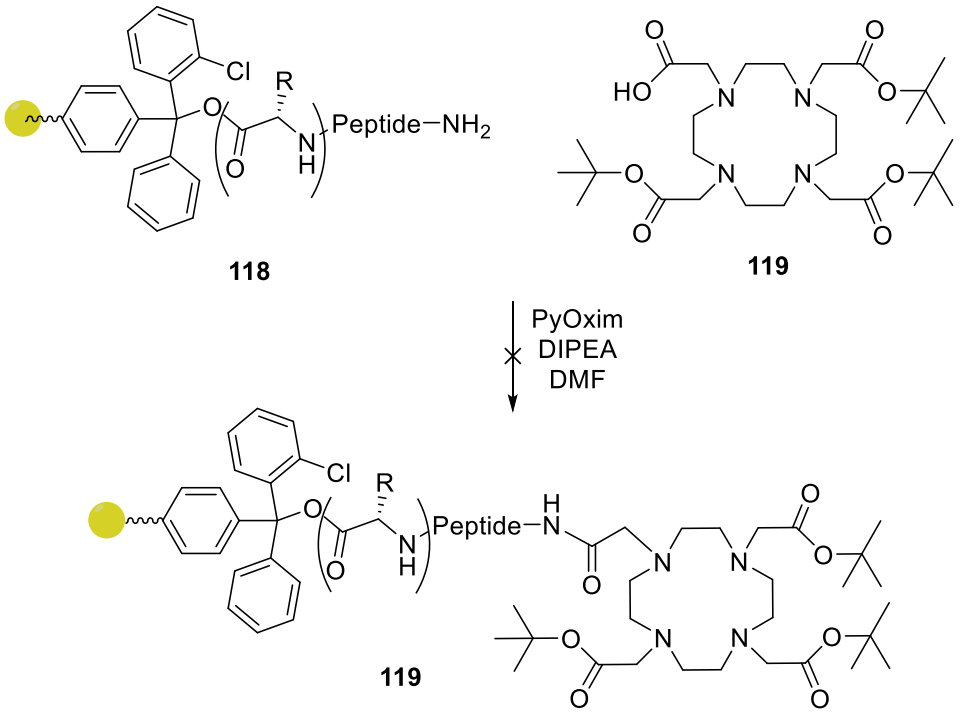

Scheme 30: Direct tris-DOTA-acid to peptide coupling

A direct coupling between DOTA-acid **117** and the amine of a bound peptide was attempted. Couplings were attempted using PyOxim **52**, HATU **53**, HBTU **54**, COMU **55**, TFFH (tetramethylfluoroformamidinium hexafluorophosphate), and DMTMM (4-(4,6-dimethoxy-1,3,5-triazin-2-yl)-4-methylmorpholin-4-ium chloride) (synthesis in appendices) to each of the peptide sequences listed in Table 3, but unfortunately each coupling was unsuccessful and showed no trace of the desired product, only the peptide without the chelator attached. It is believed that all the couplings failed due to the following reasons: firstly, the activated ester of the DOTA-acid **117** is sterically hindered, representing a problem when attempting to couple to a resin-held peptide. The *tert*-butyl groups and cage-like structure of the DOTA-acid **117** make access to the activated ester difficult. Secondly, as the peptide is bound to a resin and not free in solution, the high loading of the resin (usually greater than 85%) will cause aggregation of the peptide strands, mainly in the form of hydrogen bonding. Thirdly, for most of the peptides the terminal amino acid is proline; proline contains a secondary amine within a pyrrolidine ring, which increases the basicity but also reduces the nucleophilicity, due to sterical clashing. The proline also introduces a turn into the peptide, meaning that any coupling on the amine is at an angle with respect to the peptide, so the activated ester must be positioned in between neighbouring peptide strands. To ascertain as to whether resin loading would affect the coupling, the resin loading was adjusted by changing the amount of FAA used in the initial loading onto the resin, but no desired product was observed.

3.7.3 Coupling screen on "model" system

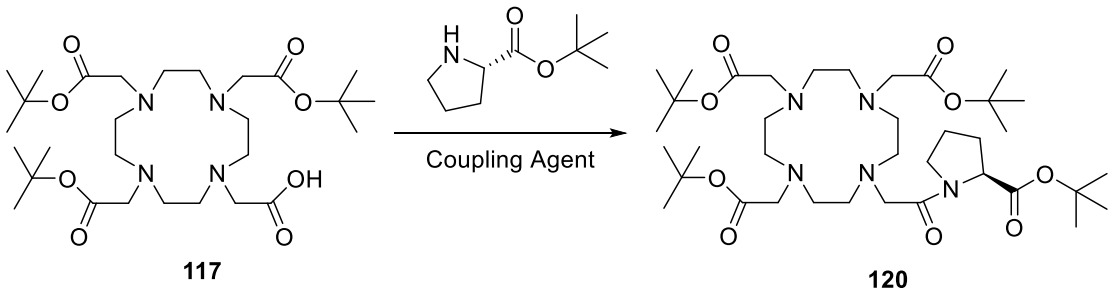

Scheme 31: Coupling screen on "model" system

Before the conjugation method detailed in the previous section was abandoned, a screen of seventeen different coupling agents was applied to a model system. Couplings were trialled between the DOTA-acid **117** and a *tert*-butyl ester protected proline. The couplings were attempted on a small scale with an internal standard of *tert*-butyl protected DOTA, analysis was conducted *via* mass spectroscopy. Whilst this method will not give quantitative results, a conclusion can still be drawn from the results. All couplings were performed under standard peptide coupling conditions (DMF, DIPEA), the results of which can be seen in Table 6. The ratio given is desired product vs. *tert*-butyl DOTA.

Once these couplings failed it was deemed to be necessary to reintroduce a "linker" compound between peptide and chelator. Beta-alanine was trialled on all the peptides, and showed no desired product.

Table 6: Coupling agent screen with DOTA-acid and Pro-^{t}Bu ester

Coupling Agent	Type	Additives	Ratio (**121**/ **116**) H^+/Na^+	Ratio total
PyOxim **52**	Phosphonium salt	None	0.705 1.467	2.172
PyBOP **51**	Phosphonium salt	None	0.890 1.370	2.260
BOP **50**	Phosphonium salt	None	0.437 0.823	1.260
HATU **53**	Aminium salt	HOBt **46**	0.425 0.374	0.799
HBTU **54**	Aminium salt	HOBt **46**	0.677 0.369	1.046
TBTU	Aminium salt	HOBt **46**	0.649 1.241	1.890
COMU **55**	Uronium salt	None	0.179 0.654	0.833
DCC **33**	Diimide	HOBt **46**	0.724 0.566	1.29
EDC **35**	Diimide	HOBt **46**	0.151 0.180	0.331
CDI	Acylazole	None	0 0	0

Acetyl-Cl	Anhydride	None	0 0	0
Oxalyl-Cl	Acyl chloride	Pyridine	0 0	0
PCl_5	Acyl chloride	Pyridine	~0 0	~0
Ethyl chloroformate	Chloroformate	NMM	0.391 0.319	0.710
Isobutyl chloroformate	Chloroformate	NMM	0.497 0.235	0.732
Phenyl chloroformate	Chloroformate	NMM	0 0	0
Allyl chloroformate	Chloroformate	NMM	0 0.173	0.173

As shown in Table 6, seventeen different coupling agents of eight different types were trialled. Three types of agent not previously discussed were used, acylazoles, acyl chlorides, and chloroformates. Acylazoles, such as CDI, form amides in a similar manner to phosgene. The acid attacks the carbonyl forming the carbonyl imidazolium, which can then directly react with another acid to form the anhydride, or an incoming amine, to form the desired amide. Oxalyl chloride and PCl_5 make the acyl chloride which then reacts with pyridine to form an activated acyl pyridinium similar to an activated ester, which then forms the desired amide. Chloroformate-based reagents form the unsymmetrical anhydride. This can directly react with the

incoming amine, or with NMM (*N*-methylmorpholine), to form the activated carbonyl morpholinium, which then reacts with the incoming amine. The unsymmetrical nature of the anhydride means that the reagent is less specific and can lead to the formation of carbamate. These mechanisms are shown in Scheme 32.

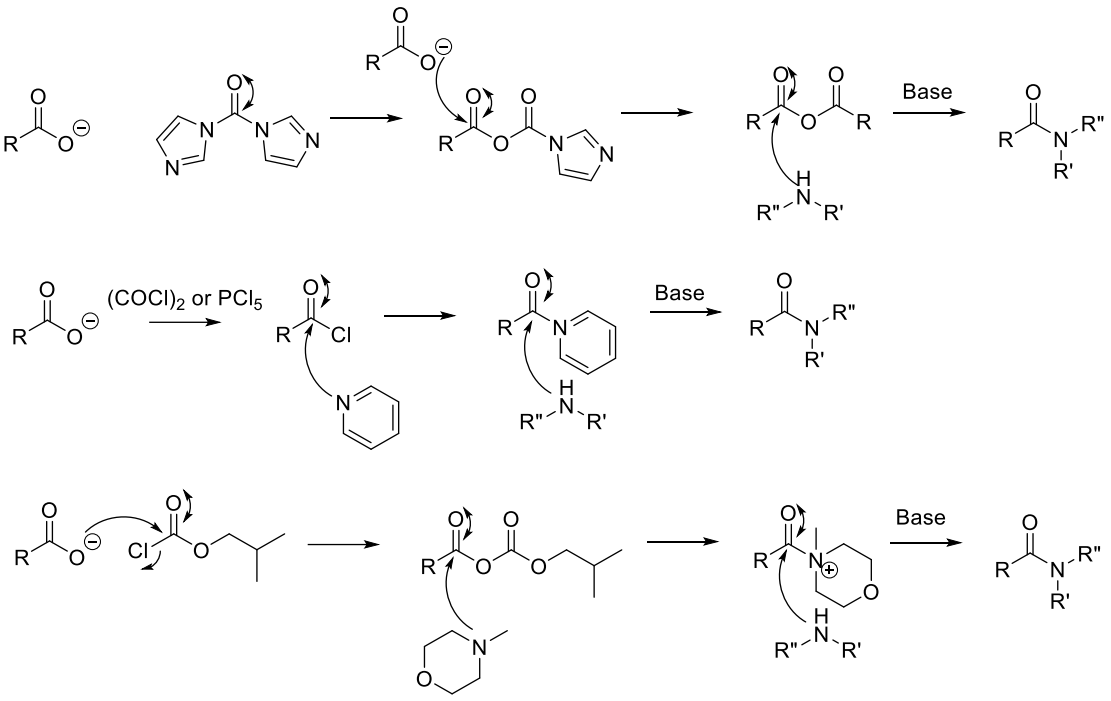

Scheme 32: Coupling mechanisms

Table 6 shows that PyBOP **51** and PyOxim **52** performed equally well, however, as PyOxim **52** has previously proved ineffective in couplings onto resin bound peptide. PyBOP **51** was then trialled and also failed, this method was then abandoned.

3.7.4 Synthesis of ethyl hydroxyl DO3A (30)

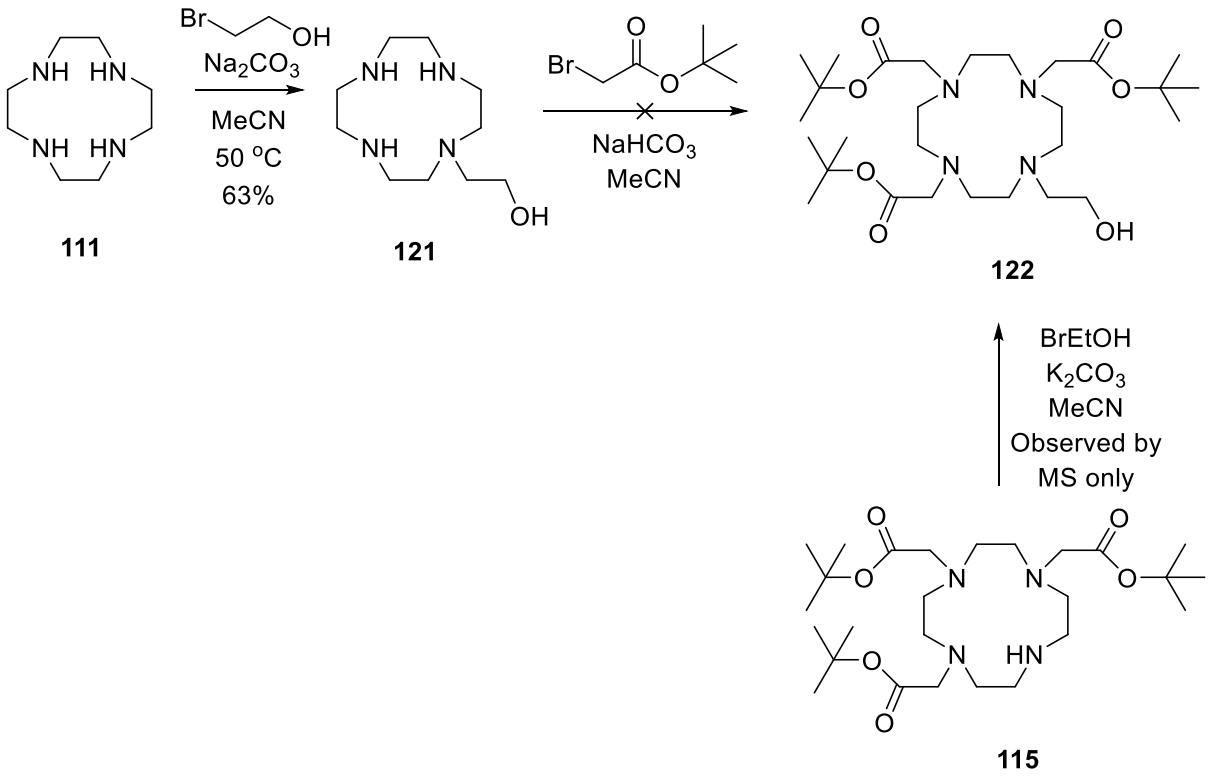

Scheme 33: Ethyl hydroxyl DO3A route

Two possible routes to the synthesis of **122** were investigated, based upon chemistries in the previous sections. These strategies were implemented, and bromoethanol was employed to incorporate an ethylene hydroxy functionality to cyclen resulting in **121**. This then would have lead into a Williamson ether synthesis in order to attach a linker, or alternatively the hydroxyl group could have been brominated under standard Appel conditions, and could then have been attached to the original linker or peptide directly. However, this DO3A analogue **122** would not be as efficient at chelating Gd^{III} as the DOTA analogue previously planned but would form a stable complex, as the loss of the carbonyl would lower the kinetic and thermodynamic stability of the chelate. This alkylation was not achieved.

Alkylation of cyclen **115** using bromoethanol gave a small conversion confirmed by ESI-MS, however, none was isolated.

3.7.5 Retrosynthetic analysis of the DOTA-PEG-COOH 115

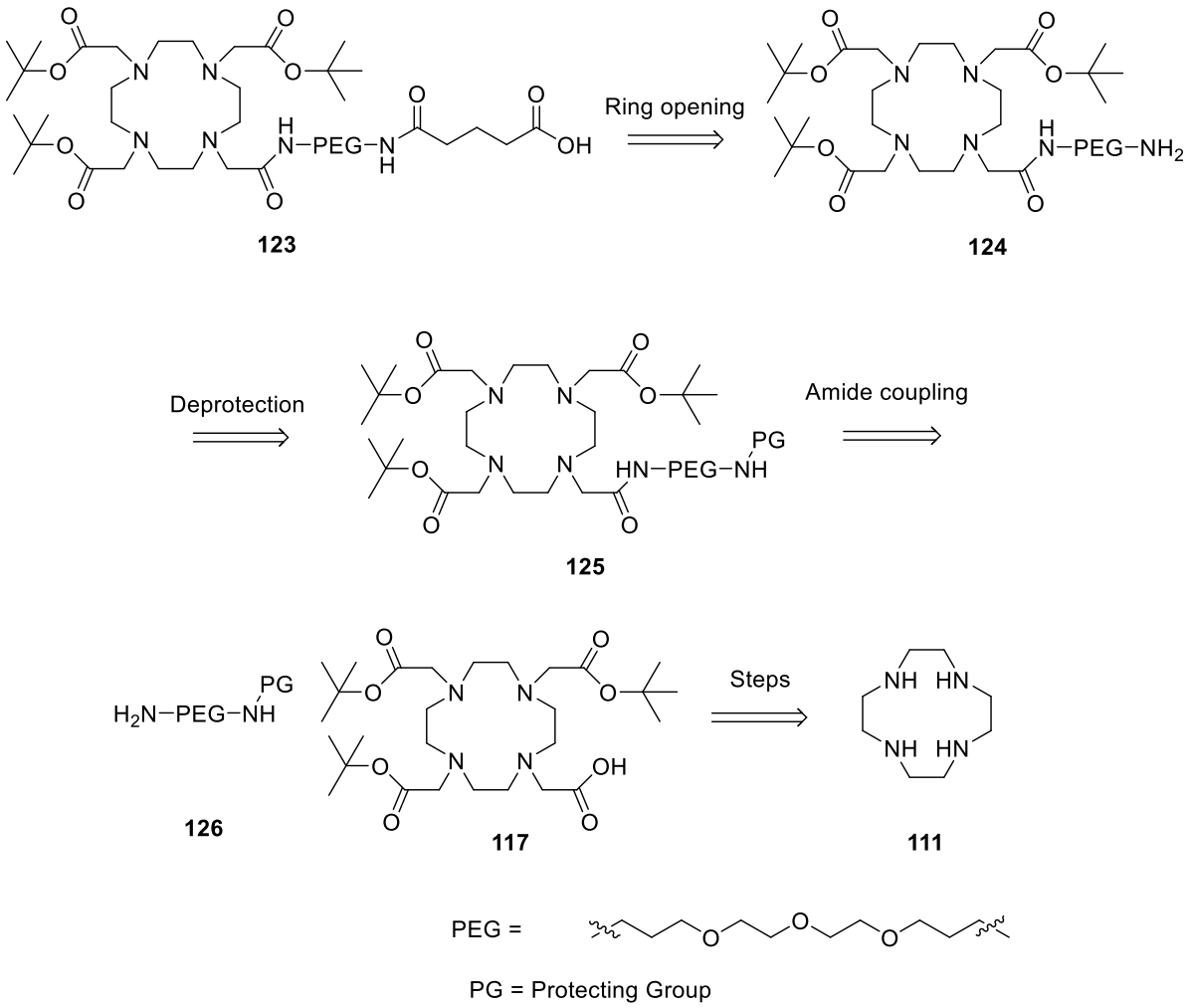

123 124 125 126 117 111

Scheme 34: Retrosynthesis of DOTA-PEG 123

Synthesis of the DOTA-PEG-COOH **123** was designed to provide the Gd^{III} ion with a strongly coordinating ligand, whilst improving the aqueous solubility of the peptide (PEG) and have SPPS compatibility (COOH). Acid **123** was intended to be prepared from a ring opening of a cyclic anhydride using DOTA-PEG **124**. The DOTA-PEG **124**

with the carboxyl groups protected as *tert*-butyl esters, was designed not to couple to the free amines of the peptide during peptide coupling to the MMP substrate. After attachment to the MMP peptide substrate, the esters were cleaved by TFA, which is also used to cleave the peptide from the resin. Following this cleavage, the Gd^{III} ion would be chelated to the ligand.

It was envisaged that the unprotected amine **124** would be made from either the Fmoc, or Cbz protected amine **125**. The PEG-PG **126** would be attached to the acid using standard coupling agents such as HBTU. The acid **117** would be synthesised *via* the route previously stated.

In order to only couple one DOTA acid **117** to one PEG **126** it would be necessary to protect one of the primary amines of that PEG. It was envisaged that one amine could be selectively BOC-protected by using an excess of diamine. Alternatively a similar approach could then be used with other carbamates, such as Fmoc-Cl or Cbz-Cl, in order to create the corresponding mono-protected diamine **119** with orthogonality to the DOTA acid **118** carboxyl protecting groups.

3.7.6 Synthesis of PEG Linkers

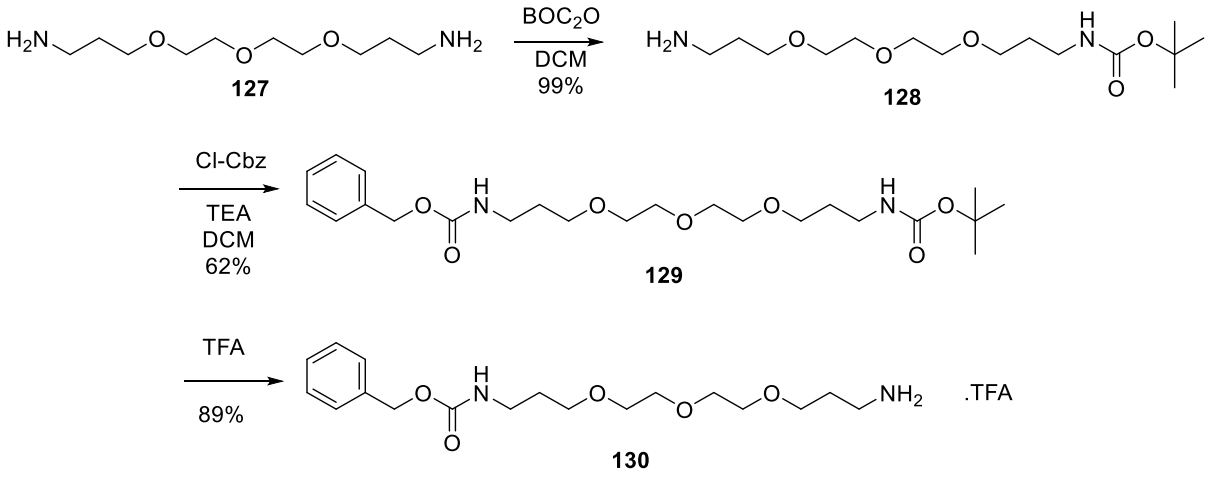

Scheme 35: Synthesis of protected PEG 130

Due to lower yields than expected with a single step approach, a three step synthesis of the PEG linkers was performed. This synthesis can be completed in a single day.

The protection of the diamine PEG **127** with BOC was based on Roelen's synthesis of a similar diamine, with some modifications.[124] Protection was simply accomplished using a seven fold excess of the PEG **127**; purification was then achieved with an organic aqueous wash and **128** was obtained in an excellent yield with respect to the BOC anhydride used.

The Cbz protection was performed on PEG-Boc **128** due to the ease with which Boc is deprotected, this was achieved using a modified literature method with Cbz-Cl and

TEA in DCM to furnish **129** in good yield.[125] Boc was easily removed from compound **129** with TFA in excellent yield giving **130**.[126]

3.7.7 DOTA-PEG-PG 126

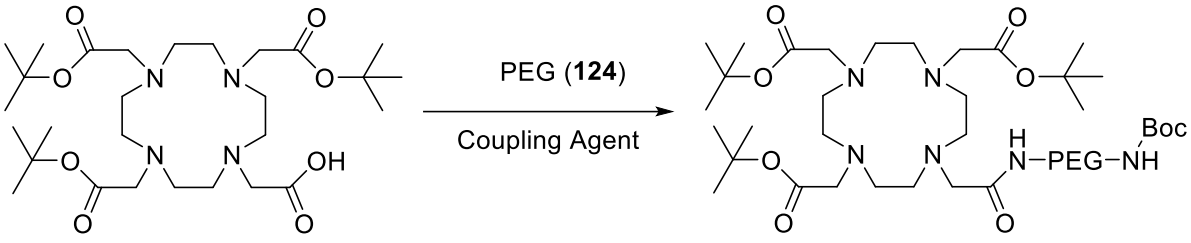

117 **131**

Coupling Agent	Yield (%)
CDI	38
EDC **35**	14
DCC **33**	Not isolated
HBTU **54**	Not isolated
PyBOP **51**	Not isolated

Scheme 36: DOTA-PEG-PG 126

The DOTA-PEG-PG **131** was synthesised using standard coupling agents in the presence of the unprotected amine of PEG **128**. Coupling reactions were also attempted with DCC **33**, HBTU **54** and PyBOP **51**, however the product could not be isolated in these cases. Low yields could be explained by the steric hindrance of the *tert*-butyl groups on the ring of acid **117**, as well as the structural conformations of the DOTA cage like structure of **117** obstructing the formation of the desired activated species. Once synthesised, the Gd^{III}-DOTA is intended to provide the

paramagnetic relaxation of the fluorine-containing section of the agent. This relaxation is proportional to the distance between the nuclei, Gd^{III} and ^{19}F, similar to FRET relaxation. A PEG linker was planned to be added between the Gd^{III}-DOTA and the peptide, in order for the peptide sequence to be more accessible to the MMP active site, as well as addressing any possible solubility problems, however, this added distance would affect the relaxation of the fluorine considerably.

The indicated yield when coupled with CDI was performed on small scale and scaling up the reaction lowered its efficiency. As a result of the low yields obtained, alternative routes were also investigated.

3.8 Functionalization of DOTA

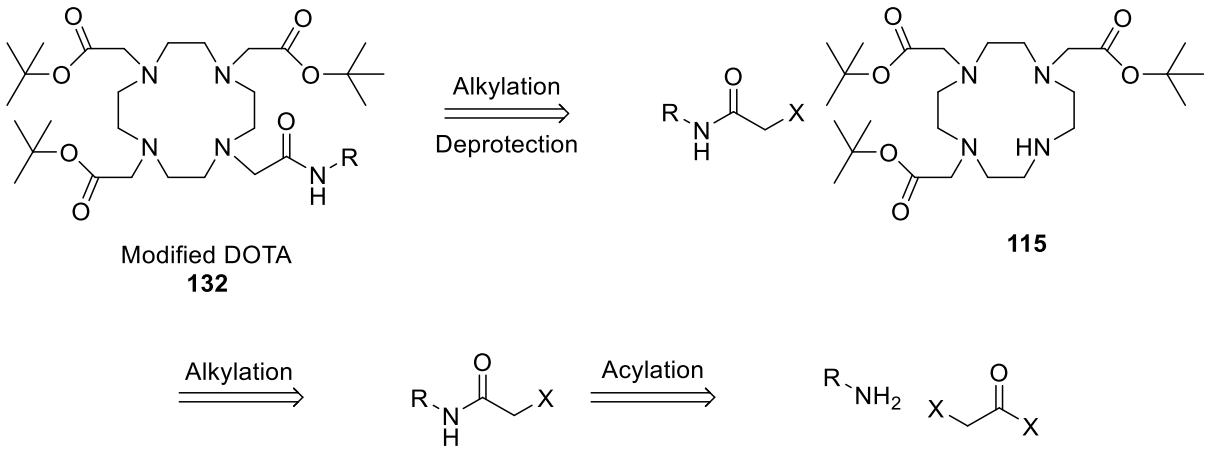

Scheme 37: Generic functionalisation of DOTA

The following sections outline how a different fourth "arm" was incorporated onto the DO3A **115**, which resulted in different DOTA analogues for different methods of conjugation onto a peptide. The modified DOTA compounds in the following sections all followed the same generic retrosynthesis shown in Scheme 37.

3.8.1 Synthesis of DOTA-PEG (135)

In order to attempt the synthesis of a DOTA-PEG which could be synthesised more reliably on a large scale the following modifications were performed.

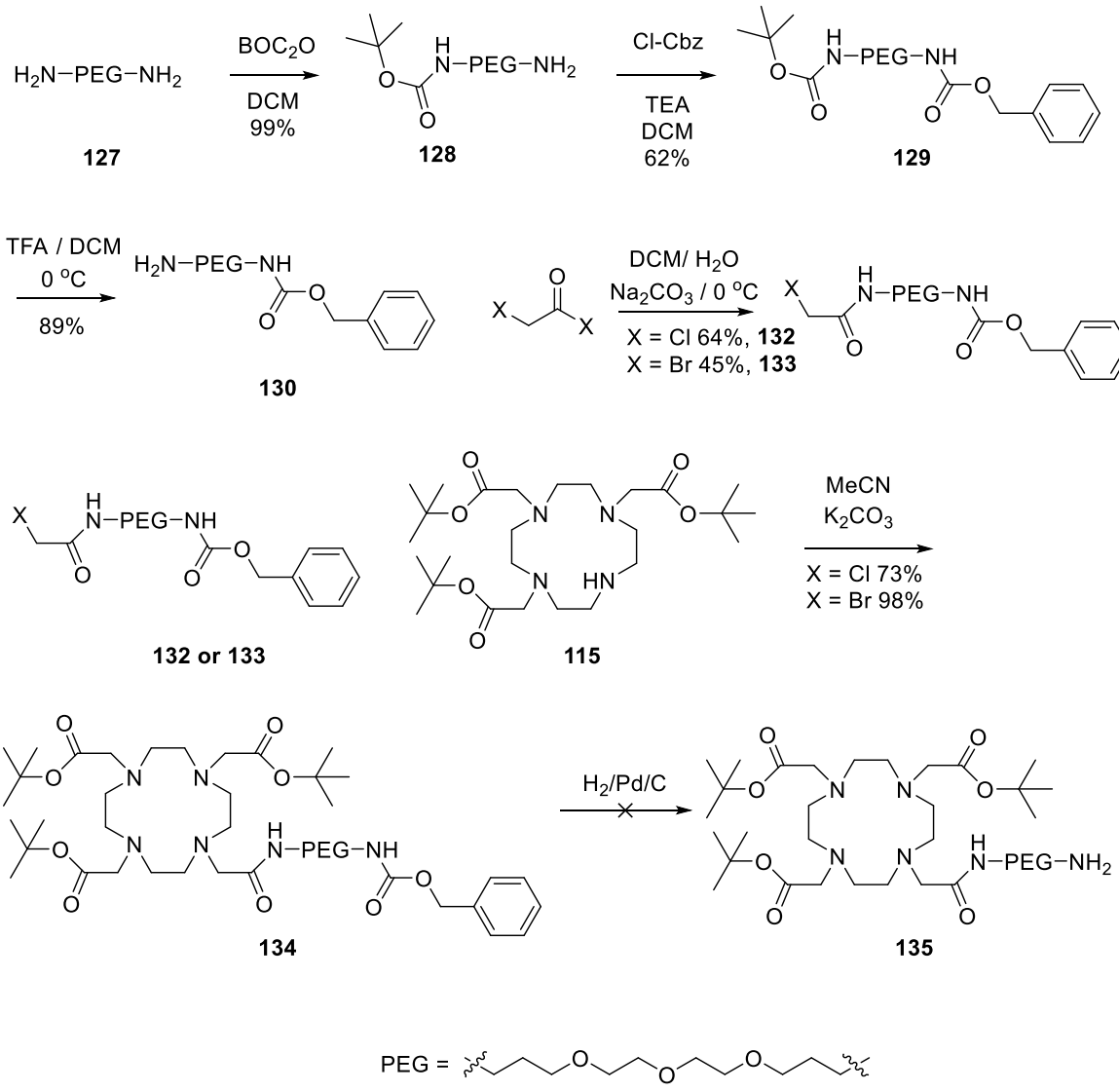

Scheme 38: Synthesis of DOTA-PEG

PEG **130** was synthesised as discussed previously. Unlike the coupling previously attempted, where a DOTA-acid **117** was coupled onto an amino-PEG **128**, here an alkylation is performed instead; at this point only the PEG-Cbz **130** was acetylated,

both bromoacetyl bromide and chloroacetyl chloride were used to compare their relative yields over two steps. As would be expected acetylation using the acyl chloride gave a higher yield than the acyl bromide. The following step was the alkylation of DO3A **115**, the secondary amine of DO3A gave excellent yields when reacted with the α-bromocarbonyl **133** and good yields with the α-chlorocarbonyl **132**. The analogues were independently extracted, yielding the pure DOTA analogue **134**, this extraction would not have been sufficient with a Boc-protected amine (synthesised later) instead of the Cbz version, as this compound is organic soluble like the DOTA-PEG-Cbz and would only remove the waste salts formed and the acyl halide. In order to produce the deprotected compound, the Cbz must be removed. Currently this has not been achieved, no deprotected product was observed using Pd on carbon (10% by weight). However, this step has not been attempted at temperatures higher than ambient temperature, under a higher pressure of hydrogen, or with any other metal catalysts.

3.8.2 Synthesis of Proline-DOTA (141)

Synthesis of the Pro-DOTA **141** was designed to avoid the steric difficulties encountered when attempting to couple the DOTA acid **117** and the amino terminus of a secondary amine on the resin bound peptide. The Pro-DOTA **141** was designed with the carboxyl groups protected as *tert*-butyl esters so as to not couple to the free amines of the peptide during peptide coupling to the MMP substrate, these esters, being amenable to hydrolysis during the TFA induced resin cleavage.

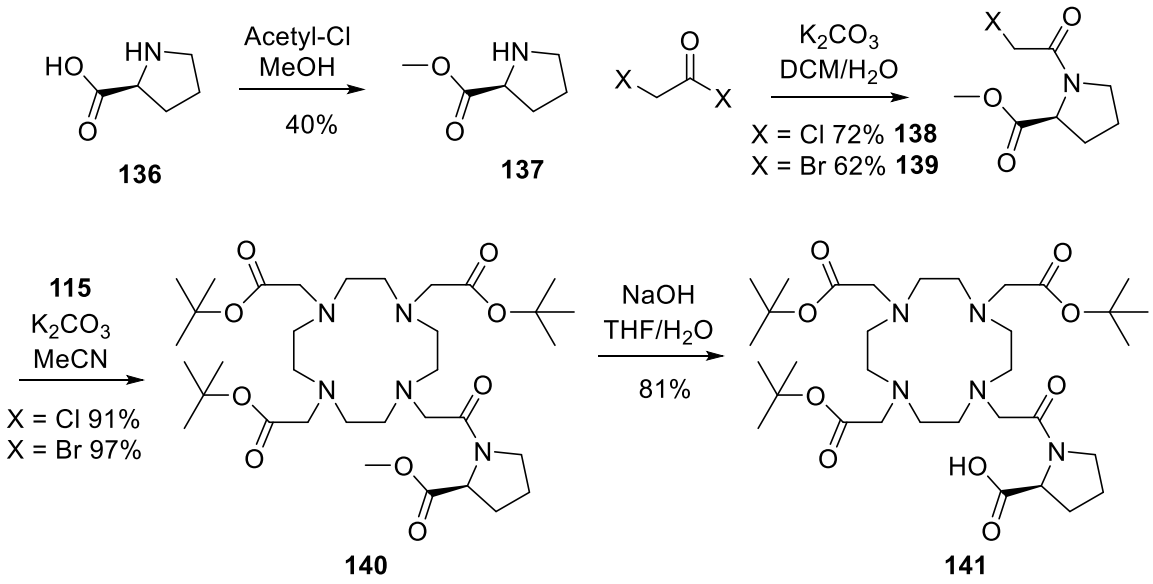

Scheme 39: Synthesis of Pro-DOTA 141

Synthesis of the Pro-DOTA **141** began with a reasonable yield of the methyl ester protection. Once the proline methyl ester had been produced both chloroacetyl chloride and bromoacetyl bromide were reacted with **137**, both giving good yields of **138** and **139** respectively. Acyl chlorides are more reactive than their bromo counterparts and as such a greater difference in yield was expected. Once the

halides were produced, an S_N2 reaction was attempted under basic conditions with cyclen **115**. Both reactions gave excellent yields with the α-bromoamide **139** giving excellent yields more consistently. Finally, the methyl ester **140** was hydrolysed using sodium hydroxide resulting in the Pro-DOTA **141** in high yield.

3.8.3 Attempts to couple Pro-DOTA onto peptide

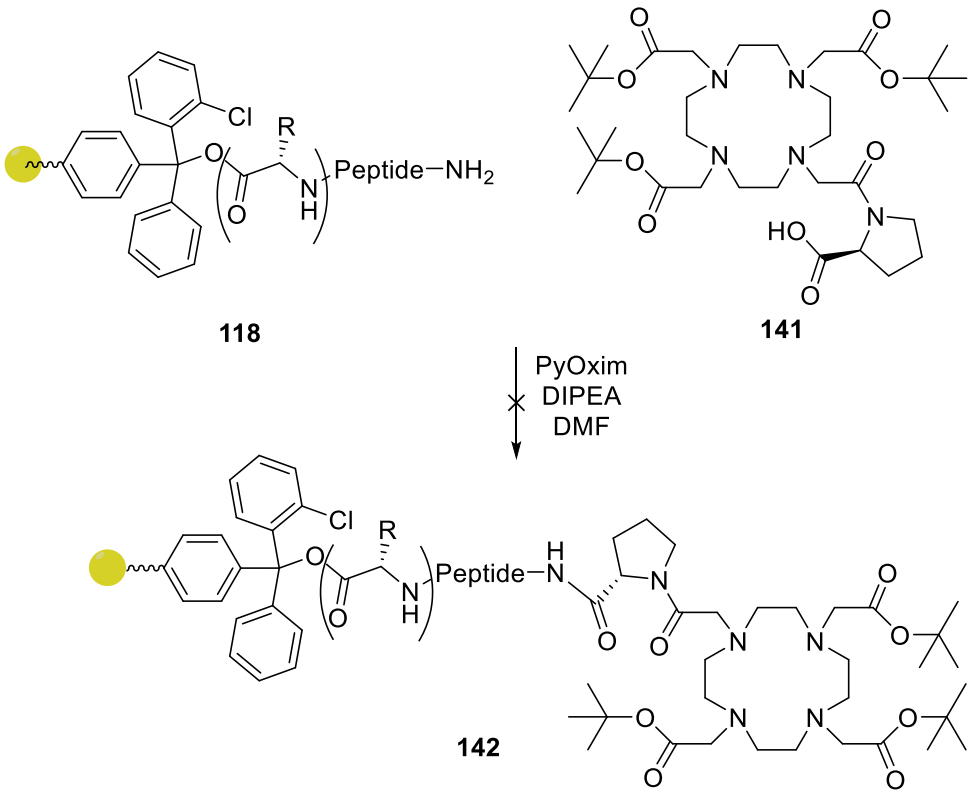

Scheme 40: Attempted coupling of Pro-DOTA onto peptide

Attempts to couple Pro-DOTA **141** onto the resin bound peptide **118** were all unsuccessful using PyOxim, TFFH, HTBU, HATU, and COMU.

3.8.4 Peptide acetylation and substitution with DO3A (115)

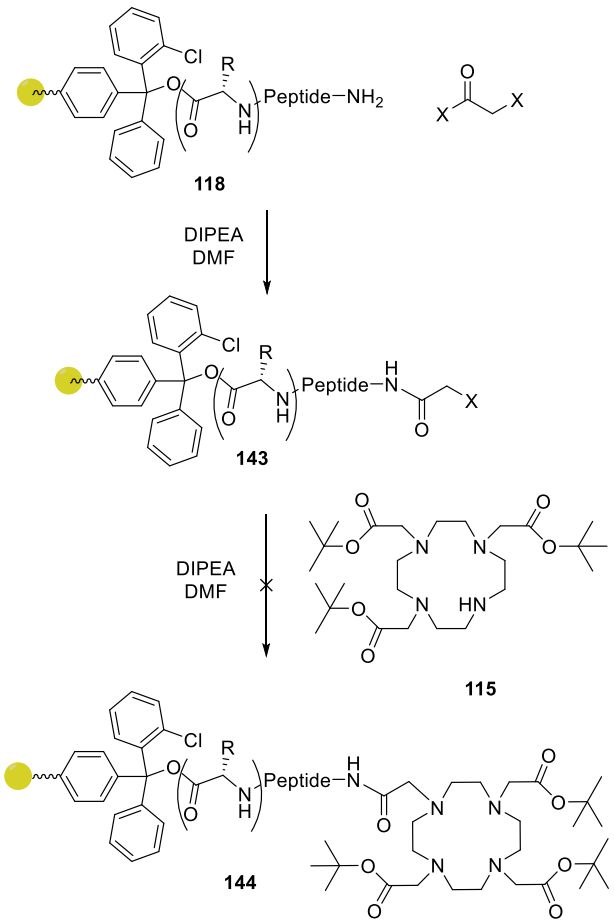

Scheme 41: Peptide acetylation, and direct DOTA mediated substitution

Following the successful substitutions of various cyclen analogues using an α-halocarbonyl, the direct nucleophilic attack onto an acetylated peptide was attempted. Using the same principles previously discussed, both bromoacetyl bromide and chloroacetyl chloride were used to acetylate the peptide Pro-Leu-Gly-Leu-Trp-Ala-Arg-FAA (**58**), under larger excesses of DIPEA to avoid acidic cleavage of the highly labile trityl ester, followed by a DMF wash. This was followed by the

addition of a large excess of DO3A **115** and DIPEA to attempt the substitution reaction of the α-halopeptide. This reaction was given two days of stirring to allow for the steric effect of the peptide; after this the peptides were then cleaved and analysed by ESI-MS to show no product. This method has been attempted previously within the literature by Meares *et al.,* who reported low yields in the range of 12-32%; it should however be noted that none of the peptides in that work contained a terminal proline.[127]

3.8.5 Synthesis of Alkyne-DOTA (147)

Alkyne-azide "click" chemistry offered an alternative to peptide coupling reactions. In order to implement this into the paramagnetic agent, an alkyne analogue was required. The synthesis of which ollows a similar synthetic route to the Pro-DOTA **141**.

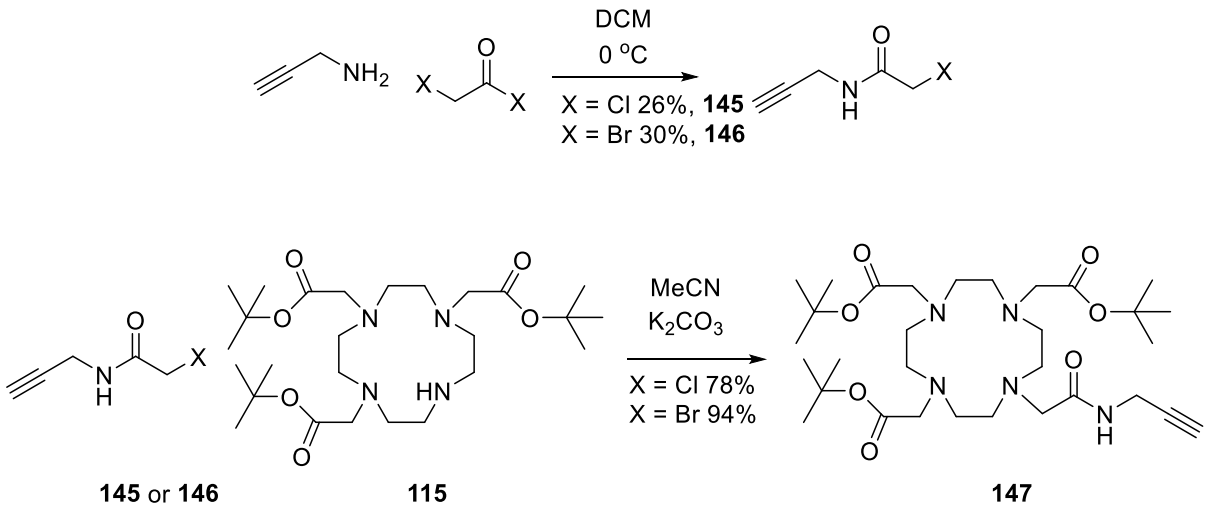

Scheme 42: Synthesis of Alykne-DOTA 147

Synthesis of the alkyne-DOTA **147** began with a low yielding reaction between propargylamine and chloroacetyl chloride resulting in the desired amide. Once the α-chloroamide had been produced, an S_N2 reaction was attempted under basic conditions with cyclen **115**, the product was obtained in good yield. In order to improve this, the same synthesis was attempted using bromoacetyl bromide. This also resulted in a low yield in the first step, although surprisingly a higher yield than with the acyl chloride; the α-bromocarbonyl compound improved the second step to result in an excellent yield. In order to utilise 'click chemistry' it was decided that the peptide would be labelled with an azide functionality.[77]

3.8.6 Proposed retrosynthesis of PEG-Azide 148

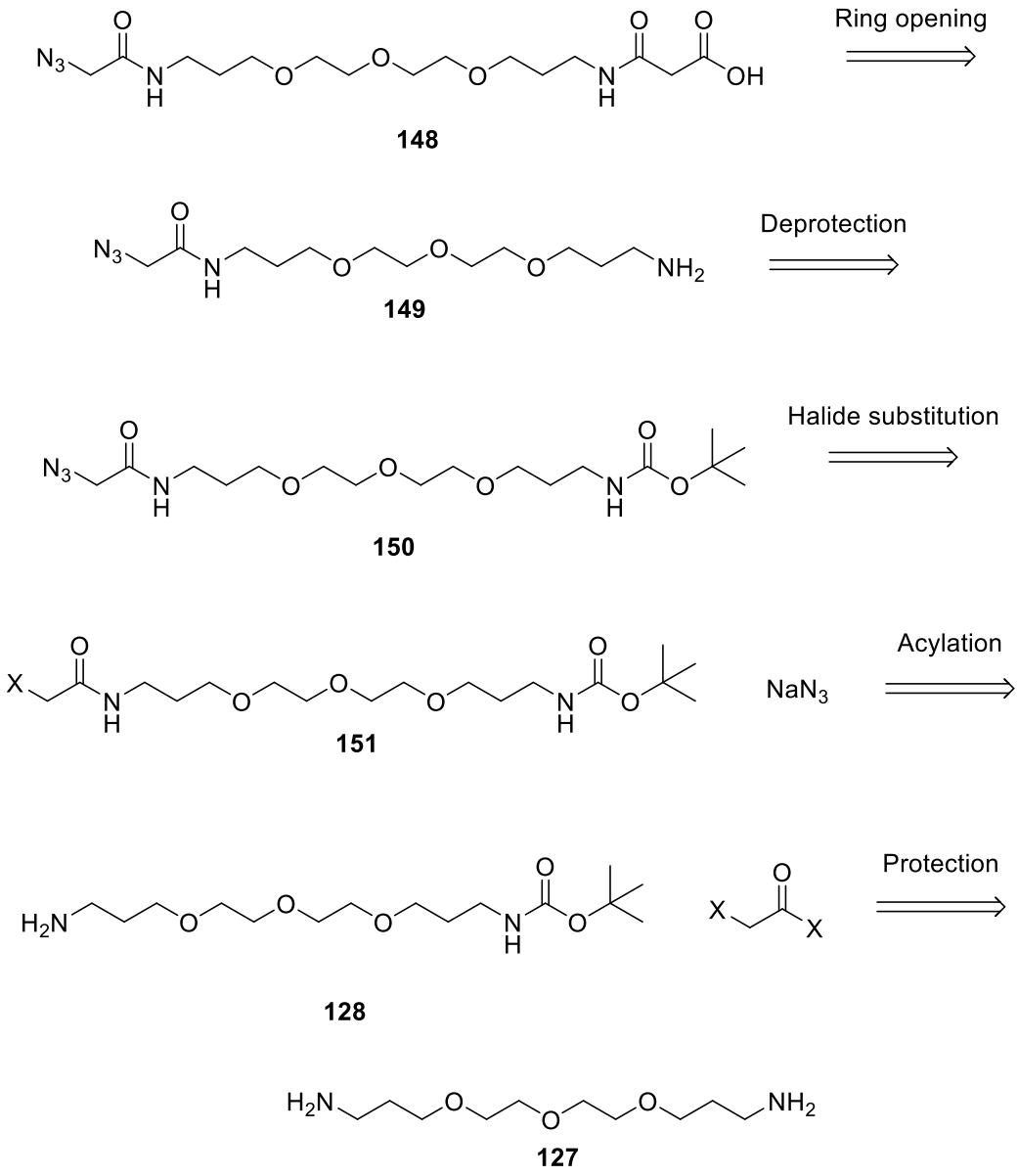

Scheme 43: Retrosynthesis of PEG-Azide

To introduce an azide onto the peptide a PEG-azide was designed. This compound would improve the solubility of the probe whilst also distancing the alkyne-DOTA **147** from the resin.

It was proposed that the free carboxylic acid **148** produced from the ring opening of a cyclic acid anhydride reacting with the amino-PEG-N_3 **149,** obtained *via* deprotection of amine **150** using TFA (deprotection conditions). The protecting group deprotection should not affect the azide; as such, reductive conditions were unsuitable. Removal of the protected amino-PEG-N_3 **1501** would be synthesised *via* an S_N2 reaction between sodium azide and α-halo amide **151**. α-Halo amide **151** would prepared from protected PEG **128** and corresponding halo-acetyl halide. The protected PEG **128** would be produced from diamine **127** and Boc anhydride, as previously described.

3.8.7 Synthesis of PEG-azide 152

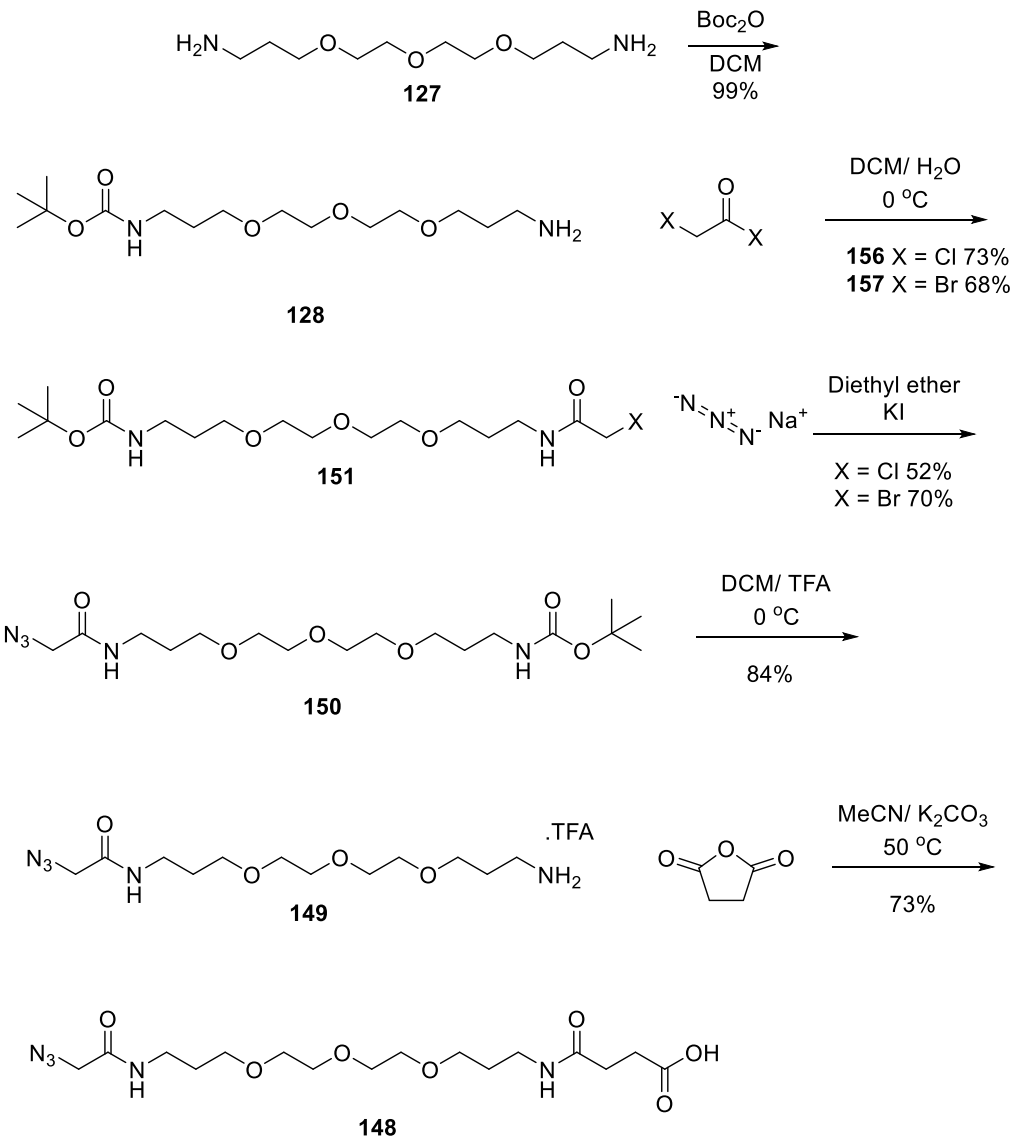

Scheme 44: Synthesis of PEG-Azide

As previously described, synthesis of Boc-protected PEG **128** was based on Roelen's synthesis.[124] The protected PEG **128** was then reacted with bromoacetyl bromide to produce the α-bromoamide **151a**, in a similar yield to the α-chloroamide **151b**

obtained by the chloroacetyl chloride method. A simple wash with DCM and water gave a pure product. Reacting α-bromoamide **151a** with sodium azide alone proved to be ineffective, and addition of a catalytic amount of potassium iodide was required to introduce Finkelstein-like conditions, the *in situ* formation of the α-iodoamide of **151** assisted in the reaction proceeding in a good yield. The deprotection of the Boc group proved facile and gave an excellent yield of the TFA salt of amine **149**. This was then followed by the ring opening of succinic anhydride. Potassium carbonate was required to deprotonate the amine salt **149** to form the free amine which then ring-opened the anhydride to form the desired acid **148**.

With acid **148** produced, the next step was the coupling to the peptide. The PEG-acid **148** is much less hindered than that of the DOTA-acid **118** and should therefore be less problematic to couple.

3.8.8 PEG-azide, peptide coupling and click chemistry

In order to couple the PEG-azide **148** to the peptide, PyOxim **52** was used. The coupling was performed whilst the peptide was still bound to the resin and was then washed with DMF and water. Following the facile coupling of the azide, there were four ways in which the DOTA-alkyne could be 'clicked' onto the azide. The four methods can be split into two types, firstly whilst resin bound, secondly after the peptide has been cleaved from the resin. The 'click' chemistry was performed with

the DOTA alkyne **147**, both with the *tert*-butyl esters cleaved and post Gd^{III} ion insertion, to both resin bound and non-bound peptide.

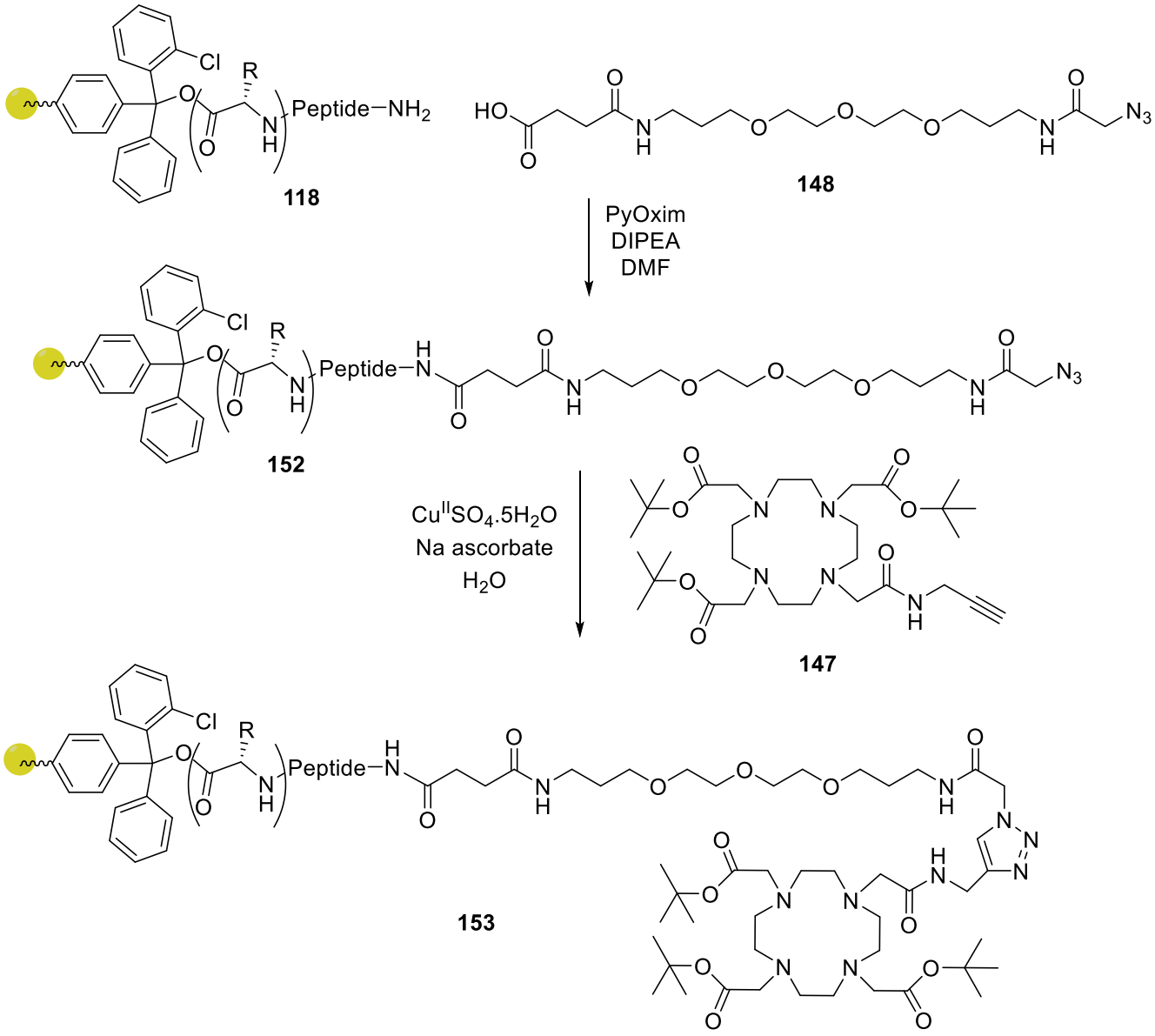

Scheme 45: Peptide, Alkyne-DOTA click chemistry

'Clicking' the peptide bound azide whilst still attached to the resin gave a low conversion by mass spectroscopy. This can potentially be explained; originally, the main issues were the conjugation of various DOTA analogues onto the peptide which were believed to be too sterically bulky to be coupled, therefore it is possible that

this rational still applies. Alternatively, the PEG units may aggregate in solution perturbing reactivity.

Attempting to 'click' the DOTA-alkyne **147** whilst free in solution proved to be more successful. By coupling in solution the peptides are more dispersed and therefore aggregation should be minimised, therefore reducing the blocking effect of neighbouring peptides. Due to low conversions for both resin bound and non-bound peptides, a modified azide was investigated. Additives such as THPTA had no effect on the "click" reaction.

3.8.9 Azido-propanoic acid synthesis

The azide **155** was synthesised from 3-bromopropanoic acid **154** using sodium azide, see Scheme 46, in good yield. Cryptophanes like DOTA-based compounds are large, causing sterical hindrance about them, it was therefore theorised that a similar stratagem may be efficient towards a DOTA based probe.

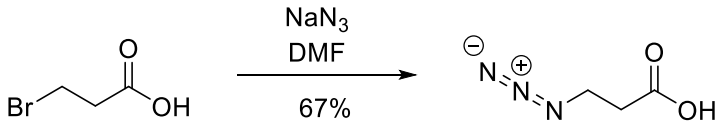

154 **155**

Scheme 46: Azido-propanoic acid synthesis

Note, extreme care was taken whilst handling **155**, low weight azides must be handled cautiously.

3.8.10 Propyl-azide, peptide coupling and click chemistry

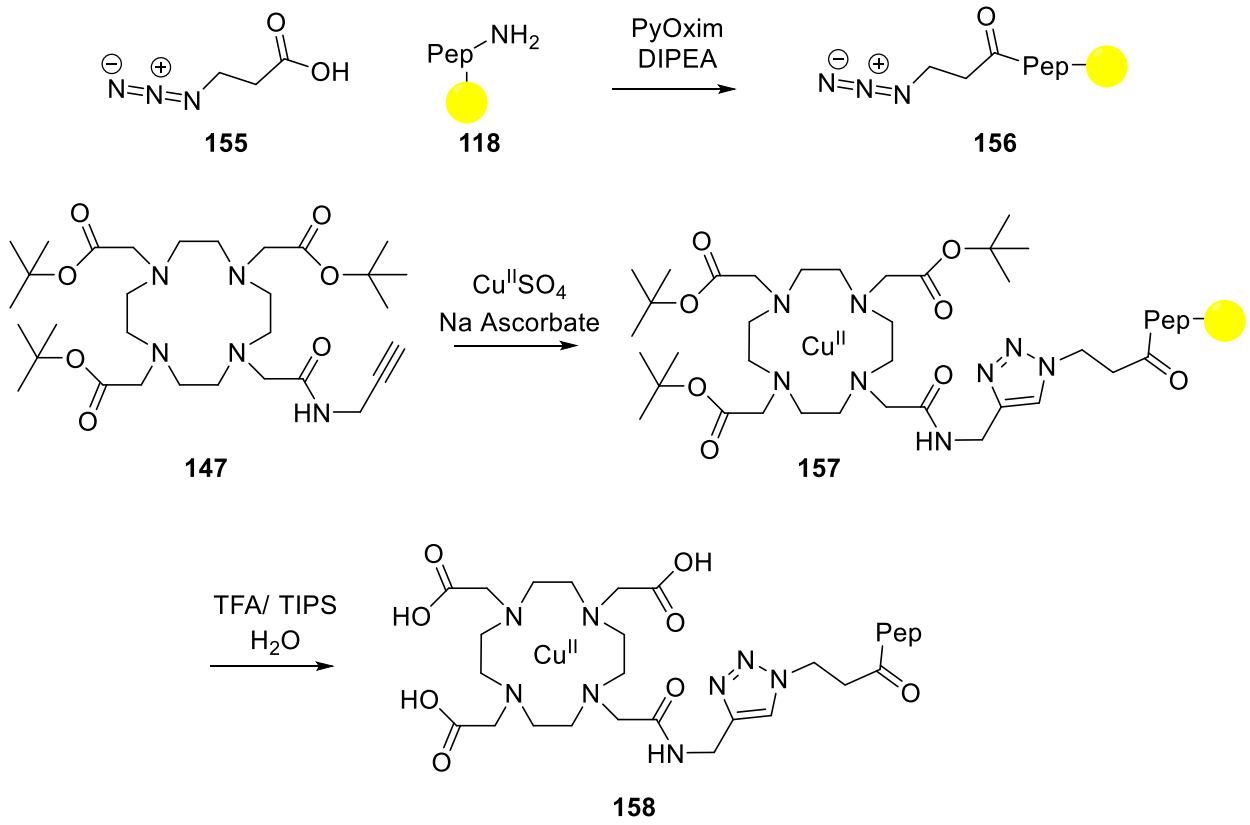

Scheme 47: Propyl-azide coupling and "click" chemistry

Azido acid **155** was then coupled onto the terminal amine of an MMP peptide sequence, using PyOxim **52** as an activator; the formation of the azide labelled peptide was observed using mass spectroscopy, by cleaving a small sample from the resin using TFA. The DOTA alkyne **147** was then “clicked” onto the peptide, using copper(II) sulphate, sodium ascorbate, and 2,4-lutidine. Once the azide was no longer observed (by a cleavage and ESI-MS, typically overnight), the peptide was cleaved from resin using TFA, the triazole formation using this azide labelled peptide **156** was substantially more successful than the PEGylated azide **152**. However, none

of the expected product was produced, instead, unsurprisingly, the DOTA moiety chelated the copper (II) used in the “click” reaction

3.8.11 Removal of Cu^{II} from DOTA 158

With peptide **158** in hand, the next step became the removal of the Cu^{II} species currently bound within the DTOA chelator. Removal of the copper *via* washing with excess solvent whilst the peptide was resin bound proved unsuccessful. $EDTA^{4-}$ dissolved in water is a common chelator of various metals including copper, but this also proved ineffective. The final method used to attempt remove a metal from a chelator (such as DO3A) was using a strong acid (5M HCl) to re-protonate the carboxylic acids, removing three binding sites and then protonating the tertiary amines to remove the amine coordination to the metal centre, but even this treatment was ineffective in removing the copper. After these failed attempts to remove the Cu^{II} a new approach was explored.

3.8.11 Click chemistry and synthesis of Gd^{III}-DOTA alkyne (164)

When the "click" reaction was attempted with DOTA alkyne **147**, Cu^{II} chelation was observed, to avoid this it was speculated that the "click" reaction with the DOTA chelated to Gd^{III} would be successful.

Continuing from the protected intermediate **147**, the *tert*-butyl esters were deprotected in excellent yield using formic acid in water to produce the tri-acid **159**. Chelation of Gd^{III} was achieved using $GdCl_3$ in water, the pH was adjusted to pH 6 completely ionising the acid groups facilitating chelation in excellent yield, and centrifugation was used to remove any insoluble salts, resulting in Gd^{III}-DOTA alkyne **160**.

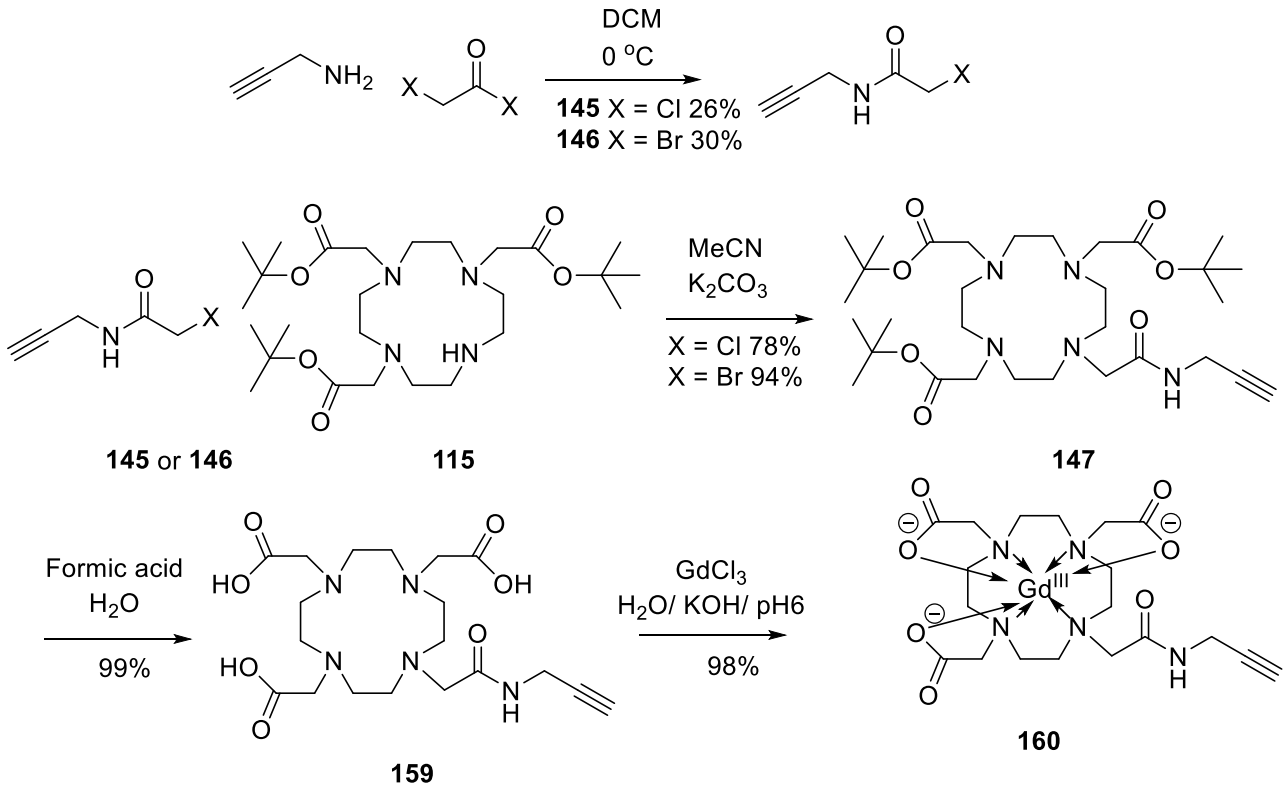

Scheme 48 Gd^{III}-DOTA alkyne 160

Once Gd^{III}-DOTA alkyne **160** was synthesised, a "click" reaction was performed with an azide labelled peptide, which resulted in triazole formation and the successful construction of the paramagnetic core of the probe and the peptide substrate. Once the method was proved to work, six different probes based on the peptide sequences discussed earlier were synthesised, see Table 12. Cleavage from the resin following washing the resin proved to remove all of the "Click" reagents. The successful formation of the probes was observed by HRMS (see appendix), and purified *via* HPLC.

3.9 Overview of the synthesis of ^{19}F NMR probes

A brief overview of the total synthesis can be found in Scheme 49.

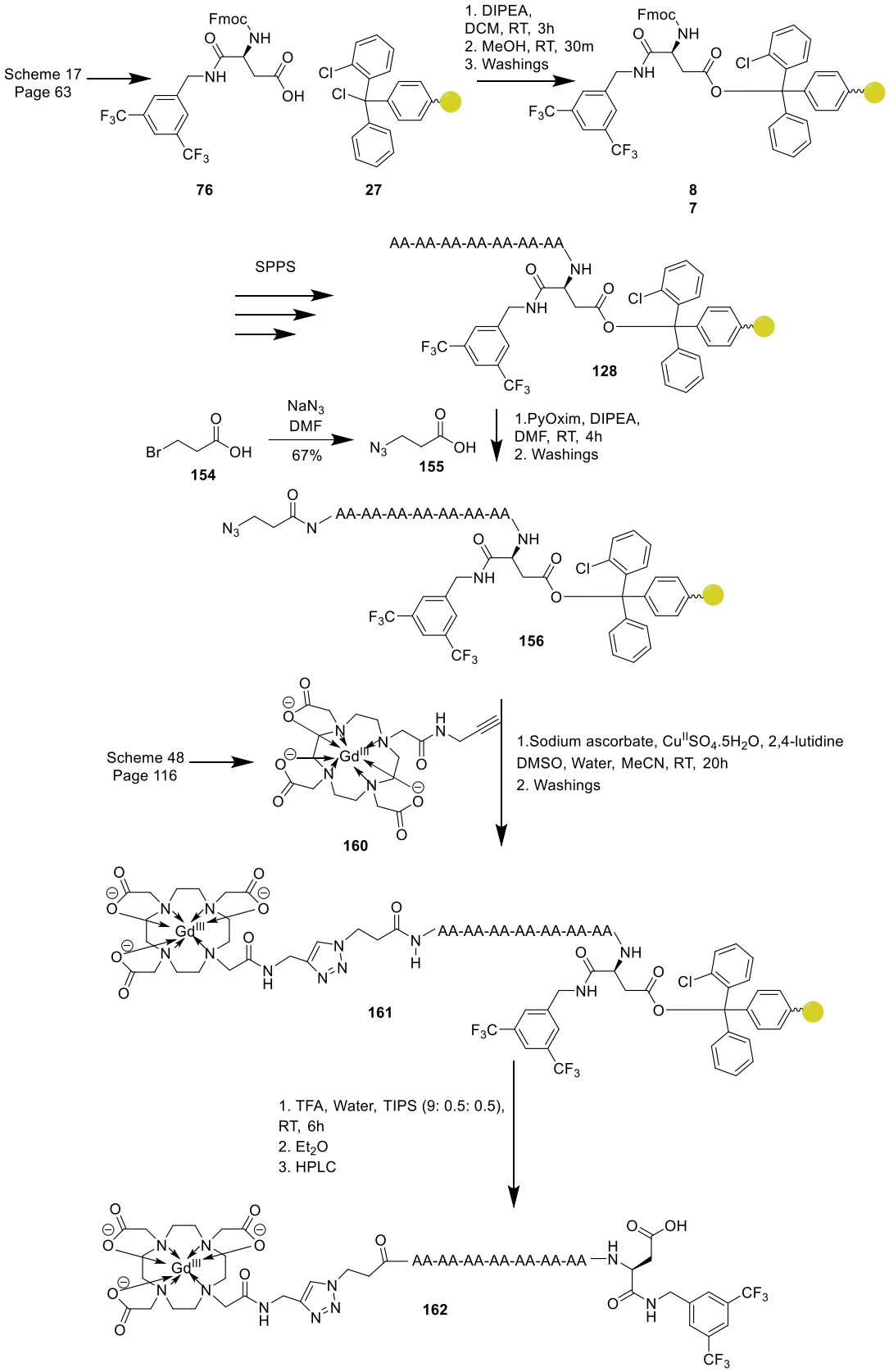

Scheme 49: Overview of the total synthesis of an MMP probe

The probes were successfully synthesised by breaking the synthesis down into segments. Initially 3,5-bis(trifluoromethyl)benzylamine was coupled *via* EDC **35** to Fmoc-Asp-tBu. This tert-butyl group was then deprotected and the free acid coupled onto a 2-chlorotrityl-chloride resin **27**, for use with Fmoc-SPPS. The second section of the probes entailed using Fmoc-SPPS which was used to produce six different peptide sequences; when the peptides were ready, 3-azidopropanoic acid **155** was synthesised from the parent bromo-compound and coupled onto each of the peptides. The third section of the probe's synthesis was a paramagnetic Gd^{III} containing metal chelator. Gd^{III}-DOTA a commercially available contrast agent for ^{1}H-MRI was chosen for modification for use as a metal chelator. Cyclen the parent tetra-secondary amine heterocycle of the DOTA ring was suitably alkylated with three tert-butyl acetylene units. The final amine was then alkylated to introduce an *N*-(prop-2yn-1yl) acetylene amide unit, for use in "click" chemistry. The *tert*-butyl protecting groups on the chelator were removed, and the Gd^{III} inserted. Finally with the probes successfully produced, semi-preparative HPLC was used to purify them.

3.10 Successfully synthesised, and purified probes

A full summary of the ^{19}F NMR MMP probes can be found in Table 7.

Full structure	Designation	MMP
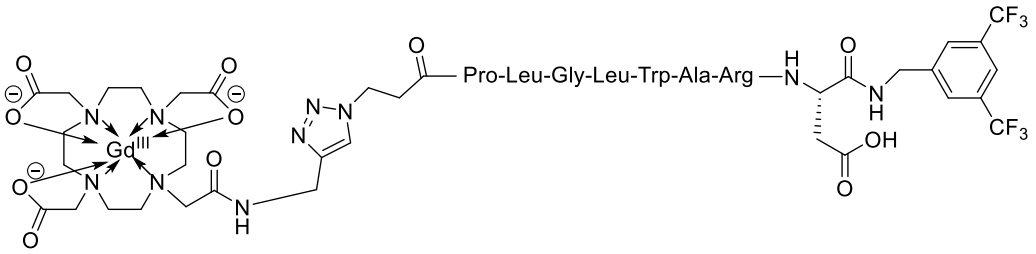	**JK-X**	Broad-range
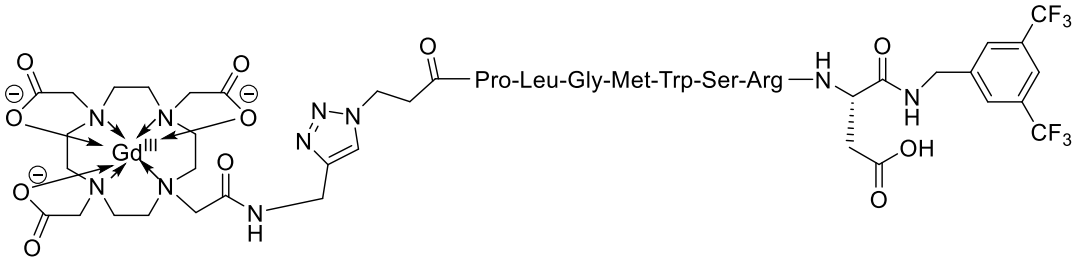	**JK-2/9**	MMP-2/-9

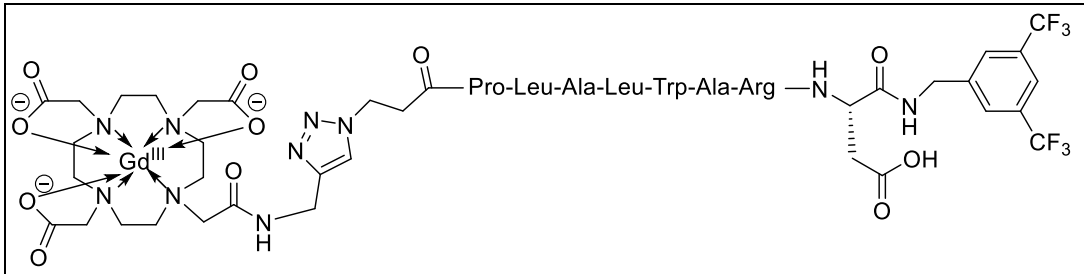	**JK-1**	MMP-1
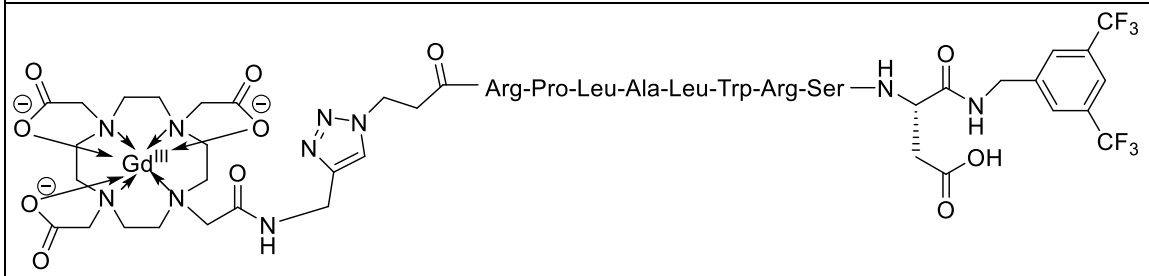	**JK-7**	MMP-7
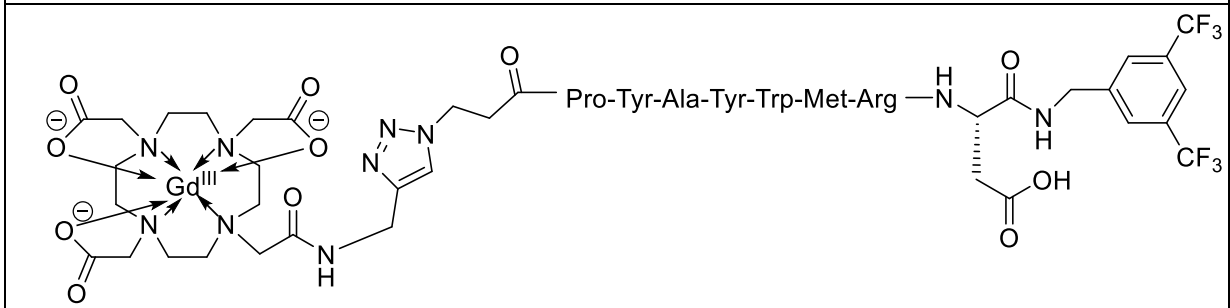	**JK-3**	MMP-3

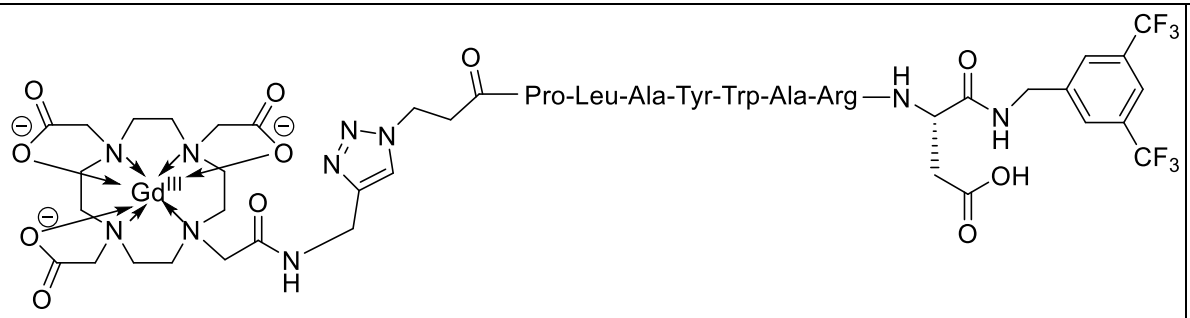	**JK-8**	MMP-8

Table 7: Completed ^{19}F NMR MMP probes

3.10.1 Purification of the ^{19}F MMP Probes via HPLC

All of the peptides produced during this work required purification *via* HPLC, which is standard when working with these types of molecules. The final step of the synthesis is the TFA-induced cleavage *via* hydrolysis of the peptide from the resin, as well as deprotection of all the protecting groups on the peptide; unfortunately the cleavage of Pbf from Arg is a long process. Exposing the ^{19}F MMP probes to strong acidic conditions for three days resulted in complete removal of the protecting groups; however, the Gd^{III} was also leached from the DO3A chelator. As a result of the loss of Gd^{III}, shortened deprotection times were used, of up to six hours, followed by removal of the cleavage mixture with a continuous nitrogen flow, proved to be the most favourable conditions at preventing leaching of the Gd^{III}. Using this shortened deprotection method did however result in high amounts of unprotected peptide which were removed during HPLC purification.

An Agilent 1200 series system was used for the all the HPLC performed. Analytical HPLC was performed using an Agilent Eclipse XDB-C18 analytical column 4.6 x 150 mm, with a 5 µm pore size, and semi-preparative HPLC was performed using an Agilent Eclipse XDB-C18 semi-preparative column 9.4 x 150 mm, which had a 5 µm pore size.

A gradient method of reversed-phase HPLC starting with eluent 100% A, increasing B to 90% to 25 minutes, followed by 95% B at 27 minutes, and then reducing B to 0%

by 30 minutes (A: milli Q water, 0.1% formic acid, B: HPLC grade acetonitrile, 0.1% formic acid). Formic acid was used instead of TFA so as to minimise the amount of TFA in the final product. This HPLC purification method was adapted from the gradient method described by Kikuchi *et al.*.[128] For the probes detailed here; the method run time was extended to improve the separation. Run times of 30 minutes proved to be optimal. All the probes had a retention time of approximately 13-14 minutes in semi-preparative columns. Following the elution of the desired products protected versions of the probes were observed. All of the probes produced were purified *via* semi-preparative HPLC.

3.11 ^{19}F NMR sample preparation

NMR and MRI are techniques which are directly comparable; however, one difference is the use of deuterium enriched solvents with NMR. Unlike MRI, high resolution NMR spectroscopic measurements requires magnetic field stabilization, typically obtained through a deuterium lock which utilizes the deuterium (^{2}H) NMR signal of a solvent such as D_2O. The deuterium lock is used for stability, negating drift of the magnet during the experiment, and also as a chemical shift reference.[129] As a result of this, for the NMR studies D_2O was used for the shim lock. The studies were performed using a Bruker AV 600 MHz spectrometer (^{19}F at 564 MHz); the minimum amount of D_2O in a H_2O/ D_2O sample required for the shim lock is 10%. Theoretically speaking the relative changes in bond enthalpy (O-D vs O-H) should increase the rate of proteolytic cleavage. Two different solvent ratios were used, 100% D_2O and 90%

H_2O/ 10% D_2O. These two ratios were chosen to show the effect of D_2O on the MMP. A D_2O insert was not trialled.

3.11.1 MMP activation and preparation

MMPs are naturally expressed in an inactive pro-form. The pro-peptide domain of pro-MMPs contains a highly conserved amino acid sequence, PRCGVPDV, and the cysteine in this peptide sequence is critical to preserving latency. The thiol-zinc bond must be removed in order to activate the proteases, this form of activation is known as a "cysteine switch", see Scheme 50.[130] MMP-1, -7 and -9 were activated using 4-aminophenylmercuric acetate (APMA). The activation consisted of diluting the MMP to a known concentration (100 µg/ mL) in a buffer (50 mM Trizma, 10 mM $CaCl_2$, 150 mM NaCl, and 0.05% (w/v) Brij35 detergent) at pH 7.5. Then APMA (1 mM) in DMSO was then added to the buffer and allowed to incubate for an hour at 37 °C, resulting in the active MMP. This active MMP was then diluted to the final desired concentration (10 µg/ mL) and was stored at -20 °C.

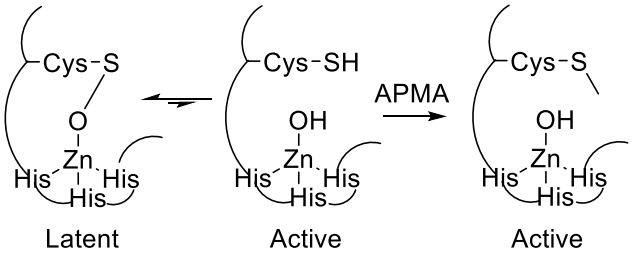

Scheme 50: APMA activation of MMPs

3.11.2 ^{19}F NMR MMP-9 studies in D_2O

All the ^{19}F NMR work in following sections, unless otherwise stated, was performed in an AV(III) 600 MHz Bruker spectrometer. MMP-9 (Gelatinase B) was used for the enzymatic studies due to its availability within the group. APMA (4-aminophenylmercuric acetate)-activated MMP-9 in PBS buffer was used as a stock solution. Initially probe **JK-X** (0.1 mM) was incubated with MMP-9 (5 µL, at 10 µg/mL, final concentration 83 ng/mL) using D_2O as solvent at 298K. D_2O was used as the only solvent to eliminate all ^{1}H background signal. This interference can make ^{19}F NMR problematic when working at high field with low concentrations of target compounds. This is especially important when monitoring small signal changes. Before the addition of MMP-9 the NMR peaks observed (on a 2048 scan ^{19}F NMR) were broad. The expected broad peak was caused by the paramagnetic effect of the Gd^{III} ion. Upon addition of MMP-9 a time-based 2D-like NMR experiment was performed to monitor the progress of the reaction, recording a 1D ^{19}F NMR spectrum (128 scans at 10 minutes, 57 seconds) per time point. The intensity of the peak at -62.4 ppm (corresponding to the two CF_3 groups of the benzylamide on the peptides) was taken and then used to plot intensity versus time graph, see Figure 23.

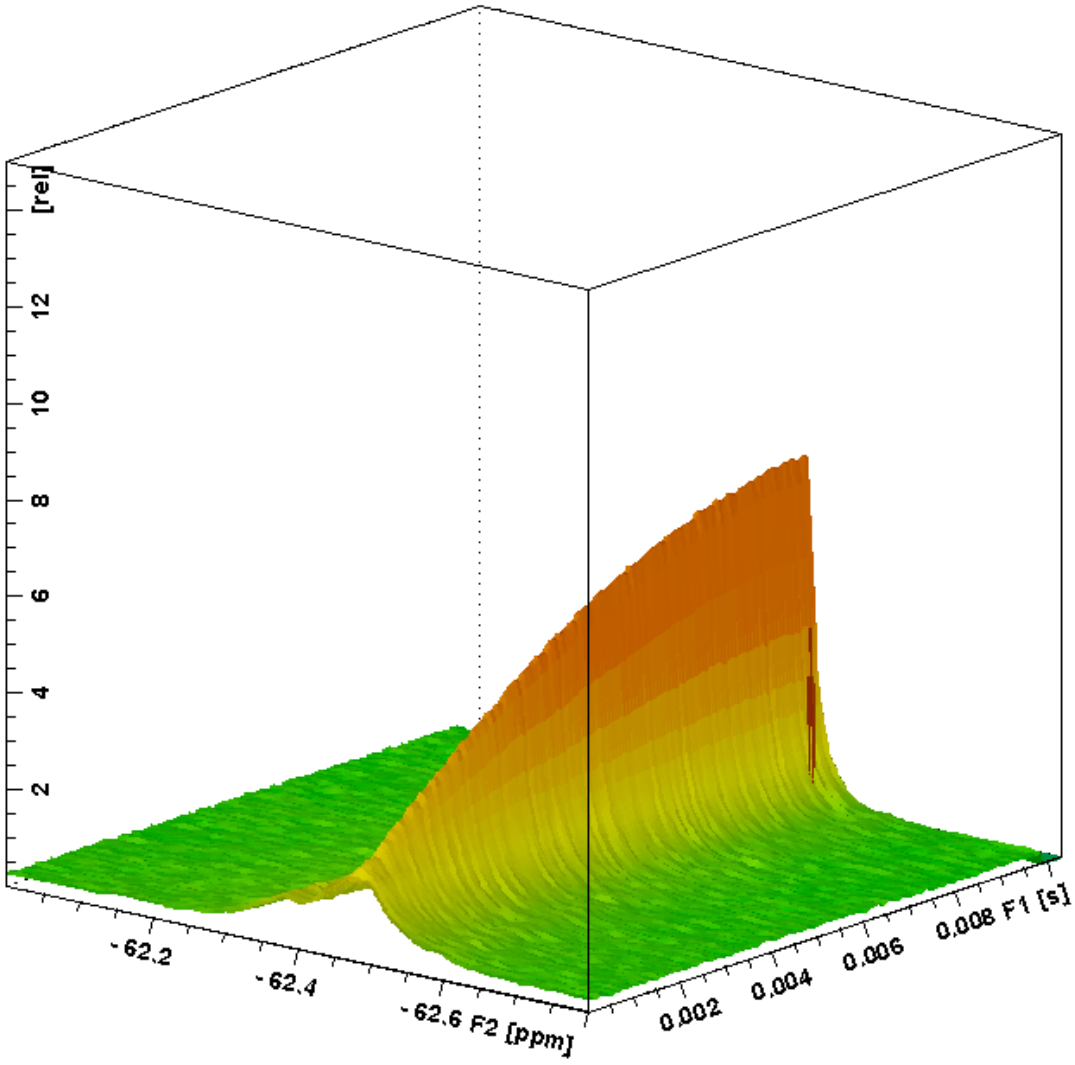

Figure 23: JK-X reaction profile, in D2O at 298K

This was then repeated with the probe **JK-2/9** under identical conditions, as shown in Figure 24.

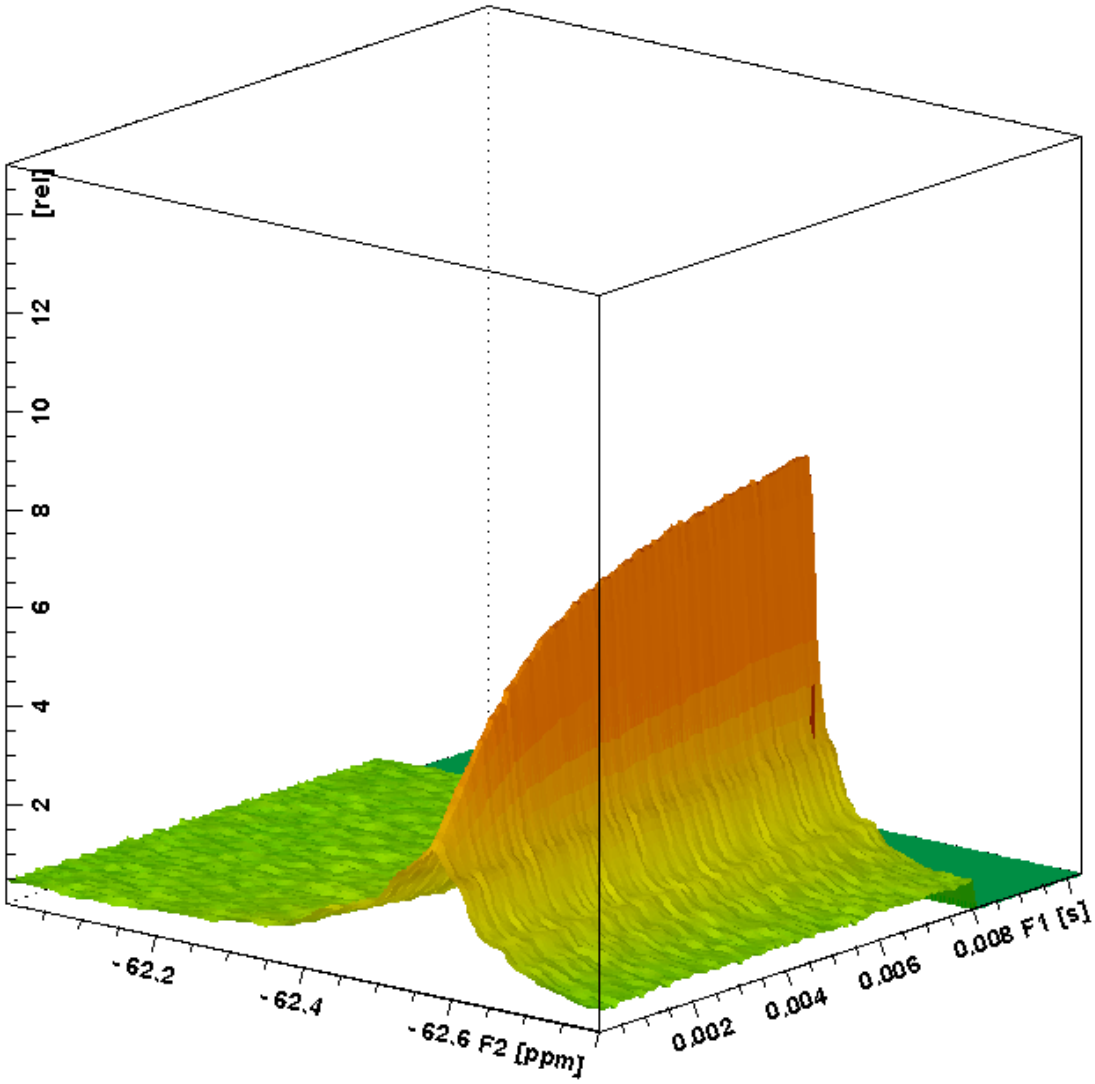

Figure 24: JK-2/9 reaction profile in D2O at 298K

3.11.3 ^{19}F NMR MMP-9 studies in 90% H_2O and 10% D_2O

The solvent system was then adjusted to 90% H_2O with 10% D_2O, the 10% D_2O being the lowest possible amount for a deuterium shim/lock to prevent magnetic drift during the experiment. The pH was adjusted to 7.5 and which was not corrected to take into account the variance for pD vs. pH. Using this solvent mixture two different time-course experiments were designed based upon the temperature studied. At

298K as described previously, 128 scans were performed per time point, at 310K this was adjusted to 32 scans (2 minutes, 59 seconds) per time point. These modified scan numbers were chosen due to the anticipated increase in rate of cleavage with increased temperature.

Figure 25 shows the combined results of the **JK-X** probe time-courses under all three conditions. Prior to cleavage, the broad-range probe was observed to have a full width at half the maximum (FWHM) of the ^{19}F NMR peak of 53 Hz at 310K. Once the probe was cleaved the FWHM changed to 13 Hz, indicating that the Gd^{III} ion was no longer affecting the ^{19}F signal. Figure 25 shows the normalised data for all three conditions, for **JK-X** probe, the normalisation of the data was achieved by taking the most intense peak as "100%" signal and then normalising everything accordingly. All the data was normalised and it is therefore displayed in arbitrary units (A.U.), data does not return to zero due to the lag time between enzyme addition and insertion into the NMR spectrometer, and then temperature equilibration, a plot back to zero was not possible. The 3D plot Figure 25a shows the narrowing of the 19F signal with time, caused by the increased distance between ^{19}F and Gd^{III} nuclei, the pseudo contact shift is therefore reduced, sharpening the peak. Surprisingly Figure 25b shows that when incubated at 310K this was turned over more slowly by the MMP-9 than at 298K, this could be due to the probe not being a natural substrate for the enzyme and at a higher temperature the probe occupying a different conformation not as easily accepted by the enzyme.

Figure 26 shows the combined results of the **JK-2/9** probe time-courses under all three conditions. Prior to cleavage the **JK-X** probe was observed to have a FWHM of 60 Hz at 310K. Once the probe was cleaved the FWHM then changed to 19 Hz, indicating that the Gd^{III} ion was no longer affecting the ^{19}F signal. Similar observations in terms of reaction profile of the **JK-2/9** probe vs. the **JK-X** was visualised. A ma jor difference between the two probes was the rate at which the **JK-2/9** probe was turned over as well as the probe being turned over most rapidly at 310K (see Figure 26). **JK-2/9** was turned over most rapidly at 310K, an expected result, this shows that the probe is a suitable substrate for the MMP-9 at physiological temperature, the accelerated rate in comparison to the **JK-X** probe shows that the **JK-2/9** probe may be a more suitable candidate for further development with a view for *in vivo* testing.

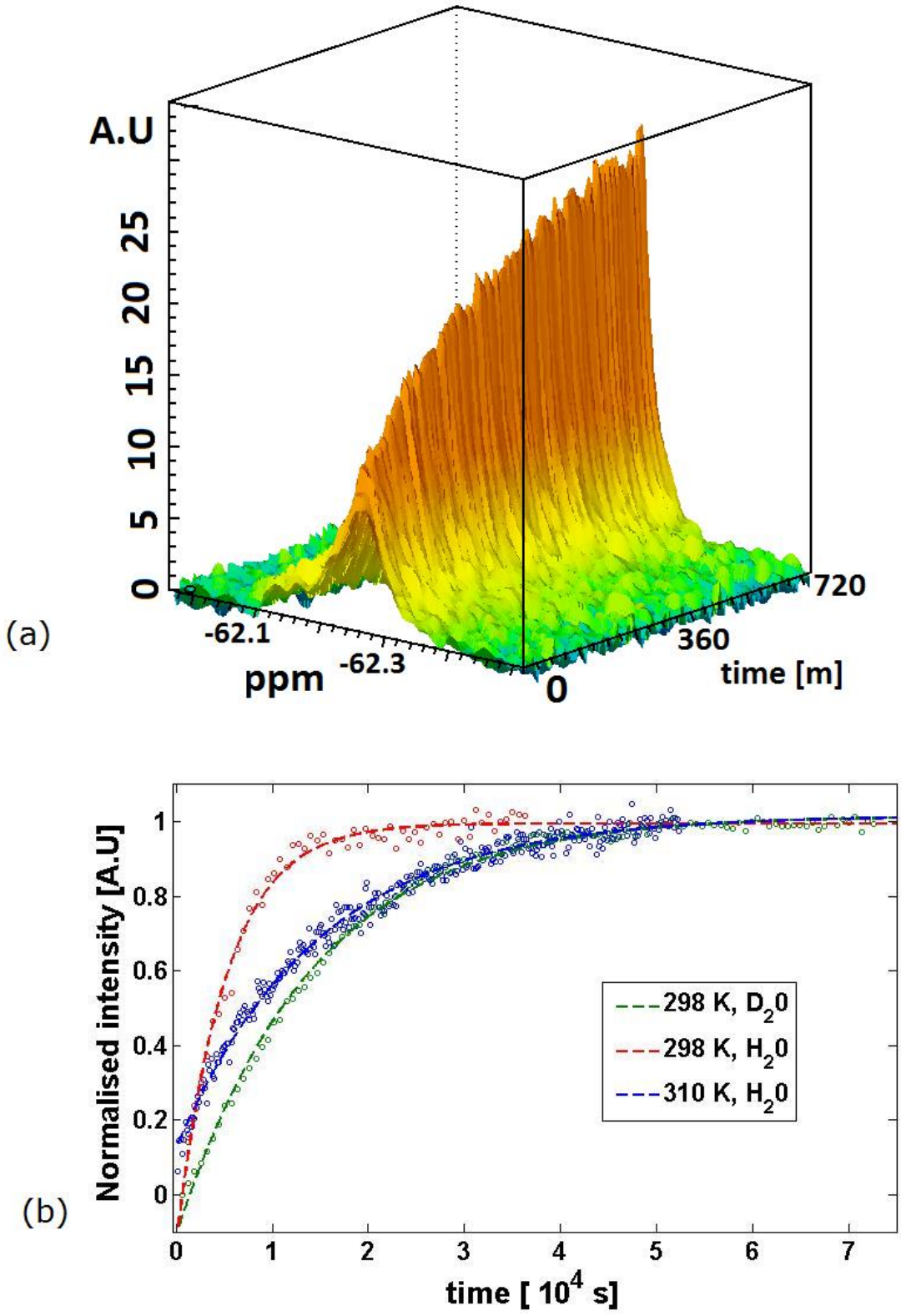

Figure 25: JK-X NMR time-courses comparison, A: 3D plot at 310K, B: a plot of normalised intensity vs. time for the incubation of JK-X with MMP-9 under all three conditions combined onto a normalised single plot

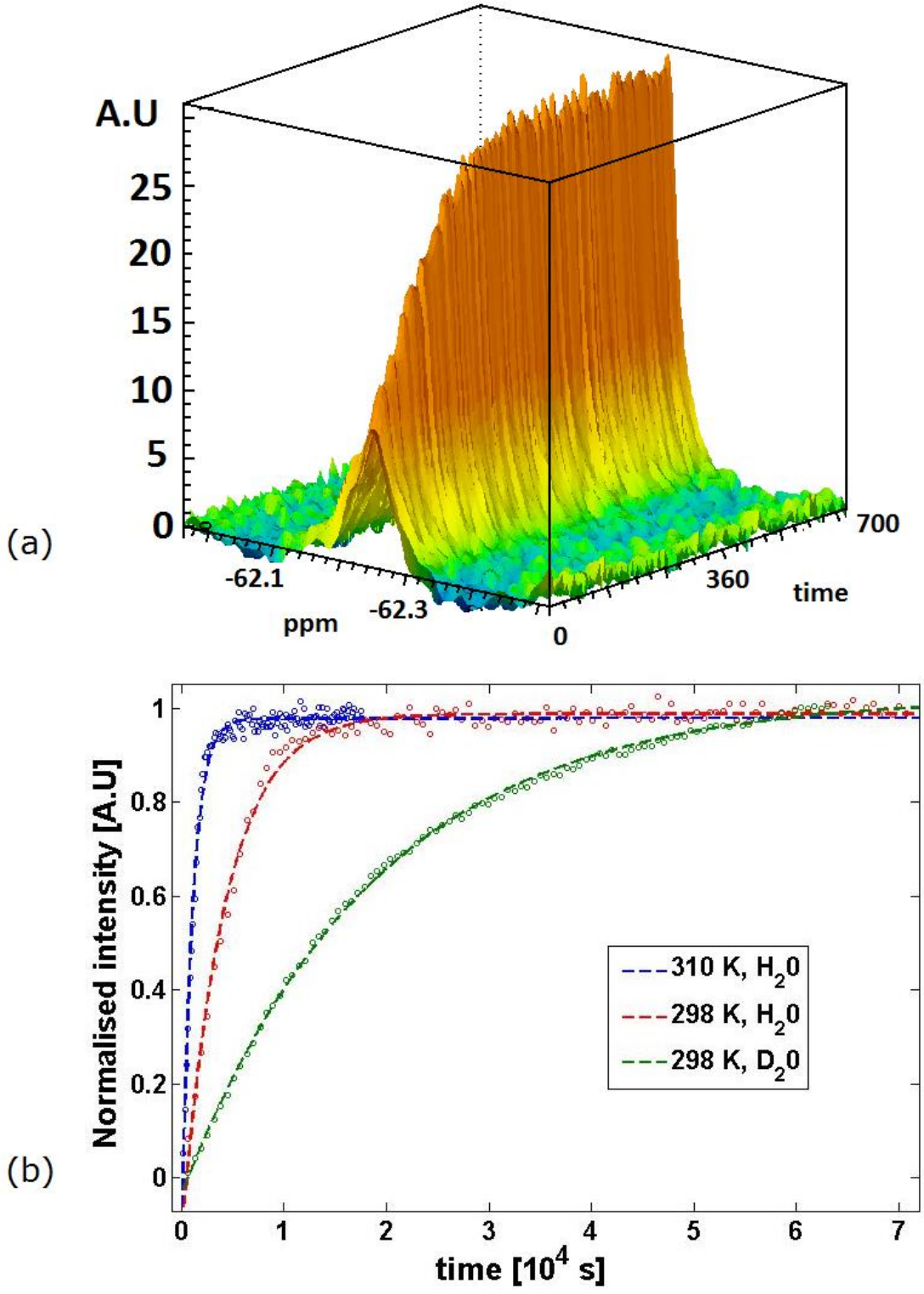

Figure 26: JK-2/9 NMR time-courses comparison, A: 3D plot at 310K, B: a plot of normalised intensity vs. time for the incubation of JK-X with MMP-9 under all three conditions combined onto a normalised single plot

3.11.4 In vitro quantification of NMR probes

In order to perform kinetic studies, absolute concentrations of the probes must be known. To this end, sodium fluoride at a known concentration was added to cleaved samples of the probes and the integration of the ^{19}F NMR peaks were used as a comparison to calculate the concentration of the cleaved probe. For example, 5 µL of a 51 mM sodium fluoride solution (21.3 mg in 10 mL H_2O), added to the 600 µL of probe gave a final concentration of 425 µM, the ^{19}F NMR integration of these spiked samples was then compared to the ^{19}F signal of the probe.

3.11.5 NMR probes, kinetic comparisons

To further compare the probes, the k_{cat}/Km values for each probe were calculated, under all three sets of experimental conditions as discussed previously (see Table 8). The enzyme efficiency, k_{cat}/K_M, of an enzymatic reaction is a measure of how efficiently an enzyme turns over its substrate, for the experiments detailed previously this is the cleavage of the NMR probes. The k_{cat} is the turnover number, i.e. the number of cleaved probes (per second) and K_M is a constant, defined as the substrate concentration at which the reaction is half of V_{max} (the maximum rate). This rate was calculated by converting the peak height data into a plot of the sensor concentration over time. A Michaelis-Menten based fitting was then applied using Lambert functions and least squares fitting to obtain the necessary parameters.

Probe	Solvent	Temp (K)	k_{cat}/ K_M ($M^{-1} s^{-1}$)
JK-X	100% D_2O	298	108
JK-X	90% H_2O, 10% D_2O	298	207
JK-X	90% H_2O, 10% D_2O	310	75.9
JK-2/9	100% D_2O	298	56.5
JK-2/9	90% H_2O, 10% D_2O	298	267
JK-2/9	90% H_2O, 10% D_2O	310	726

Table 8: kcat/K_M comparison of NMR probes

Initially the D_2O experiments were performed to establish a reliable method for further study, thereby eliminating a potential issue of the ^1H signal in H_2O interfering with the experiment. Prior to the NMR studies, it was believed that going to higher % amounts of H_2O and increased temperature would increase the rates of reaction, however, on comparing the data, this was not always the case.

Table 8 shows relative rates of reaction. It was observed that the **JK-2/9** probe was cleaved fastest at higher temperature and most efficiently by the MMP-9. The **JK-2/9** probe exhibited the expected reaction profile, at 298K the k_{cat}/ K_M showed that the enzyme was fivefold more efficient when using less D_2O. The **JK-X** probe at 298K followed a similar pattern, the enzyme was twice as efficient using less D_2O as solvent, possibly due to a change in the rate determining step. The most interesting and surprising result was achieved using the **JK-X** probe at 310K; at physiological temperature the **JK-X** probe was slower than at 298K, this was repeated (as with all the experiments detailed) which showed the result was reliable. It is possible that

the reason behind this unexpected result was that at higher temperature the broad-range probe may occupy a different conformation which is not as readily accepted by the MMP-9 as a substrate. When comparing this result to previous literature precedent using a FRET substrate with the same sequence, described by Knight *et al.*[112] the NMR probe had a significantly increased turnover time, an observation which could potentially be attributed to the Gd^{III}-DOTA chelate reducing the MMP-9 affinity for the NMR probe, see Table 9.

Table 9: Rate comparison of MRI probes to FRET probes

	Substrate/ sequence k_{cat}/ K_M ($M^{-1} s^{-1}$)			
Enzyme	Mca-PLGL-Dpa-A-R	Dnp-PLGLWAr	JK-X	JK2/9
MMP-1[a]	14,800	830	X	X
MMP-2[b]	629,000	58,000	X	X
MMP-7[a]	169,000	11,700	X	X
MMP-9[a]	X	X	207	267
MMP-9[b]	X	X	75.9	726
MMP-11[a]	23,000	3,200	X	X

Where [a] is 37 °C, and [b] is 25 °C. Mca, Dpa, Dnp are the FRET agents Knight *et al.*[112] used to label their peptide sequences, Dpa can be used as a replacement for tryptophan.

For an unknown reason **JK-3** was not accepted as substrate by MMP-3 and **JK-8** was not cleaved due to MMP-8 not being available. The **JK-1** probe does not have any

rate values as the probe was turned over so rapidly making it not possible to measure this correctly. Due to his result the JK-1 probe may (as with JK-29) be suitable candidate for further development for in vivo work, the rapi turnover is a highly desirable quality for such a probe as for an in vivo study the probe would be cleared at an unknown rate, therefore a rapid ""ON" signal would be beneficial. However, it should also be noted that if JK-1 is "too readily" turned over then the probe would deliver unreliable "ON" results. Conversely **JK-7** showed a very slow cleavage profile (too slow to plot for the rate data) possibly due to its amino acid chain length in comparison to the other probes.

3.11.6 Relaxation times; elucidation of T_1 and T_2*

To determine the T_1 values for the probes, a calibration curve of intensity vs. time was produced. An inversion recovery experiment was designed to measure the T_1 values for each of the probes both before and after cleavage. The experiment used between 14 (pre) and 28 (post) inversion times, with a repetition of up to 8 seconds, depending on whether it was pre or post-cleavage. The curve fitting was performed on Matlab (The Mathworks Inc, Nattick, MA) and R (version 3.1.3) as detailed in the following section, with assistance from Alexander Taylor (School of Medicine, UoN) and Dr. Huw Williams (School of Chemistry, UoN), using a two component model, given by Equation 11.

$$(I = 1 - a(be^{-\frac{t}{c}} - (1-b)e^{-\frac{t}{d}})$$

Equation 11: Two component fitting equation

Where *I* is the signal intensity, *t* is time, *a* and *b* are constants and *c* and *d* represent T_1 components. Deconvolution of the NMR data obtained showed that two different compounds were contributing to the ^{19}F peak which was measured; both were affected during the cleavage reactions.

The rationale for a two component fit originates in the mixture of cleaved and uncleaved or unknown ^{19}F signals. Spectrally the two signals cannot be resolved, and are observed as a broad component at the base of the 'sharp' peak. When using the inversion recovery experiment, the measurement is achieved using peak intensity, as the two separate components are non-resolvable, a superimposition is observed therefore it is not possible to fit to single component (as you would expect) for the pre-cleaved probes, it is however possible for the cleaved probes.

The inversion recovery experiments were then performed on all of the probes in their pre-cleaved state, and post cleavage for **JK-X**, **JK-1**, **JK-2-/-9**, and **JK-7**. **JK-3** and **JK-8** were not cleaved enzymatically, as such they do not have post-cleavage times. Plotting of the data was performed in Matlab and inversion recovery plots were generated by Alexander Taylor.

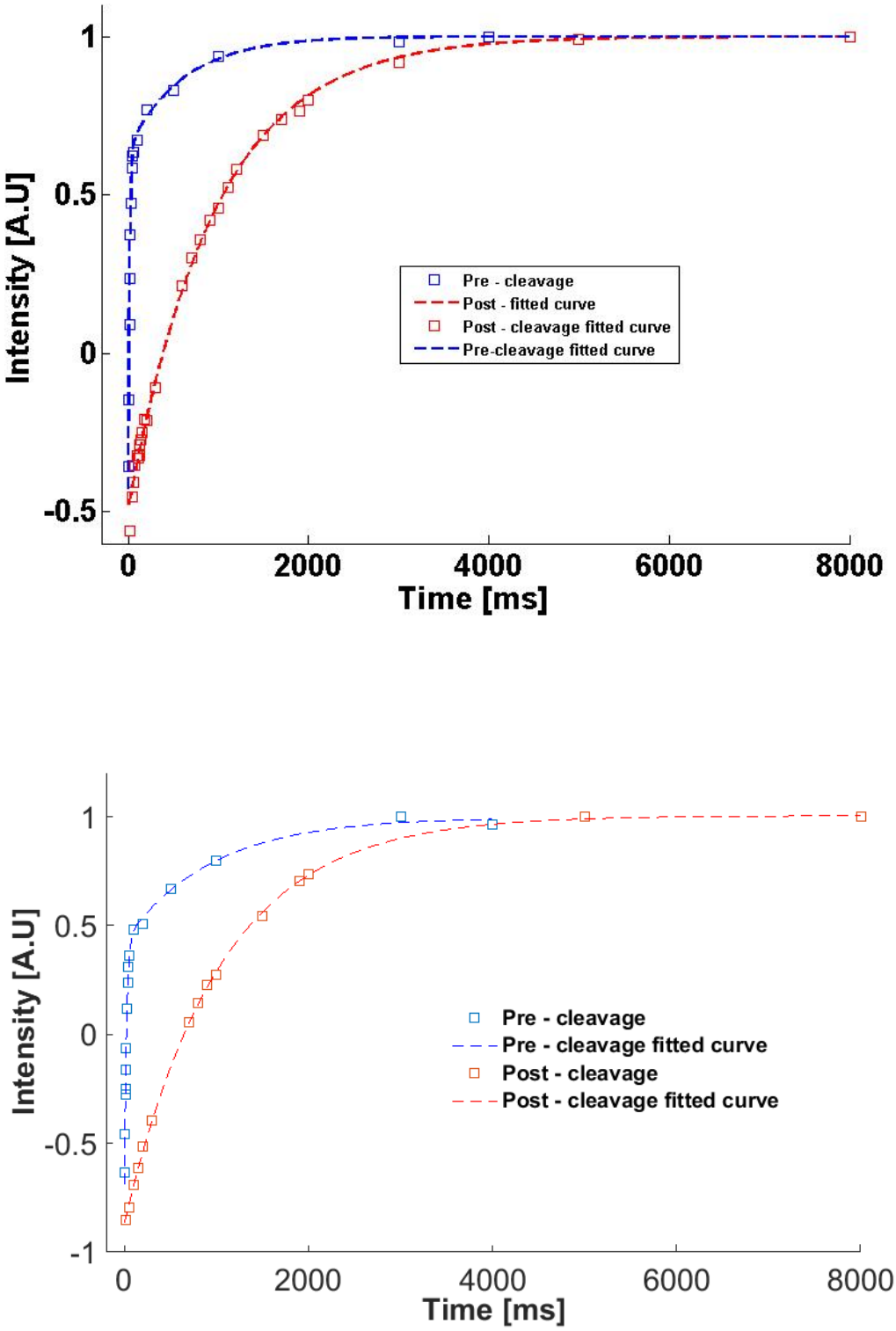

Figure 28: JK-1 inversion recovery plots

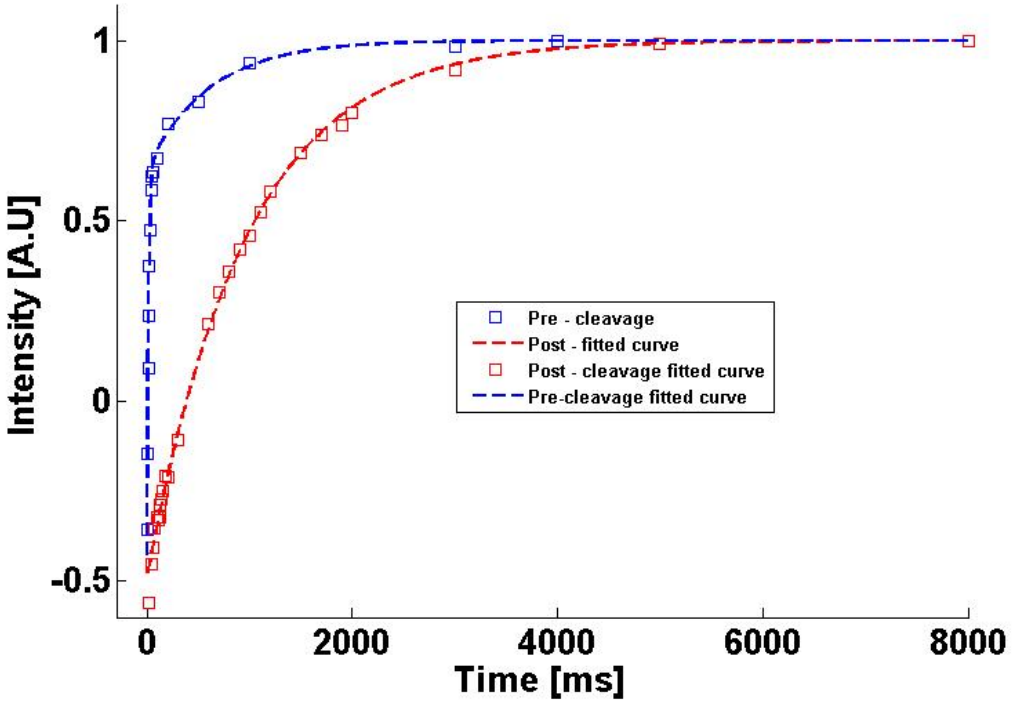

Figure 29: JK-2-9 inversion recovery data plot

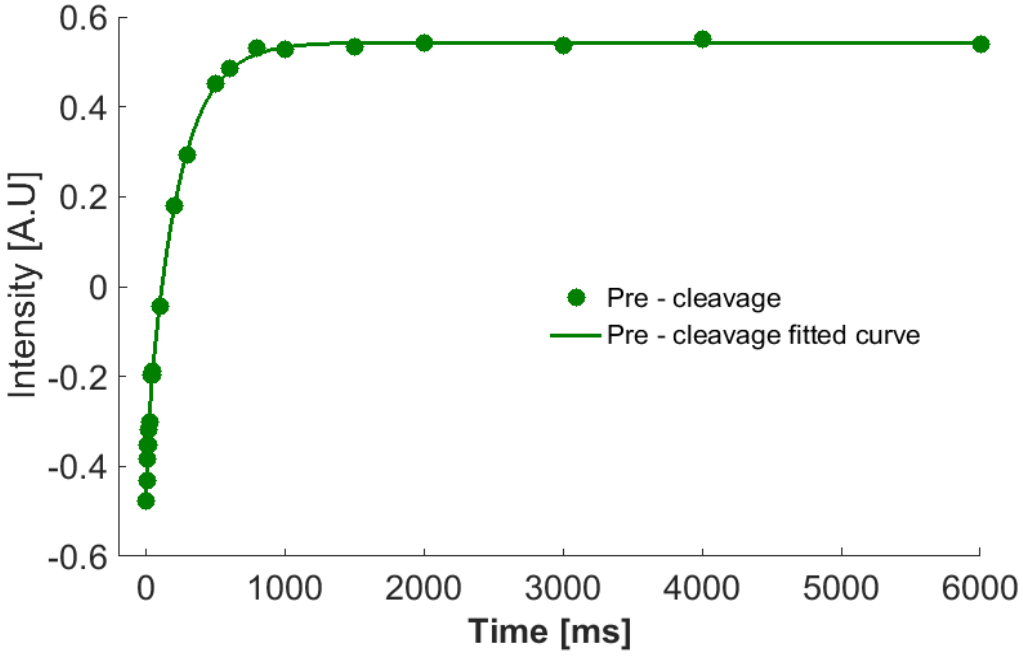

Figure 30: JK-3 inversion recovery plot

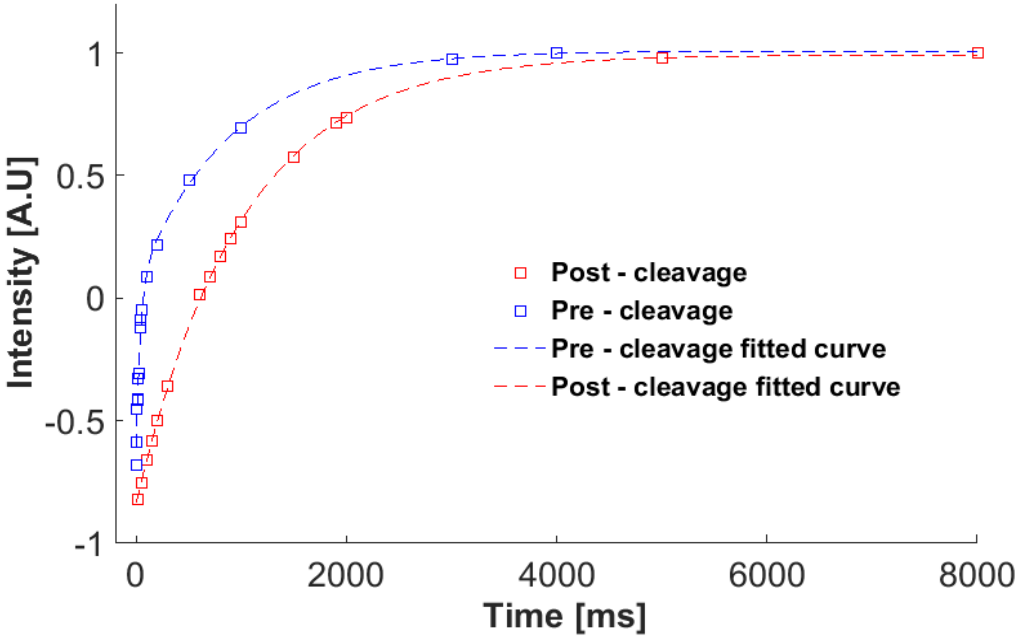

Figure 31: JK-7 inversion recovery plots

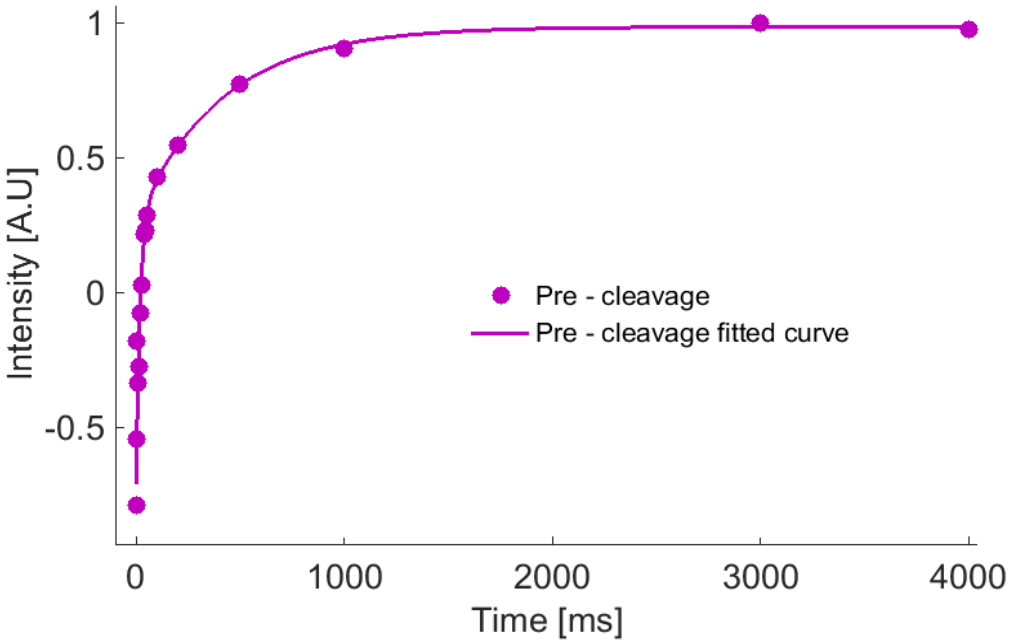

Figure 32: JK-8 inversion recovery plot

Table 10: Probe T_1 and T_2^* values

Probe	Cleavage state	T_1(ms)	T_2*(ms)
JK-X	Pre	12.8	3.4
JK-X	Post	960	13.8
JK-1	Pre	14.7	3.7
JK-1	Post	1040	10.0
JK-2/9	Pre	15.1	3.8
JK-2/9	Post	961	9.4
JK-3	Pre	17.2	3.9
JK-7	Pre	29.5	5.6
JK-7	Post	1003	11.2
JK-8	Pre	18.5	3.8

With these T_1 values in hand the fluorine linewidth was then used as a measure of the T_2*, as given by Equation 12.

$$T_2^* = (\pi \Delta v)^{-1}$$

Equation 12: Linewidth to T_2*

Where Δv is the linewidth of fluorine peak at FWHM. As such, as the linewidth increases, T_2* decreases.

3.11.7 Relaxation times; comparisons of T_1 and T_2*

The changes in both longitudinal and transverse relaxation times show the effect of the Gd^{III} ion on the system. The T_1 value of the probes changes between on and off modes by a factor of 75 for **JK-X**, and by a factor of 64 for **JK-2/9**. The T_1 values achieved all show a similar trend of approximately one second post cleavage, and with the exception of **JK-7** a pre-cleavage time of below 20 ms. **JK-7** had the longest T_1 pre-cleave most probably due to it containing an additional amino acid in comparison to the other sequences, thereby increasing the distance between the Gd^{III} and the ^{19}F reducing the pseudo contact shift.

The T_2* was affected to a lesser extent, resulting in approximately a one order of magnitude change, as expected for Gd^{III}.

Relaxometry data for the probes can be found in Table 11, which lists the T_1, FWHM, T_2^* values for all of the pre-cleaved probes as well as the probes post-cleavage, with the exception of **JK-3** and **JK-8**. Only the pre-cleavage data was achieved for **JK-3** and **JK-8**, this was due to **JK-3** not being cleaved by prepared samples of MMP-3, after multiple attempts. **JK-8** was not cleaved as MMP-8 was not available.

Table 11: ^{19}F MMP MRI probe relaxometry data

Full structure	Probe name	T_1 (ms)	T_1 cleaved (ms)	FWHM (Hz)	FWHM cleaved	T_2^* (ms)	T_2^* cleaved (ms)
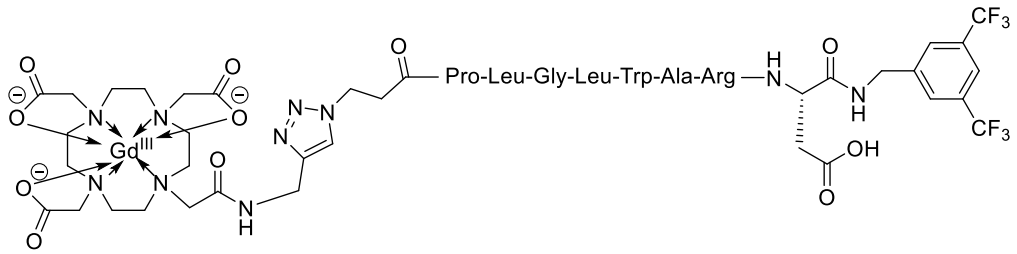	**JK-X**	12.8	960	53	13	3.4	13.8
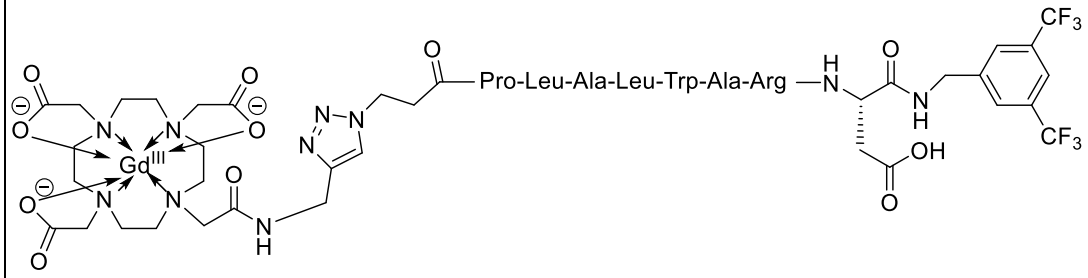	**JK-1**	14.7	1.040	48	18	3.7	10.0

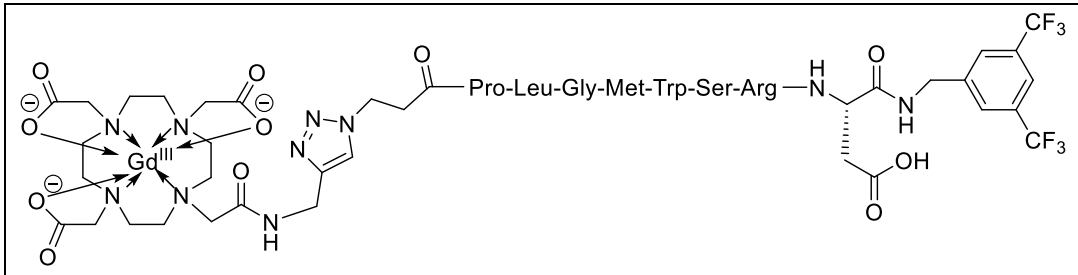	**JK-2/9**	15.1	961	47	19	3.8	9.4
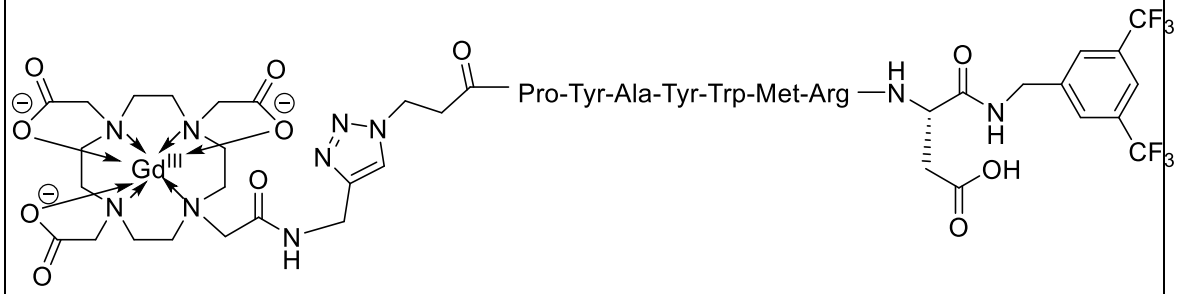	**JK-3**	17.2	X	46	X	3.9	X
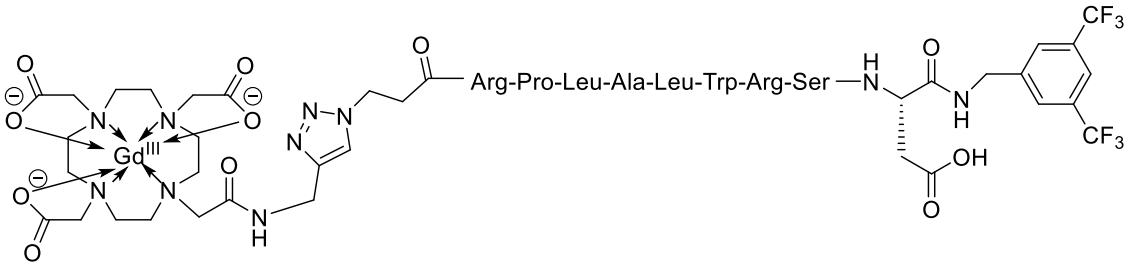	**JK-7**	29.5	1.003	32	16	5.6	11.2

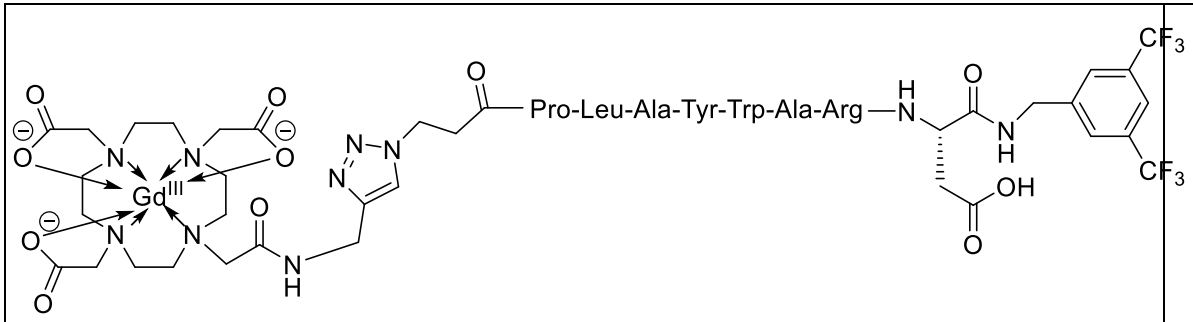	**JK-8**	18.5	X	47	X	3.8	X

3.11.8 In vitro MR imaging of JK-X

All MRI studies were conducted in the Sir Peter Mansfield Imaging Centre, UoN, in the laboratory of Prof. Thomas Meersmann, on a wide bore AV(III) 400 MHz Bruker spectrometer, using a 25 mm fluorine volume coil, with sample in a Wilmad 535-PP-7 NMR tube. Fast low angle shot (FLASH) is a sequence used to reduce the amount of time taken to take an MR image. A FLASH image was taken (for both) before and after incubation with the MMP (using a repetition time (TR) of 5000 ms, echo time (TE) of 10 ms, acquisition time of 22 hours and 45 minutes, number of scans (NS) of 128, and a post processing zero filling to a 64 x 64 matrix size). The image of **JK-X** post-cleavage can be seen in Figure 33, unfortunately an image was not obtained for the pre-cleaved probe.

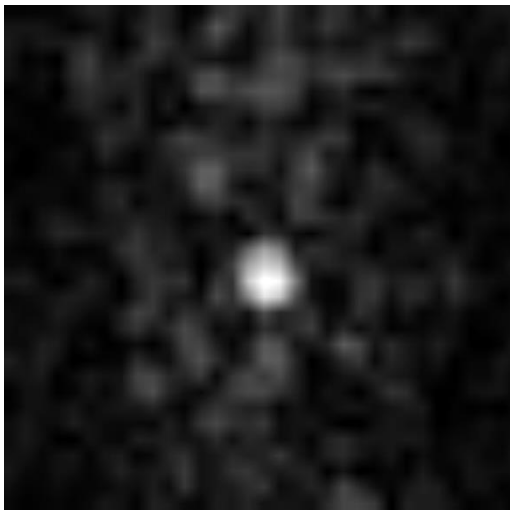

Figure 33: MRI of JK-X post-cleavage with MMP-9

The signal to noise ratio (SNR) is defined as the ratio of the signal intensity divided by the standard deviation of the intensity of a region with no signal (only noise). For the **JK-X** probe post-cleavage an SNR of 14.89 ± 1.1 was achieved, which is in line with similar works.[36]

In order to compare the sensitivity of different NMR/ MRI spectrometer a single scan on a test sample can be performed, then direct comparison of the SNR achieved in the experiment shows the variance in sensitivity. To this end an α,α,α-trifluorotoluene in d6-benzene was used to compare the SNR of 5mm probe in the AV(III) 600 MHz spectrometer used for the time-course work described previously, and the wide bore probe fitted into the AV 400 MHz spectrometer used for the MR imaging. The SNR for the AV(III) 600 MHz was 100 off a single scan, compared to the AV 400 MHz which achieved an SNR of 3, however, the SNR achieved is not linear with time using NMR so in order to achieve the same SNR a substantial increase in the number of scans would be required.

3.12 Fluorine alternative: ^{129}Xe@cryptophane

The sensitivity issues associated with ^{19}F NMR/MRI led to the investigation of an alternative spin ½ nuclei. Xe has multiple stable isotopes, ^{129}Xe is one of these which is NMR active. A process called hyperpolarisation is used in conjugation with ^{129}Xe NMR, this process pushes all of the ^{129}Xe nuclei into a high energy state, because all of the nuclei enter this state a hugely increased signal is observed by NMR. ^{129}Xe has a large chemical shift range, when temporarily encapsulated in a cryptophane cage this signal shifts, modifications to the cryptophane then cause further shifts in the ^{129}Xe spectrum. In order to exploit the enhanced sensitivity; a cryptophane cage was required.

3.12.1 Design of a cryptophane-Gd^{III} MMP probe

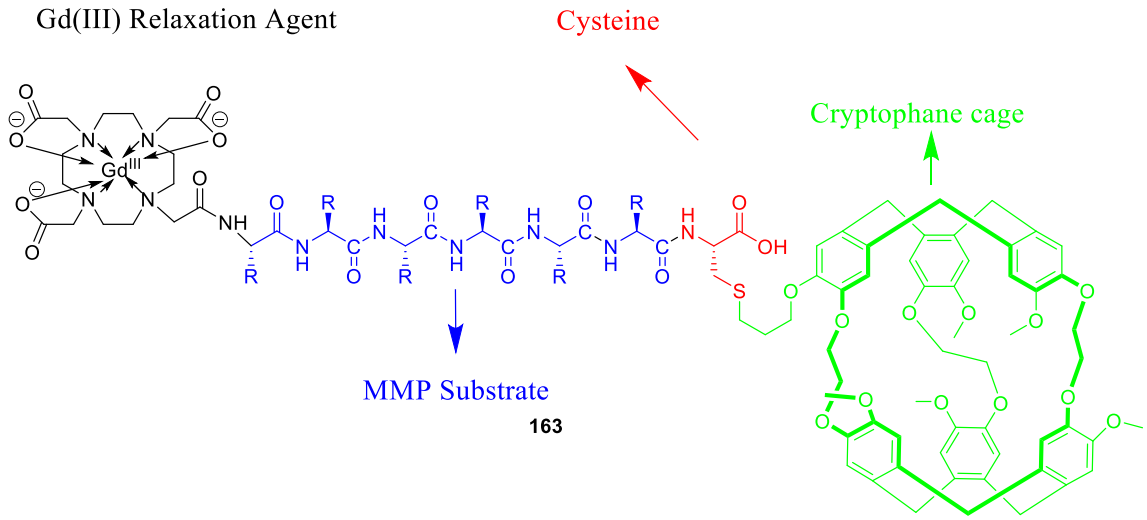

Scheme 51: Design of a ^{129}Xe@cryptophane-Gd^{III} MMP Probe

As described previously Wei *et al.* used alkyne-azide "click" chemistry to add a cryptophane cage onto a peptide sequence, with the ^{19}F probes the paramagnetic moiety was incorporated using this approach, therefore it cannot be used for the addition of a cryptophane instead an orthogonal methodology is required. It was envisaged that a thiol ene "click" reactions could instead be used, this approach uses a thiol group and an a alkene to form a thioether. To this end a cysteine would be required to at the carboxy terminus of a peptide, by using SPPS with a cysteine as the first loaded amino acid, the substrate sequence could then built onto the resin, finally the Gd^{III} DO3A alkyne would be attached as described for the ^{19}F MRI MMP probe. Following this step, the peptide would undergo hydrolysis from the resin and the protecting groups of the peptide also hydrolysed, resulting in a thiol capable of being used in the thiol ene reaction.

3.12.2 Synthesis of the cryptophane

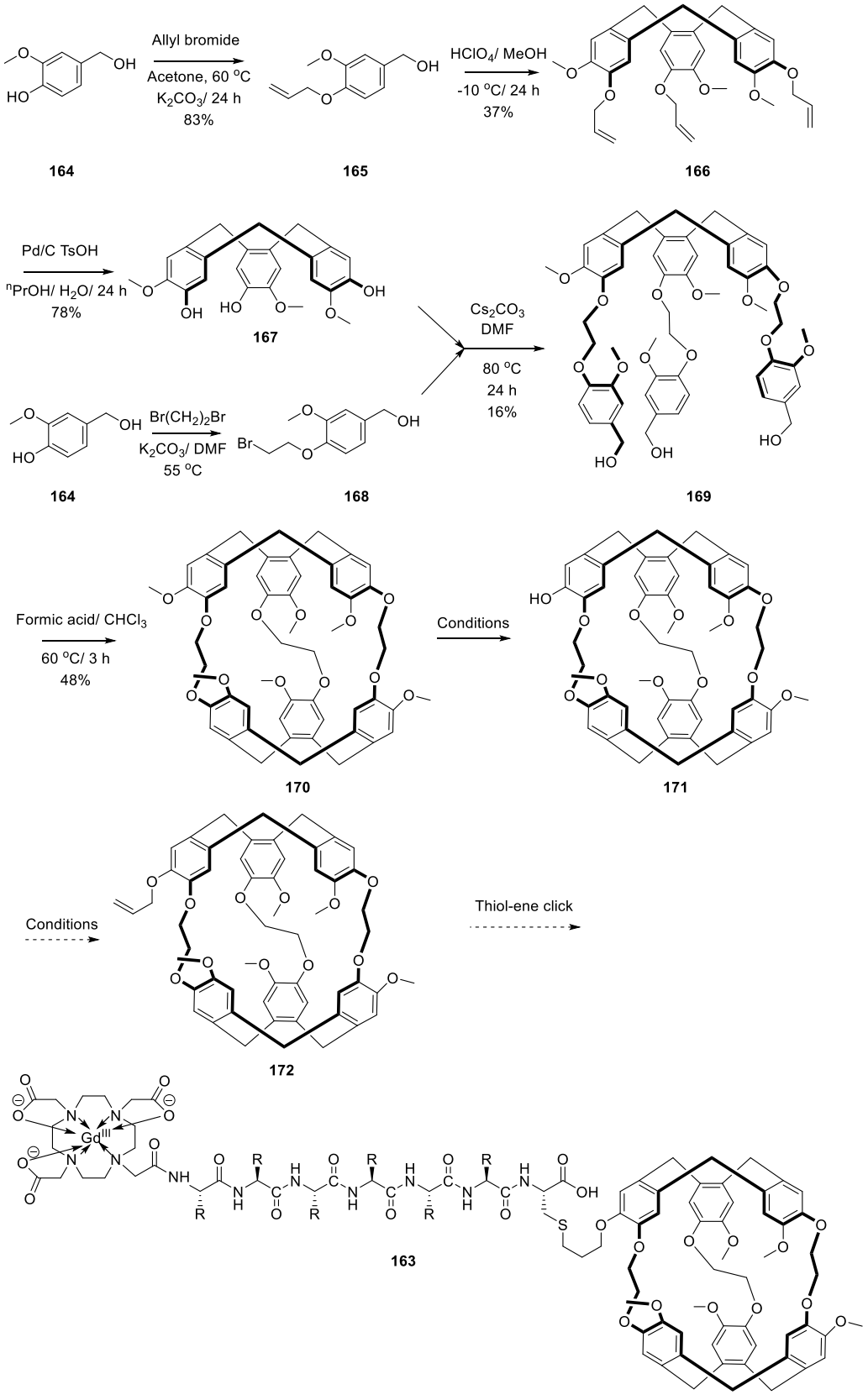

Scheme 52: Cryptophane synthesis

The synthesis of cryptophane was based upon current literature methods, and was modified when required.[77, 131] The first step involved the alkylation of the phenolic hydroxy instead of the benzylic alcohol on vanillyl alcohol **164** to form the protected allyl ether **165**, this was achieved by a selective deprotonation using a carbonate base, and purified *via* work up affording the ether in good yield. The protected vanillyl compound **165** was then dissolved in hypochloric acid to initiate an acid-mediated ring forming condensation reaction to form the northern hemisphere of a cryptophane cage **166** in high yield. With this half hemisphere **166** in hand, the following step was the reductive deprotection of the allyl protecting groups, which was achieved using a literature modified method palladium on charcoal, resulting in the triol **167** in a good yield. During these steps a vanillyl alcohol **164** was mono-alkylated with a large excess of 1,2-dibromoethane, which after column chromatography resulted in the bromo compound **168**. The alkyl-bromide **168** was then used to alkylate triol **167** to form open cryptophane **169** and purified using silica. The southern hemisphere of the cryptophane **170** was then formed using a similar acid-mediated ring closing condensation instead utilising formic acid to form the full cage. The following step was the mono-demethylation of one methyl ether to give alcohol **171**, which was performed in house.[73] This will then be followed by alkylation with allyl bromide which would result in the allyl-cryptophane **172**. Following the successful synthesis of allyl-crytophane **172** it could then be conjugated onto the cysteine of a Gd^{III}-DO3A labelled peptide using a thiol ene "click" reaction.

3.12.3 Proof of concept: ^{129}Xe bio-sensor design

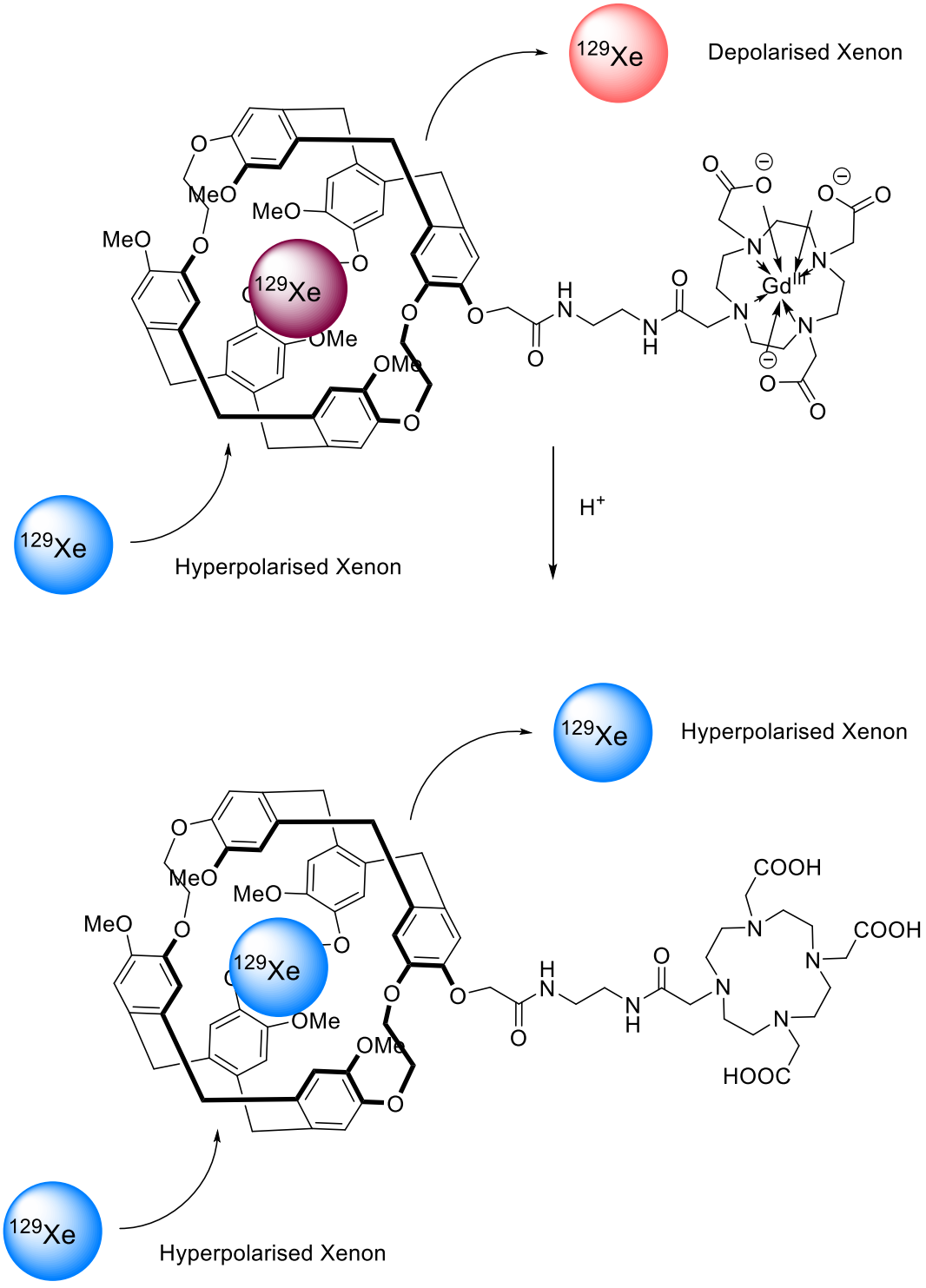

Scheme 53: Mode of action of ^{129}Xe NMR Probe

A ^{129}Xe based bio-sensor would has a different mechanism of action in comparison to the ^{19}F NMR probe described previously. Instead of imaging the signal of the ^{129}Xe inside of the cage, the free ^{129}Xe signal would be affected due to the high chemical exchange rate of free ^{129}Xe in solvent and within the cage, see Scheme 53. This high exchange rate then results in an accelerated rate of decay of the hyperpolarised ^{129}Xe signal. The publication containing this work be found within the Appendix of this work. This is not described here as the author only contributed to the synthesis of the ^{129}Xe probe and not with any following experiments.

3.13 Conclusions and Future work

The initial goal of this work was to design and synthesise four MMP activated ^{19}F MRI probes, with a view to perform ^{19}F NMR and MRI studies based on their proteolytic cleavage of the probes in question. Thus, the synthesis of a source of ^{19}F, with six ^{19}F nuclei was accomplished, furnishing a ^{19}F-labelled amino acid which was used to begin SPPS. Following this the paramagnetic unit was to be added. The first obstacle to this end was the addition of a paramagnetic unit (stabilised free radical, Gd^{III}-DOTA, or Gd^{III}-AAZTA based compound) onto the terminal amine of a proline residue, a problematic step which was eventually overcome by using "click" chemistry. The MRI MMP probes were then purified using semi-preparative HPLC. Once a method was established, four probes were synthesised and purified; this was then applied to two additional sequences, also containing terminal proline residues.

The initial four MRI MMP probes were successfully shown to be substrates for the corresponding MMPs using mass spectroscopy; following these steps the NMR testing of the probes began. Using an AV(III) 600 MHz NMR spectrometer the probes were successfully tested, showing expected activity profiles, although slightly slower than originally anticipated. The ^{19}F NMR peaks prior to cleavage were broad as expected, due to the PRE of the Gd^{III}, whilst their cleaved counter-parts were sharp singlets, indicative of the increased distance between the ^{19}F and Gd^{III} nuclei. With these proofs of principle in hand the following step was to undergo MRI experiments.

The key difference between NMR and MRI experimentally is the sensitivity of the techniques, whilst ^{19}F NMR in a AV(III) 600 MHz spectrometer is very sensitive to a µM concentration, the move over to an AV(III) 400 MHz spectrometer presents an obvious drop in sensitivity, with the increase in bore sizes from 5mm to 25mm further effecting the sensitivity, an issue currently affecting this project.

The first ^{19}F MRI was performed in 1973, four years after ^{1}H MRI was first used, the main obstacle within this field is the inherent lower sensitivity of ^{19}F MRI. This decrease in sensitivity is the main obstacle for ^{19}F MRI vs. ^{1}H MRI, in order to advance the area from an *in vivo* perspective; improvements in the imaging equipment are required. Once developments in the equipment are achieved ^{19}F MRI will become more of a clinical possibility.

An alternative approach to tackle the sensitivity issue with ^{19}F MRI is a synthetic modification; the limiting factor behind such probes as those described previously is the ^{19}F signal, therefore, by increasing the number of equivalent ^{19}F nuclei on the probe the signal would increase, reducing also the time required to perform MRI experiments. Currently the probes synthesised contains six equivalent ^{19}F nuclei, the future of this project would be to continue the work on increasing this by such methods as those shown in Scheme 18. It is however, important that highly fluorinated compounds do not then make the final probe soluble in water.

Table 12 shows the peptide sequences used for the probing of MMPs, with the probes synthesised in this work, the peptide sequence can be completely changed,

as a result any protease with a recognition sequence of seven amino acids or less can be explored using this approach. As the peptide sequence decreases in length the Gd^{III} PRE would increase, therefore other enzymes could be used for similar future proteolytic studies.

Table 12: MMP selective peptides

Sequence	Substrate for MMP
Pro-Leu-Gly-Leu-Trp-Ala-Arg[112]	General
Pro-Leu-Ala-Leu-Trp-Ala-Arg[113]	MMP-1
Pro-Leu-Gly-Met-Trp-Ser-Arg[114]	MMP-2/9
Pro-Tyr-Ala-Tyr-Trp-Met-Arg	MMP-3
Arg-Pro-Leu-Ala-Leu-Trp-Arg-Ser[115]	MMP-7
Pro-Leu-Ala-Tyr-Trp-Ala-Arg	MMP-8

To briefly summarize, six peptide based bio-sensors for ^{19}F NMR/MRI were designed, synthesised, and purified, and tested *in vitro*. These probes consist of three separate regions: the signal source, an MMP peptide substrate, and a paramagnetic modulator of the NMR signal. The probes were incubated with MMPs and their rate of activity on the probes measured from NMR studies, elucidating rate constants. These probes were then taken forward for MRI studies; however, poor sensitivity of the MRI systems led to the project not progressing further into cell line or mouse models. Future work on addressing this sensitivity issue is required to push this area of work forward into an *in vivo* system.

Chapter 4 - General experimental

Commercial reagent grade and HPLC grade solvents purchased from Fischer Scientific® were used for all reactions, DMF (peptide synthesis grade) was supplied by Rathburn Chemicals Ltd, anhydrous DMF was purchased from Sigma Aldrich®. All reagents were purchased from either Sigma Aldrich®, Alfa Aesar®, Merck Chemicals Ltd, or Strem Chemicals Inc.

Chemical shifts (δ) are given in parts per million (ppm) and *J* values in Hertz (Hz). Multiplets are designated by the following notations: singlet (s), doublet (d), triplet (t), quartet (q), multiplet (m). All ^{1}H NMR spectra were recorded on Bruker™ AV400, AV(III)400, or DPX 400 spectrometers at 400 MHz, or AV(III)500 at 500 MHz and at ambient temperature. Spectra were recorded in solutions of deuterated chloroform ($CDCl_3$, δ_{solv} = 7.26), deuterated methanol (CD_3OD, δ_{solv} = 3.31), deuterated water (D_2O, δ_{solv} = 4.79), or deuterated DMSO ($(CD_3)_2SO$, δ_{solv} = 2.50).[132] All ^{13}C NMR spectra were recorded on Bruker™ AV400, AV(III)400, or DPX 400 spectrometers at 100 MHz, or AV(III)500 at 125 MHz and at ambient temperature. All spectra were recorded relative to residual solvent peaks. Spectra were recorded in solutions of deuterated chloroform ($CDCl_3$, δ_{solv} = 77.1), deuterated methanol (CD_3OD, δ_{solv} = 49.0), deuterated water (D_2O, δ_{solv} = no signal), or deuterated DMSO ($(CD_3)_2SO$, δ_{solv} = 39.5).[132] All ^{19}F NMR spectra were recorded on a Bruker™ AV(III)400, or DPX 400 spectrometer at 376 MHz and at ambient temperature. Assignments were based on DEPT 90, DEPT 135, and HMQC spectra. High field NMR work was performed on a AV(III) 600 MHz or an AV(III) 800 MHz spectrometer. High field ^{19}F NMR was

performed solely on the AV(III) 600 MHz which was fitted with an fluorine observe probe.

High resolution mass spectroscopy (HRMS) was recorded on a Bruker^{TM} microTOF, an orthogonal Time of Flight instrument with electrospray ionisation (ESI, both positive and negative ion) sources as indicated. Values of mass to charge ratio (m/z), are given to four decimal places. The mass of the counter ions are H^+ 1.0078, and Na^+ 22.9898.

Infared spectroscopy was recorded on either a Thermo Scientific NICOLET IR200 FT-IR infared spectrometer, with samples prepared as a nujol mull on NaCl discs or as KBr discs. Solution IR was recorded on a Bruker Tensor 27 FT-IR instrument using spectroscopic grade chloroform or methanol.

UV spectroscopy to monitor amino acid resin loadings was measured on either a Cary 100 Bio UV-visible spectrophotometer, or a WPA lightwave set to 290 nm.

Thin layer chromatography was performed using Merck Kieselgel 60 F_{254} plates. Visualisation was by UV light and staining with phosphomolybdic acid (PMA) or ninhydrin with heating. Flash column chromatography was performed using Merck Kieselgel silica gel 60 Å, 230-400 mesh, 40-63µm, unless otherwise stated.

Melting points were determined on a Stuart Scientific melting point apparatus (SMP3), values are given in degrees Celsius (˚C) and are uncorrected.

Solid phase peptide synthesis was performed using a NovaSyn®gem Peptide Synthesiser set to a flow rate of 2.8 mL/min, attached to a Gilson 115 UV detector to monitor Fmoc absorbance at 290 nm. All resins were loaded into Omnifit Ltd Solventplus 10 mm x 100 mm Columns.

All HPLC was run an Agilent 1200 series system. Analytical HPLC was performed using an Agilent Eclipse XDB-C18 analytical column 4.6 x 150 mm, with a 5 µm pore size. Semi-preparative HPLC was performed using either an Agilent Eclipse XDB-C18 semi-preparative column 9.4 x 150 mm, with a 5 µm pore size, or an Agilent Eclipse XDB-C18 semi-preparative column 9.4 x 250 mm, with a 5 µm pore size. Solvent A was 0.1% formic acid in milli Q water, and solvent B was 0.1% formic acid in HPLC grade acetonitrile.

Chemical names were generated using ChemBioDraw 12.0, ChemBioDraw 13.0 or ChemBioDraw 14.0.

Gadolinium complexes were characterised using HRMS only. ^{1}H NMR and ^{13}C NMR are not recorded for gadolinium complexes and only the final probes have been characterised using ^{19}F NMR due to their paramagnetic nature.

Organic azides, especially small organic azides are potentially explosive as such they must be handled very carefully. The organic azides prepared in this thesis were only produced on small scale, not isolated in a concentrated form for an extended period

and stored in solution at -20 °C. Heat, halogenated solvents and acids should be avoided when using sodium azides and organic azides.

All peptide coupling agents have been written as their associated shortened name:

CDI - Carbodiimidazole

DCC - *N,N'*-Dicyclohexylcarbodiimide

EDC - 1-Ethyl-3-(3-dimethylaminopropyl) carbodiimide

PyOxim - [Ethyl cyano(hydroxyimino)acetato-O2) tri-1-pyrrolidinylphosphonium hexafluorophosphate

Fluorinated section syntheses

Synthesis of sodium 1,1,1,3,3,3-hexafluoro-2-(trifluoromethyl)propan-2-olate (66)[133]

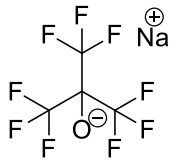

Sodium hydroxide (50.0 mg, 1.25 mmol, 1.0 eq.) and nonafluorotertbutanol **65** (260 mg, 1.10 mmol, 1.0 eq.) in water (3 mL) was stirred at 0 ˚C for 1 hour, followed by an 18 hour stir. The mixture was then lyophilized to yield the *sodium oxide* as a white powder (280 mg, quantitative). Mp. 102 ˚C; IR V_{max} (KBr solid)/cm^{-1} 1261 (C-O), 1198 (C-F), 1167 (C-F), 965 (C-F) cm^{-1}; ^{13}C NMR (100 MHz, MeOD) δ 123.2 (q, *J* = 293 Hz, 3 x CF_3), 83.0 (q, *J* = 27 Hz, Cq); ^{19}F NMR (376 MHz, MeOD) δ -76.9 (s, 3 x CF_3, 9F). HRMS (ESI) required for $C_4F_9O^-$ 234.9811 observed MH^- 234.9838.

Synthesis of 2-(2,2,2-trifluoroacetamido)acetic acid (74)[110]

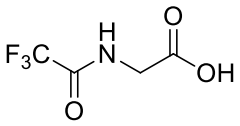

Glycine (1.10 g, 14.6 mmol, 1.0 eq.) in THF (25 mL) was stirred at 0 ˚C under a nitrogen atmosphere, trifluoroacetic anhydride (3.10 mL, 22.0 mmol, 1.5 eq.) was added dropwise and stirred for 30 minutes at 0 ˚C, before being warmed to ambient temperature and stirred for a further 45 minutes, and then concentrated *in vacuo*. Mixed solvent (15 mL, 1:1 petroleum ether(40/60): chloroform) was added and refluxed at 60 ˚C for 10 minutes and then cooled to ambient temperature and

filtered, to yield the *fluorinated acetamide* as a white wax (2.24 g, 90%). Mp. 108-110 ˚C (Lit. 117-118 ˚C);[110] IR V_{max} (Nujol)/ cm^{-1} 3323 (O-H), 3103 (N-H), 1711 (C=O), 1563 (C=O), 1182 (C-F); ^{1}H NMR (400 MHz, MeOD) δ 4.01 (s, 2H); ^{13}C NMR (100 MHz, MeOD) δ 40.3 (s, CH_2), 115.9 (q, J = 280 Hz, CF_3), 157.8 (q, J = 37 Hz, C=O), 169.1 (C=O). ^{19}F NMR (376 MHz, MeOD) δ -77.49 (s, 3F). HRMS (ESI) required for $C_4H_5F_3NO_3^+$ 172.0177 observed MH^+ 172.0225. HRMS (ESI) required for $C_4H_4F_3NO_3Na^+$ 194.0035 observed MNa^+ 194.0043.

Synthesis of (S)-tert-butyl 3-((((9H-fluoren-9-yl)methoxy)carbonyl)amino)-4-oxo-4-((4-(trifluoromethoxy)benzyl)amino)butanoate (57)[37]

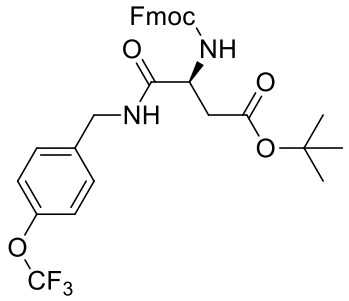

Fmoc-Asp-O^{t}Bu-OH **56** (90 mg, 0.22 mmol, 1.0 eq.), *p*-(trifluoromethoxy)benzylamine (37 uL, 0.24 mmol, 1.0 eq.), EDC (50 mg, 0.32 mmol, 1.2 eq.) and HOBt (40 mg, 0.3 mmol, 1.2 eq.) were dissolved in anhydrous dimethylformamide (2 mL) and stirred at 0 ˚C for 2 hours under argon, followed by a ambient temperature stir for 1 hour. The resulting mixture was then concentrated *in vacuo*, the crude product was dissolved in ethyl acetate (10 mL) before being successively extracted with sat. Na_2CO_3 (3 x 10 mL), 10% aqueous citric acid (3 x 10 mL), and brine (3 x 10 mL). The organic phase was dried with magnesium sulphate filtered and concentrated *in vacuo* to give the

amide as a white solid. Mp. 103-104 ˚C (Lit. not given). IR ($CDCl_3$): V_{max} = 3607, 1602, 1262; ^{1}H NMR (400 MHz, $CDCl_3$) δ 1.44 (s, 9H, -C(C*H*$_3$)$_3$), 2.63 (dd, *J* = 17.2, 6.8 Hz, 1H), 3.0 (dd, *J* = 17.2, 3.6 Hz, 1H), 4.22 (t, *J* = 6.8 Hz, 1H), 4.46-4.48 (m, 4H), 6.00 (d, *J* = 7.6 Hz, 1H), 6.70 (bs, 1H), 7.16 (d, *J* = 8.0 Hz, 2H), 7.28-7.3 (m, 4H), 7.4 (q, *J* =6.8 Hz, 2H), 7.57 (d, *J* = 7.6 Hz, 2H), 7.79 (m, 2H). ^{13}C NMR (100 MHz, $CDCl_3$) δ 28.0 (-C(*C*H$_3$)$_3$), 37.3 (CH_2), 42.8 (CH_2), 47.2 (CH), 60.4, 67.2 (CH_2), 82.1 (-*C*(CH$_3$)$_3$), 120.1 (Ar-CH), 121.2 (Ar-CH), 125.0 (Ar-CH), 127.1 (Ar-CH), 127.8 (Ar-CH), 128.9 (Ar-CH), 136.8 (Ar-Cq), 141.3 (Ar-Cq), 143.6 (Ar-Cq), 143.7 (Ar-Cq), 170.6 (C=O). ^{19}F NMR (376 MHz, $CDCl_3$) δ -57.90 (s, 3F). HRMS (ESI) required for $C_{31}H_{31}N_2O_6Na^+$ 607.5726 observed MNa^+ 607.2202. HRMS (ESI) required for $C_{31}H_{32}N_2O_6^+$ 585.2168 observed MH^+ 585.2202.

Synthesis of (S)-3-((((9H-fluoren-9-yl)methoxy)carbonyl)amino)-4-oxo-4-((4-(trifluoromethoxy)benzyl)amino)butanoic acid (58)[37]

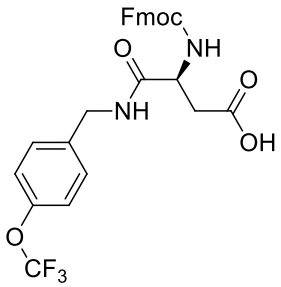

Ester **57** (130 mg, 0.220 mmol, 1.0 eq.) was dissolved in trifluoroacetic acid (2.0 mL, 26 mmol) and stirred for 2 hours at ambient temperature, the solution turned a bright yellow, before being concentrated *in vacuo*, to yield the acid as an off white solid. Mp. 174-177 °C (Lit. not given); IR (KBr): V_{max} = 3289, 1702 (C=O), 1651 (C=O);

^{1}H NMR (400 MHz, $CDCl_3$) δ 2.96 (m, 2H), 4.22 (t, *J* =6.8 Hz, 1H), 4.32-4.45 (m, 4H), 4.58 (t, *J* =6.8 Hz, 1H), 7.16 (d, *J* =8.0 Hz, 2H), 7.29 (t, *J* =7.2 Hz, 2H), 7.27-7.40 (m, 4H), 7.66 (d, *J* =7.2 Hz, 2H), 7.79 (d, *J* =7.6 Hz, 2H). ^{13}C NMR (100 MHz, MeOD) δ 35.6 (CH_2), 41.9 (CH_2), 47.0 (CH), 51.7 (CH), 66.8 (CH_2).119.5 (Ar-CH), 120.6 (Ar-CH), 124.8 (Ar-CH), 124.9 (Ar-CH) 126.8 (Ar-CH), 127.4 (Ar-CH) 128.6 (Ar-CH) 141.2 (Ar-Cq), 143.8 (Ar-Cq), 172.2 (C=O), 172.6 (C=O). ^{19}F NMR (376 MHz, $CDCl_3$) δ -57.90 (s, 3F). HRMS (ESI) required for $C_{27}H_{24}F_3N_2O_6^+$ 529.1542 observed MH^+ 529.1599. HRMS (ESI) required for $C_{27}H_{23}F_3N_2O_6Na^+$ 551.1406 observed MNa^+ 551.1417. HRMS (ESI) required for $C_{27}H_{22}F_3N_2O_6$ 527.1435 observed MH^- 527.1406.

Synthesis of (S)-tert-butyl 3-((((9H-fluoren-9-yl)methoxy)carbonyl)amino)-4-((3,5-bis(trifluoromethyl)benzyl)amino)-4-oxobutanoate (75)

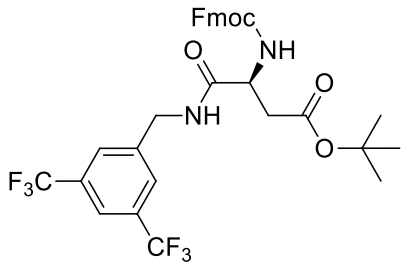

The title compound was synthesised using a procedure adapted from the literature.[37] Fmoc-Asp-OtBu-OH **56** (90 mg, 0.22 mmol, 1.0 eq.), 3,5-bis(trifluoromethyl)benzylamine (60 mg, 0.24 mmol, 1.0 eq.), EDC·HCl (40 mg, 0.25 mmol, 1.0 eq.) and HOBt (40 mg, 0.30 mmol, 1.2 eq.) were dissolved in anhydrous dimethylformamide (2 mL) and stirred at 0 ˚C for 2 hour under argon, followed by a ambient temperature stir for 1 hour. The resulting mixture was then concentrated *in vacuo*, the crude product was dissolved in ethyl acetate (10 mL) before being

successively extracted with sat. Na_2CO_3 (3 x 10 mL), 10% aqueous citric acid (3 x 10 mL), and brine (3 x 10 mL). The organic phase was dried with magnesium sulphate filtered and concentrated *in vacuo* to give the *amide* as a white solid. Mp. 98-101 ˚C. IR V_{max} (Nujol)/cm^{-1} 3286 (N-H), 1726 (C=O), 1686 (C=O), 1659 (C=O). ^{1}H NMR (400 MHz, $CDCl_3$) δ 1.46 (s, 9H, -C(CH_3)$_3$), 2.6 (dd, *J* = 16.8, 6.4 Hz, 1H), 3.0 (dd, *J* = 17.2, 3.6 Hz, 1H), 4.23 (t, *J* = 7.2 Hz, 1H), 4.49-4.51 (m, 5H), 6.0 (bs, 1H), 6.7 (bs, 1H), 7.28 (m, 2H), 7.4-7.42 (m, 2H), 7.8 (d, *J* = 7.6 Hz, 2H), 7.76-7.81 (m, 5H). ^{13}C NMR (100 MHz, $(CD_3)_2SO$) δ 28.1 (-C(*C*H_3)$_3$), 37.7 (CH_2), 42.0 (CH_2), 47.1 (CH), 52.1 (CH), 66.2 (CH_2), 80.6 (-*C*(CH_3)$_3$), 95.7 (CF_3), 120.6 (Ar-CH), 120.9 (Ar-CH), 122.5 (Ar-Cq), 125.2 (Ar-Cq), 125.7 (Ar-CH), 127.5 (Ar-CH), 128.1 (Ar-CH), 128.4 (Ar-CH), 130.6 (q, *J* = 33 Hz, Ar-Cq), 156.3 (C=O), 169.8 (C=O), 171.4 (C=O). ^{19}F NMR (376 MHz, $CDCl_3$) δ -62.79 (s, 6F). HRMS (ESI) required for $C_{32}H_{30}F_6N_2O_5Na^+$ 659.1957 observed MNa^+ 659.1942. HRMS (ESI) required for $C_{32}H_{31}F_6N_2O_5^+$ 637.2092 observed MH^+ 637.2130.

Synthesis of (S)-3-((((9H-fluoren-9-yl)methoxy)carbonyl)amino)-4-((3,5-bis(trifluoromethyl)benzyl)amino)-4-oxobutanoic acid (76)

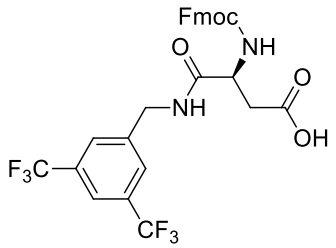

The title compound was synthesised using a procedure adapted from the literature.[37] Ester **75** (100 mg, 0.16 mmol, 1.0 eq.) was dissolved in trifluoroacetic acid (2.0 mL, 26 mmol) and stirred for 2 hours at ambient temperature, before being

concentrated *in vacuo* to yield the *acid* as a white solid. Mp. 216-219 ˚C. IR V_{max} (Nujol)/cm^{-1} 3266 (O-H), 1724 (C=O), 1655 (C=O), 1547 (N-H), 1376, 1293, 1175, 1126. ^{1}H NMR (400 MHz, MeOD) δ 2.76 (dd, 1H, C*H*$_2$COOH, *J* = 8.0 Hz, 16 Hz), 2.88 (dd, 1H, C*H*$_2$COOH, *J* = 8.0 Hz, 16 Hz), 4.25, (t, 1H, C*H*CH_2COOH, *J* = 8.0 Hz)4.36 (dd, 1H, CC*H*$_2$-Fmoc, J = 8.0 Hz, 12 Hz), 4.44 (dd, 1H, CC*H*$_2$-Fmoc, *J* = 8.0 Hz, 12 Hz), 7.31 (t, 2H, *J* = 8.0 Hz, Fmoc 2 Ar-H), 7.40 (t, 2H, *J* = 8.0 Hz, Fmoc 2 Ar-H), 7.67 (d, 2H, Fmoc 2 Ar-H), 7.80 (s, 1H, Bnz H), 7.82 (s, 1H, Bnz H), 7.84 (s, 1H, Bnz H), 7.92 (d, 2H, Fmoc 2 Ar-H, *J* = 4.0 Hz). ^{13}C NMR (100 MHz, $(CD_3)_2SO$) δ 36.5 (CH_2), 42.0 (CH_2), 47.1 (CH), 52.05 (CH), 66.3 (CH_2), 95.7 (CF_3), 119.8 (Ar-Cq), 120.6 (Ar-CH), 120.8 (Ar-CH), 122.5 (Ar-Cq), 125.2 (Ar-Cq), 125.7 (Ar-CH), 127.5 (Ar-CH), 128.1 (Ar-CH), 128.2 (Ar-CH), 130.6 (q, *J* = 32 Hz, Ar-Cq), 156.4 (C=O), 171.8 (C=O), 172.2 (C=O). ^{19}F NMR (376 MHz, MeOD) δ -64.24 (s, 6F, 2 C*F*$_3$). HRMS (ESI) required for $C_{28}H_{23}F_6N_2O_5^+$ 581.1466 observed MH^+ 581.1506. HRMS (ESI) required for $C_{28}H_{22}F_6N_2O_5Na^+$ 603.4649 observed MNa^+ 603.1331. HRMS (ESI) required for $C_{27}H_{21}F_3N_2O_6^-$ 579.4677 observed MH^- 579.1335.

Synthesis of tert-butyl (S)-3-((((9H-fluoren-9-yl)methoxy)carbonyl)amino)-4-((1,3-dihydroxy-2-(hydroxymethyl)propan-2-yl)amino)-4-oxobutanoate (79)

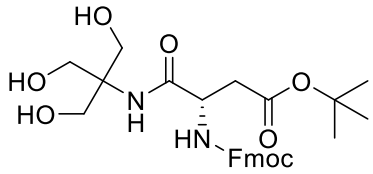

The title compound was synthesised using a procedure adapted from the literature. Fmoc-Asp-OtBu-OH **56** (296 mg, 0.576 mmol, 1.0 eq.), Trizma (107 mg, 0.884 mmol, 1.5 eq.), EEDQ (302 mg, 1.22 mmol, 2.0 eq.) were dissolved in ethanol (10 mL) and stirred under reflux at 78 ˚C for 20 hours. The residue was then purified using column chromatography (DCM: methanol, 100, 99:1, 98:2, 97:3, 96:4, 95:5) to give the *amide* as a white solid (rf.= 0.05 (DCM: methanol, 95:5), 301 mg, 81%). ^{1}H NMR (400 MHz, MeOD) δ 1.46 (s, 9H, -C(C*H*$_3$)$_3$), 2.61 (dd, *J* = 16.2, 8.0 Hz, 1H), 2.81 (dd, *J* = 16.2, 5.6 Hz, 1H), 3.72 (s, 6H), 4.24 (appt, *J* = 6.4 Hz, 1H), 4.38-4.40 (m, 2H), 4.51-4.55 (m, 1H), 7.30-7.34 (m, 2H), 7.38-7.42 (m, 2H), 7.65-7.68 (m, 2H), 7.80-7.81 (m, 2H). ^{13}C NMR (100 MHz, MeOD) δ 26.9 (-C(*C*H$_3$)$_3$), 37.2 (CH$_2$), 46.9 (CH), 52.2 (CH), 60.7 (CH$_2$), 62.0 (Cq), 66.9 (CH$_2$), 81.1 (-*C*(CH$_3$)$_3$), 119.5 (Ar-CH), 124.8 (Ar-CH), 124.8 (Ar-CH), 126.8 (Ar-CH), 127.4 (Ar-CH), 141.2 (Ar-Cq), 143.7 (Ar-Cq), 143.8 (Ar-Cq), 157.0 (C=O), 170.3 (C=O), 172.5 (C=O). HRMS (ESI) required for $C_{27}H_{35}N_2O_8^+$ 515.2388 observed MH^+ 515.2389. HRMS (ESI) required for $C_{27}H_{34}N_2O_8Na^+$ 537.2207 observed MNa^+ 537.2204.

Synthesis of tert-butyl (1,3-dihydroxy-2-(hydroxymethyl)propan-2-yl) carbamate (82)

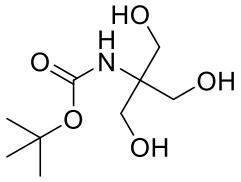

Trizma® **83** (6.66 g, 55.0 mmol, 1.0 eq.) was dissolved in methanol (180 mL), di-*tert* butyl bicarbonate (12.1 g, 55.5 mmol, 1.0 eq.) in methanol (40 mL) was then added over 30 minutes and stirred overnight at ambient temperature, before being concentrated *in vacuo* to yield the *protected amine* as a white solid (11.5 g, 95%). IR V_{max} (Nujol)/cm^{-1} 1683 (C=O); ^{1}H NMR (400 MHz, MeOD) δ 1.46 (s, 9H, -C(C*H*$_3$)$_3$), 3.71 (s, 6H, CH_2). ^{13}C NMR (100 MHz, MeOD) δ 27.3 (-C(*C*H$_3$)$_3$), 60.1 (Cq), 61.4 (CH_2), 79.2 (*C*(CH$_3$)$_3$), 156.7 (C=O). HRMS (ESI) required for $C_9H_{19}NO_5Na^+$ 244.1060 observed MNa$^+$ 244.1166. HRMS (ESI) required for $C_9H_{18}NO_5^-$ 220.1185 observed MH$^-$ 220.1181.

Synthesis of (S)-methyl 2-amino-3-hydroxypropanoate (68)[134]

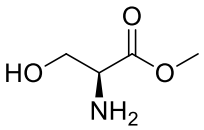

L-Serine (560 mg, 5.33 mmol, 1.0 eq.) in anyhdrous methanol (10 mL) was cooled to 0 ˚C and stirred under a nitrogen atmosphere. Acetyl chloride (3.31 g, 42.2 mmol, 8.0 eq.) was added dropwise, and then allowed to warm to ambient temperature and

stirred for 18 hours. Diethyl ether was added until no more precipitate formed and was filtered and collected, to yield the *methyl ester* as the hydrochloride salt (820 mg, quantitative). Mp. 160-162 ˚C (Lit. mp. not given). IR V_{max} ($CHCl_3$)/cm^{-1} 3386 (OH), 1743 (C=O); ^{1}H NMR (400 MHz, D_2O) δ 3.80 (s, 3H, C*H*$_3$), 3.94 (dd, 1H, *J* = 12, 4.0 Hz, C(H)*H*), 4.04 (dd, 1H, *J* = 12, 4.0 Hz, C(H)*H*), 4.22 (t, 1H, *J* = 4.0 Hz); ^{13}C NMR (100 MHz, D_2O) δ 53.7 (*C*H_3), 54.7 (*C*H), 59.2 (*C*H_2), 168.9 (C=O). HRMS (ESI) required for $C_4H_9NO_3Na^+$ 142.0480 observed MNa^+ 142.0463.

Synthesis of (S)-methyl 2-((((9H-fluoren-9-yl)methoxy)carbonyl)amino)-3-hydroxypropanoate (69)

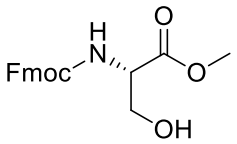

L-Serine(OMe) **68** (100 mg, 0.840 mmol, 1.0 eq.) was dissolved in a mixture of dioxane (5 mL) and sat $NaHCO_3$ (5 mL). Fmoc-Cl (350 mg, 1.40 mmol, 1.5 eq.) was added and stirred overnight. The mixture was then concentrated in *vacuo* and extracted using chloroform (3 x 10 mL) and water (10 mL) with the organic phase retained and then dried over sodium sulphate to give the *protected amine* as a clear oil (182 mg, 63%). IR V_{max} (Nujol)/cm^{-1} 1693w (C=O); ^{1}H NMR (400 MHz, MeOD) δ 3.57 (s, 3H, CH_3) 3.7 (s, 1H), 3.85 (d, *J* = 4.0 Hz, 2H, C*H*$_2$), 3.98 (t, *J* = 4.0 Hz, 1H, C*H*), 4.23-4.39 (m, 2H, C*H*$_2$), 7.21-7.27 (m, 2H, Ar-C*H*), 7.31 (t, *J* = 8.0 Hz, 2H, Ar-C*H*), 7.60 (d, *J* = 4.0 Hz, 2H, Ar-C*H*), (t, *J* = 8.0 Hz, 2H, Ar-C*H*); ^{13}C NMR (100 MHz, MeOD) δ 46.9 (CH), 50.2 (CH3), 56.5 (CH), 61.7 (CH2), 64.5 (CH2), 119.5 (Ar-CH), 124.8 (Ar-CH),

126.6 (Ar-CH), 127.1 (Ar-CH), 141.2 (Ar-Cq), 144.9 (Ar-Cq), 157.1 (C=O), 171.4 (C=O). HRMS (ESI) required for $C_{19}H_{19}NO_5Na^+$ 364.1161 observed MNa^+ 364.1146.

Radical containing compounds

Synthesis of 2-bromo-N-(1-oxyl radical-2,2,6,6-tetramethylpiperidin-4-yl)acetamide (94)

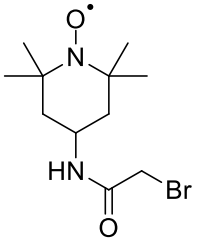

4-Amino-TEMPO **93** (25 mg, 0.15 mmol, 1.0 eq.) and bromoacetyl bromide (50 mg, 0.25 mmol, 1.7 eq.) were dissolved in anhydrous THF (0.75 mL) and stirred under a nitrogen atmosphere in darkness until all the 4-amino-TEMPO had been consumed, approximately 3 hours. The orange solution was then concentrated *in vacuo* protected in darkness at ambient temperature to yield the *bromo acetamide* as an orange wax. IR V_{max} (Nujol)/cm^{-1} 1660 (C=O). HRMS (ESI) required for $C_{11}H_{20}BrNNaO_2^+$ 314.0606 observed MNa^+ 314.0593. HRMS (ESI) required for $C_{11}H_{20}BrNNaO_2^+$ 316.0586 observed MNa^+ 316.0583.

Synthesis of 4-((1-oxy radical-2,2,6,6-tetramethylpiperidin-4-yl)amino)-4-oxobutanoic acid

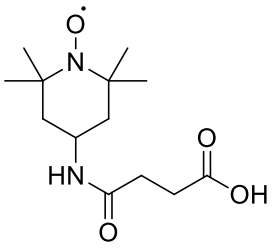

4-Amino-TEMPO **93** (23 mg, 0.14 mmol, 1.0 eq.) and succinic anhydride (13 mg, 0.13 mmol, 1.7 eq.) were dissolved in anhydrous THF (0.75 mL) and stirred under a nitrogen atmosphere in darkness until all the 4-amino-TEMPO had been consumed, approximately 3 hours. The orange solution was then concentrated *in vacuo* protected in darkness at ambient temperature to yield the *acid* as an orange wax. IR V_{max} (Nujol)/cm^{-1} 1705 (C=O), 1641 (C=O). HRMS (ESI) required for $C_{13}H_{24}N_2O_4^+$ 272.1736 observed MH^+ 272.1706. HRMS (ESI) required for $C_{13}H_{22}N_2O_4^-$ 270.1580 observed MH^- 270.1574.

Synthesis of 2,2,6,6-tetramethyl-4-(prop-2-yn-1-ylamino)piperidin-1-oxy radical and 4-(di(prop-2-yn-1-yl)amino)-2,2,6,6-tetramethylpiperidin-1-oxy radical

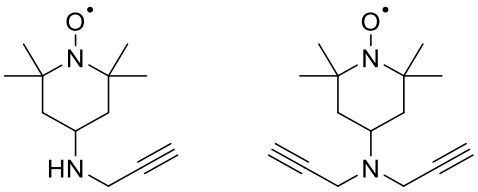

4-Amino-TEMPO **93** (116 mg, 0.678 mmol, 1.0 eq.) was dissolved in 5 mL of acetonitrile; potassium carbonate (163 mg, 1.18 mmol, 2 eq.) was added to give a white suspension that was stirred for 15 minutes under a nitrogen atmosphere. To this propargyl bromide (105 mg, 0.897 mmol, 1.1 eq.) as an 80% solution in toluene was added and stirred under a nitrogen atmosphere in darkness until all the 4-amino-TEMPO had been consumed, approximately 3 hours. The orange solution was then concentrated *in vacuo* protected in darkness at ambient temperature. The residue was then purified using column chromatography (petroleum ether 40/60: ethyl acetate, 2:8) to yield the mono alkylated product as an orange wax (rf.= 0.25, 79 mg)., and the di-alkylated product as an orange wax (rf.= 0.75, 10 mg). Mono alkylated; HRMS (ESI) required for $C_{12}H_{22}N_2O^+$ 210.1727 observed MH^+ 210.1730. Di-alkylated; HRMS (ESI) required for $C_{15}H_{24}N_2O^+$ 248.1883 observed MH^+ 248.1884.

Synthesis of the AAZTA based complexes

Synthesis of (1,4-dibenzyl-6-nitro-1,4-diazepan-6-yl)methanol (98)

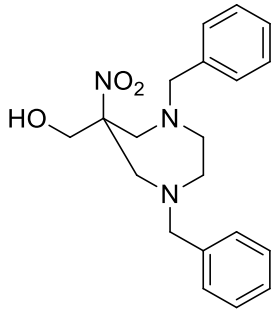

To a solution of *N,N'*-dibenzylethylendiamine diacetate **99** (3.00 g, 8.33 mmol, 1.0 eq.) and 2-nitroethanol (650 µL, 8.72 mmol, 1.0 eq.) in toluene: ethanol (1:1 to total 120 mL), paraformaldehyde (1.00 g, 33.3 mmol, 3.5 eq.) was added in portions. The suspension was then heated to 95 ˚C for 6 hours before concentration *in vacuo.* The residue was then dissolved in dichloromethane (10 mL) and the organic solution was then washed with water (3 x 10 mL). It was then dried with sodium sulphate and concentration *in vacuo.* This residue was then purified using column chromatography (petroleum ether 40/60: ethyl acetate, 4:1) to yield the final product as a sticky light yellow oil (R_f = 0.7, 2.30 g, 77%). IR V_{max} (Nujol)/cm^{-1} 3435w (O-H), 1742 (C=O), 1538 (NO_2), 1056 (C-O); ^{1}H NMR (400 MHz, $CDCl_3$) δ 2.54-2.85 (m, 4H, CH_2CH_2), 3.10 (d, *J* = 14.3 Hz, 2H, CH_2), 3.59 (d, *J* = 14.3 Hz, 2H, CH_2), 3.69 (d, *J* = 13.0 Hz, 2H, CH_2), 3.77 (m, 4H, CH_2), 7.27-7.43 (m, 10H, Ar-*H*). ^{13}C NMR (100 MHz, $CDCl_3$) δ 58.5 (*C*H_2), 59.3 (*C*H_2), 63.8 (*C*H_2), 65.8 (*C*H_2), 95.0 (*C*q), 127.5 (Ar-*C*H), 128.5 (Ar-*C*H), 129.1 (Ar-*C*H), 138.9 (Ar-*C*q). HRMS (ESI) required for $C_{20}H_{26}N_3O_3^+$ 356.1974 observed MH^+ 356.1972.

Synthesis of (6-amino-1,4-diazepan-6-yl)methanol (97)

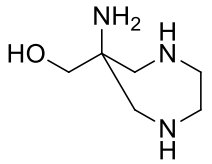

Ammonium formate (153 mg, 2.43 mmol, 3.3 eq.) was added to Pd/C (65 mg, 10% weight loading) in water (3 mL), followed by formic acid (102 mg, 2.21 mmol, 3.0 eq.). Nitro **98** (223 mg, 0.628 mmol, 1.0 eq.) in methanol (30 mL) was then added to the suspension. The system atmosphere was then evacuated, flushed with nitrogen three times; and the evacuation process repeated with hydrogen three times. The resulting black suspension was stirred for 24 hours at ambient temperature. The suspension was filtered, concentrated *in vacuo* and then lyophilised. The residue was then dissolved in water (10 mL) and washed with dichloromethane (3 x 10 mL) before drying *via* lyophilisation yield the *amine* as a clear-yellow oil (84 mg, 92%). IR V_{max} ($CHCl_3$)/cm^{-1} 3340 (O-H); ^{1}H NMR (400 MHz, D_2O) δ 2.59-2.71 (m, 2H, C*H*$_2$), 2.74-2.93 (m, 6H, C*H*$_2$), 3.36 (s, 2H, C*H*$_2$OH); ^{13}C NMR (100 MHz, D_2O) δ 50.3 (*C*H_2), 55.2 (*C*H_2), 57.4 (*C*q), 66.5 (*C*H_2). HRMS (ESI) required for $C_6H_{16}N_3O^+$ 146.1293 observed MH^+ 146.1295.

Synthesis of di-*tert*-butyl 2,2'-((1,4-bis(2-(*tert*-butoxy)-2-oxoethyl)-6-(hydroxymethyl)-1,4-diazepan-6-yl)azanediyl)diacetate (96)

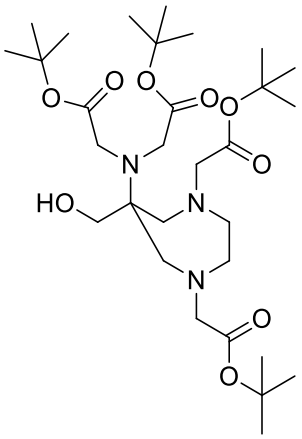

tert-Butyl bromoacetate (285 mg, 1.47 mmol, 4.0 eq.) was dissolved in acetonitrile (2 mL) slowly added to a solution of amine **97** (50 mg, 0.34 mmol, 1.0 eq.) in acetonitrile (3 mL). Potassium carbonate (60 mg, 0.43 mmol, 1.2 eq.) was then added and stirred for 24 hours under a nitrogen atmosphere. The suspension was then filtered and the filter washed with dichloromethane (20 mL), and concentrated *in vacuo* at ambient temperature. The residue was then dissolved in dichloromethane (10 mL) and washed with water (3 x 10 mL) followed by concentration *in vacuo* to yield the *protected ester* (147 mg, 71%) as a yellow oil. IR V_{max} (Nujol)/cm^{-1} 3449b (O-H), 1735 (C=O); ^{1}H NMR (400 MHz, $CDCl_3$) δ 1.42 (s, 36H, 3 x -C(CH_3)$_3$), 2.50-3.75 (m, 18 H, CH_2); ^{13}C NMR (100 MHz, $CDCl_3$) δ 28.0 (-C(*C*H_3)$_3$), 28.2 (-C(*C*H_3)$_3$), 52.5 (*C*H_2), 58.8 (*C*H_2), 61.3 (*C*H_2), 62.0 (*C*H_2), 64.2 (*C*q), 66.1 (*C*H_2), 80.8 (-*C*(CH_3)$_3$), 80.9 (-*C*(CH_3)$_3$), 170.7 (C=O), 172.6 (C=O). HRMS (ESI) required for $C_{30}H_{56}N_3O_9^+$ 602.4016 observed MH^+ 602.4005.

Synthesis of di-*tert*-butyl 2,2'-((1,4-bis(2-(*tert*-butoxy)-2-oxoethyl)-6-(chloromethyl)-1,4-diazepan-6-yl)azanediyl)diacetate (95)

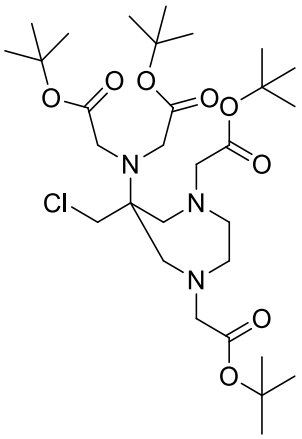

Thionyl chloride (0.10 mL, 1.4 mmol, 7.0 eq.) was added to hydroxyl **96** (124 mg, 0.206 mmol, 1.0 eq.) in dichloromethane (3 mL), and stirred under a nitrogen atmosphere until no starting material remained by MS, approximately 1 hour. The solution was then concentrated *in vacuo* to yield the crude *chloro-alkyl* as a yellow oil (128 mg, 100%). NMR not achieved due to stability; HRMS (ESI) required for $C_{30}H_{55}ClN_3O_8^+$ 620.3676 observed MH^+ 620.3669. HRMS (ESI) required for $C_{30}H_{55}ClN_3O_8^+$ 622.3648 observed MH^+ 622.3648.

Synthesis of di-tert-butyl 2,2'-(ethane-1,2-diylbis(benzylazanediyl))diacetate (101)

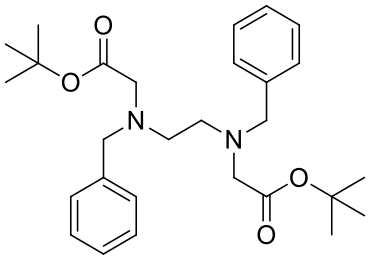

Tert-butyl bromoacetate (1.78 g, 9.18 mmol, 2.1 eq.) dissolved in acetonitrile (20 mL) was slowly added to a solution of *N1,N2*-dibenzylethane-1,2-diamine **99** (1.05 g, 4.38

mmol, 1.0 eq.) in acetonitrile (60 mL). Sodium carbonate (1.74 g, 16.4 mmol, 4.0 eq.) was then added, and the reaction heated to 60 ˚C and stirred under a nitrogen atmosphere for 24 hours. The suspension was then filtered and the filtrate washed with dichloromethane (20 mL), and concentrated *in vacuo*. This residue was then purified using column chromatography (DCM: methanol, 9:1) to yield the final product as a light orange solid (R_f = 0.8, 1.47 g, 72%). IR V_{max} (Nujol)/cm^{-1} 1734 (C=O); ^{1}H NMR (400 MHz, $CDCl_3$) δ 1.49 (s, 18H, -C(C*H*$_3$)$_3$), 2.86 (s, 4H, C*H*$_2$), 3.30 (s, 4H, C*H*$_2$), 3.83 (s, 4H, C*H*$_2$), 7.22-7.39 (m, 10H, Ar*H*); ^{13}C NMR (100 MHz, $CDCl_3$) δ 28.2 (-C(*C*H$_3$)$_3$), 51.5 (CH_2), 54.9 (CH_2), 58.4 (CH_2), 80.9 (-*C*(CH$_3$)$_3$), 127.2 (Ar-*C*H), 128.3 (Ar-*C*H), 129.1 (Ar-*C*H), 138.5 (Ar-*C*q), 170.5 (C=O). HRMS (ESI) required for $C_{28}H_{41}N_2O_4^+$ 469.3066 observed MH^+ 469.3064.

Synthesis of di-*tert*-butyl 2,2'-(ethane-1,2-diylbis(azanediyl))diacetate (102)

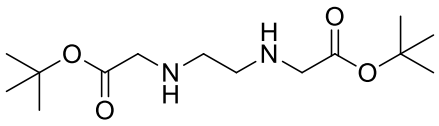

To a solution of protected amine **101** (0.92 g, 2.0 mmol, 1.0 eq.) in methanol (10 mL), Pd/C (90 mg, 10% weight loading) in water (1 mL) was then added. The system atmosphere was then evacuated, flushed with nitrogen three times; and the evacuation process repeated with hydrogen three times. The resulting black suspension was stirred for 24 hours at ambient temperature. The suspension was filtered, concentrated *in vacuo* and then lyophilised. The residue was then purified by silica chromatography (DCM: methanol, 9:1) to give the title compound as a clear

oil (R_f.= 0.4, 0.56 g, 99%). IR V_{max} (Nujol)/cm^{-1} 1739 (C=O), 1565 (N-H); ^{1}H NMR (400 MHz, $CDCl_3$) δ 1.39 (s, 18H, -C(CH_3)$_3$), 1.89 (s, 2H, NH), 2.80 (s, 4H, CH_2), 3.34 (s, 4H, CH_2). ^{13}C NMR (100 MHz, $CDCl_3$) δ 28.0 (-C(*C*H_3)$_3$), 47.1 (CH_2), 50.2 (CH_2), 81.8 (-*C*(CH_3)$_3$), 170.3 (C=O). HRMS (ESI) required for $C_{14}H_{29}N_2O_4^+$ 288.2161 observed MH^+ 289.2110.

Synthesis of di-tert-butyl 2,2'-(6-(3-methoxy-3-oxopropyl)-6-nitro-1,4-diazepane-1,4-diyl)diacetate (103)

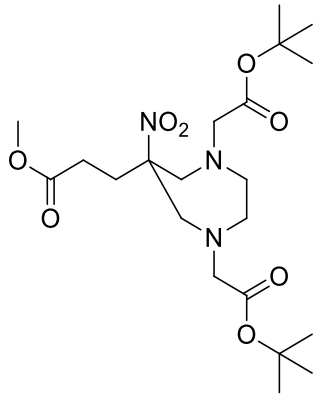

To a solution of diamine **102** (186 mg, 647 µmol, 1.0 eq.) and methyl 4-nitrobutanoate (115 mg, 782 µmol, 1.0 eq.) in toluene: ethanol (1:1 to total 120 mL), paraformaldehyde (93.1 mg, 3.10 mmol, 3.5 eq.) was added in portions. The suspension was then heated to 95 ˚C for 6 hours before concentration *in vacuo.* The residue was then dissolved in dichloromethane (10 mL) and washed with water (3 x 10 mL) before drying with sodium sulphate and concentrated *in vacuo.* This residue was then purified using column chromatography (petroleum ether 40/60: ethyl acetate, 1:1) to yield the final product as a yellow oil (R_f = 0.8, 296 mg, 100%). IR V_{max}

(Nujol)/cm^{-1} 1738s (C=O), 1555s (NO_2); ^1H NMR (400 MHz, $CDCl_3$) δ to be ascertained; ^{13}C NMR (100 MHz, $CDCl_3$) δ 22.2 (*C*H_2CH_2C=O), 28.0 (-C(*C*$H_3)_3$), 30.1 (CH_2*C*H_2C=O), 51.6 (*C*H_3), 56.8 (N*C*H_2*C*H_2N), 60.9 (N*C*H_2CNO_2), 61.2 (*C*H_2Ph), 74.2 (N*C*H_2C(O)), 81.0 (-*C*$(CH_3)_3$), 94.1 (*C*qNO_2), 170.4 (*C*=O), 172.2 (*C*=O). HRMS (ESI) required for $C_{21}H_{38}N_3O_8^+$ 460.2659 observed MH^+ 460.2664.

Synthesis of di-tert-butyl 2,2'-(6-amino-6-(3-methoxy-3-oxopropyl)-1,4-diazepane-1,4-diyl)diacetate (108)

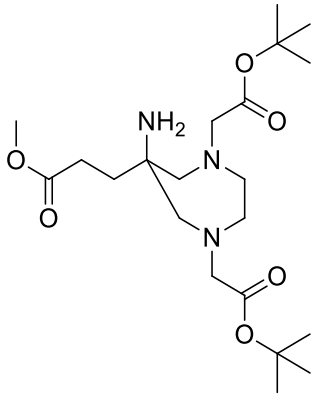

To a solution of nitro **103** (60.4 mg, 132 µmol, 1.0 eq.) in methanol (5 mL), Pd/C (16.6 mg, 10% weight loading) in water (1 mL) was then added, followed by formic acid (0.1 mL). The system atmosphere was then evacuated, flushed with nitrogen three times; and the evacuation process repeated with hydrogen three times. The resulting black suspension was stirred for 24 hours at ambient temperature. The suspension was filtered, concentrated *in vacuo* and then lyophilised, to yield the *amine* as an orange oil (49.4 mg, 88%). IR V_{max} (Nujol)/cm^{-1} 1735 (C=O), 1671 (C=O);

^{1}H NMR (400 MHz, $CDCl_3$) to be ascertained; ^{13}C NMR (100 MHz, $CDCl_3$) δ to be ascertained. HRMS (ESI) required for $C_{21}H_{40}N_3O_6^+$ 430.2917 observed MH^+ 430.2909.

Synthesis of methyl 3-(1,4-dibenzyl-6-nitro-1,4-diazepan-6-yl)propanoate (104)

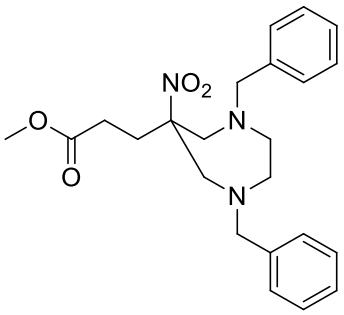

Hydroxy **98** (1.71 g, 4.82 mmol, 1.0 eq.), and methyl acrylate (0.900 mL, 9.94 mmol, 2.0 eq.) were dissolved in THF (12 mL) and stirred for 5 minutes before slowly adding potassium tert-butoxide (650 mg, 5.37 mmol, 1.2 eq.), the solution was then stirred for 24 hours. The solution was then concentrated *in vacuo* and the residue dissolved in ethyl acetate (50 mL). The organic solution was then washed with brine (3 x 30 mL) before being dried over sodium sulphate and concentrated *in vacuo*. The residue was then purified using column chromatography (petroleum ether 40/60: ethyl acetate, 9:1) to yield the final product as a clear yellow oil (rf.= 0.35, 1.86 g, 94%). IR V_{max} (Nujol)/cm^{-1} 1739s (C=O), 1536s (NO_2); ^{1}H NMR (400 MHz, $CDCl_3$) δ 1.75-1.87 (m, 2H, C*H*$_2$CH$_2$C=O), 1.95-2.04 (m, 2H, CH$_2$C*H*$_2$C=O), 2.52-2.73 (m, 4H, NC*H*$_2$C*H*$_2$N), 3.00 (d, *J* = 14.3 Hz, NC*H'*$_2$CNO$_2$), 3.51-3.67 (m, 4H, NC*H*$_2$CNO$_2$ and C*H'*$_2$Ph), 3.63 (s, 3H, C*H*$_3$), 3.76 (d, *J* = 12.9 Hz, 2H, C*H*$_2$Ph), 7.23-7.40 (m, 10H, ArH); ^{13}C NMR (100 MHz, $CDCl_3$) δ 27.7 (*C*H$_2$CH$_2$C=O), 31.3 (CH$_2$*C*H$_2$C=O), 51.6 (*C*H$_3$), 58.7 (N*C*H$_2$*C*H$_2$N), 61.4 (N*C*H$_2$CNO$_2$), 63.9 (*C*H$_2$Ph), 93.9 (*C*qNO$_2$), 127.3 (Ar-*C*H), 128.4 (Ar-*C*H), 129.1 (Ar-*C*H), 138.9 (Ar-*C*q), 172.2 (*C*=O). HRMS (ESI) required for $C_{23}H_{30}N_3O_4^+$ 412.2231 observed MH^+ 412.2229.

Synthesis of 3-(1,4-dibenzyl-6-nitro-1,4-diazepan-6-yl)propanoic acid (107)

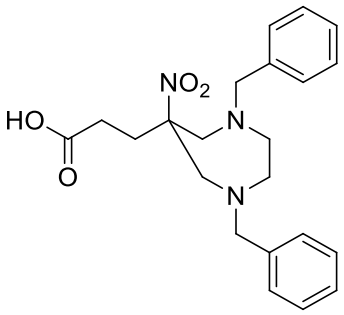

Ester **104** (860 mg, 2.09 mmol, 1.0 eq.) and sodium hydroxide (200 mg, 5.00 mmol, 2.5 eq.) were dissolved in a mixture of water: THF (1:1 to total 10 mL). The solution was then stirred for 24 hours, and then concentrated *in vacuo*. The residue was then dissolved in dichloromethane (20 mL) and successively washed with citric acid (10% wt solution, 3 x 10 mL). The organic phase was then dried over sodium sulphate, filtered, and concentrated *in vacuo* to yield the acid (830 mg, 64%) as a brown oil. HRMS (ESI) required for $C_{22}H_{28}N_3O_4^+$ 398.2080 observed MH^+ 396.2092. IR V_{max} (Nujol)/cm^{-1} 1714 (C=O), 1536 (NO_2); ^{1}H NMR (400 MHz, $CDCl_3$) δ 1.83-1.94 (m, 2H, C*H*$_2$CH$_2$C=O), 1.96-2.10 (m, 2H, CH$_2$C*H*$_2$C=O), 2.57-2.77 (m, 4H, NC*H*$_2$C*H*$_2$N), 3.02 (d, *J* = 14.1 Hz, NC*H'*$_2$CNO$_2$), 3.52-3.70 (m, 4H, NC*H*$_2$CNO$_2$ and C*H'*$_2$Ph), 3.79 (d, *J* = 13.1 Hz, 2H, C*H*$_2$Ph), 7.25-7.42 (m, 10H, ArH), 10.63 (COO*H*); ^{13}C NMR (100 MHz, $CDCl_3$) δ 28.6 (*C*H$_2$CH$_2$C=O), 31.9 (CH$_2$*C*H$_2$C=O), 58.2 (N*C*H$_2$*C*H$_2$N), 61.6 (N*C*H$_2$CNO$_2$), 63.8 (*C*H$_2$Ph), 94.1 (*C*qNO$_2$), 127.4 (Ar-*C*H), 128.4 (Ar-*C*H), 129.1 (Ar-*C*H), 138.9 (Ar-*C*q), 172.8 (*C*=O). HRMS (ESI) required for $C_{22}H_{26}N_3O_4^-$ 396.1924 observed MH^+ 396.1926.

Synthesis of linkers and spacers

Synthesis of tert-butyl (3-(2-(2-(3-aminopropoxy)ethoxy)ethoxy)propyl)carbamates (128)

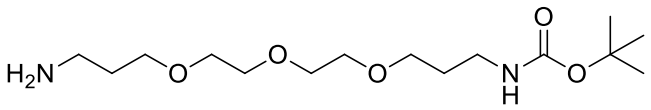

The title compound was synthesised using a procedure adapted from the literature.[135] To a solution of diamine **127** (18.2 g, 82.5 mmol, 7.0 eq.) in dichloromethane (200 mL), di-*tert*-butyl dicarbonate (2.50 g, 11.4 mmol, 1.0 eq.) was added dropwise at 0 ˚C and the mixture stirred for 30 minutes, followed by a further 18 hour stir at ambient temperature. The reaction was then extracted with water (2 x 150 mL), and brine (2 x 150 mL), dried over magnesium sulphate, filtered and concentrated *in vacuo*, to yield the title compound as a light yellow-brown oil (3.88 g, 99% with respect to Boc anhydride). IR V_{max} (Nujol)/cm^{-1} 1711 (C=O), 1171 (C-O), 1043 (C-O); ^{1}H NMR (400 MHz, $CDCl_3$) δ 1.29 (s, 9H, -C(C*H*$_3$)$_3$), 1.61 (quin, *J* = 4.0 Hz, 4H, C*H*$_2$), 2.14 (s, 2H, C*H*$_2$), 2.68 (t, *J* = 8.0 Hz, 2H, C*H*$_2$), 3.06 (m, 2H, C*H*$_2$), 3.37-3.53 (m, 12H, HN-C*H*$_2$- C*H*$_2$- C*H*$_2$-O), 5.27 (bs, 1H, N*H*); ^{13}C NMR (100 MHz, $CDCl_3$) δ 28.4 (-C(*C*H$_3$)$_3$), 29.6 (O-CH$_2$-*C*H$_2$-O), 31.7 (O-CH$_2$-*C*H$_2$-O), 38.4 (O-CH$_2$-*C*H$_2$-O), 39.3 (O-CH$_2$-*C*H$_2$-O), 53.4 (-*C*(CH$_3$)$_3$), 70.1 (O-CH$_2$-CH$_2$-CH$_2$-N), 70.1 (O-CH$_2$-CH$_2$-CH$_2$-N), 70.2 (O-CH$_2$-CH$_2$-CH$_2$-N), 70.4 (O-CH$_2$-CH$_2$-CH$_2$-N), 70.5 (O-CH$_2$-CH$_2$-CH$_2$-N), 70.5 (O-CH$_2$-CH$_2$-CH$_2$-N), 156.1 (*C*=O). HRMS (ESI) required for $C_{15}H_{33}N_2O_5^+$ 321.2384 observed MH^+ 321.2350.

Synthesis of benzyl tert-butyl (((oxybis(ethane-2,1-diyl))bis(oxy))bis(propane-3,1-diyl))dicarbamate (129)

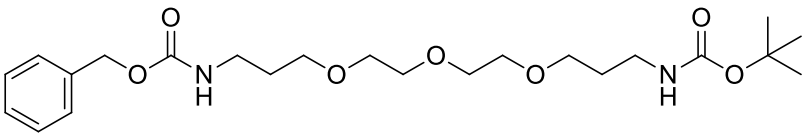

The title compound was synthesised using a procedure adapted from the literature.[125] Protected diamine **128** (1.00 g, 3.13 mmol, 1.0 eq.) and triethylamine (530 mg, 5.24 mmol, 1.5 eq.) in dichloromethane (10 mL) were stirred as benzyl chloroformate (600 mg, 3.53 mmol, 1.1 eq.) in dichloromethane (1 mL), was added and the mixture stirred at ambient temperature until no starting material was observed by TLC (ethyl acetate: dichloromethane (3:7)) (approximately 2 hours). Water (10 mL) was then added and aqueous phase extracted with dichloromethane (3 x 10 mL). The organic phases were combined and washed with brine (10 mL), dried over sodium sulphate filtered and concentrated *in vacuo*. The crude mixture was then purified by silica chromatography (ethyl acetate: dichloromethane, 3:7) to give the title compound (**9**) as a light yellow oil (R_f = 0.2, 900 mg, 62%). IR V_{max} (Nujol)/cm^{-1} 1742b (C=O), 1047 (C-O); ^{1}H NMR (400 MHz, $CDCl_3$) δ 1.45 (s, 9H, -C(C*H*$_3$)$_3$), 1.71-1.82 (m, 4H, C*H*$_2$), 3.06 (m, 2H, C*H*$_2$), 3.35 (m, 2H, C*H*$_2$), 3.47-3.68 (m, 11H, HN-C*H*$_2$- C*H*$_2$- C*H*$_2$-O), 4.97 (br s, 1H, N*H*), 5.41 (bs, 1H, N*H*), 7.3-7.37 (m, 5H, Ar*H*); ^{13}C NMR (100 MHz, $CDCl_3$) δ 28.4 (-C(*C*H$_3$)$_3$), 29.4 (O-CH$_2$-*C*H$_2$-O), 29.6 (O-CH$_2$-*C*H$_2$-O), 38.6 (O-CH$_2$-*C*H$_2$-O), 39.2 (O-CH$_2$-*C*H$_2$-O), 66.4 (Bnz-CH$_2$), 69.5 (O-CH$_2$-CH$_2$-CH$_2$-N), 70.2 (O-CH$_2$-CH$_2$-CH$_2$-N), 70.5 (O-CH$_2$-CH$_2$-CH$_2$-N), 70.6 (O-CH$_2$-CH$_2$-CH$_2$-N), 127.9 (2 x Ar-C), 128.1 (Ar-C), 128.4 (2 x Ar-C), 138.8 (Ar-Cq), 156.0 (C=O), 156.5

(C=O). HRMS (ESI) required for $C_{23}H_{38}N_2O_7Na^+$ 477.2571 observed MNa^+ 477.2569. HRMS (ESI) required for $C_{23}H_3N_2O_7^+$ 455.2713 observed MH^+ 455.2750.

Synthesis of benzyl (3-(2-(2-(3-aminopropoxy)ethoxy)ethoxy)propyl)carbamates. TFA (130)

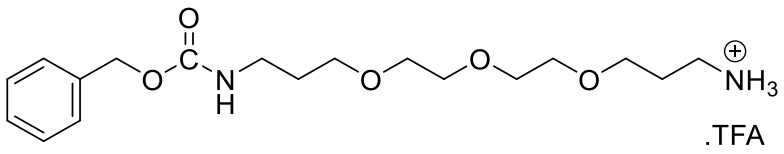

The title compound was synthesised using a procedure adapted from the literature.[126] Protected diamine **129** (390 mg, 0.859 mmol, 1.0 eq.) in dichloromethane (1 mL) was stirred at 0 ˚C as trifluoroacetic acid (0.50 mL, 6.5 mmol, 6.0 eq.) was added slowly and the mixture stirred for 1 hour. The mixture was then concentrated *in vacuo* to afford the *protected diamine* trifluoroacetic acid salt as a yellow oil (360 mg, 89%). IR V_{max} (Nujol)/cm^{-1} 1686 (C=O), 1203 (C-O); ^{1}H NMR (400 MHz, $CDCl_3$) δ 1.76 (quin, *J* = 4.0 Hz, 2H, C*H*$_2$), 1.89-2.03 (m, 2H, C*H*$_2$), 3.17 (q, *J* = 8.0 Hz, 2H, C*H*$_2$), 3.28 (t, *J* = 4.0 Hz, 2H, C*H*$_2$), 3.46-3.67 (m, 11H, HN-C*H*$_2$- C*H*$_2$- C*H*$_2$-O), 3.67-3.78 (m, 2H, C*H*$_2$), 5.36 (bs, N*H*C(O)O), 7.29-7.41 (m, 5H, Ar*H*); ^{13}C NMR (100 MHz, $CDCl_3$) δ 26.4 (CH_2), 29.6 (CH_2), 38.6 (CH_2), 39.1 (CH_2), 39.6 (CH_2), 66.7 (CH_2), 68.9 (CH_2), 69.5 (CH_2), 69.7 (CH_2), 69.8 (CH_2), 70.2 (CH_2), 116.2 (q, *J* = 289 Hz, trifluoroacetic acid CF_3), 127.9 (Ar-*C*H), 128.1 (2 x Ar-*C*H), 128.5 (2 x Ar-*C*H), 136.6 (Ar-*Cq*) 157.0 (C=O), 161.4 (q, *J* = 36 Hz, trifluoroacetic acid C=O); ^{19}F NMR (376MHz, $CDCl_3$) δ 75.98 (s, 3F). HRMS (ESI) required for $C_{18}H_{31}N_2O_5^+$ 355.2188 observed MH^+ 355.2218.

Synthesis of benzyl (1-bromo-2-oxo-7,10,13-trioxa-3-azahexadecan-16-yl)carbamates (132)

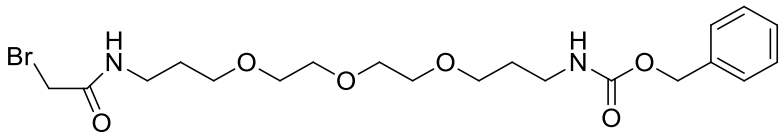

Amine salt **130** (110 mg, 0.235 mmol, 1.0 eq.) and potassium carbonate (130 mg, 0.942 mmol, 4.0 eq.) were stirred at 0 ˚C in dichloromethane (5 mL) and water (3 mL) as bromoacetyl bromide (90 mg, 0.45 mmol, 2 eq.) in dichloromethane (1 mL) was slowly added, once added the biphasic solution was stirred for an hour followed by 24 hours at ambient temperature. The aqueous phase was then removed and the organic successively washed with water (2 x 10 mL) and brine (1 x 10 mL). The organic phase was dried over sodium sulphate, filtered and concentrated *in vacuo* to give the *α-bromo amide* as a yellow oil (70 mg, 63%). IR V_{max} (Nujol)/cm^{-1} 3318 (NH), 1714 (C=O), 1666 (C=O), 1123 (C-O-C). ^{1}H NMR (400 MHz, $CDCl_3$) δ 1.79 (quin, *J* = 5.9 Hz, 4H, C*H*$_2$), 3.26-3.37 (m, 2H, C*H*$_2$), 3.38-3.46 (m, 2H, C*H*$_2$), 3.47-3.72 (m, 13H, HN-C*H*$_2$- C*H*$_2$- C*H*$_2$-O), 3.84 (s, 2H, C*H*$_2$Br), 5.42 (bs, N*H*C(O)O), 7.20 (bs, N*H*), 7.27-7.42 (m, 5H, Ar*H*); ^{13}C NMR (100 MHz, $CDCl_3$) δ 28.5 (*C*H$_2$), 29.3 (*C*H$_2$), 29.4 (*C*H$_2$), 39.0 (*C*H$_2$), 39.3 (*C*H$_2$), 66.5 (*C*H$_2$Br), 69.6 (*C*H$_2$), 70.2 (*C*H$_2$), 70.3 (*C*H$_2$), 70.3 (*C*H$_2$), 70.5 (*C*H$_2$), 128.0 (Ar-*C*H), 128.1 (Ar-*C*H), 128.5 (Ar-*C*H), 136.8 (Ar-*C*q), 156.5 (*C*=O), 165.6 (BrCH$_2$*C*=O). HRMS (ESI) required for $C_{20}H_{32}BrN_2O_6^+$ 475.1443 observed MH^+ 475.1425. HRMS (ESI) required for $C_{20}H_{32}BrN_2O_6^+$ 477.1423 observed MH^+ 477.1415.

Synthesis of benzyl (1-chloro-2-oxo-7,10,13-trioxa-3-azahexadecan-16-yl)carbamates (133)

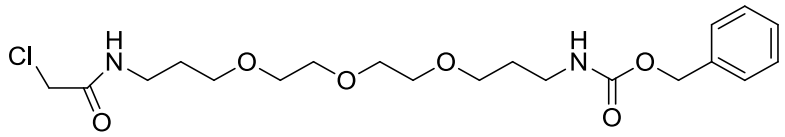

Amine salt **130** (110 mg, 0.235 mmol, 1.0 eq.) and potassium carbonate (130 mg, 0.942 mmol, 4.0 eq.) were stirred at 0 ˚C in dichloromethane (5 mL) and water (3 mL) as chloroacetyl chloride (43.0 mg, 0.380 mmol, 1.5 eq.) in dichloromethane (1 mL) was slowly added, once added the biphasic solution was stirred for an hour followed by 24 hours at ambient temperature. The aqueous phase was then removed and the organic successively washed with water (2 x 10 mL) and brine (1 x 10 mL). The organic phase was dried over sodium sulphate, filtered and concentrated *in vacuo* to give the *α-chloro amide* as a brown oil (88 mg, 87%). IR V_{max} (Nujol)/cm^{-1} 3318 (NH), 1716 (C=O), 1667 (C=O), 1108 (C-O-C), 759 (C-Cl); ^{1}H NMR (400 MHz, $CDCl_3$) δ 1.72-88 (m, 4H, C*H*$_2$), 3.27-3.37 (m, 2H, C*H*$_2$), 3.38-3.47 (m, 2H, C*H*$_2$), 3.51-3.72 (m, 11H, HN-C*H*$_2$- C*H*$_2$- C*H*$_2$-O), 4.02 (s, 2H, C*H*$_2$Cl), 5.42 (bs, N*H*C(O)O), 7.25-7.41 (m, 5H, Ar*H*); ^{13}C NMR (100 MHz, $CDCl_3$) δ 28.6 (*C*H$_2$), 28.6 (*C*H$_2$), 29.4 (*C*H$_2$), 38.7 (*C*H$_2$), 39.3 (*C*H$_2$), 42.7 (CH$_2$), 66.5 (*C*H$_2$Br), 69.6 (*C*H$_2$), 70.2 (*C*H$_2$), 70.4 (*C*H$_2$), 70.4 (*C*H$_2$), 70.5 (*C*H$_2$), 128.0 (Ar-*C*H), 128.1 (Ar-*C*H), 128.5 (Ar-*C*H), 136.8 (Ar-*C*q), 156.5 (*C*=O), 165.9 (ClCH$_2$*C*=O). HRMS (ESI) required for $C_{20}H_{31}ClN_2O_6K^+$ 469.1503 observed MK$^+$ 469.1518. HRMS (ESI) required for $C_{20}H_{31}ClN_2O_6K^+$ 471.1473 observed MK$^+$ 471.1496.

Synthesis of tert-butyl (1-bromo-2-oxo-7,10,13-trioxa-3-azahexadecan-16-yl)carbamates (155a)

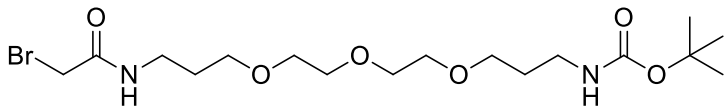

Amine salt **128** (810 mg, 1.88 mmol, 1.0 eq.) and potassium carbonate (1.17 g, 8.48 mmol, 3.5 eq.) were stirred at 0 ˚C in dichloromethane (60 mL) and water (10 mL) as bromoacetyl bromide (0.30 mL, 3.5 mmol, 1.4 eq.) in dichloromethane (10 mL) was slowly added, once added the biphasic solution was stirred for an hour followed by 24 hours at ambient temperature. The aqueous phase was then removed and the organic successively washed with water (2 x 10 mL) and brine (1 x 10 mL). The organic phase was dried over sodium sulphate, filtered and concentrated *in vacuo* to give the *α-bromo amide* as an orange/brown oil (760 mg, 92%). IR V_{max} (Nujol)/cm^{-1} 1709 (C=O), 1692 (C=O); ^{1}H NMR (400 MHz, $CDCl_3$) δ 1.40 (s, 9H (-C(CH_3)$_3$), 1.67-1.81 (m, 4H, CH_2), 3.17 (t, *J* = 6.4 Hz, 2H, CH_2), 3.37 (q, *J* = 5.8 Hz, 2H, CH_2), 3.47-3.52 (m, 2H, CH_2), 3.53-3.65 (m, 10H, CH_2), 3.81 (s, 2H, CH_2Br), 4.99 (bs, NHC(O)O), 7.23 (bs, NH); ^{13}C NMR (100 MHz, $CDCl_3$) δ 28.4 (-C(*C*H_3)$_3$), 28.5 (*C*H_2), 29.2 (*C*H_2), 30.0 (*C*H_2), 38.5 (*C*H_2), 38.9 (*C*H_2), 70.1 (*C*H_2), 70.2 (*C*H_2), 70.3 (*C*H_2), 70.5 (*C*H_2), 70.5 (*C*H_2), 70.5 (*C*H_2), 78.8 (-*C*(CH_3)$_3$), 156.0 (C=O), 165.6 (BrCH_2*C*=O). HRMS (ESI) required for $C_{17}H_{33}BrN_2O_6Na^+$ 463.1420 observed MNa^+ 463.1408. HRMS (ESI) required for $C_{17}H_{33}BrN_2O_6Na^+$ 465.1400 observed MNa^+ 465.1391.

Synthesis of tert-butyl (1-chloro-2-oxo-7,10,13-trioxa-3-azahexadecan-16-yl)carbamates (155b)

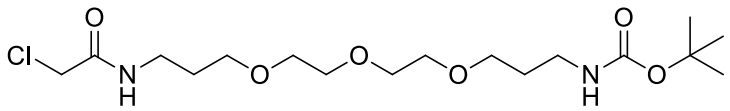

Amine salt **128** (820 mg, 1.89 mmol, 1.0 eq.) and potassium carbonate (1.17 g, 8.48 mmol, 3.0 eq.) were stirred at 0 ˚C in dichloromethane (60 mL) and water (10 mL) as chloroacetyl chloride (0.40 mL, 5.0 mmol, 2.0 eq.) in dichloromethane (10 mL) was slowly added, once added the biphasic solution was stirred for an hour followed by 24 hours at ambient temperature. The aqueous phase was then removed and the organic successively washed with water (2 x 10 mL) and brine (1 x 10 mL). The organic phase was dried over sodium sulphate, filtered and concentrated *in vacuo* to give the *α-bromo amide* as an orange/brown oil (740 mg, 99%). IR V_{max} (Nujol)/cm^{-1} 1711 (C=O), 1694 (C=O); ^{1}H NMR (400 MHz, $CDCl_3$) δ 1.33 (s, 9H (-C(C*H*$_3$)$_3$), 1.65 (quin, *J* = 6.3 Hz, 2H, CH_2), 1.72 (quin, *J* = 5.6 Hz, 2H, CH_2), 3.02-3.15 (m, 2H, CH_2), 3.33 (q, *J* = 5.8 Hz, 2H, CH_2), 3.40-3.46 (m, 2H, CH_2), 3.46-3.58 (m, 10H, CH_2), 3.92 (s, 2H, CH_2Cl), 5.04 (bs, NHC(O)O), 7.25 (bs, NH) ; ^{13}C NMR (100 MHz, $CDCl_3$) δ 28.4 (-C(*C*H_3)$_3$), 28.6 (*C*H_2), 29.6 (*C*H_2), 38.5 (*C*H_2), 42.6 (*C*H_2), 69.4 (*C*H_2), 70.1 (*C*H_2), 70.1 (*C*H_2), 70.2 (*C*H_2), 70.3 (*C*H_2), 70.4 (*C*H_2), 70.5 (*C*H_2), 78.7 (-*C*$(CH_3)_3$), 156.0 (C=O), 165.9 ($ClCH_2$*C*=O). HRMS (ESI) required for $C_{17}H_{34}ClN_2O_6^+$ 397.2106 observed MH^+ 397.2107. HRMS (ESI) required for $C_{17}H_{34}ClN_2O_6^+$ 399.2076 observed MH^+ 399.2075.

Synthesis of tert-butyl (1-azido-2-oxo-7,10,13-trioxa-3-azahexadecan-16-yl)carbamates (150)

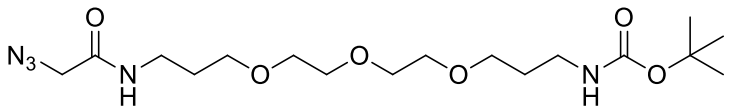

α-Bromoamide **155a** (660 mg, 1.42 mmol, 1.0 eq.), sodium azide (230 mg, 3.54 mmol, 2.3 eq.) and potassium iodide (160 mg, 0.964 mmol, 0.7 eq.) in diethyl ether (20 mL) were stirred for 24 hours under a nitrogen atmosphere. At which point additional sodium azide (140 mg, 2.15 mmol, 2.0 eq.) and potassium iodide (140 mg, 0.843 mmol, eq.) was added, and stirred for a further 48 hours. The solvent was then concentrated *in vacuo* at ambient temperature, the residue was then dissolved in dichloromethane (30 mL) and successively washed with water (3 x 30 mL). The organic phase was retained and dried over sodium sulphate, filtered and concentrated *in vacuo* to give the *azide* (510 mg, 70%) as a clear oil. IR V_{max} (Nujol)/cm^{-1} 2105 (N_3), 1709 (C=O), 1692 (C=O); ^{1}H NMR (400 MHz, $CDCl_3$) δ 1.40 (s, 9H (-C(C*H*$_3$)$_3$), 1.73 (quin, *J* = 6.1 Hz, 2H, CH_2), 1.78 (quin, *J* = 5.6 Hz, 2H, CH_2), 3.19 (t, *J* = 6.6 Hz, 2H, CH_2), 3.39 (q, *J* = 5.8 Hz, 2H, CH_2), 3.48-3.54 (m, 2H, CH_2), 3.54-3.71 (m, 10H, CH_2), 3.90 (s, 2H, CH_2N_3), 4.96 (bs, NHC(O)O), 7.02 (bs, NH); ^{13}C NMR (100 MHz, $CDCl_3$) δ 28.4 (-C(*C*H_3)$_3$), 28.7 (*C*H_2), 29.7 (*C*H_2), 38.2 (*C*H_2), 38.6 (*C*H_2), 52.6 (*C*H_2N_3), 69.5 (*C*H_2), 69.5(*C*H_2), 70.2 (*C*H_2), 70.2 (*C*H_2), 70.3 (*C*H_2), 70.5 (*C*H_2), 70.5 (*C*H_2), 70.6 (*C*H_2), 79.0 (-*C*(CH_3)$_3$), 156.0 (C=O), 166.9 (N_3CH_2*C*=O). HRMS (ESI) required for $C_{17}H_{34}N_5O_6^+$ 404.2509 observed MH^+ 404.2517.

Synthesis of *N*-(3-(2-(2-(3-aminopropoxy)ethoxy)ethoxy)propyl)-2-azidoacetamide. TFA (149)

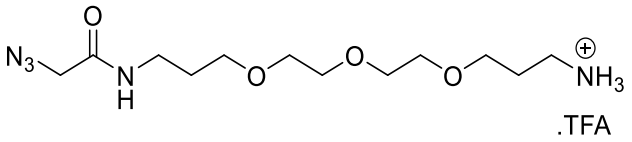

Protected amine **150** (230 mg, 0.571 mmol, 1.0 eq.) in dichloromethane (5 mL) was stirred at 0 ˚C as trifluoroacetic acid (5.0 mL, 65 mmol, 11.0 eq.) was added slowly and the mixture stirred for 1 hour. The mixture was then concentrated *in vacuo*, the residue was then dissolved in dichloromethane (30 mL) and successively washed with water (3 x 30 mL). The aqueous phase was retained and lyophilised to give the *azide trifluoroacetic acid salt* (200 mg, 84%) as a orange/brown oil. IR V_{max} (Nujol)/cm^{-1} 2108 (N_3), 1679b (C=O); (400 MHz, $CDCl_3$) δ 1.81 (quin, *J* = 6.0 Hz, 2H, CH_2), 1.94-2.02 (m, 2H, CH_2), 3.25-3.22 (m, 2H, CH_2), 3.40 (q, *J* = 6.6 Hz, 2H, CH_2), 3.57 (t, *J* = 5.6 Hz, 2H, CH_2), 3.61-3.74 (m, 10H, CH_2), 3.78 (t, *J* = 5.3 Hz, 2H, CH_2), 4.10 (s, 2H, CH_2N_3), 7.15 (bs, NH_3), 7.38 (bs, NH); ^{13}C NMR (100 MHz, $CDCl_3$) δ 25.8 (*C*H_2), 28.3 (*C*H_2), 37.6 (*C*H_2), 41.2 (*C*H_2), 51.8 (*C*H_2N_3), 68.9 (*C*H_2), 69.3 (*C*H_2), 69.5 (*C*H_2), 69.5 (*C*H_2), 69.6 (*C*H_2), 69.8 (*C*H_2), 70.8 (*C*H_2), 115.1 (q, *J* = 285.0 Hz, *C*F_3), 160.2 (q, *J* = 40.4 Hz, CF_3*C*O), 169.8 (N_3CH_2*C*=O); ^{19}F NMR (376 MHz, $CDCl_3$) δ 76.34 (s, 3F, C*F*$_3$). HRMS (ESI) required for $C_{12}H_{25}N_5O_4^+$ 304.1985 observed MH^+ 304.1978.

Synthesis of 1-azido-2,18-dioxo-7,10,13-trioxa-3,17-diazahenicosan-21-oic acid (148)

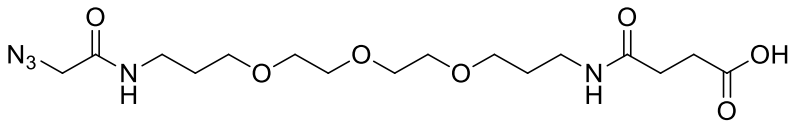

Amine salt **149** (230 mg, 0.551 mmol, eq.), succinic anhydride (80 mg, 0.80 mmol, 1.0 eq.) and sodium carbonate (80 mg, 0.58 mmol, 0.7 eq.) were stirred in acetonitrile (10 mL) at 50 ˚C for 24 hours. The suspension was then filtered, and the filtrate concentrated *in vacuo*. The residue was then dissolved in dichloromethane (30 mL) and successively washed with water (3 x 30 mL). The aqueous phase was retained and lyophilised, to give the *acid* (201 mg, 91%) as a orange/brown oil. 2108 (N_3), 1680b (C=O); HRMS (ESI) required for $C_{16}H_{29}N_5O_7^+$ 404.2140 observed MH^+ 404.2133.

Synthsis of L-proline methyl ester (137)

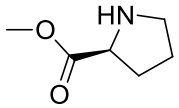

L-proline (1.04 g, 9.01 mmol, 1.0 eq.) in anhydrous methanol (20 mL) was stirred under a nitrogen atmosphere at 0 ˚C. Acetyl chloride (5.66 g, 72.1 mmol, 8.0 eq.) was slowly added over 30 minutes, and stirred for an additional 30 minutes at 0 ˚C, followed by 24 hours at ambient temperature. The solution was concentrated *in vacuo*, the residue was then dissolved in dichloromethane (10 mL) and successively

washed with water (3 x 10 mL). The aqueous phase was retained; saturated aqueous sodium carbonate (30 mL) added and successively washed with dichloromethane (3 x 20 mL). The organic was retained and dried over magnesium sulphate, filtered and concentrated *in vacuo* to give the *ester* (0.470 g, 40%) as a clear oil. IR V_{max} (Nujol)/cm^{-1} 1667s (C=O); ^{1}H NMR (400 MHz, $CDCl_3$) δ 1.66-1.76 (m, 2H, C*H*$_2$), 1.76-1.85 (m, 1H, C*H*$_2$), 2.05-2.14 (m, 1H, C*H*$_2$), 2.84-2.90 (m, 1H, C*H*$_2$), 3.00-3.07 (m, 1H, C*H*$_2$), 3.68 (s, 3H, C*H*$_3$), 3.72-3.76 (m, 1H, C*H*) 5.26 (s, 1H, N*H*). ^{13}C NMR (100 MHz, $CDCl_3$) δ 25.4 (*C*H_2), 30.2 (*C*H_2), 47.0 (*C*H_2), 52.0 (*C*H_3), 60.0 (*C*H), 175.7 (C=O). HRMS (ESI) required for $C_6H_{11}NO_2^+$ 130.0868 observed MH^+ 130.0838.

Synthesis of (S)-methyl 1-(2-bromoacetyl)pyrrolidine-2-carboxylate (139)

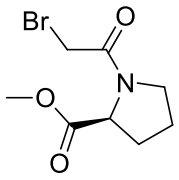

L-Proline methyl ester **137** (160 mg, 1.24 mmol, 1.0 eq.) and potassium carbonate (430 mg, 3.12 mmol, 3.0 eq.) were stirred at 0 ˚C in dichloromethane (15 mL) and water (9 mL) as bromoacetyl bromide (300 mg, 1.49 mmol, 1.2 eq.) in dichloromethane (2 mL) was slowly added, once added the biphasic solution was stirred for an hour followed by 24 hours at ambient temperature. The aqueous phase was then removed and the organic successively washed with water (2 x 10 mL) and brine (1 x 10 mL). The organic phase was dried over magnesium sulphate, filtered and concentrated *in vacuo* to give the *amide* as a clear oil (310 mg, 62%). IR

V_{max} (Nujol)/cm^{-1} 1745 (C=O), 1653 (C=O); ^{1}H NMR (400 MHz, $CDCl_3$) δ 1.82-2.28 (m, 4H, CH_2), 3.56-3.85 (m, 4H, CH_2), 3.67 (s, 3H, CH_3), 4.44 (dd, 1H, *J* = 8.6, 4.0 Hz, C*H*). ^{13}C NMR (100 MHz, $CDCl_3$) δ 24.8 (*C*H_2), 27.1 (*C*H_2), 29.2 (*C*H_2), 47.5 (*C*H_2), 52.3 (*C*H_3), 59.2 (*C*H), 165.2 (C=O), 172.1 (C=O). HRMS (ESI) required for $C_8H_{13}BrNO_3^+$ 250.0079 observed MH^+ 250.0070. HRMS (ESI) required for $C_8H_{13}BrNO_3^+$ 252.0059 observed MH^+ 252.0054.

Synthesis of (S)-methyl 1-(2-chloroacetyl)pyrrolidine-2-carboxylate (138)

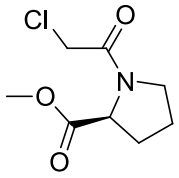

L-Proline methyl ester **138** (160 mg, 1.24 mmol, 1.0 eq.) and potassium carbonate (450 mg, 3.26 mmol, 3.0 eq.) were stirred at 0 ˚C in dichloromethane (15 mL) and water (9 mL) as chloroacetyl chloride (170 mg, 1.50 mmol, 1.2 eq.) in dichloromethane (2 mL) was slowly added, once added the biphasic solution was stirred for an hour followed by 24 hours at ambient temperature. The aqueous phase was then removed and the organic successively washed with water (2 x 10 mL) and brine (1 x 10 mL). The organic phase was dried over magnesium sulphate, filtered and concentrated *in vacuo* to give the *amide* (180 mg, 72%) as a clear oil. IR V_{max} (Nujol)/cm^{-1} 1746 (C=O), 1660 (C=O); ^{1}H NMR (400 MHz, $CDCl_3$) δ 1.93-2.12 (m, 3H, CH_2), 2.12-2.28 (m, 1H, CH_2), 3.56-3.67 (m, 2H, CH_2), 3.70 (s, 3H, CH_3), 4.04 (q, 2H, *J* = 12.8 Hz, CH_2Cl), 4.47 (dd, *J* = 8.7, 4.8 Hz, 1H, C*H*). ^{13}C NMR (100 MHz, $CDCl_3$) δ

24.8 (*C*H_2), 29.1 (*C*H_2), 41.9 (*C*H_2Cl), 47.0 (*C*H_2), 52.3 (*C*H_3), 59.2 (*C*H), 165.0 (C=O), 172.1 (C=O). HRMS (ESI) required for $C_8H_{13}ClNO_3^+$ 206.0584 observed MH^+ 206.0593. HRMS (ESI) required for $C_8H_{13}ClNO_3^+$ 208.0554 observed MH^+ 208.0569.

Synthesis of 2-bromo-*N*-(prop-2-yn-1-yl)acetamide (146)

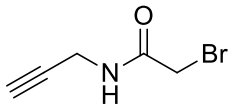

Bromoacetyl bromide (460 mg, 2.28 mmol, 1.1 eq.) and potassium carbonate (590 mg, 4.28 mmol, 2.0 eq.) were stirred under a nitrogen atmosphere at 0 ˚C in anhydrous dichloromethane (5 mL). Propargyl amine (120 mg, 2.18 mmol, 1.0 eq.) in anhydrous dichloromethane (1 mL) was slowly added over 30 minutes, and stirred for two hour at ambient temperature before being quenched with water (2 mL), followed by a 24 hour stir at ambient temperature. The product was then extracted with water (20 mL), dichloromethane (3 x 10 mL), and washed with citric acid (5% solution, 2 x 10 mL) and water (2 x 10 mL). The organic phase was then dried over sodium sulphate, filtered and concentrated *in vacuo* to yield the *propargyl amide* (110 mg, 30%) as an off white solid. Mp. 72-73 ˚C; IR V_{max} (Nujol)/cm^{-1} 3291 (NH), 1642 (C=O); ^{1}H NMR (400 MHz, $CDCl_3$) δ 2.30 (t, *J* = 4.0 Hz, 1H, alkyne-H), 3.90 (s, 2H, CH_2), 4.09 (dd, *J* = 5.4, 2.6 Hz, 2H, CH_2), 6.94 (bs, 1H, N*H*). ^{13}C NMR (100 MHz, $CDCl_3$) δ 28.6 (*C*H_2-Br), 29.9 (*C*H_2NH), 72.2 (*C*q alkyne), 78.6 (*C*H), 165.5 (*C*=O). HRMS (ESI) required for $C_5H_6BrNONa^+$ 197.9525 observed MNa^+ 197.9552. HRMS (ESI) required for $C_5H_6BrNONa^+$ 199.9505 observed MNa^+ 199.9525.

Synthesis of 2-chloro-*N*-(prop-2-yn-1-yl)acetamide (145)

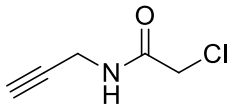

Chloroacetyl chloride (260 mg, 2.30 mmol, 1.1 eq.) and potassium carbonate (590 mg, 4.28 mmol, 2.0 eq.) were stirred under a nitrogen atmosphere at 0 ˚C in anhydrous dichloromethane (5 mL). Propargyl amine (120 mg, 2.18 mmol, 1.0 eq.) in anhydrous dichloromethane (1 mL) was slowly added over 30 minutes, and stirred for two hour at ambient temperature before being quenched with water (2 mL), followed by a 24 hour stir at ambient temperature. The product was then extracted with water (20 mL), dichloromethane (3 x 10 mL), and washed with citric acid (5% solution, 2 x 10 mL) and water (2 x 10 mL). The organic phase was then dried over sodium sulphate, filtered and concentrated *in vacuo* to yield the *propargyl amide* (70 mg, 26%) as an off white solid. IR V_{max} (Nujol)/cm^{-1} 3291 (NH), 1642 (C=O); ^{1}H NMR (400 MHz, $CDCl_3$) δ 2.30 (t, *J* = 2.6 Hz, 1H, alkyne-H), 4.08 (s, 2H, CH_2), 4.10 (dd, *J* = 5.4, 2.5 Hz, 2H, CH_2), 6.93 (bs, 1H, N*H*). ^{13}C NMR (100 MHz, $CDCl_3$) δ 29.6 (*C*H_2NH), 42.4 (*C*H_2-Cl), 72.1 (*C*q alkyne), 78.7 (*C*H), 165.8 (*C*=O). HRMS (ESI) required for $C_5H_6ClNO^+$ 131.0138 / 133.0108 not observed potentially due to a low mr.

Synthesis of 3-azidopropanoic acid (155)

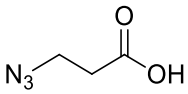

3-Bromopropanoic acid (1.93 g, mmol, 1 eq.) was dissolved in dimethylformamide (30 mL), and water (10 mL), to this stirred solution sodium azide (0.87 g, mmol, 1.1 eq.) was then slowly added over 10 minutes. The solution was then heated to 55 ˚C for 18 hours, followed by 6 hours at 67 ˚C. Once at ambient temperature water (150mL) and ethyl acetate (20 mL) were then added and the aqueous phase successively washed with ethyl acetate (2 x 20 mL), and diethyl ether (2 x 20 mL), the organic phases were then combined and dried over magnesium sulphate, filtered and concentrated *in vacuo* with the water bath at 30 ˚C, to yield the *azide* as a free flowing light yellow liquid (1.45 g, 69 %), which was then re-dissolved in ethyl acetate (5 mL) for storage. IR V_{max} (Nujol)/cm^{-1} 3454 (O-H), 2103 (N_3), 1727 (C=O), 1255 (C-O); ^{1}H NMR (400 MHz, $CDCl_3$) δ 2.66 (t, J = 6.5 Hz, 2H), 3.61 (t, J = 6.5 Hz, 2H), 10.17 (bs, 1H); ^{13}C NMR (100 MHz, $CDCl_3$) δ 33.7 (CH_2), 46.4 (CH_2), 176.4 (C=O).

Please see general experimental for brief notes on azide safety

Synthesis of the cyclen based complexes

Synthesis of tri-*tert*-butyl 2,2',2''-(1,4,7,10-tetraazacyclododecane-1,4,7-triyl)triacetate. HBr (115)[123]

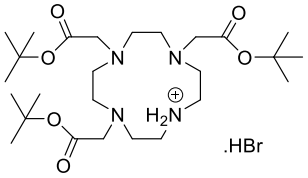

To a solution of cyclen **111** (200 mg, 1.16 mmol, 1.0 eq.) in acetonitrile (150 mL), sodium carbonate (350 mg, 3.30 mmol, 3.0 eq.) was added to give a white suspension that was stirred for 15 minutes under a nitrogen atmosphere. A solution of *tert*-butyl bromoacetate (660 mg, 3.40 mmol, 3.0 eq.) in acetonitrile (50 mL) was slowly added over 15 minutes and the resulting mixture stirred for 30 minutes at ambient temperature, followed by an 18 hour reflux at 80 ˚C. The white precipitate was then filtered and recrystallised from the minimum amount of boiling toluene and washed with ice cold diethyl ether (20 mL) to yield the *tri-substituted cyclen* (**6**) (590 mg, 85%) as a fine white powder. Mp. 192-193 °C (Lit. 190-191 °C);[136] IR V_{max} (KBr)/cm^{-1} 3428 (N-H), 1712 (C=O); ^{1}H NMR (400 MHz, $CDCl_3$) δ 1.46 (s, 27H, 3 x -C(CH_3)$_3$), 2.85-2.95 (m, 12H, 6 x CH_2), 3.11 (s, 4H, 2 x CH_2), 3.29 (s, 2H, CH_2), 3.37 (s, 4H, 2 x CH_2). ^{13}C NMR (100 MHz, $CDCl_3$) δ 28.2 (-C(*C*H_3)$_3$), 28.3 (-C(*C*H_3)$_3$), 47.6 (*C*H_2), 49.1 (*C*H_2), 51.1 (*C*H_2), 58.2 (*C*H_2), 81.7 (2 x -*C*(CH_3)$_3$), 81.9 (-*C*(CH_3)$_3$), 169.6 (*C*=O), 170.5 (2 x *C*=O). HRMS (ESI) required for $C_{26}H_{51}N_4O_6^+$ 515.3803 observed MH^+ 515.3819.

Synthesis of tri-*tert*-butyl 2,2',2''-(10-(2-(benzyloxy)-2-oxoethyl)-1,4,7,10-tetraazacyclododecane-1,4,7-triyl)triacetate (116)[123]

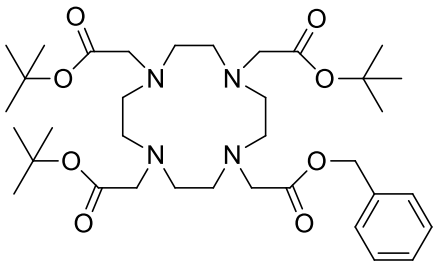

To a solution of compound **115** (100 mg, 0.168 mmol, 1.0 eq.) in acetonitrile (2 mL), potassium carbonate (40 mg, 0.29 mmol, 1.3 eq.) was added to give a white suspension that was stirred for 15 minutes under a nitrogen atmosphere. A solution of benzyl bromoacetate (90 mg, 0.39 mmol, 2.0 eq.) in acetonitrile (1 mL) was added and the mixture stirred at ambient temperature for 16 hours. The white precipitate was then filtered and the filtrate concentrated *in vacuo*. The residue was then dissolved in chloroform (10 mL) and successively washed with water (3 x 10 mL). The organic phase was dried over magnesium sulphate, filtered and concentrated *in vacuo* to give the *benzyl ester* (**5**) (103 mg, 93%) as a yellow-brown oil. IR V_{max} ($CHCl_3$)/cm^{-1} 3691, 2931, 1727 (C=O), 1602 (C=O); 1456 (C-O); ^{1}H NMR (400 MHz, $CDCl_3$) δ 1.4 (s, 27H, 3 x -C(C*H*$_3$)$_3$), 2.05-3.75 (m, 24H, 12 x C*H*$_2$), 7.35-7.42 (m, 5H, 5 x Ar*H*); ^{13}C NMR (100 MHz, $CDCl_3$) δ 25.9 (CH_2), 27.9 (-C(*C*H$_3$)$_3$), 28.0 (-C(*C*H$_3$)$_3$), 28.2 (-C(*C*H$_3$)$_3$), 55.1 (-*C*(CH$_3$)$_3$), 55.7 (-*C*(CH$_3$)$_3$), 55.8 (-*C*(CH$_3$)$_3$), 66.9 (CH_2), 67.9 (CH_2), 128.4 (2 x Ar-*C*H), 128.6 (Ar-*C*H), 128.7 (2 x Ar-*C*H), 135.0 (Ar-*C*q), 167.1 (C=O), 173.0 (C=O), 173.1 (C=O), 173.6 (C=O). HRMS (ESI) required for $C_{35}H_{59}N_4O_8^+$ 663.4327 observed MH^+ 663.4326.

Synthesis of 2-(4,7,10-tris(2-(*tert*-butoxy)-2-oxoethyl)-1,4,7,10-tetraazacyclododecan-1-yl)acetic acid (117)[123]

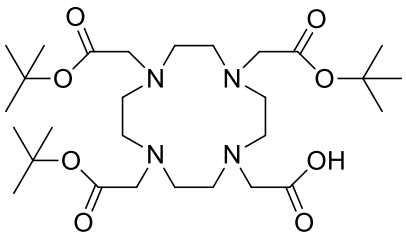

To a solution of cyclen **115** (32 mg, 48 µmol, 1.0 eq.) in methanol (10 mL), Pd/C (7 mg, 10% weight loading) in water (3 mL) was then added. The system atmosphere was then evacuated, flushed with nitrogen three times; and the evacuation process repeated with hydrogen three times. The resulting black suspension was stirred for 24 hours at ambient temperature. The suspension was filtered, concentrated *in vacuo* and then lyophilised, to yield the *free acid* as a clear-yellow oil (27 mg, 98%). IR V_{max} ($CHCl_3$)/cm^{-1} 1727 (C=O), 1155 (C-O); ^{1}H NMR (400MHz, $CDCl_3$) δ 1.49 (s, 27H, 3 x -C(CH_3)$_3$), 2.15-4.51 (m, 24H, 12 CH_2); ^{13}C NMR (100 MHz, $CDCl_3$) δ 27.9 (CH_3), 28.1 (CH_3), 28.2 (CH_3), 53.4 (CH_2), 55.7 (CH_2), 81.8 (-*C*(CH_3)$_3$), 128.5 (C=O), 128.7 (C=O). HRMS (ESI) required for $C_{28}H_{53}N_4O_8^+$ 573.3858 observed MH^+ 573.3878.

Synthesis of tri-*tert*-butyl 2,2',2''-(10-(2,2-dimethyl-4,20-dioxo-3,9,12,15-tetraoxa-5,19-diazahenicosan-21-yl)-1,4,7,10-tetraazacyclododecane-1,4,7-triyl)triacetate (131)

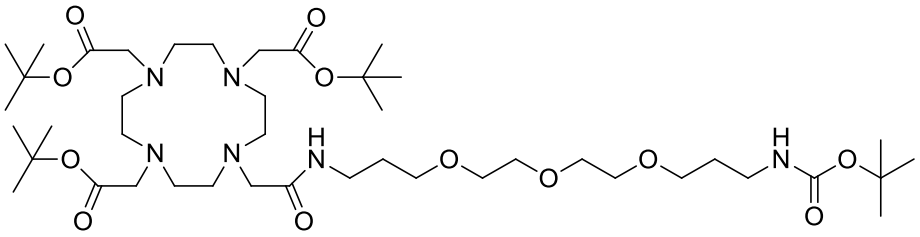

The title compound was synthesised using a procedure adapted from the literature.[137] Cyclen acid **117** (54 mg, 0.094 mmol, 1.0 eq.), CDI (18 mg, 0.11 mmol, 1.0 eq.) and protected diamine **128** (40 mg, 0.13 mmol, 1.2 eq.) were dissolved in dichloromethane (5 mL) and stirred for 18 hours at ambient temperature. The solution was then concentrated *in vacuo* and purified *via* column chromatography (chloroform: ethanol; 9:1) to give the *amide* as a dark orange wax (31 mg, 38%). IR V_{max} ($CHCl_3$)/cm^{-1} 3154, 1710, 1596, 1470, 1159, 1096; ^{1}H NMR (400 MHz, $CDCl_3$) δ 1.40-1.55 (m, 36H, 4 x -C(CH_3)$_3$), 1.67-1.80 (m, 4H, 2 x CH_2), 1.89-1.98 (m, 2H, CH_2), 2.05-3.44 (m, 20H, 10 x cyclen-CH_2), 3.48 (t, *J* = 6.0 Hz, 2H), 3.52-3.62 (m, 8H, O-CH_2-CH_2-O), 3.63-3.73 (m, 12H, HN-CH_2- CH_2- CH_2-O); ^{13}C NMR (100 MHz, $CDCl_3$) δ 27.9 (-C(*C*H_3)$_3$), 28.5 (3 x -C(*C*H_3)$_3$), 29.7 (*C*H_2), 38.3 (*C*H_2), 40.2 (*C*H_2), 44.8 (*C*H_2), 54.3 (*C*H_2), 55.6 (*C*H_2), 55.7 (-*C*(CH$_3$)$_3$), 57.5 (*C*H_2), 59.7 (*C*H_2), 67.1 (*C*H_2), 67.7 (*C*H_2), 69.3 (*C*H_2), 69.7 (*C*H_2), 70.1 (*C*H_2), 70.2 (*C*H_2), 70.2 (*C*H_2), 70.3 (*C*H_2), 70.6 (*C*H_2), 70.8 (*C*H_2), 82.2 (-*C*(CH$_3$)$_3$), 82.3 (-*C*(CH$_3$)$_3$), 82.6 (-*C*(CH$_3$)$_3$), 148.7 (*C*=O), 156.1 (*C*=O), 172.8 (*C*=O), 172.9 (*C*=O). HRMS (ESI) required for $C_{43}H_{83}N_6O_{12}^+$ 875.6069 observed MH^+ 875.5792 (in 1% trifluoroacetic acid/ methanol).

Synthesis of 2-(1,4,7,10-tetraazacyclododecan-1-yl)ethanol (121)[138]

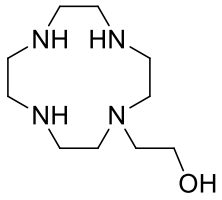

Bromoethanol (27 mg, 0.22 mmol, 1.0 eq.) was added to a suspension of cyclen **111** (77 mg, 0.45 mmol, 2.0 eq.) in acetonitrile (40 mL), followed by the addition of potassium carbonate (145 mg, 1.05 mmol, 5.0 eq.). This reaction mixture was heated to 55 ˚C and stirred under a nitrogen atmosphere for 7 hours. The suspension was then filtered and concentrated *in vacuo* to yield the crude title *alcohol* as a white solid (29 mg, 63%). IR V_{max} (Nujol)/cm^{-1} 3271w (O-H), 1595s (N-H); ^{1}H NMR (400 MHz, $CDCl_3$) δ 2.53-3.58 (m, 20H, 10 x CH_2); ^{13}C NMR (100 MHz, $CDCl_3$) δ 46.4 (*C*H_2), 46.0 (*C*H_2), 47.0 (*C*H_2), 51.9 (*C*H_2), 52.2 (*C*H_2), 56.6 (*C*H_2), 56.8 (*C*H_2), 59.1 (*C*H_2), 60.1 (*C*H_2), 64.6 (*C*H_2). HRMS (ESI) required for $C_{10}H_{24}N_4O^+$ 217.1984 observed MH^+ 217.2043.

Synthesis of tri-*tert*-butyl 2,2',2''-(10-(3,19-dioxo-1-phenyl-2,8,11,14-tetraoxa-4,18-diazaicosan-20-yl)-1,4,7,10-tetraazacyclododecane-1,4,7-triyl)triacetate (134)

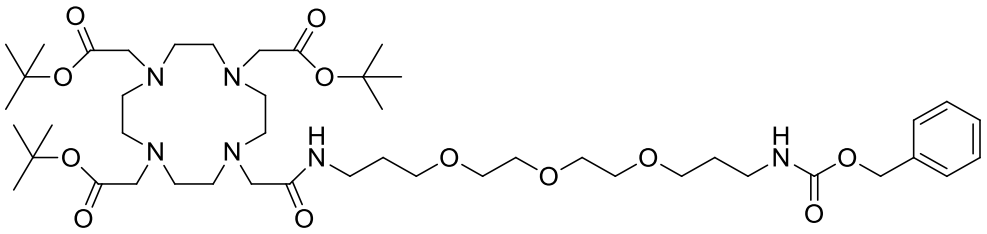

Cyclen **111** (72 mg, 0.14 mmol, 1.1 eq.), α-bromo amide **133** (67 mg, 0.13 mmol, 1eq.) and potassium carbonate (23 mg, 0.17 mmol, 1.3 eq.) were stirred under a nitrogen atmosphere in acetonitrile for 24 hours. The white precipitate was then filtered and the filtrate concentrated *in vacuo*. The residue was then dissolved in dichloromethane (10 mL) and successively washed with water (3 x 10 mL). The organic phase was dried over magnesium sulphate, filtered and concentrated *in vacuo* to give the *amide* (118 mg, 98%) as a brown oil. IR V_{max} (Nujol)/cm^{-1} 1727s (C=O), 1669 (C=O); ^{1}H NMR (400 MHz, $CDCl_3$) δ 1.43 (s, 27H, -C(CH_3)$_3$), 1.70-1.78 (m, 4H, O-CH_2-CH_2-O), 1.91-3.19 (m, 24H, CH_2), 3.24-3.32 (m, 4H, O-CH_2-CH_2-O), 3.45-3.64 (m, 12H, HN-CH_2- CH_2- CH_2-O), 5.06 (s, 2H, O-CH_2-Ph), 7.23-7.37 (m, 5H, Ar). ^{13}C NMR (100 MHz, $CDCl_3$) δ 27.9 (-C(*C*H_3)$_3$), 27.9 (-C(*C*H_3)$_3$), 28.0 (-C(*C*H_3)$_3$), 29.3 (CH_2), 36.7 (CH_2), 69.3 (CH_2), 69.5 (CH_2), 70.0 (CH_2), 70.1 (CH_2), 70.4 (CH_2), 70.5 (CH_2), 81.7 (-*C*(CH_3)$_3$), 81.8 (-*C*(CH_3)$_3$), 82.0 (-*C*(CH_3)$_3$), 127.9 (Ar-*C*H), 128.0 (Ar-*C*H), 128.4 (Ar-*C*H), 156.5 (Cq), 171.6 (C=O), 172.4 (C=O), 172.9 (C=O). HRMS (ESI) required for $C_{46}H_{81}N_6O_{12}^+$ 909.5907 observed MH^+ 909.5891.

Synthesis of (S)-tri-*tert*-butyl 2,2',2''-(10-(2-(2-(methoxycarbonyl)pyrrolidin-1-yl)-2-oxoethyl)-1,4,7,10-tetraazacyclododecane-1,4,7-triyl)triacetate (140)

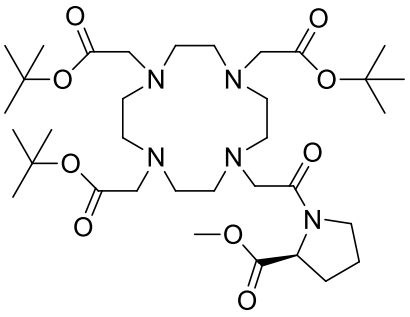

Cyclen **111** (350 mg, 0.681 mmol, 1.0 eq.), α-bromo amide **139** (190 mg, 0.770 mmol, 1.1 eq.) and potassium carbonate (190 mg, 1.38 mmol, 2.0 eq.) were stirred under a nitrogen atmosphere in acetonitrile (10 mL) for 24 hours. The white precipitate was then filtered and the filtrate concentrated *in vacuo*. Resulting in the crude *amide* (118 mg, 98%) as a brown oil. IR V_{max} (Nujol)/cm^{-1} 1724b (C=O), 1651 (C=O); ^{1}H NMR (400 MHz, $CDCl_3$) δ 1.38-1.47 (m, 27H, C(C*H*$_3$)$_3$), 2.03-3.62 (m, 30H, C*H*$_2$), 4.39-4.52 (m, 1H, C*H*); ^{13}C NMR (100 MHz, $CDCl_3$) δ 27.8 (C(*C*H$_3$)$_3$), 27.9 (C(*C*H$_3$)$_3$), 27.9 (C(*C*H$_3$)$_3$), 46.2 (*C*H$_2$), 46.7 (*C*H$_2$), 55.6 (*C*H$_2$), 55.7 (*C*H$_2$), 58.8 (*C*H), 81.9 (*C*(CH$_3$)$_3$), 81.8 (*C*(CH$_3$)$_3$), 81.7 (*C*(CH$_3$)$_3$), 172.7 (C=O), 172.7 (C=O), 172.9 (C=O). HRMS (ESI) required for $C_{34}H_{62}N_5O_9^+$ 684.4547 observed MH$^+$ 684.4581

Synthesis of (S)-1-(2-(4,7,10-tris(2-(*tert*-butoxy)-2-oxoethyl)-1,4,7,10-tetraazacyclododecan-1-yl)acetyl)pyrrolidine-2-carboxylic acid (141)

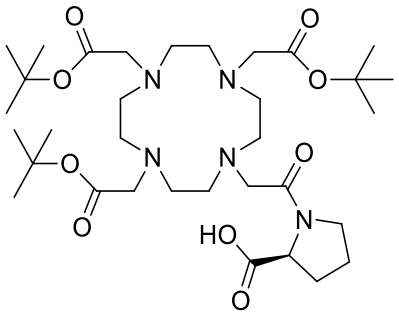

Cyclen **140** (450 mg, 6.59 mmol, 1.0 eq.) and sodium hydroxide (70.0 mg, 1.75 mmol, 2.5 eq.) were dissolved in a mixture of water (5 mL) and THF (5 mL). The solution was stirred for 24 hours, and then concentrated *in vacuo*. The residue was then dissolved in water (20 mL) and successively washed with dichloromethane (3 x 10 mL). The aqueous phase was then lyophilised to yield the acid () (360 mg, 81%) as a fine orange powder. Mp. 66-67 ˚C; IR V_{max} (Nujol)/cm^{-1} 1729 (C=O), 1591w (C=O); ^{1}H NMR (400 MHz, MeOD) δ 1.45-1.58 (m, 27H, C(C*H*$_3$)$_3$), 1.76-3.29 (m, 34H, CH$_2$), 4.04-4.13 (m, 1H, CH); ^{13}C NMR (100 MHz, MeOD) δ 27.1 (C(*C*H$_3$)$_3$), 27.1 (C(*C*H$_3$)$_3$), 28.6 (CH$_2$), 29.9 (CH$_2$), 34.0 (CH$_2$), 55.3 (CH$_2$), 55.5 (CH$_2$), 55.7 (CH$_2$), 61.3 (CH), 81.1 (*C*(CH$_3$)$_3$), 81.3 (*C*(CH$_3$)$_3$), 81.6 (*C*(CH$_3$)$_3$), 169.2 (C=O), 170.5 (C=O), 172.8 (C=O), 173.0 (C=O), 173.2 (C=O). HRMS (ESI) required for $C_{33}H_{60}N_5O_9^+$ 670.4391 observed MH$^+$ 670.4400.

Synthesis of tri-*tert*-butyl 2,2',2''-(10-(2-oxo-2-(prop-2-yn-1-ylamino)ethyl)-1,4,7,10-tetraazacyclododecane-1,4,7-triyl)triacetate (147)

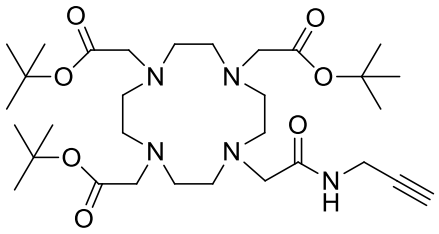

Cyclen **111** (210 mg, 0.490 mmol, 1.0 eq.) and α-bromo alkyne **146** (80 mg, 0.44 mmol, 1.1 eq.) were dissolved in acetonitrile (10 mL). Potassium carbonate (120 mg, 0.870 mmol, 2.0 eq.) was then added. The solution was then stirred for 24 hours at 60 °C, and then concentrated *in vacuo*. The residue was then dissolved in dichloromethane (10 mL) and successively washed with water (3 x 10 mL). The organic phase was dried over sodium sulphate, filtered and concentrated *in vacuo* to give the *amide* (250 mg, 94%) as an off white solid. Mp. 94-95 ˚C; IR V_{max} (Nujol)/cm^{-1} 1721 (C=O), 1680 (C=O); ^{1}H NMR (400 MHz, $CDCl_3$) δ 1.39 (s, 27H, C(C*H*$_3$)$_3$), 2.15 (s, 1H, CH_2CCH), 2.16-3.94 (m, 24H, NC*H*$_2$C*H*$_2$N, and C*H*$_2$), 3.98 (m, 2H, C*H*$_2$CCH), 8.80 (t, *J* = 5.5 Hz, 1H, N*H*); ^{13}C NMR (100 MHz, $CDCl_3$) δ 27.8 (C(*C*H$_3$)$_3$), 27.9 (C(*C*H$_3$)$_3$), 28.0 (C(*C*H$_3$)$_3$), 28.5 (*C*H$_2$), 29.3 (*C*H$_2$), 29.4 (*C*H$_2$), 55.6 (*C*H$_2$), 56.1 (*C*H$_2$), 56.2 (N*C*H2*C*H2N, *C*H2), 69.6 (Alkyne *C*H), 71.2 (Alkyne Cq), 80.8 (*C*(CH$_3$)$_3$), 81.8 (*C*(CH$_3$)$_3$), 82.0 (*C*(CH$_3$)$_3$), 171.8 (C=O), 172.4 (*C*=O), 172.8 (C=O). HRMS (ESI) required for $C_{31}H_{55}N_5O_7^+$ 610.4179 observed MH^+ 610.4174.

Synthesis of 2,2',2''-(10-(2-oxo-2-(prop-2-yn-1-ylamino)ethyl)-1,4,7,10-tetraazacyclododecane-1,4,7-triyl)triacetic acid (**160**)

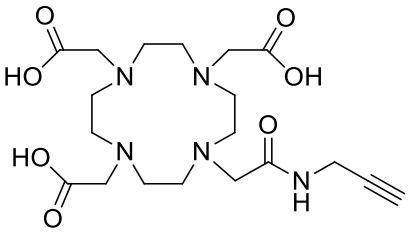

Protected Alkyne **147** (383mg, 0.629 mmol, 1 eq.) was dissolved in formic acid (10 mL), and water (0.5 mL) and heated to 60 ˚C for 18 hours under nitrogen. Once at ambient temperature the solvent was removed in vacuo to yield the title compound (261 mg, 94%). Decomp 224 ˚C; IR V_{max} (Nujol)/cm^{-1} 1646 (C=O); ^{1}H NMR (400 MHz, D_2O) δ 2.53 (apparent q, J = 4.0 Hz, alkyne CH), 2.77-3.99 (m, 26H, NC*H*$_2$C*H*$_2$N, and C*H*$_2$); ^{13}C NMR (100 MHz, D_2O) δ 28.8 (*C*H$_2$), 28.9 (*C*H$_2$), 29.0 (*C*H$_2$), 48.3 (*C*H$_2$), 48.6 (*C*H$_2$), 50.5 (*C*H$_2$), 51.3 (*C*H$_2$), 53.4 (*C*H$_2$), 55.2 (*C*H$_2$), 55.6 (*C*H$_2$), 56.1 (*C*H2), 69.1 (*C*H$_2$), 71.7 (Alkyne CH), 73.4 (Alkyne Cq), 170.1 (C=O), 172.3 (*C*=O), 174.3 (C=O); HRMS (ESI) required for $C_{19}H_{32}N_5O_7^+$ 442.2296 observed MH$^+$ 442.2294. HRMS (ESI) required for $C_{19}H_{30}N_5O_7^-$ 440.2145 observed MH$^-$ 440.2148.

Synthesis of Gadolinium 2,2',2''-(10-(2-oxo-2-(prop-2-yn-1-ylamino)ethyl)-1,4,7,10-tetraazacyclododecane-1,4,7-triyl)triacetate (160)

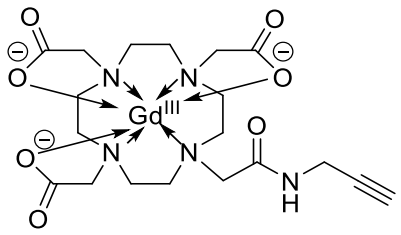

Gadolinium (III) chloride hexahydrate (237 mg, 0.639 mmol, 1 eq.) in water (3 mL), was added to chelate **160** (277 mg, 0.628 mmol, 1 eq.) dissolved in water (10 mL). The pH was then adjusted to pH 5 using aqueous potassium hydroxide (0.2 M), after 1 hour the pH was readjusted to pH 5, again using aqueous potassium hydroxide (0.2 M), followed by an 18 hour stir. The solution was then concentrated in vacuo, once dry the white solid was redissolved in ethanol (10 mL), stirred for 30 minutes and then filtered, and concentrated in vacuo to yield the gadolinium complex (370 mg, 98%). HRMS (ESI) required for $C_{19}H_{29}GdN_5O_7^+$ 593.1491, 594.1509, 595.1504, 596.1522, 597.1524, 599.1553 observed MH^+ 593.1345, 594.1294, 595.1276, 596.1288, 597.1291, 599.1309. HRMS (ESI) required for $C_{19}H_{28}ClGdN_5O_7^-$ 631.0918 observed MCl^- 627.0892, 628.0891, 630.0910, 631.0908, 632.0940, 633.0948, 635.0925, 635.0913.

Compounds towards cryptophane

Synthesis of 3-methoxy-4-(2-propenyloxy) benzenemethanol (165)

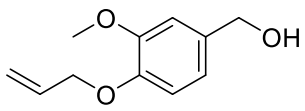

Allyl bromide (3.1 mL, 35.9 mmol, 1.1 eq.) was added to vanillyl alcohol (5.09 g, 33.1 mmol, 1 eq.) in acetone (20 mL) and stirred for 10 minutes. Potassium carbonate (4.56 g, 33.0 mmol, 1 eq.) was then added slowly which briefly resulted in the formation of a pink colour. The mixture was then heated to 60 °C for 20 hours. After cooling to room temperature, the mixture was then concentrated in vacuo, yielding a white residue which was dissolved in dichloromethane (30 mL) before being successively washed with water (100 mL), and 1M aqueous sodium hydroxide (3 x 100 mL), and brine (100 mL). The organic phase was dried over magnesium sulphate and concentrated *in vacuo* to furnish the title compound as an off white solid (5.32 g, 83%). IR V_{max} KBrcm^{-1} 3400 (O-H), 1620 (C=C); MP. 70-72 ˚C ; ^{1}H NMR (400 MHz, $CDCl_3$) δ 3.91 (s, 3H, CH_3) 4.63 (appt, J = 1.53, 1H, C*H*H-CH), 4.63-4.65 (m, 3H, CH_2-OH, CH*H*-CH), 5.30 (appdq, J = 10.4, 2.8 Hz, 1H, C*H*H alkene), 5.42 (appdq, J = 17.2, 1.6 Hz, 1H, CH*H* alkene) 6.04-6.18 (m, 1H), 6.88 (s, Ar-CH), 6.88 (s, Ar-CH), 6.96 (Ar-CH); ^{13}C NMR (100 MHz, $CDCl_3$) δ 55.9 (CH3), 65.3 (CH2), 69.9 (CH2), 110.8 (Ar-CH), 113.3 (Ar-CH), 118.0 (CH2), 119.3 (Ar-CH), 133.3 (CH), 134.0 (Ar-Cq), 147.5 (Ar-Cq), 149.6 (Ar-Cq). HRMS (ESI) required for $C_{11}H_{14}O_3Na^+$ 217.0841 observed MNa^+ 217.0841.

Synthesis of 2,7,12-tris(allyloxy)-3,8,13-trimethoxy-10,15-dihydro-5H-tribenzo[a,d,g][9]annulene (166)

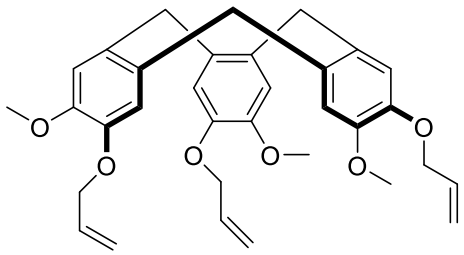

Compound **165** (5.32 g, 27.4 mmol, 1 eq.) was dissolved in methanol (40 mL) and stirred at -10 °C before hypochloric acid (70% aq, 15 mL) was slowly added over 20 minutes, resulting in the temporary formation of a purple colour. The solution was allowed to warm to room temperature and stirred for 24 hours. The solution was cooled to -10 °C before dichloromethane (40 mL) was added, generating a red/ brown colour. Aqueous sodium hydroxide (5M, 40 mL) was then added slowly over 20 minutes, before adding aqueous sodium carbonate (sat. 40 mL), turning the solution yellow. The aqueous phase was then successively extracted with dichloromethane (2 x 200 mL), and then dried over sodium sulphate, filtered and concentrated *in vacuo*. The residue was then dissolved in diethyl ether (100 mL) and digested for 24 hours. The suspension was then filtered and the solid collected, and washed with ether to yield the title compound as a white solid (rf.= 0.6 (Pet Ether: Ethyl acetate, 1:1) 1.80 g, 37%). IR V_{max} (KBr)/cm^{-1} 1608 (C=C); MP. 165-167 ˚C ; ^{1}H NMR (400 MHz, $CDCl_3$) δ 3.54 (d, J = 13.9, 1H, C*H*H), 3.87 (s, 3H, CH3), 4.56-4.68 (m, 2H, OCH_2), 4.76 (d, J = 13.7, 1H, CH*H*), 5.28 (appdd, J = 10.4, 1.2 Hz, 1H), 5.41 (appdd, J = 17.2, 1.2 Hz, 1H), 6.04-6.14 (m, 1H, OCH_2CHCH_2), 6.83 (s, 1H, Ar-CH), 6.88 (s, 1H,

Ar-CH); ^{13}C NMR (100 MHz, $CDCl_3$) δ 36.5 (CH2), 56.1 (CH3), 70.2 (CH2), 113.6 (Ar-CH), 115.5 (Ar-CH), 117.5 (CH2), 131.7 (Ar-Cq), 132.3 (Ar-Cq), 133.7 (CH), 146.7 (Ar-Cq), 148.2 (Ar-Cq). HRMS (ESI) required for $C_{33}H_{36}O_6Na^+$ 551.2410 observed MNa^+ 551.2414.

Synthesis of 3,8,13-trimethoxy-10,15-dihydro-5H-tribenzo[a,d,g][9]annulene-2,7,12-triol (167)

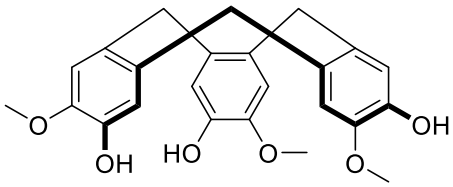

Compound **166** (5.42 g, 10.3 mmol, eq.) was dissolved in 3-propanol (250 mL), Pd/C (1.61 g, 10% weight loading) in water (20 mL), and para-toluenesulfonic acid (320 mg, mmol, eq.) were then added in that order. The suspension was stirred at 100 °C for 24 hours under a nitrogen atmosphere. The black suspension was then filtered, and concentrated in vacuo. The residue was taken up in ethyl acetate (100 mL) and washed with brine (3 x 100 mL), the organic phase was then dried over magnesium sulphate, filtered and concentrated *in vacuo*. The crude residue was then digested in chloroform (10 mL) for one hour, filtered and the solid collected yielding the title compound as an off white solid (3.28 g, 78%). IR V_{max} (KBr)/cm^{-1} 3433 (O-H); MP. 147-149 ˚C ; ^{1}H NMR (400 MHz, d-DMSO) δ ; 3.35 (d, J = 13.4 Hz, 3H, C*H*H, water overlap), 3.73 (s, 3H, CH3), 4.59 (d, J = 13.4 Hz, 1H, CH*H*), 6.84 (s, 1H, Ar-CH), 6.86 (s, 1H, Ar-CH); ^{13}C NMR (100 MHz, d-DMSO) δ 35.5 (CH_2), 56.4 (CH_3), 114.4 (Ar-CH),

117.3 (Ar-CH), 130.9 (Ar-Cq), 133.1 (Ar-Cq), 145.3 (Ar-Cq), 146.4 (Ar-Cq). HRMS (ESI) required for $C_{24}H_{24}O_6Na^+$ 431.1471 observed MNa^+ 431.1475.

Synthesis of (((((3,8,13-trimethoxy-10,15-dihydro-5H-tribenzo [a,d,g][9] annulene-2,7,12-triyl) tris(oxy))tris(ethane-2,1-diyl))tris(oxy))tris(3-methoxybenzene-4,1-diyl))trimethanol (169)

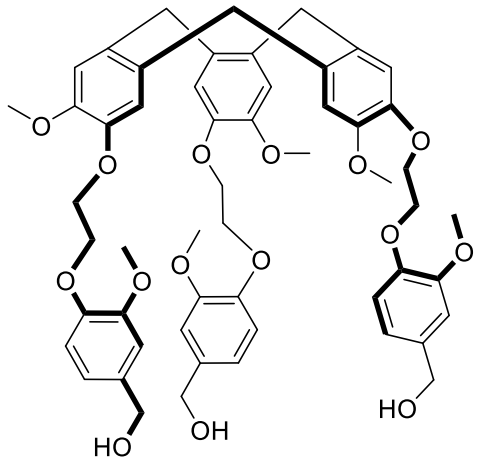

Tri-ol **167** (674 mg, 1.65 mmol, 1 eq.), bromo **168** (1.43 g, 5.50 mmol, 3.3 eq.) and caesium carbonate (1.87 g, mmol, 3.3 eq.) were dissolved in dimethylformamide (30 mL) and stirred for 24 hours at 80 °C under a nitrogen atmosphere. The suspension was concentrated in vacuo and the resultant sludge was dissolved in brine (100 mL), and extracted with ethyl acetate (3 x 100 mL). The organic extracts were then combined and successively washed with HCl (1M aq, 3 x 100 mL), sodium carbonate (sat. aq, 3 x 100 mL), and brine (3 x 100 mL), before being dried over sodium sulphate, filtered and concentrated in vacuo. The residue was then purified using column chromatography (DCM: methanol, 100, 99:1, 98:2, 97:3, 96:4, 95:5) to give the *ether* as an off white solid (rf.= 0.2 (DCM: methanol, 95:5), 243 mg, 16%). Decomp 275 ˚C; ^{1}H NMR (400 MHz, d-DMSO) δ ; 3.53 (d, J = 13.6 Hz, 1H, C*H*H), 3.68

(s, 3H, CH3), 3.74 (s, 3H, CH3), 4.18-4.32 (m, 4H, CH2CH2), 4.43 (appd, J = 6.0 Hz, 2H, CH2-OH), 4.72 (d, J = 13.2 Hz, 1H, CH*H*), 6.79-6.84 (m, 1H, Ar-CH), 6.92-6.94 (m, 2H, Ar-CH), 7.11 (s, 1H, Ar-CH), 7.18 (s, 1H, Ar-CH); ^{13}C NMR (100 MHz, d-DMSO) δ 35.5 (CH2), 55.8 (CH3), 56.3 (CH3), 63.2 (CH2), 67.7 (CH2), 67.9 (CH2), 111.3 (Ar-CH), 113.7 (Ar-CH), 114.4 (Ar-CH), 115.6 (Ar-CH), 119.0 (Ar-CH), 132.5 (Ar-Cq), 133.0 (Ar-Cq), 136.1 (Ar-Cq), 146.7 (Ar-Cq), 147.0 (Ar-Cq), 147.9 (Ar-Cq), 149.3 (Ar-Cq). HRMS (ESI) required for $C_{54}H_{60}O_{15}Na^+$ 971.3830 observed MNa^+ 971.3958.

Synthesis of cryptophane (170)

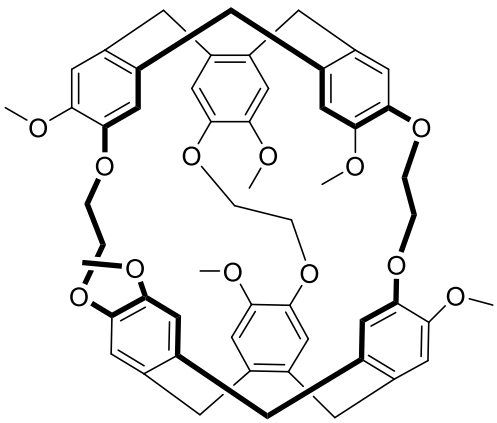

Compound **169** (223 mg, 0.235 mmol, 1 eq.) was dissolved in chloroform (15 mL) and formic acid (230 mL), and stirred for three hours at 60 °C. The solution was then concentrated in vacuo. The residue was then purified using column chromatography (ethyl acetate: petroleum ether 40/60, 4/1) to give the *cryptophane* as a white solid (rf.= 0.7 (ethyl acetate: petroleum ether 40/60, 4/1), 100 mg, 48%). Decomp. 270 ˚C; IR V_{max} (Nujol)/cm^{-1} ; ^{1}H NMR (400 MHz, $CDCl_3$) δ 3.43 (d, J = 13.9 Hz, 1H, C*H*H), 3.82

(s, 3H, CH_3) 4.18-4.20 (m, 2H, CH_2CH_2), 4.62 (d, J = 13.7 Hz, 1H, CH*H*), 6.70 (s, 1H, Ar-CH), 6.78 (s, 1H, Ar-CH); ^{13}C NMR (100 MHz, $CDCl_3$) δ 36.2 (CH2), 55.7 (CH3), 69.3 (CH2), 113.7 (Ar-CH), 120.8 (Ar-CH), 131.6 (Ar-Cq), 134.2 (Ar-Cq), 146.6 (Ar-Cq), 149.6 (Ar-Cq). HRMS (ESI) required for $C_{54}H_{55}O_{12}^+$ 895.3693 observed MH^+ 895.3603. HRMS (ESI) required for $C_{54}H_{54}O_{12}Na^+$ 917.3513 observed MNa^+ 917.3670.

Synthesis of 4-(4,6-dimethoxy-1,3,5-triazin-2-yl)-4-methylmorpholin-4-ium chloride (DMTMM)

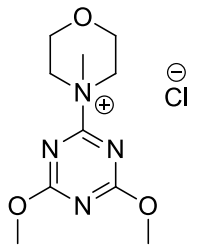

2-Chloro-4,6-dimethoxy-1,3,5-triazine (180 mg, 1.04 mmol, 1.0 eq.) and *N*-methyl morpholine (100 mg, 1.00 mmol, 1eq.) were stirred under a nitrogen atmosphere in anhydrous THF (5 mL) for one hour. The white solid precipitate was filtered, collected and washed with anhydrous THF (10 mL) to yield chloride salt (280 mg, 68%) as a white solid. Mp. 112-114 °C; IR V_{max} (Nujol)/cm^{-1} 1619 (aromatic C-N), 1128 (aliphatic C-N); ^{1}H NMR (400 MHz, MeOD) δ 3.65 (s, 3H, CH_3N), 3.86-3.97 (m, 2H, CH_2), 3.99-4.07 (m, 2H, CH_2), 4.11-4.15 (m, 1H, CH_2), 4.15-4.19 (m, 1H, CH_2), 4.24 (s, 6H, CH_3); ^{13}C NMR (100 MHz, MeOD) δ 55.2 (CH_3), 56.4 (CH_3), 60.1 (CH_2), 61.9 (CH_2), 170.6 (Cq), 174.1 (Cq). HRMS (ESI) required for $C_{10}H_{17}N_4O_3^+$ 241.1295 observed MH^+ 241.1313.

General SPPS methodology

All flow rates are 3 mL/ second.

General procedure 1 - Resin loading

2-Chlorotrityl chloride resin was suspended in dichloromethane (2 mL) and very slowly stirred. Fmoc-AA-OH (1.2 eq.) was added followed by diisopropylethylamine (2.0 eq.), once no more HCl gas was observed the resin was stirred for 3 hours. Excess methanol (2 mL) was then added and stirred for a further 20 minutes. The resin was then filtered and washed with dimethylformamide (3 mL x 2), dichloromethane (5 mL x 2), hexane (5 mL x 2), dimethylformamide (3 mL x 2), dichloromethane (5 mL x 2) and finally hexane (5 mL x 2). The resin was then dried *in vacuo*, and a sample removed for testing. Once tested the resins were soaked overnight in dichloromethane / dimethylformamide (3 mL, 1:1).

General procedure 2 – Loading testing

Loaded resin (~10 mg) was stirred in piperidine/ dimethylformamide (3 mL, 2:8) for 2 hours, the absorbance at 290 nm was then measured indicating Fmoc presence, and therefore amino acid loaded, according to the Beer-Lambert equation. The remaining resin was transferred to a peptide synthesiser column.[111]

General procedure 3 – Fmoc deprotection

The resin was washed by a steady stream of dimethylformamide, followed by a piperidine / dimethylformamide (2:8) mix until the absorbance at 290nm was reduced to start point, followed by an additional dimethylformamide wash.

General procedure 4 - Subsequent Fmoc-AA-OH

For all acid couplings, Fmoc-AA-OH (4.0 eq.), PyOxim **52** (4.0 eq.), and diisopropylethylamine (4.5 eq.) in dimethylformamide (1.5 mL) were added to pre-treated resin in a peptide synthesiser column and stirred intermittently for 3 hours.

General procedure 5 – "Click" chemistry

The azide labelled substrate was slowly stirred in DMSO, water and acetonitrile (2:1:1, 1 mL). To this the Gd^{III}-DO3A alkyne was added (3 eq.) in DMSO (0.5 mL), copper (II) sulphate pentahydrate (1 eq. wt.) and sodium ascorbate (1 eq. wt.) were then added. The suspension was allowed to slowly stir for 20 hours.

General procedure 6 – "Click" washings

The resin bound product was successively washed with water, methanol, acetonitrile and dichloromethane.

General procedure 7 – Cleavage

The desired peptide on resin was loaded into a syringe pre-fitted with cotton wool and a needle. The loaded resin was then washed with cleavage mixture (TFA: TIPS: H_2O, 9: 0.5: 0.5, 20 mL) and the solution slowly stirred for 6 hours before being concentrated *in vacuo*. The cleaved residue was then washed with cold diethyl ether and filtered. The collected peptide was then dried *in vacuo*.

General procedure 8 – HPLC

Reversed-phase HPLC starting with eluent 100% A, increasing B to 90% to 25 minutes on a gradient, followed by 95% B at 27 minutes. The chromatogram was monitored at 215nm. A: water, 0.1% formic acid, B: acetonitrile, 0.1% formic acid.

Final peptide structures

Synthesis of JK-X

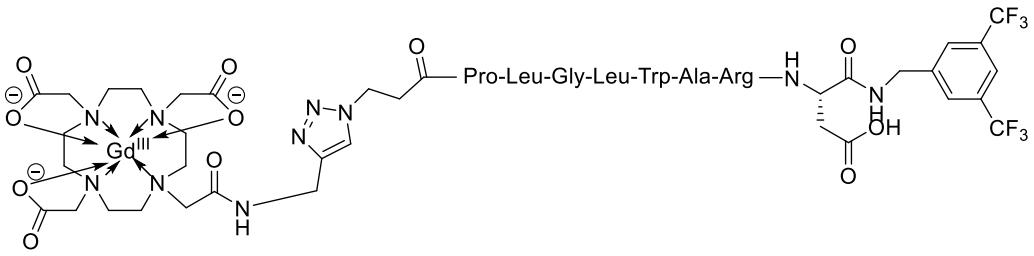

FAA **76** was loaded on to the resin general procedure 1, and tested using general procedure 2. Using the Fmoc chemistry in general procedure 3, Fmoc-Arg(Pbf)-OH, Fmoc-Ala-OH, Fmoc-Trp(Boc)-OH, Fmoc-Leu-OH, Fmoc-Gly-OH, Fmoc-Leu-OH, Fmoc-Pro-OH, and azido-acid **155** were successively conjugated. General method 4 was then used to "Click" alkyne **160** on to the peptide, followed by general procedure 5. Cleavage was then achieved using general method 6 with a cleavage mixture of trifluoroacetic acid: TIPS: H_2O (95:2.5:2.5), followed by purification using general method 7. HRMS (ESI) observed MH^{2+} 921.8118, 922.3961, 922.9092, 923.4510, 923.9075, 924.4067.

Synthesis of JK-1

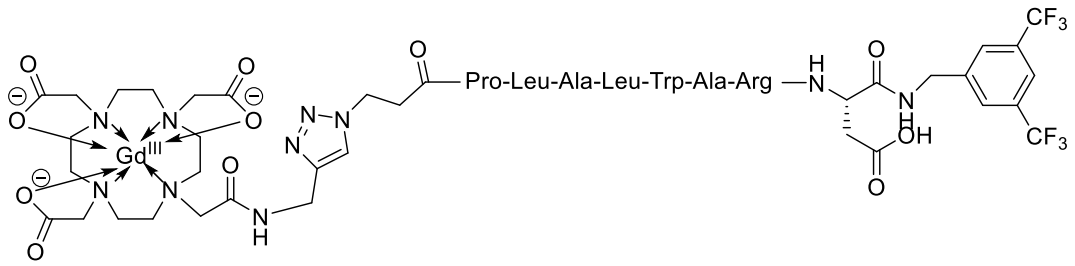

FAA **76** was loaded on to the resin general procedure 1, and tested using general procedure 2. Using the Fmoc chemistry in general procedure 3, Fmoc-Arg(Pbf)-OH, Fmoc-Ala-OH, Fmoc-Trp(Boc)-OH, Fmoc-Leu-OH, Fmoc-Ala-OH, Fmoc-Leu-OH, Fmoc-Pro-OH, and azido-acid **155** were successively conjugated. General method 4 was then used to "Click" alkyne **160** on to the peptide, followed by general procedure 5. Cleavage was then achieved using general method 6 with a cleavage mixture of trifluoroacetic acid: TIPS: H_2O (95:2.5:2.5), followed by purification using general method 7. HRMS (ESI) observed MH^{2+} 928.8567, 929.3553, 929.8542, 930.3542, 931.3538, 931.8563.

Synthesis of JK-2/9

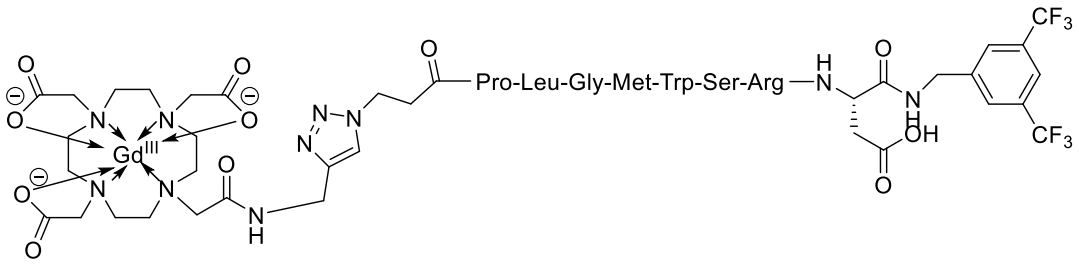

FAA **76** was loaded on to the resin general procedure 1, and tested using general procedure 2. Using the Fmoc chemistry in general procedure 3, Fmoc-Arg(Pbf)-OH, Fmoc-Ser(O^{t}Bu)-OH, Fmoc-Trp(Boc)-OH, Fmoc-Met-OH, Fmoc-Gly-OH, Fmoc-Leu-OH, Fmoc-Pro-OH, and azido-acid **155** were successively conjugated. General method 4 was then used to "Click" alkyne **160** on to the peptide, followed by general procedure 5. Cleavage was then achieved using general method 6 with a cleavage mixture of trifluoroacetic acid: TIPS: H_2O (95:2.5:2.5), followed by purification using general method 7. HRMS (ESI) observed MH^{2+} 938.6716, 939.1606, 939.6497, 940.1388, 940.6282, 941.1608.

Synthesis of JK-3

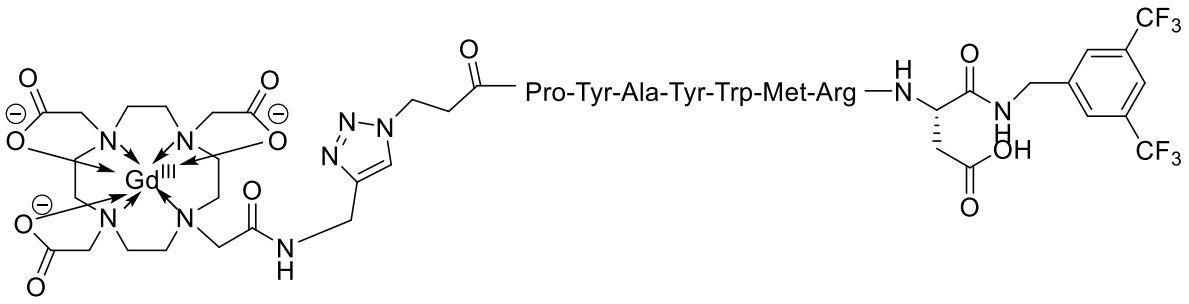

FAA **76** was loaded on to the resin general procedure 1, and tested using general procedure 2. Using the Fmoc chemistry in general procedure 3, Fmoc-Arg(Pbf)-OH, Fmoc-Met-OH, Fmoc-Trp(Boc)-OH, Fmoc-Tyr(Trt)-OH, Fmoc-Ala-OH, Fmoc-Tyr(Trt)-OH, Fmoc-Pro-OH, and azido-acid **155** were successively conjugated. General method 4 was then used to "Click" alkyne **160** on to the peptide, followed by general procedure 5. Cleavage was then achieved using general method 6 with a cleavage mixture of trifluoroacetic acid: TIPS: H_2O (95:2.5:2.5), followed by purification using general method 7. MH^{2+} 1008.4237, 1008.9196, 1009.4211, 1010.4232, 1010.9216.

Synthesis of JK-7

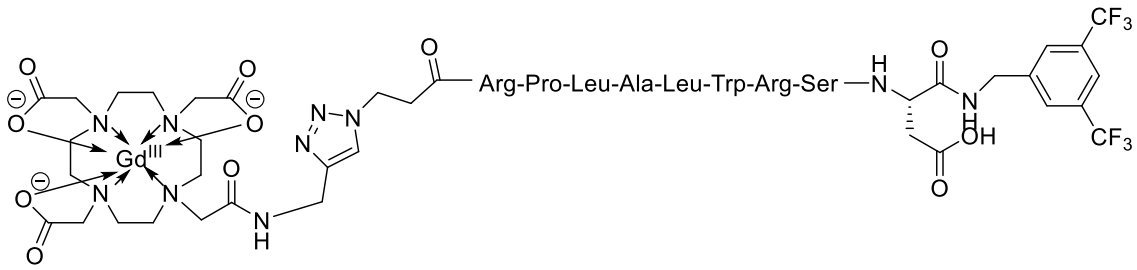

FAA **76** was loaded on to the resin general procedure 1, and tested using general procedure 2. Using the Fmoc chemistry in general procedure 3, Fmoc-Ser(O^{t}Bu)-OH, Fmoc-Arg(Pbf)-OH, Fmoc-Trp(Boc)-OH, Fmoc-Leu-OH, Fmoc-Ala-OH, Fmoc-Leu-OH, Fmoc-Pro-OH, Fmoc-Arg(Pbf)-OH and azido-acid **155** were successively conjugated. General method 4 was then used to "Click" alkyne **160** on to the peptide, followed by general procedure 5. Cleavage was then achieved using general method 6 with a cleavage mixture of trifluoroacetic acid: TIPS: H_2O (95:2.5:2.5), followed by purification using general method 7. MH^{2+} 1015.3204, 1015.8188, 1016.3178, 1016.8198, 1017.8242, 1018.3277.

Synthesis of JK-8

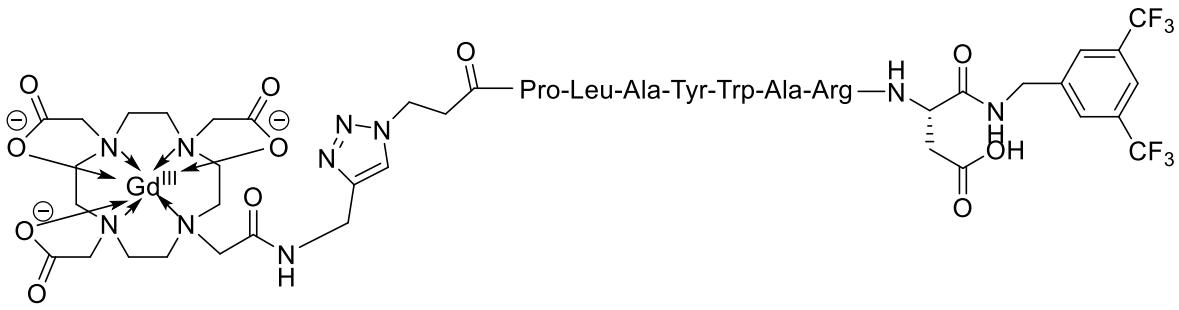

FAA **76** was loaded on to the resin general procedure 1, and tested using general procedure 2. Using the Fmoc chemistry in general procedure 3, Fmoc-Arg(Pbf)-OH, Fmoc-Ala-OH, Fmoc-Trp(Boc)-OH, Fmoc-Tyr(Trt)-OH, Fmoc-Ala-OH, Fmoc-Leu-OH, Fmoc-Pro-OH, and azido-acid **155** were successively conjugated. General method 4 was then used to "Click" alkyne **160** on to the peptide, followed by general procedure 5. Cleavage was then achieved using general method 6 with a cleavage mixture of trifluoroacetic acid: TIPS: H_2O (95:2.5:2.5), followed by purification using general method 7. HRMS (ESI) observed MH^{2+} 953.7017, 954.2007, 954.6995, 955.7017, 956.2011, 956.6810.

Activation of pro-MMP to active form

Stock A: Aqueous (50 mM Tris, 10 mM $CaCl_2$, 150 mM NaCl, 0.05% (w/v) Brij35) at pH 7.5.

Stock B: *P*-aminophenylmercuric acetate (APMA) (100 mM) in DMSO.

The desired MMP was diluted to 100 µg/ mL in stock A with a final concentration of APMA of 1mM and incubate for one hour 37 °C. Following removal from the incubator, the solution was diluted to 10 µg/ mL and stored at -20 °C.

^{19}F time-course methods and data handling

Data generation from TopSpin

In order generate data which can be used for plotting purposes; the data must be converted into a suitable format, for example as an intensity or area plot from the time course experiments.

Topspin was used to generate a data set for fitting purposes. To create a .txt file containing the relevant information, the data-set containing the time course was opened, and the baseline corrected as well as being correctly phased. The baseline and phase correction must be done otherwise the resultant data would have been incorrect, this was corrected by selecting multi-display, and the time course was then checked through to ensure that the data did not fluctuate and was constant. Then “analaysis”, “T1/T2”, “baseline”, “Fid” were selected, followed by “spectrum” to access the time course as a 2D plot with the ability to go through slices of the experiment. The desired region of the plot was selected by using the “peak/ranges” function. Once the desired area was selected this was saved as a “Relaxation Module Return”. Returning to the “D plot, accessing the relaxation module, gave a graph of the desired plots as either area or intensity, selecting “fit” to gave a graph of the

selected peak, which was then saved as a .txt file containing the data sets for the plotting. This .txt file was then modified to remove the information which was not required (empty columns and spacings etc.).

R Studio plotting methodology

The generated .txt file was then opened in R Studio. A package called LambertW was installed (this was only done on the initial use of the program). The LambertW function contains a solution for a non-linear Michaelis-Menten plot.

The initial concentration of the probe in the sample was loaded into the program (S_0 as the initial concentration). In R Studio the "i" (intensity) was copied to create an "s" (concentration) then any modifcations were performed on the "s", from the raw data file, "t" (time) was also a component used during the fit.

An array of data from the sets taken from "t" and "s" were chosen for the plot. This data was then added into a linear Michaelis-Menten plot giving a straight line equation, VMax (1/ gradient), K_M (y intercept), these were the approximate values which were used in the next step. The numbers generated from the linear plot were then fed into the LambertW function, in the co summary of R Studio. The LambertW function was then used to give a plot for the data. The values generated from the linear plot and non-linear plot can then be mapped on the same plot area as the raw data showing that the non-linear plot fits with the experimental data.

Inversion recovery experiments

The times used for the inversion were:

Pre cleavage (s): 0.001, 0.005, 0.01, 0.015, 0.02, 0.025, 0.04, 0.045, 0.05, 0.1, 0.2, 0.5, 1, 3, 4.

Post cleavage (s): 0.01, 0.05, 0.1, 0.15, 0.2, 0.3, 0.6, 0.7, 0.8, 0.9, 1, 1.5, 1.9, 2, 5, 8.

References

1. A. Jemal, R. C. Tiwari, T. Murray, A. Ghafoor, A. Samuels, E. Ward, E. J. Feuer and M. J. Thun, *Ca-Cancer J. Clin.*, 2004, **54**, 8-29.
2. J. Gross and C. M. Lapiere, *Proc. Natl. Acad. Sci. U. S. A.*, 1962, **48**, 1014-&.
3. K. Kessenbrock, V. Plaks and Z. Werb, *Cell*, 2010, **141**, 52-67.
4. J. O. McIntyre and L. M. Matrisian, *J. Cell. Biochem.*, 2003, **90**, 1087-1097.
5. I. Massova, L. P. Kotra, R. Fridman and S. Mobashery, *FASEB J.*, 1998, **12**, 1075-1095.
6. E. B. Springman, E. L. Angleton, H. Birkedalhansen and H. E. Vanwart, *Proc. Natl. Acad. Sci. U. S. A.*, 1990, **87**, 364-368.
7. C. Gialeli, A. D. Theocharis and N. K. Karamanos, *FEBS J.*, 2011, **278**, 16-27.
8. L. A. Liotta, K. Tryggvason, S. Garbisa, I. Hart, C. M. Foltz and S. Shafie, *Nature*, 1980, **284**, 67-68.
9. A. M. Weaver, *Clin. Exp. Metastasis*, 2006, **23**, 97-105.
10. K. Oda, Y. Matsuoka, A. Funahashi and H. Kitano, *Mol. Syst. Biol.*, 2005, **1**, 17.
11. M. Suzuki, G. Raab, M. A. Moses, C. A. Fernandez and M. Klagsbrun, *J. Biol. Chem.*, 1997, **272**, 31730-31737.
12. W. H. Yu, J. F. Woessner, J. D. McNeish and I. Stamenkovic, *Genes Dev.*, 2002, **16**, 307-323.
13. J. E. Rundhaug, *Clin. Cancer Res.*, 2003, **9**, 551-554.
14. G. Bergers, R. Brekken, G. McMahon, T. H. Vu, T. Itoh, K. Tamaki, K. Tanzawa, P. Thorpe, S. Itohara, Z. Werb and D. Hanahan, *Nat. Cell Biol.*, 2000, **2**, 737-744.
15. M. S. O'Reilly, D. Wiederschain, W. G. Stetler-Stevenson, J. Folkman and M. A. Moses, *J. Biol. Chem.*, 1999, **274**, 29568-29571.

16. K. Wolf, Y. I. Wu, Y. Liu, J. Geiger, E. Tam, C. Overall, M. S. Stack and P. Friedl, *Nat. Cell Biol.*, 2007, **9**, 893-U839.

17. V. Noe, B. Fingleton, K. Jacobs, H. C. Crawford, S. Vermeulen, W. Steelant, E. Bruyneel, L. M. Matrisian and M. Mareel, *J. Cell Sci.*, 2001, **114**, 111-118.

18. N. Beckmann, *Braz. J. Phys.*, 2006, **36**, 16-22.

19. D. W. a. I. Fleming, *Spectroscopic Methods in Organic Chemistry*, McGraw-Hill Education, 6th edn., 2008.

20. A. C. Guyton, *Textbook of Medical Physiology (8th ed.).* , 1991.

21. R. K. Harris, E. D. Becker, S. M. C. de Menezes, R. Goodfellow and P. Granger, *Solid State Nucl. Magn. Reson.*, 2002, **22**, 458-483.

22. G. N. Holland, P. A. Bottomley and W. S. Hinshaw, *J. Magn. Reson.*, 1977, **28**, 133-136.

23. E. McFarland, J. A. Koutcher, B. R. Rosen, B. Teicher and T. J. Brady, *Journal of Computer Assisted Tomography*, 1985, **9**, 8-15.

24. Z.-X. Jiang, Y. Feng and Y. B. Yu, *Chem. Commun.*, 2011, **47**, 7233-7235.

25. V. W. R. H. A. Harper, P. A. Mayes,, *Review of Physiological Chemistry, 16th ed.*, Lange Medical Publications, 1977.

26. B. Drahos, I. Lukes and E. Toth, *Eur. J. Inorg. Chem.*, 2012, 1975-1986.

27. C.-H. Fan, C.-Y. Ting, H.-J. Lin, C.-H. Wang, H.-L. Liu, T.-C. Yen and C.-K. Yeh, *Biomaterials*, 2013, **34**, 3706-3715.

28. S. N. Misra, M. A. Gagnani, I. Devi and R. S. Shukla, *Bioinorg. Chem. Appl.*, 2004, **2**, 155-192.

29. G. J. Strijkers, W. J. M. Mulder, G. A. F. van Tilborg and K. Nicolay, *Anti-Cancer Agents Med. Chem.*, 2007, **7**, 291-305.

30. M. R. Prince, H. L. Zhang, G. H. Roditi, T. Leiner and W. Kucharczyk, *Journal of Magnetic Resonance Imaging*, 2009, **30**, 1298-1308.

31. E. L. Que, E. Gianolio, S. L. Baker, A. P. Wong, S. Aime and C. J. Chang, *J. Am. Chem. Soc.*, 2009, **131**, 8527-8536.

32. A. C. Esqueda, J. A. Lopez, G. Andreu-de-Riquer, J. C. Alvarado-Monzon, J. Ratnakar, A. J. M. Lubag, A. D. Sherry and L. M. De Leon-Rodriguez, *J. Am. Chem. Soc.*, 2009, **131**, 11387-11391.

33. M. C.F., *Zinc in Human Biology*, Springer-Verlag, New York, 1989.

34. A. Y. Louie, M. M. Huber, E. T. Ahrens, U. Rothbacher, R. Moats, R. E. Jacobs, S. E. Fraser and T. J. Meade, *Nat. Biotechnol.*, 2000, **18**, 321-325.

35. S. Mizukami, R. Takikawa, F. Sugihara, Y. Hori, H. Tochio, M. Walchli, M. Shirakawa and K. Kikuchi, *J. Am. Chem. Soc.*, 2008, **130**, 794-+.

36. X. Yue, Z. Wang, L. Zhu, Y. Wang, C. Qian, Y. Ma, D. O. Kiesewetter, G. Niu and X. Chen, *Molecular Pharmaceutics*, 2014, **11**, 4208-4217.

37. R. Takikawa, S. Mizukami, F. Sugihara, M. Shirakawa and K. Kikuchi, *J. Pharm. Soc. Jpn.*, 2008, **128**, 45-45.

38. R. Trokowski, J. M. Ren, F. K. Kalman and A. D. Sherry, *Angew. Chem., Int. Ed.*, 2005, **44**, 6920-6923.

39. J. Paris, C. Gameiro, V. Humblet, P. K. Mohapatra, V. Jacques and J. F. Desreux, *Inorg. Chem.*, 2006, **45**, 5092-5102.

40. T. N. Parac-Vogt, L. V. Elst, K. Kimpe, S. Laurent, C. Burtea, F. Chen, R. Van Deun, Y. Ni, R. N. Muller and K. Binnemans, *Contrast Media & Molecular Imaging*, 2006, **1**, 267-278.

41. U. Himmelreich, S. Aime, T. Hieronymus, C. Justicia, F. Uggeri, M. Zenke and M. Hoehn, *Neuroimage*, 2006, **32**, 1142-1149.

42. E. L. Que and C. J. Chang, *J. Am. Chem. Soc.*, 2006, **128**, 15942-15943.

43. J. L. Major, G. Parigi, C. Luchinat and T. J. Meade, *Proc. Natl. Acad. Sci. U. S. A.*, 2007, **104**, 13881-13886.

44. Y.-T. Chang, C.-M. Cheng, Y.-Z. Su, W.-T. Lee, J.-S. Hsu, G.-C. Liu, T.-L. Cheng and Y.-M. Wang, *Bioconjugate Chem.*, 2007, **18**, 1716-1727.

45. M. Giardiello, M. P. Lowe and M. Botta, *Chem. Commun.*, 2007, 4044-4046.

46. M. Lepage, W. C. Dow, M. Melchior, Y. You, B. Fingleton, C. C. Quarles, C. Pepin, J. C. Gore, L. M. Matrisian and J. O. McIntyre, *Molecular Imaging*, 2007, **6**, 393-403.

47. M. Querol, D. G. Bennett, C. Sotak, H. W. Kang and A. Bogdanov, Jr., *Chembiochem*, 2007, **8**, 1637-1641.

48. K. Dhingra, P. Fouskova, G. Angelovski, M. E. Maier, N. K. Logothetis and E. Toth, *J. Biol. Inorg. Chem.*, 2008, **13**, 35-46.

49. T. Chauvin, P. Durand, M. Bernier, H. Meudal, B.-T. Doan, F. Noury, B. Badet, J.-C. Beloeil and E. Toth, *Angew. Chem., Int. Ed.*, 2008, **47**, 4370-4372.

50. E. Schellenberger, F. Rudloff, C. Warmuth, M. Taupitz, B. Hamm and J. Schnorr, *Bioconjugate Chem.*, 2008, **19**, 2440-2445.

51. K. Dhingra, M. E. Maier, M. Beyerlein, G. Angelovski and N. K. Logothetis, *Chem. Commun.*, 2008, 3444-3446.

52. J. M. Chambers, P. A. Hill, J. A. Aaron, Z. Han, D. W. Christianson, N. N. Kuzma and I. J. Dmochowski, *J. Am. Chem. Soc.*, 2009, **131**, 563-569.

53. B. Yoo, V. R. Sheth and M. D. Pagel, *Tetrahedron Lett.*, 2009, **50**, 4459-4462.

54. B. Jastrzebska, R. Lebel, H. Therriault, J. O. McIntyre, E. Escher, B. Guerin, B. Paquette, W. A. Neugebauer and M. Lepage, *J. Med. Chem.*, 2009, **52**, 1576-1581.

55. C. Tu, E. A. Osborne and A. Y. Louie, *Tetrahedron*, 2009, **65**, 1241-1246.

56. M. Suchy, R. Ta, A. X. Li, F. Wojciechowski, S. H. Pasternak, R. Bartha and R. H. E. Hudson, *Org. Biomol. Chem.*, 2010, **8**, 2560-2566.

57. K. H. Chalmers, E. De Luca, N. H. M. Hogg, A. M. Kenwright, I. Kuprov, D. Parker, M. Botta, J. I. Wilson and A. M. Blamire, *Chem.--Eur. J.*, 2010, **16**, 134-148.

58. V. Kubicek, T. Vitha, J. Kotek, P. Hermann, L. Vander Elst, R. N. Muller, I. Lukes and J. A. Peters, *Contrast Media Mol. Imaging*, 2010, **5**, 294-296.

59. S. Figueiredo, J. N. Moreira, C. F. G. C. Geraldes, S. Aime and E. Terreno, *Bioorg. Med. Chem.*, 2011, **19**, 1131-1135.

60. G. A. Rolla, L. Tei, M. Fekete, F. Arena, E. Gianolio and M. Botta, *Bioorg. Med. Chem.*, 2011, **19**, 1115-1122.

61. K. H. Chalmers, A. M. Kenwright, D. Parker and A. M. Blamire, *Magnetic Resonance in Medicine*, 2011, **66**, 931-936.

62. D. Granot and E. M. Shapiro, *Magn. Reson. Med.*, 2011, **65**, 1253-1259.

63. S. Matsumura, I. Aoki, T. Saga and K. Shiba, *Molecular Pharmaceutics*, 2011, **8**, 1970-1974.

64. A. J. M. Lubag, L. M. De Leon-Rodriguez, S. C. Burgess and A. D. Sherry, *Proc. Natl. Acad. Sci. U. S. A.*, 2011, **108**, 18400-18405.

65. A. Keliris, I. Mamedov, G. E. Hagberg, N. K. Logothetis, K. Scheffler and J. Engelmann, *Contrast Media & Molecular Imaging*, 2012, **7**, 478-483.

66. Z. Zhelev, V. Gadjeva, I. Aoki, R. Bakalova and T. Saga, *Mol. Biosyst.*, 2012, **8**, 2733-2740.

67. D. V. Hingorani, E. A. Randtke and M. D. Pagel, *J. Am. Chem. Soc.*, 2013, **135**, 6396-6398.

68. R. Napolitano, G. Pariani, F. Fedeli, Z. Baranyai, M. Aswendt, S. Aime and E. Gianolio, *J. Med. Chem.*, 2013, **56**, 2466-2477.

69. F. Schmid, C. Hoeltke, D. Parker and C. Faber, *Magnetic Resonance in Medicine*, 2013, **69**, 1056-1062.

70. J. H. Jang, S. Bhuniya, J. Kang, A. Yeom, K. S. Hong and J. S. Kim, *Org. Lett.*, 2013, **15**, 4702-4705.

71. B. Yoo, V. R. Sheth, C. M. Howison, M. J. K. Douglas, C. T. Pineda, E. A. Maine, A. F. Baker and M. D. Pagel, *Magn. Reson. Med.*, 2014, **71**, 1221-1230.

72. H.-W. Zhang, L.-Q. Wang, Q.-F. Xiang, Q. Zhong, L.-M. Chen, C.-X. Xu, X.-H. Xiang, B. Xu, F. Meng, Y.-Q. Wan and D. Y. B. Deng, *Biomater.*, 2014, **35**, 356-367.

73. F. Zamberlan, C. Lesbats, N. J. Rogers, J. L. Krupa, G. E. Pavlovskaya, N. R. Thomas, H. M. Faas and T. Meersmann, *ChemPhysChem*, 2015, **16**, 2294-2298.

74. J. L. Krupa, A. J. Taylor, H. M. Faas, S. R. Johnson, T. Meersmann, H. E. L. Williams and N. R. Thomas, *Chem.--Eur. J.*, 2015.

75. B. Driehuys, *Science*, 2006, **314**, 432-433.

76. M. M. Spence, S. M. Rubin, I. E. Dimitrov, E. J. Ruiz, D. E. Wemmer, A. Pines, S. Q. Yao, F. Tian and P. G. Schultz, *Proceedings of the National Academy of Sciences of the United States of America*, 2001, **98**, 10654-10657.

77. Q. Wei, G. K. Seward, P. A. Hill, B. Patton, I. E. Dimitrov, N. N. Kuzma and I. J. Dmochowski, *J. Am. Chem. Soc.*, 2006, **128**, 13274-13283.

78. L. Stryer, *Annu. Rev. Biochem.*, 1978, **47**, 819-846.

79. J. R. Mansfield, K. W. Gossage, C. C. Hoyt and R. M. Levenson, *J. Biomed. Opt.*, 2005, **10**.

80. T. Forster, *Naturwissenschaften*, 1946, **33**.

81. G. T. Wang, E. Matayoshi, H. J. Huffaker and G. A. Krafft, *Tetrahedron Lett.*, 1990, **31**.

82. E. D. Matayoshi, G. T. Wang, G. A. Krafft and J. Erickson, *Science*, 1990, **247**.

83. A. H. Coons, H. J. Creech and R. N. Jones, *Proc. Soc. Exp. Biol. Med.*, 1941, **47**.

84. R. B. Merrifield, *J. Am. Chem. Soc.*, 1963, **85**, 2149-&.

85. P. Alewood, D. Alewood, L. Miranda, S. Love, W. Meutermans and D. Wilson, *Solid-Phase Peptide Synthesis*, 1997, **289**, 14-29.

86. H. Rink, *Tetrahedron Lett.*, 1987, **28**, 3787-3790.

87. M. S. Bernatowicz, S. B. Daniels and H. Koster, *Tetrahedron Lett.*, 1989, **30**, 4645-4648.

88. P. Sieber, *Tetrahedron Lett.*, 1987, **28**, 2107-2110.

89. S. S. Wang, *J. Am. Chem. Soc.*, 1973, **95**, 1328-1333.

90. M. Mergler, R. Nyfeler, R. Tanner, J. Gosteli and P. Grogg, *Tetrahedron Lett.*, 1988, **29**, 4009-4012.

91. A. Florsheimer and B. Riniker, *Pept. 1990*, 1991, 131-133.

92. K. Barlos, D. Gatos, J. Kallitsis, G. Papaphotiu, P. Sotiriu, W. Q. Yao and W. Schafer, *Tetrahedron Lett.*, 1989, **30**, 3943-3946.

93. J. C. Sheehan and G. P. Hess, *J. Am. Chem. Soc.*, 1955, **77**, 1067-1068.

94. N. L. Benoiton and F. M. F. Chen, *J. Chem. Soc., Chem. Commun.*, 1981, 543-545.

95. J. R. Vaughan and R. L. Osato, *J. Am. Chem. Soc.*, 1951, **73**, 5553-5555.

96. J. R. Vaughan and R. L. Osato, *J. Am. Chem. Soc.*, 1952, **74**, 676-678.

97. L. A. Carpino, *J. Am. Chem. Soc.*, 1993, **115**, 4397-4398.

98. J. C. Sheehan and D. A. Johnson, *J. Am. Chem. Soc.*, 1954, **76**, 158-160.

99. M. Fujino, Kobayash.S, M. Obayashi, T. Fukuda, Shinagaw.S and Nishimur.O, *Chem. Pharm. Bull.*, 1974, **22**, 1857-1863.

100. R. Subiros-Funosas, R. Prohens, R. Barbas, A. El-Faham and F. Albericio, *Chem.--Eur. J.*, 2009, **15**, 9394-9403.

101. G. Gawne, G. W. Kenner and R. C. Sheppard, *J. Am. Chem. Soc.*, 1969, **91**, 5669-&.

102. B. Castro, J. R. Dormoy, G. Evin and C. Selve, *Tetrahedron Lett.*, 1975, 1219-1222.

103. J. Coste, D. Lenguyen and B. Castro, *Tetrahedron Lett.*, 1990, **31**, 205-208.

104. R. Subiros-Funosas, A. El-Faham and F. Albericio, *Org. Biomol. Chem.*, 2010, **8**.

105. V. Dourtoglou, J. C. Ziegler and B. Gross, *Tetrahedron Lett.*, 1978, 1269-1272.

106. I. Abdelmoty, F. Albericio, L. A. Carpino, B. M. Foxman and S. A. Kates, *Lett. Pept. Sci.*, 1994, **1**, 57-67.

107. A. El-Faham, R. S. Funosas, R. Prohens and F. Albericio, *Chem.--Eur. J.*, 2009, **15**, 9404-9416.

108. D. L. Hughes, J. J. Bergan and E. J. J. Grabowski, *J. Org. Chem.*, 1986, **51**, 2579-2585.

109. P. M. T. Ferreira, H. L. S. Maia, L. S. Monteiro and J. Sacramento, *J. Chem. Soc., Perkin Trans. 1*, 1999, 3697-3703.

110. L. Bi, M. Zhao, K. Gu, C. Wang, J. Ju and S. Peng, *Bioorg. Med. Chem.*, 2008, **16**.

111. W. C. C. a. P. D. White, *Fmoc Solid Phase Peptide Synthesis: A Practical Approach*, Oxford University Press, 1999.

112. C. G. Knight, F. Willenbrock and G. Murphy, *FEBS J.*, 1992, **296**, 263-266.

113. J. H. Cha, M. V. Pedersen and D. S. Auld, *Biochemistry*, 1996, **35**, 15831-15838.

114. S. Netzelarnett, S. K. Mallya, H. Nagase, H. Birkedalhansen and H. E. Vanwart, *Anal. Biochem.*, 1991, **195**, 86-92.

115. A. R. Welch, C. M. Holman, M. F. Browner, M. R. Gehring, C. C. Kan and H. E. VanWart, *Arch. Biochem. Biophys.*, 1995, **324**, 59-64.

116. A. I. Nalepa, J. J. Taing, A. Savitsky and M. Knipp, *Protein Expression Purif.*, 2013, **88**, 33-40.

117. T. Goffman, D. Cuscela, J. Glass, S. Hahn, C. M. Krishna, G. Lupton and J. B. Mitchell, *Int. J. Radiat. Oncol., Biol., Phys.*, 1992, **22**, 803-806.

118. D. Cuscela, D. Coffin, G. P. Lupton, J. A. Cook, M. C. Krishna, R. F. Bonner and J. B. Mitchell, *Canc. J. Sci. Am.*, 1996, **2**, 273-278.

119. J. M. Metz, D. Smith, R. Mick, R. Lustig, J. Mitchell, M. Cherakuri, E. Glatstein and S. M. Hahn, *Clin. Cancer Res.*, 2004, **10**, 6411-6417.

120. S. Aime, L. Calabi, C. Cavallotti, E. Gianolio, G. B. Giovenzana, P. Losi, A. Maiocchi, G. Palmisano and M. Sisti, *Inorg. Chem.*, 2004, **43**, 7588-7590.

121. G. Gugliotta, M. Botta, G. B. Giovenzana and L. Tei, *Bioorg. Med. Chem. Lett.*, 2009, **19**, 3442-3444.

122. S. Mizukami, R. Takikawa, F. Sugihara, Y. Hori, H. Tochio, M. Walchli, M. Shirakawa and K. Kikuchi, *Journal of the American Chemical Society*, 2008, **130**, 794-+.

123. C. Waengler, B. Waengler, M. Eisenhut, U. Haberkorn and W. Mier, *Bioorg. Med. Chem.*, 2008, **16**, 2606-2616.

124. C. Nativi, O. Francesconi, G. Gabrielli, A. Vacca and S. Roelens, *Chem.--Eur. J.*, 2011, **17**.

125. S. H. Yoo, B. J. Lee, H. Kim and J. Suh, *J. Am. Chem. Soc.*, 2005, **127**.

126. B. I. Morinaka, M. N. Masuno, J. R. Pawlik and T. F. Molinski, *Org. Lett.*, 2007, **9**.

127. J. J. Peterson, R. H. Pak and C. F. Meares, *Bioconjugate Chem.*, 1999, **10**, 316-320.

128. S. Mizukami, R. Takikawa, F. Sugihara, M. Shirakawa and K. Kikuchi, *Angew. Chem., Int. Ed.*, 2009, **48**, 3641-3643.

129. R. K. Harris, E. D. Becker, S. M. C. De Menezes, R. Goodfellow and P. Granger, *Pure Appl. Chem.*, 2001, **73**, 1795-1818.

130. G. Galazka, L. J. Windsor, H. BirkedalHansen and J. A. Engler, *Biochemistry*, 1996, **35**, 11221-11227.

131. J. Canceill, L. Lacombe and A. Collet, *J. Chem. Soc., Chem. Commun.*, 1987, 219-221.

132. H. E. Gottlieb, V. Kotlyar and A. Nudelman, *J. Org. Chem.*, 1997, **62**.

133. D. Szabo, J. Mohl, A. M. Balint, A. Bodor and J. Rabai, *J. Fluorine Chem.*, 2006, **127**, 1496-1504.

134. Y. F. Huang, D. R. Dalton and P. J. Carroll, *J. Org. Chem.*, 1997, **62**.

135. C. Nativi, O. Francesconi, G. Gabrielli, A. Vacca and S. Roelens, *Chemistry-a European Journal*, 2011, **17**.

136. B. Jagadish, G. L. Brickert-Albrecht, G. S. Nichol, E. A. Mash and N. Raghunand, *Tetrahedron Lett.*, 2011, **52**.

137. L. Doszczak and J. Rachon, *J. Chem. Soc., Perkin Trans. 1*, 2002.

138. C. Li and W. T. Wong, *Tetrahedron Lett.*, 2002, **43**.

139. D. Bahulayan, L. John and M. Lalithambika, *Synth. Commun.*, 2003, **33**.

140. B. D. Kelly and T. H. Lambert, *J. Am. Chem. Soc.*, 2009, **131**.

141. K.-Q. Ling and L. M. Sayre, *J. Org. Chem.*, 2009, **74**.

142. L. S. Barnes, K. R. Kaneshige, J. S. Strong, K. Tan, H. F. von Bremen and R. Mogul, *J. Inorg. Biochem.*, 2011, **105**.

143. S. J. Ratnakar and V. Alexander, *Eur. J. Inorg. Chem.*, 2005.

144. E. Terreno, M. Botta, F. Fedeli, B. Mondino, L. Milone and S. Aime, *Inorg. Chem.*, 2003, **42**.

Appendices

^{19}F MMP HRMS-LCMS

JK-X

Pre-cleavage

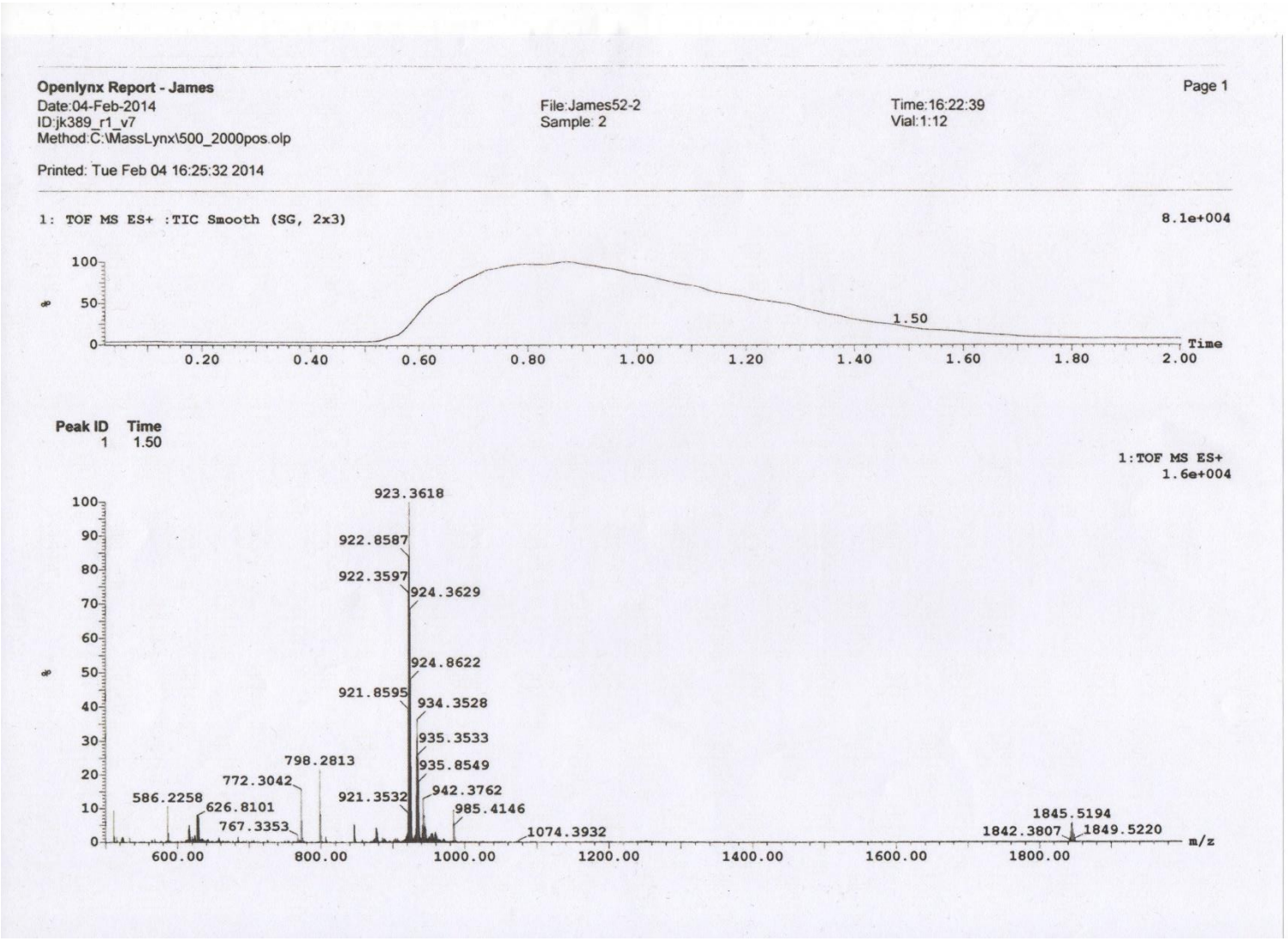

Post-cleavage

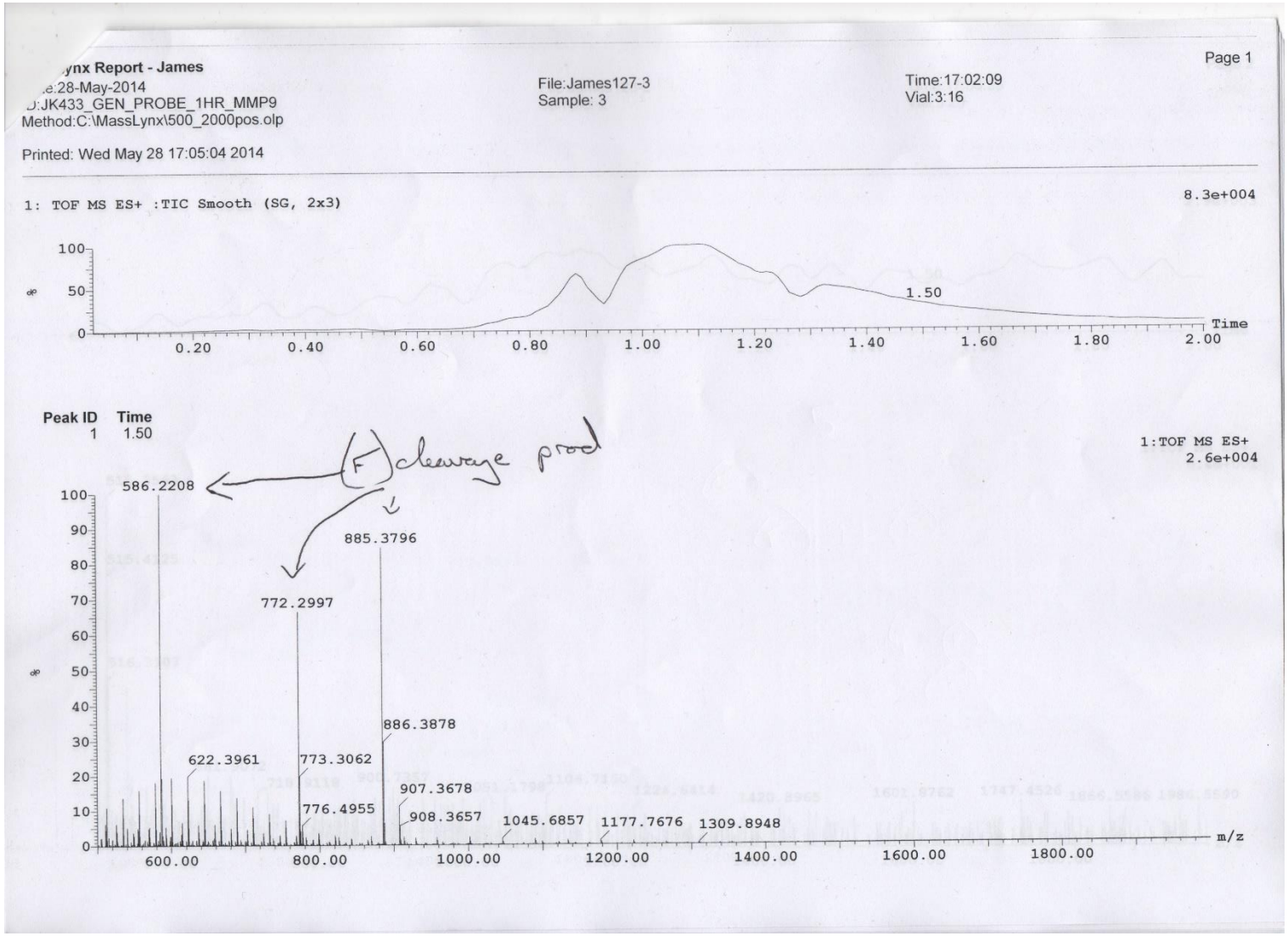

JK-1

Openlynx Report - James
Date:28-Nov-2014
ID:jk500_r1_v12
Method:C:\MassLynx\Leemassspec.PRO\500_2000pos.olp

Printed: Fri Nov 28 13:29:54 2014

File:James244-1
Sample: 1

NMP-1

Time:13:26:51
Vial:2:42

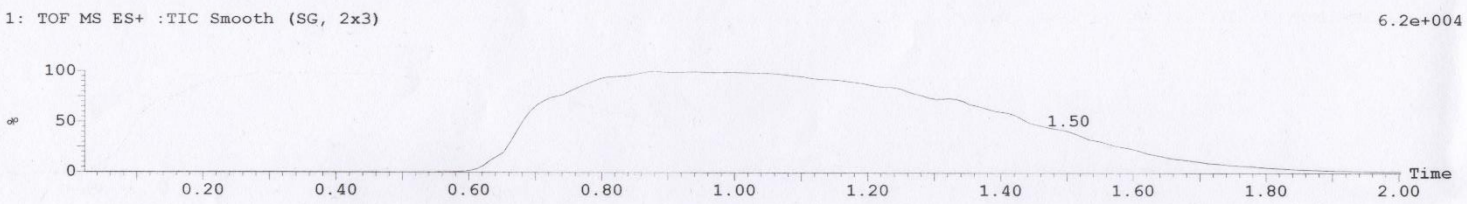

Peak ID	Time
1	1.50

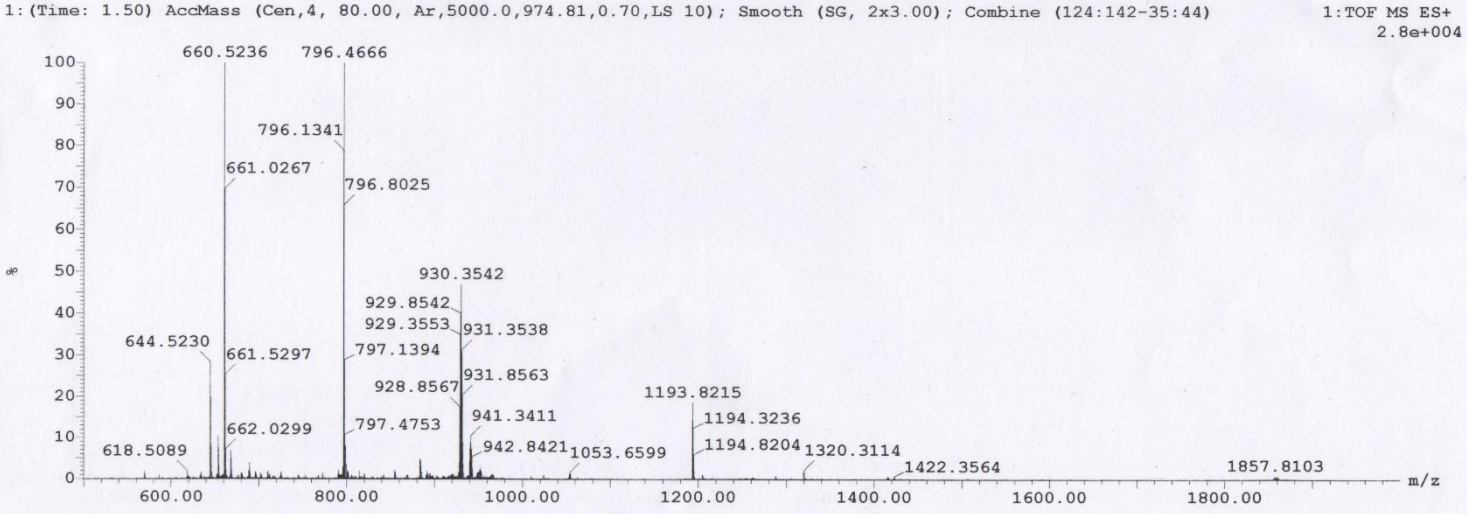

JK-2/9

Pre-cleavage

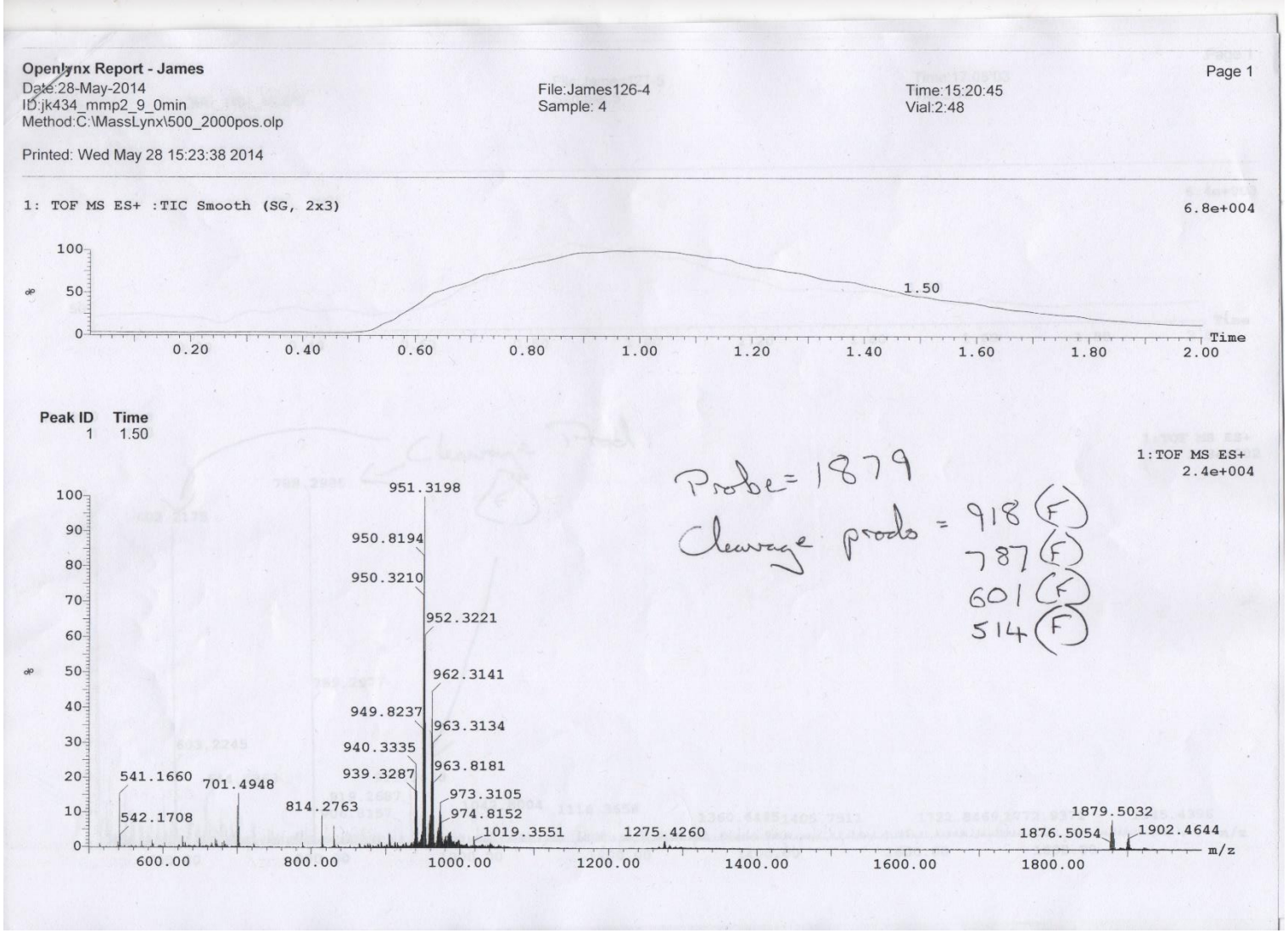

Post-cleavage

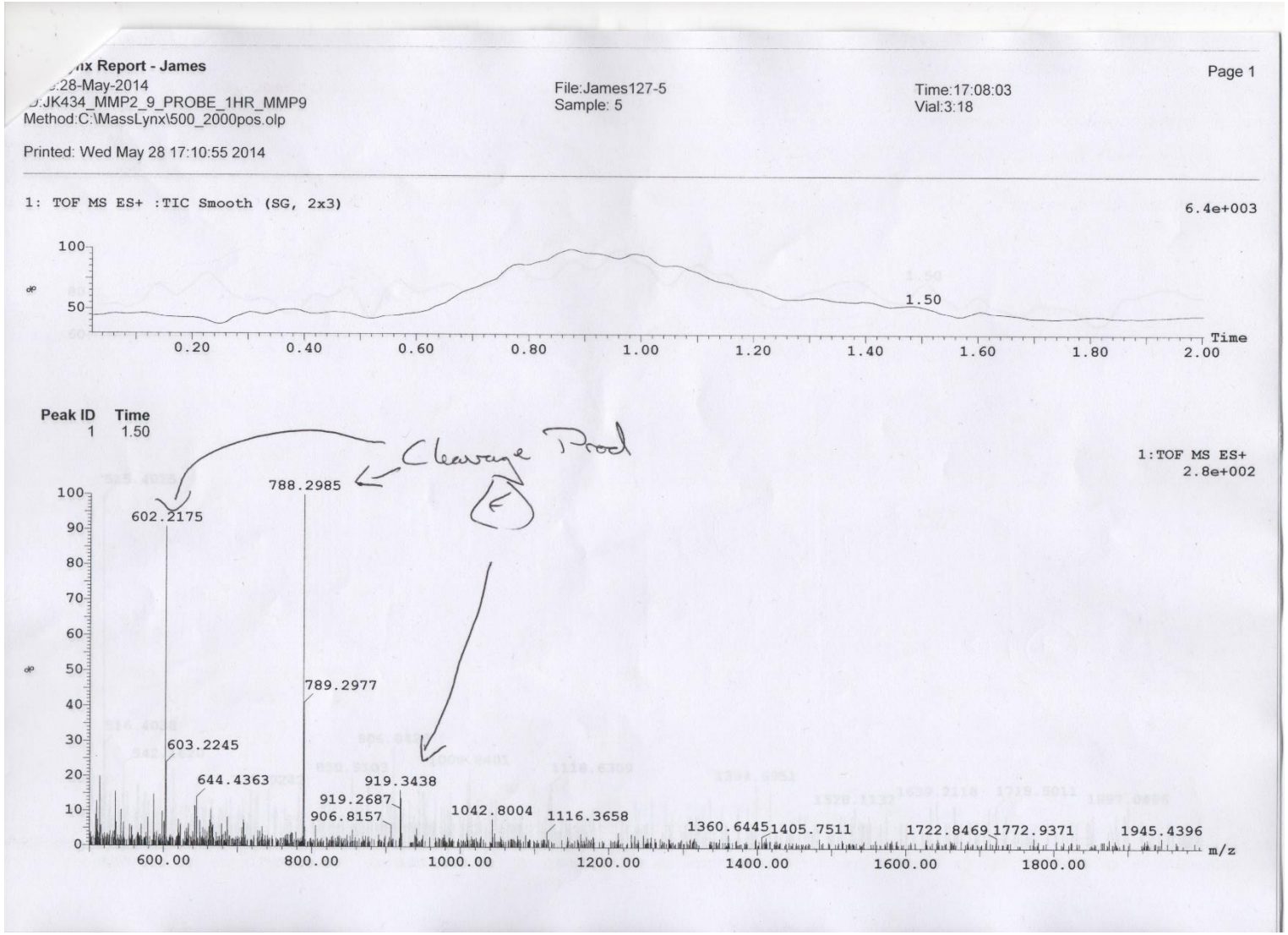

JK-3

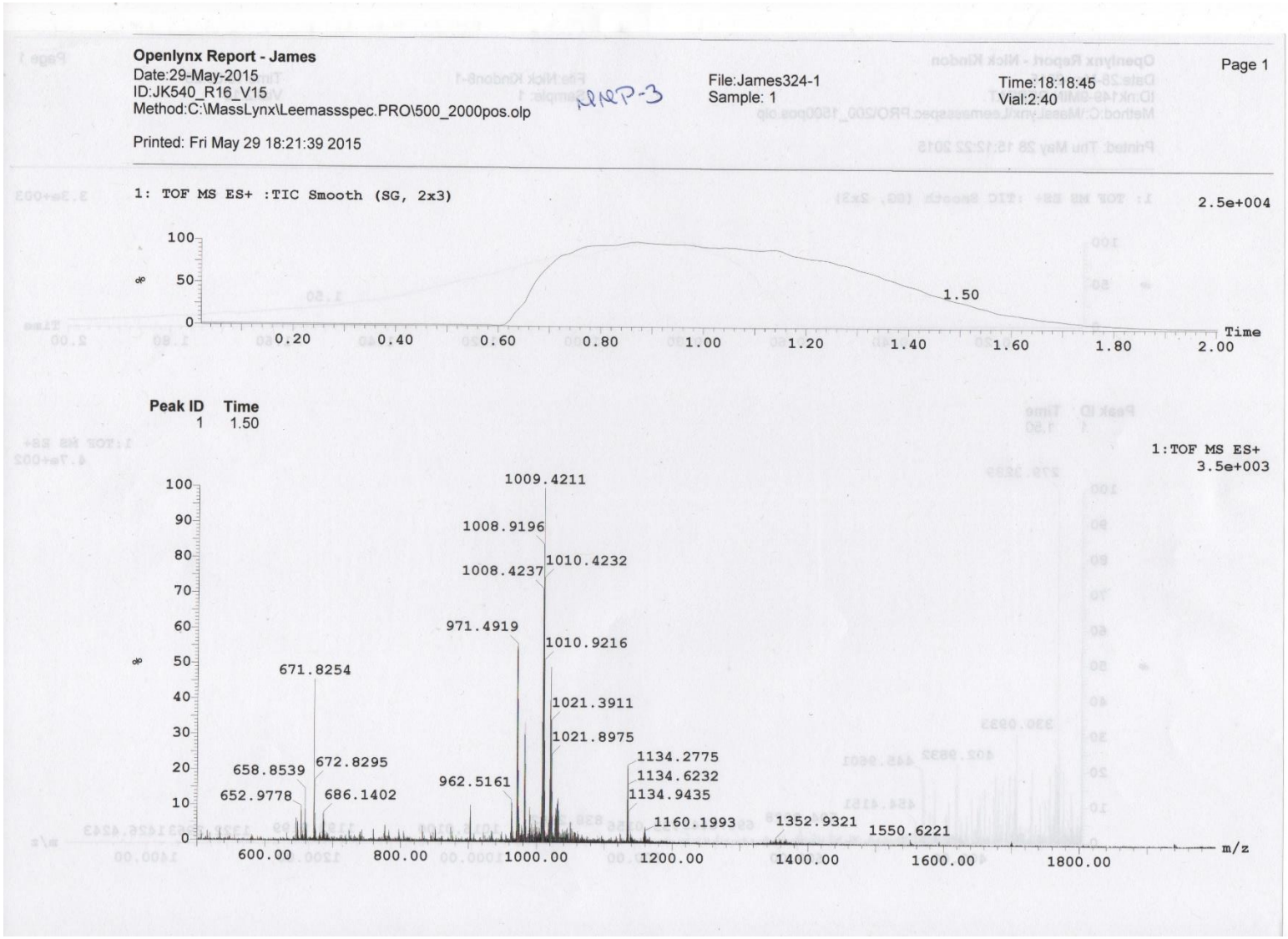
Openlynx Report - James
Date:29-May-2015
ID:JK540_R16_V15
Method:C:\MassLynx\Leemassspec.PRO\500_2000pos.olp
Printed: Fri May 29 18:21:39 2015
AMP-3
File:James324-1
Sample: 1
Time:18:18:45
Vial:2:40
Page 1
1: TOF MS ES+ :TIC Smooth (SG, 2x3)
2.5e+004
1.50
Time
Peak ID Time
1 1.50
1:TOF MS ES+
3.5e+003
1009.4211
1008.9196
1008.4237
1010.4232
971.4919
1010.9216
671.8254
1021.3911
1021.8975
1134.2775
1134.6232
1134.9435
658.8539
672.8295
652.9778
686.1402
962.5161
1160.1993
1352.9321
1550.6221
m/z

JK-7

Openlynx Report - James
Date:10-Dec-2014
ID:jk501_r8_v5
Method:C:\MassLynx\Leemassspec.PRO\500_2000pos.olp

Printed: Wed Dec 10 18:37:53 2014

File:James257-1
Sample: 1

Time:18:34:43
Vial:2:24

MMP-7

1: TOF MS ES+ :TIC Smooth (SG, 2x3)

8.7e+004

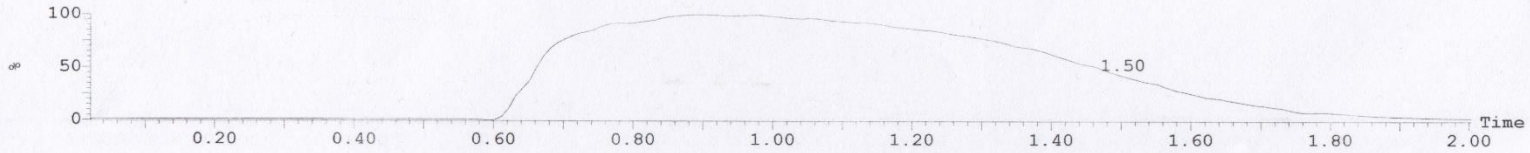

Peak ID	Time
1	1.50

1:(Time: 1.50) AccMass (Cen,4, 80.00, Ar,5000.0,974.81,0.70,LS 10); Smooth (SG, 2x3.00); Combine (124:142-35:44)

1:TOF MS ES+
2.4e+004

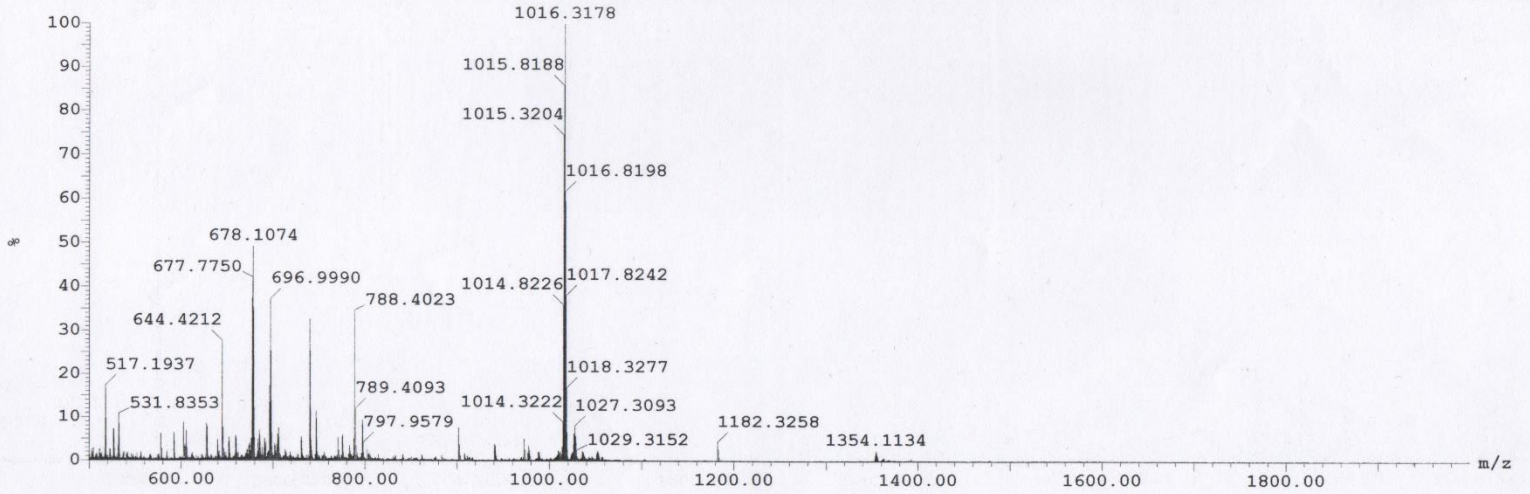

JK-8

Openlynx Report - James
Date:03-Jun-2015
ID:JK541_R7_V7
Method:C:\MassLynx\Leemassspec.PRO\500_2000pos.olp

Printed: Wed Jun 03 18:16:23 2015

MPP-8

File:James335-7
Sample: 7

Time:18:13:29
Vial:2:5

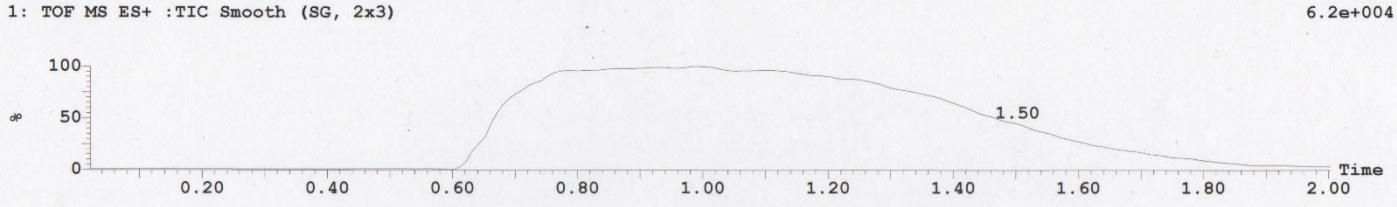

Peak ID **Time**
1 1.50

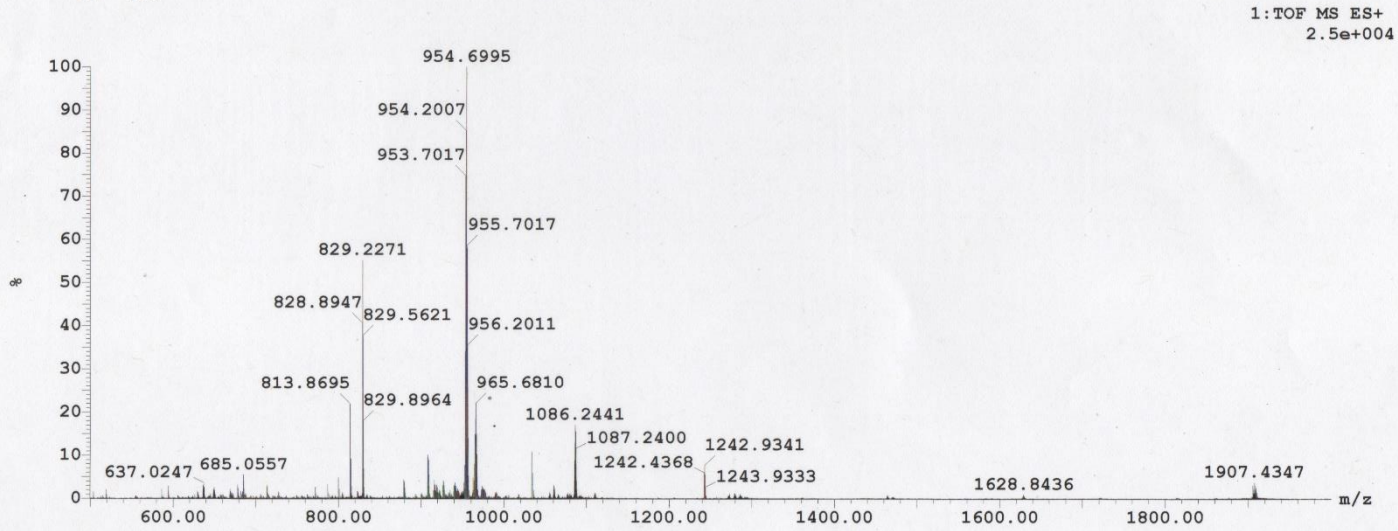

JK-X time course 19F NMR incubated with MMP-9, 19F NMR sampled from data throughout time course at 310K.

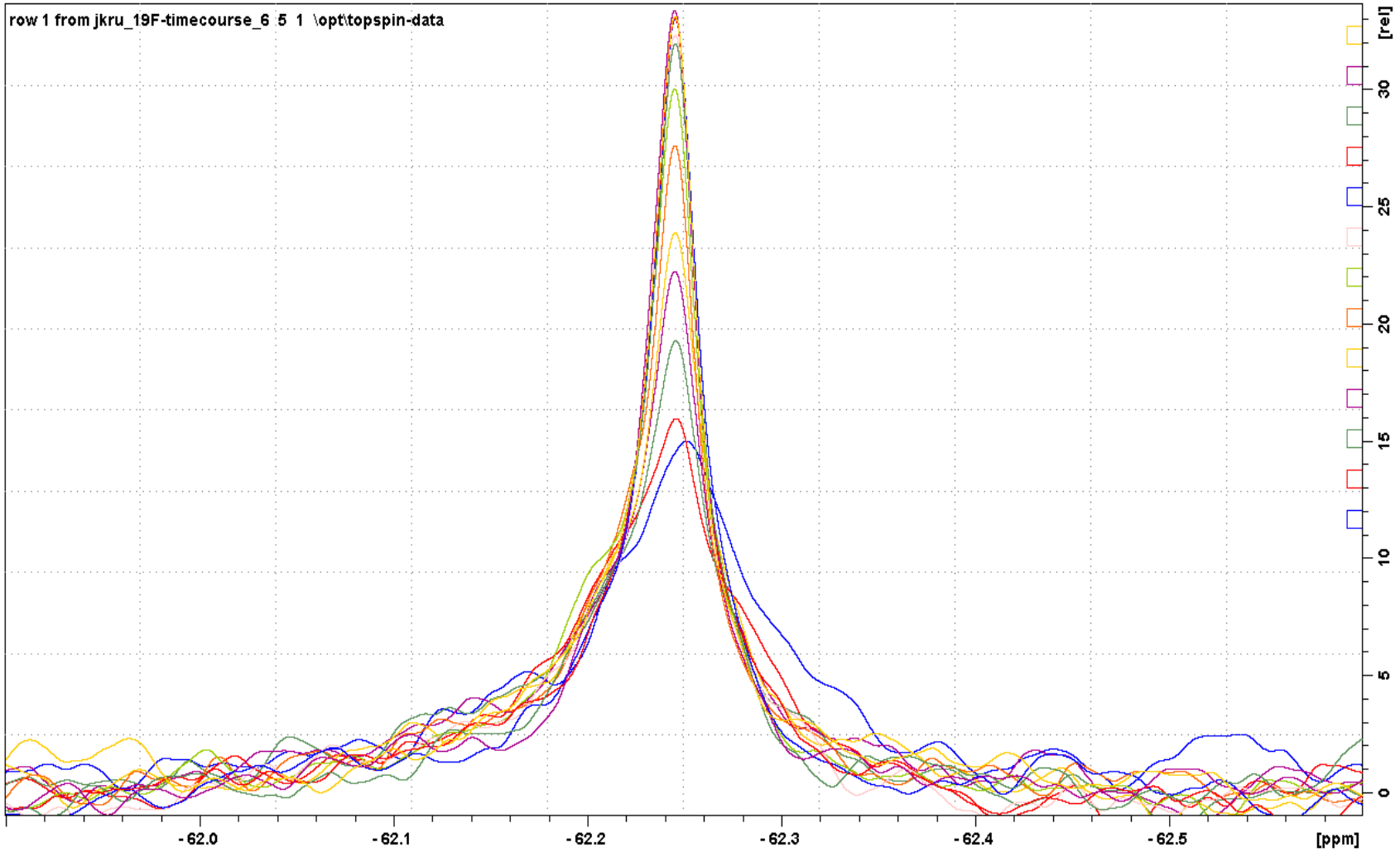

JK-2/9 time course 19F NMR incubated with MMP-9, 19F NMR sampled from data throughout time course at 310K.

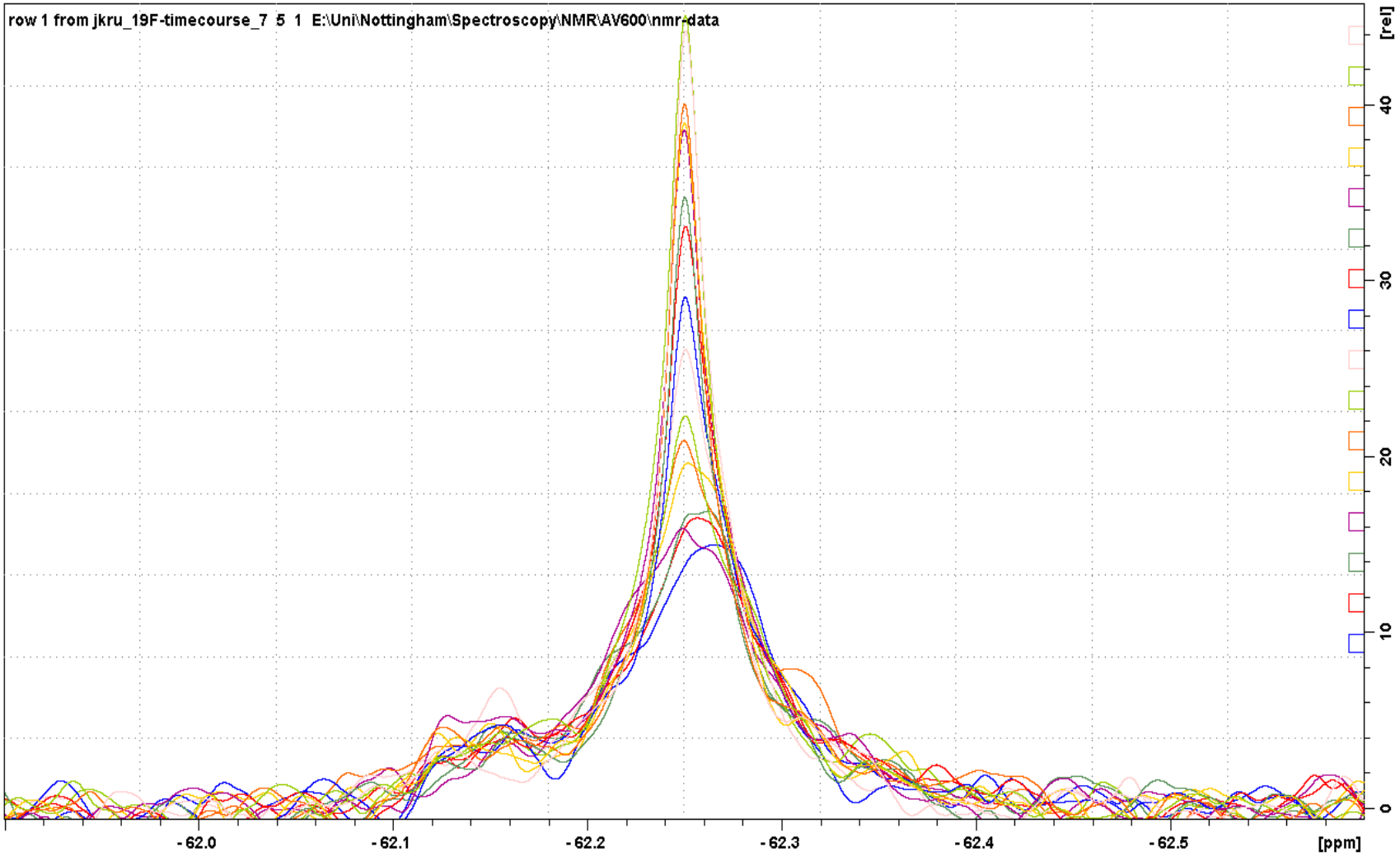

FRET active compounds

FRET labelled substrates have been used to determine the activity of enzymes. Whilst the FRET labelled peptide is a whole unit, emission will be detected from the acceptor fluorochromes. Once the peptide is cleaved the only detectable emission will be from the donor fluorochrome. A FRET labelled MMP substrates will therefore be synthesised to compare to the Gd^{III} MMP agent.

EDANS – Fmoc-Aspartic acid analogue

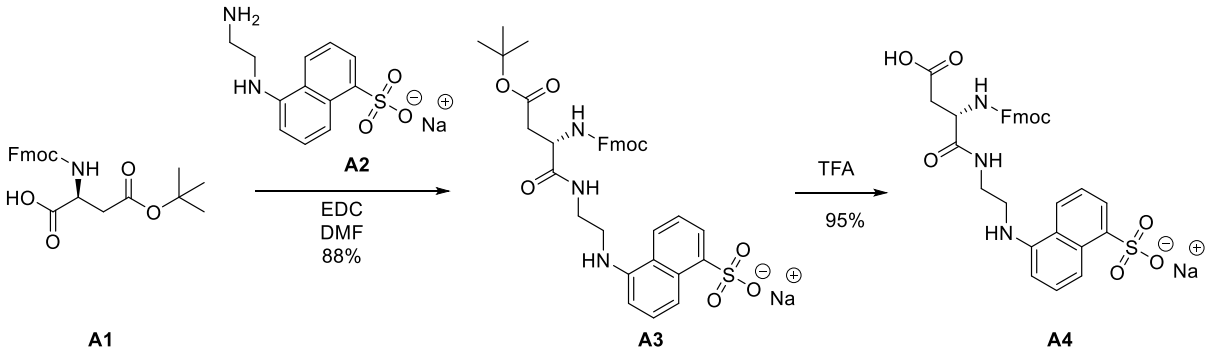

Scheme 54:EDANS – Fmoc-Aspartic acid

Using the same methodology as for FAA **76**, aspartic acid **A1** was used as the Fmoc-amino acid functionality to EDANS **A2**, a donor fluorochrome.

The coupling reaction to form EDANS-Asp-O^{t}Bu **A3** was performed in a high yield of 88% using EDC, HOBt and DMF. This was then dissolved in ethyl acetate, an aqueous basic wash which removed any unreacted AA, followed by an aqueous acid wash to

remove unreacted EDANS, and finally a brine wash to remove any EDC remaining to yield the EDANS-Asp-OtBu **A3** in high yield. The *tert*-butyl ester was then easily deprotected using TFA to yield EDANS-Asp **A4**, without further purification.

EDANS-Asp **A4** was then attached to a SPPS resin in order to synthesize a FRET-labelled MMP substrate.

Dabcyl (A7)

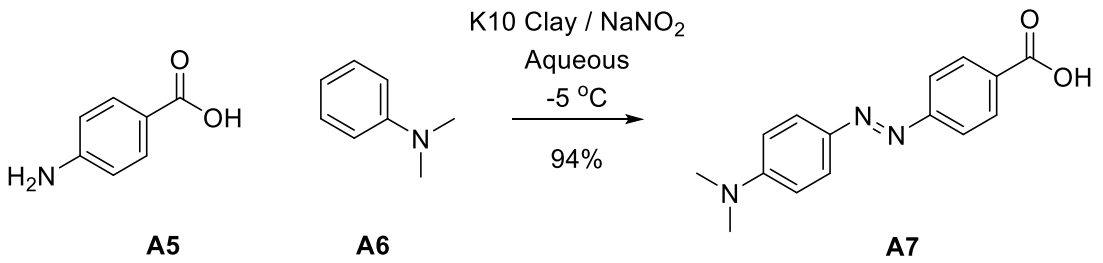

A5 **A6** **A7**

Scheme 55: Synthesis of Dabcyl

Dabcyl **A7** is a complementary acceptor to the fluorochrome donor EDANS. Dabcyl is an expensive fluorochrome, with 100 mg of the succinimidyl ester costing approximately £130; it can be synthesised simply and at a substantially lower price as the acid.

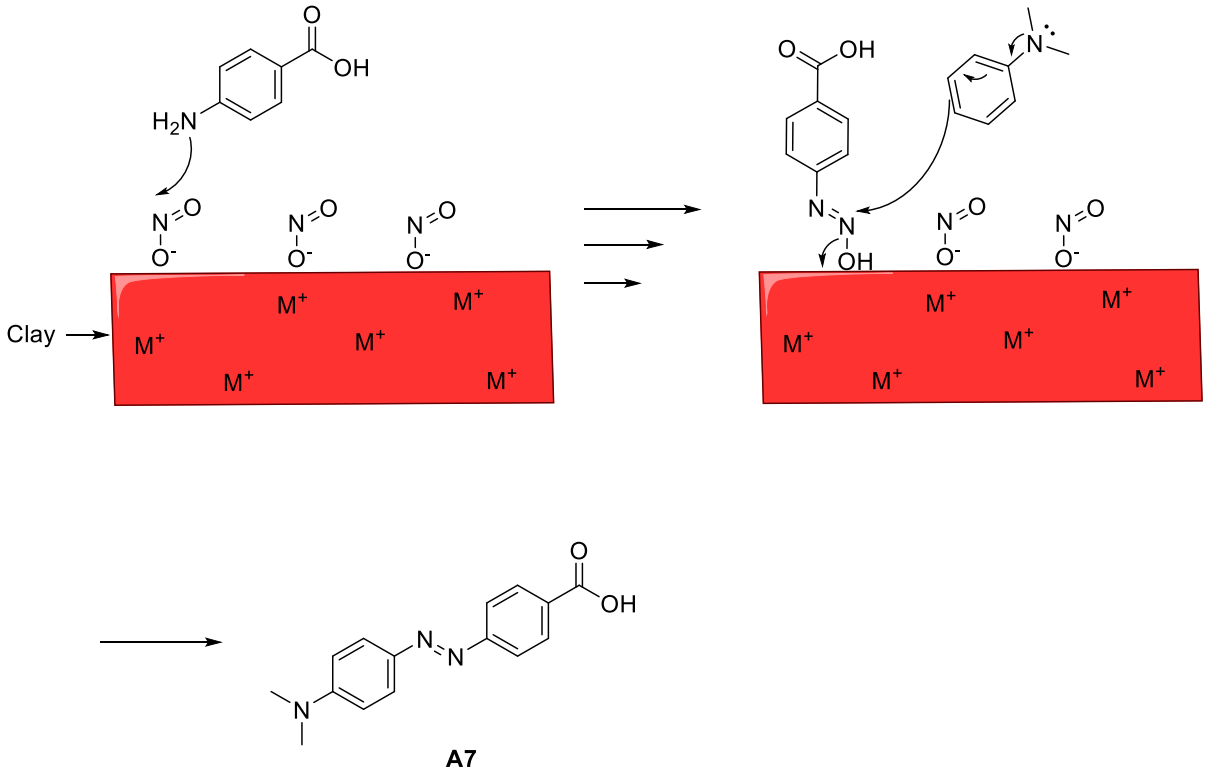

Scheme 56: Potential mechanism for Dabcyl formation

The synthesis of Dabcyl **A7** was based on the use of clays as catalysts for similar substrates by Bahulayan *et al*.[139] *para*-Amino benzoic was mixed with montmorilonite K10 clay at -5 ˚C. Then sodium nitrite was then added, which potentially may have chelated to metals within the clay, and followed by the formation of the hydroxy diazene compound as shown in Scheme 56. The clay became a strong yellow in colour potentially indicating the formation of the diazo, until the *N,N*-dimethyl aniline was added, the tertiary amine makes the phenyl ring nucleophilic at the *ortho* and *para* positions. Due to steric clashes, the *para* position was favoured, resulting in nucleophilic aromatic attack and deprotonation at the *para* position to yield the deep dark red of Dabcyl. The Dabcyl was then washed off

the clay with an excess of methanol, dried protected from light and heat. Once dried it was then stored at -15 ˚C still protected from light.

FRET syntheses

Synthesis of sodium (S)-5-((2-(2-((((9H-fluoren-9-yl)methoxy)carbonyl)amino)-4-(tert-butoxy)-4-oxobutanamido)ethyl)amino)naphthalene-1-sulfonate (A3)

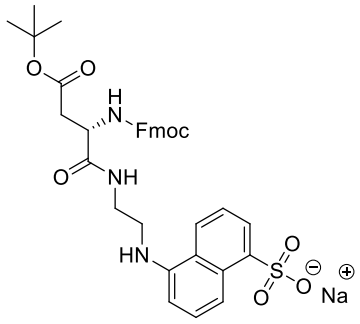

The title compound was synthesised using a procedure adapted from the literature.[128] Fmoc-Asp-OtBu (0.710 g, 1.73 mmol, 1.0 eq.) and EDANS (0.510 g, 1.77 mmol, 1.0 eq.) were dissolved in anhydrous dimethylforamide (20 mL). The solution was cooled to 0 °C, followed by the addition EDC (0.400 g, 2.58 mmol, 1.0 eq.), HOBt (0.300 g, 2.22 mmol). The reaction mixture was stirred at 0 °C for 2 hours. The resulting solution was concentrated *in vacuo*, the residue was dissolved in ethyl acetate (10 mL) before being successively extracted with sat. Na_2CO_3 (3 x 10 mL). The organic phase was dried over sodium sulphate and concentrated *in vacuo* to yield the *amide* as a light yellow solid (1.04 g, 88%); Mp. 78-80 °C; IR V_{max} ($CHCl_3$)/cm^{-1} 3431, 3051, 1724 (C=O), 1506, 1242, 1155; ^{1}H NMR (400 MHz, MeOD) δ 1.41 (s, 9H, -C(CH_3)$_3$), 2.61 (dd, 1H, NCHCH_2COO, *J* = 8.0 Hz, 16 Hz), 2.82 (dd, 1H, NCHCH_2COO, *J* =

8.0 Hz, 16 Hz), 3.42 (m, 2H, NHC*H*$_2$CH$_2$N), 3.59 (m, 2H, NHC*H*$_2$CH$_2$N), 4.21 (t, 1H, C*H*CH$_2$COO, *J* = 4.0 Hz), 6.69 (d, 1H, Fmoc H, *J* = 8.0 Hz, Ar-C*H*), 7.30 (t, 2H, *J* = 8.0 Hz, Ar-C*H*), 7.39 (quin, 5H, *J* = 8.0 Hz, Ar-C*H*), 7.62 (d, 2H, *J* = 8.0 Hz, Ar-C*H*), 7.78 (d, 2H, *J* = 8.0 Hz, Ar-C*H*), 8.15 (d, 2H, *J* = 8.0 Hz, Ar-C*H*), 8.22 (d, 2H, *J* = 8.0 Hz, Ar-C*H*); ^{13}C NMR (100 MHz, MeOD) δ 26.9 (-C(*C*H$_3$)$_3$), 37.3 (CH$_2$), 38.4 (CH$_2$), 43.3 (CH$_2$), 46.9 (CH), 66.7 (CH$_2$), 76.7 (-*C*(CH$_3$)$_3$), 103.8 (Ar-CH), 115.2 (Ar-CH), 119.5 (Ar-CH), 120.7 (Ar-Cq), 122.2 (Ar-CH), 124.0 (Ar-CH), 124.8 (Ar-CH), 124.9 (Ar-CH), 125.3 (Ar-CH), 126.8 (Ar-CH), 127.1 (Ar-CH), 127.4 (Ar-CH), 128.5 (Ar-Cq), 130.1 (Ar-Cq), 141.2 (Ar-Cq), 170.0 (C=O), 171.6 (C=O), 172.7 (C=O). HRMS (ESI) required for $C_{35}H_{38}N_3O_8S^+$ 660.2335 observed MH^+ 660.2357. HRMS (ESI) required for $C_{35}H_{36}N_3O_8S^-$ 658.2228 observed MH^- 658.2283.

Synthesis of sodium (S)-5-((2-(2-((((9H-fluoren-9-yl)methoxy)carbonyl)amino)-3-carboxypropanamido)ethyl)amino)naphthalene-1-sulfonate (A4)

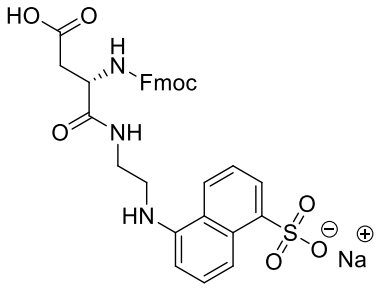

The title compound was synthesised using a procedure adapted from the literature.[122] Ester (**17**) (850 mg, 1.25 mmol) was dissolved in trifluoroacetic acid (15.0 mL, 195 mmol) and stirred for 2 h at rt. The yellow solution was concentrated *in vacuo*, resulting in the title *acid* as an off yellow solid (95%); Mp. 230-233 °C; IR

V_{max} (Nujol)/cm^{-1} 1713 (C=O), 1661 (C=O); ^{1}H NMR (400 MHz, MeOD) δ 2.75-2.86 (m, 1H, NCHC*H*$_2$COO), 2.87-2.96 (m, 1H, NCHC*H*$_2$COO), 3.54-3.60 (m, 2H, NHC*H*$_2$CH$_2$N), 3.61-3.74 (m, 2H, NHC*H*$_2$CH$_2$N), 4.22 (t, 1H, C*H*CH$_2$COO, *J* = 8.0 Hz), 7.24-7.34 (m, 3H, Ar-C*H*), 7.35-7..42 (m, 2H, Ar-C*H*), 7.47-7.55 (m, 2H, Ar-C*H*), 7.63 (d, 2H, *J* = 8.0 Hz, Ar-C*H*), 7.78 (d, 2H, *J* = 4.0 Hz, Ar-C*H*), 8.06 (d, 1H, *J* = 8.0 Hz, Ar-C*H*), 8.18 (d, 1H, *J* = 4.0 Hz, Ar-C*H*), 8.68 (d, 1 H, *J* = 8.0 Hz, Ar-C*H*); ^{13}C NMR (100 MHz, MeOD) δ 24.5 (CH_2), 37.3 (CH_2) 46.3 (CH), 44.4 (CH_2), 66.2 (CH_2), 118.9 (Ar-CH), 123.0 (Ar-CH), 123.5 (Ar-CH), 124.2 (Ar-CH), 124.2 (Ar-CH), 126.2 (Ar-CH), 126.8 (Ar-CH), 127.2 (Ar-CH), 127.6 (Ar-CH), 130.2 (Ar-Cq), 140.5 (Ar-Cq), 143.1 (Ar-Cq), 164.8 (Ar-Cq). HRMS (ESI) required for $C_{31}H_{30}N_3O_8S^+$ 604.1709 observed MH^+ 604.1756. HRMS (ESI) required for $C_{31}H_{28}N_3O_8S^-$ 602.1602 observed MH^- 602.1644.

Synthesis of (E)-4-((4-(dimethylamino)phenyl)diazenyl)benzoic acid (DABCYL) (A7)[139]

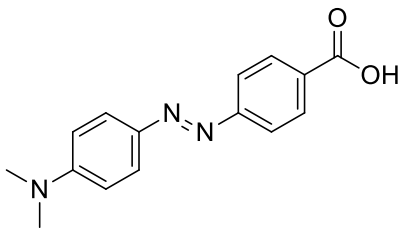

para-Aminobenzoic acid (6.89 g, 50.3 mmol, 1.0 eq.) was adsorbed onto untreated montmorilonite K10 clay (8.07 g) and then cooled to -5 ˚C. To this sodium nitrite (6.93 g, 100 mmol, 2.0 eq.) in water (15 mL) was added dropwise over the course of

an hour. After the addition of sodium nitrite, *N,N*-dimethylaniline (5.80 mL, 45.8 mmol, 1.0 eq.) was added and stirred for 1 hour at ambient temperature. After this the red solid crude DABCYL mixture was taken and washed with methanol to yield the *diazo compound* as a dark red solid (11.6 g, 94%). This was then stored protected from light and below -15 ˚C. Decomposing at 164 °C; IR V_{max} (Nujol)/cm^{-1} 1603 (C=O), 1459 (N=N); ^{1}H NMR (400 MHz, D_2O) δ 2.87 (s, 6H, CH_3), 6.76 (m, 2H, Ar-CH), 7.10 (m, 2H, Ar-CH), 7.35 (m, 2H, Ar-CH), 7.67 (m, 2H, Ar-CH); ^{13}C NMR (100 MHz, D_2O) δ 41.5 (Me), 115.1 (Ar-CH), 116.1 (Ar-CH), 120.3 (Ar-Cq), 126.2 (Ar-Cq), 129.4 (Ar-CH), 130.9 (Ar-CH), 149.7 (Ar-Cq), 175.7 (COOH). HRMS (ESI) required for $C_{15}H_{16}N_3O_2^+$ 270.1198 observed MH^+ 270.1230. HRMS (ESI) required for $C_{15}H_{14}N_3O_2^-$ 268.1091 observed MH^- 268.1102.

THPTA synthesis (click additive)

Synthesis of 3-bromopropyl acetate (A8)

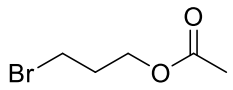

3-Bromopropanol (7 mL, 77.4 mmol, 1 eq.) and diisopropylethylamine (7.4 mL, 42.3 mmol, 0.5 eq.) was dissolved in dichloromethane (60 mL). To this acetic anhydride (7.3 mL, 77.3 mmol, 1 eq.) was slowly added over 10 minutes at 0 ˚C, under a nitrogen atmosphere and stirred. Once added the solution was allowed to warm to ambient temperature and stirred for a further two hours. The solution was then successively extracted with sat. Na_2CO_3 (3 x 20 mL), and brine (3 x 20 mL). The

organic was then taken and dried over magnesium sulphate, filtered and concentrated *in vacuo* to yield the *ester* as a clear free flowing liquid (8.02 g, 57%). HRMS (ESI) required for $C_5H_{10}O_2Br^+$ 183.0493 observed 183.0631.

Synthesis of 3-azidopropyl acetate (A9)

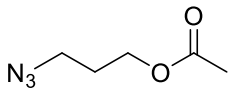

3-Bromopropyl acetate **A8** (1.05 g, mmol, 1 eq.) was dissolved in water (10 mL), to this stirred solution sodium azide (561.70 mg, mmol, 1.5 eq.) was then slowly added over 10 minutes. The solution was then heated to 90 ˚C for 20 hours. Once at ambient temperature ethyl acetate (20 mL) was then added and the aqueous phase successively washed with ethyl acetate (2 x 20 mL), the organic phase was then dried over magnesium sulphate, filtered and concentrated *in vacuo* with the water bath at 30 ˚C, to yield the *azide* as a free flowing light yellow liquid (690 mg, 83 %), which was then re-dissolved in tetrahydrofuran (5 mL). HRMS (ESI) required for $C_5H_{10}N_3O_2^+$ 144.1538 observed 144.1366.

Synthesis of ((nitrilotris(methylene))tris(1H-1,2,3-triazole-4,1-diyl)) tris (propane-3,1-diyl) triacetate (A10)

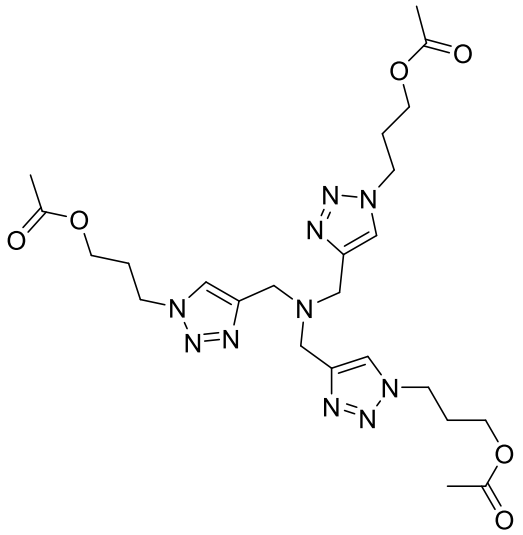

Tripropargylamine **A9** (93 mg, 0.71 mmol, 1 eq.) in tetrahydrofuran (5 mL) was added to 3-azidopropyl acetate (680 mg, 4.8 mmol, 7 eq.) in tetrahydrofuran (5 mL), followed by copper (I) acetate (8 mg, 63 μmol, 0.1 eq.). The green solution was then stirred at 60 ˚C for 20 hours. The solution was then concentrated in vacuo and re-dissolved in dichloromethane: methanol (9:1). The residue was then purified using column chromatography (dichloromethane: methanol, 9:1) to yield the *triazole* as a yellow oil (100 mg, 26 %). ^{1}H NMR (400 MHz, $CDCl_3$) δ 2.06 (s, 9H, 3 x CH_3), 2.27 (m, 6H, CH_2), 3.77 (s, 6H, $N(CH_2)_3$), 4.01 (t, 6H, J = 6.0 Hz, CH_2), 4.48 (t, 6H, J = 7.0 Hz, CH_2), 7.84 (s, 3H, Ar-CH); ^{13}C NMR (100 MHz, $CDCl_3$) δ 20.9 (*C*H_3), 29.4 (*C*H_2), 46.9 (*C*H_2), 47.1 (*C*H_2), 60.8 (*C*H_2), 124.4 (Ar-*C*H), 143.4 (Ar-*C*q), 170.9 (*C*=O). HRMS (ESI) required for $C_{24}H_{36}N_{10}O_6^+$ 561.2897 observed 561.2900.

Synthesis of 3,3',3''-((nitrilotris(methylene))tris(1H-1,2,3-triazole-4,1-diyl))tris(propan-1-ol) (A11)

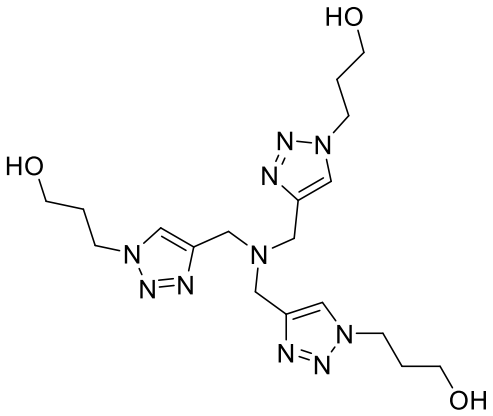

Acetyl precursor **A10** (51 mg, 91 µmol) was dissolved in ammonia in methanol (2M, 2mL) and stirred overnight at ambient temperature. The mixture as then concentrated in vacuo to yield the crude tile compound (45 mg) which was not purified further before use. ^{1}H NMR (400 MHz, $CDCl_3$) δ 2.12 (m, CH_2), 3.58 (s, $N(CH_2)_3$), 3.94 (m, CH_2), 4.54 (m, CH_2), 8.08 (s, Ar-CH); ^{13}C NMR (100 MHz, $CDCl_3$) δ 32.5 (*C*H_2), 47.0 (*C*H_2), 47.1 (*C*H_2), 57.9 (*C*H_2), 125.0 (Ar-*C*H), 163.1 (Ar-*C*q). HRMS (ESI) required for $C_{18}H_{31}N_{10}O_3^+$ 435.2580 observed 435.2584.

Miscellaneous

Synthesis of 1,3-dibromo-1,3-diphenylpropan-2-one A12[140]

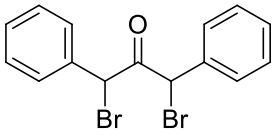

1,3-Diphenylacetone (5.08 g, 24.2 mmol, 1.0 eq.) was added to glacial acetic acid (18 mL). Bromine (2.6 mL, 50 mmol, 2.1 eq.) in glacial acetic acid (36 mL, 0.63 mol, 3.0 eq.) was slowly added over 15 minutes, and stirred for a further 15 minutes. Water (75 mL) was then added followed by Na_2SO_3 until the yellow colour had faded. This was then filtered and washed with water until any residue Na_2SO_3 had been removed, followed by wash with petroleum ether (40/60). This was then concentrated *in vacuo* to yield the title compound as a yellow-grey solid (7.29 g, 82%). Mp. 83-85 °C; IR V_{max} (Nujol)/cm^{-1} 1723s (C=O), 695 (C-Br); ^{1}H NMR (400 MHz, $CDCl_3$) δ 5.77 (s, 1H), 5.82 (s, 1H), 7.34-7.46 (m, 10H); ^{13}C NMR (100 MHz, $CDCl_3$) δ 50.1 (a*C*H), 51.0 (b*C*H), 129.0 (Ar-*C*), 129.1 (Ar-*C*), 129.1 (Ar-*C*), 129.2 (Ar-*C*). 129.6 (Ar-*C*), 134.3 (bAr-*Cq*), 134.5 (aAr-*Cq*), 192.0 (bC=O), 192.4 (aC=O). HRMS (ESI) required for $C_{15}H_{12}Br_2ONa^+$ 388.9145 observed MH^+ 388.9147.

Synthesis of tert-butyl (2-bromoethyl)carbamates[141]

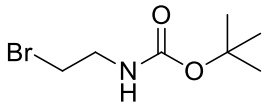

2-Bromoethylamine hydrobromide (410 mg, 2.00 mmol, 1.0 eq.) and di-*tert* butyl bicarbonate (440 mg, 2.02 mmol, 1.0 eq.) were dissolved in dichloromethane (25 mL), diisopropylethylamine (1.10 mL, 6.32 mmol, 3.0 eq.) in dichloromethane (20 mL) was then added and stirred overnight at ambient temperature, before being concentrated *in vacuo*, re-dissolved in diethyl ether (10 mL) and successively extracted with water (3 x 10 mL). The organic phase was then collected and dried over $NaSO_4$ to yield the *protected amine* as a clear oil (400 mg, 90%). IR V_{max} (Nujol)/cm^{-1} 1681 (C=O); ^{1}H NMR (400 MHz, $CDCl_3$) δ 1.53 (s, 9H, -(CH_3)$_3$), 3.45 (m, 2H, N$CH_2$$CH_2$Br), 3.54 (m, 2H, N$CH_2$$CH_2$Br), 5.01 (bs, 1H, N*H*); ^{13}C NMR (100 MHz, $CDCl_3$) δ 28.3 (-C(CH_3)$_3$), 32.8 (N$CH_2$$CH_2$Br), 42.3 (N$CH_2$$CH_2$Br), 85.2 (-$C$($CH_3$)$_3$), 155.6. HRMS (ESI) required for $C_7H_{14}BrNO_2Na^+$ 246.0106, 248.0085 observed MH^+ 246.0097, 248.0078. HRMS (ESI) required for $C_7H_{13}BrNO_2^-$ 222.0130, 224.0109 observed MH^- 222.7627, 224.7676.

Synthesis of benzyl (2-bromoethyl)carbamate

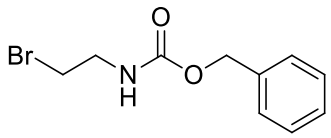

Bromoethylamine hydrobromide (410 mg, 2.01 mmol, 1.0 eq.) in dichloromethane (20 mL) was stirred at ambient temperature. Cbz-Cl (370 mg, 2.16 mmol, 1.0 eq.) and diisopropylethylamine (1.00 mL, 5.75 mmol, 3.0 eq.) in dichloromethane (20 mL) were slowly added and stirred under a nitrogen atmosphere for 72 hours. The

solution was then successively washed with water (3 x 20 mL). The organic phase was dried over magnesium sulphate, filtered and concentrated *in vacuo* to give the *Cbz-amine* as a clear brown liquid (520 mg, 99%). IR V_{max} (Nujol)/cm^{-1} 3332 (NH), 1733 (C=O); ^{1}H NMR (400 MHz, $CDCl_3$) δ 3.47 (t, *J* = 5.8 Hz, 2H, CH_2), 3.61 (q, *J* = 5.8 Hz, CH_2), 5.14 (s, 2H, O-CH_2-Ph), 7.32-7.45 (m, 5H, Ar-H); ^{13}C NMR (100 MHz, $CDCl_3$) δ 32.4 (CH_2), 42.8 (CH_2), 67.0 (CH_2), 128.2 (Ar-CH), 128.3 (Ar-CH), 128.6 (Ar-CH), 136.3 (Ar-Cq), 156.2 (C=O). HRMS (ESI) required for $C_{10}H_{12}NO_2BrNa^+$ 279.9954 observed MNa^+279.9914, HRMS (ESI) required for $C_{10}H_{12}NO_2BrNa^+$ 281.9939 observed MNa^+ 281.9892.

Synthesis of 2,2',2''-(1,4,7,10-tetraazacyclododecane-1,4,7-triyl)triacetic acid[142]

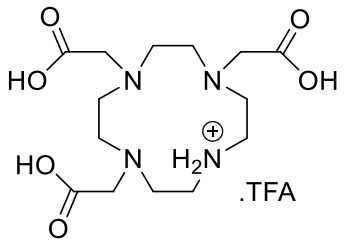

Compound **115** (190 mg, 0.319 mmol) was dissolved in a mixture of dichloromethane (2 mL) and trifluoroacetic acid (3 mL) to give a clear solution that was stirred for 18 hours at ambient temperature. The solution was then concentrated *in vacuo* to yield the *deprotected tri-acid* trifluoroacetic acid salt as a white solid (120 mg, 82%). Mp. 252-253 °C (Lit. 260 °C);[143] IR V_{max} (MeOH)/cm^{-1} 1929 (C=O); ^{1}H NMR (400 MHz, MeOD) δ 2.75-2.90 (m, 2H, CH_2), 3.01-3.29 (m, 6H, CH_2), 3.42-3.86 (m, 12H, CH_2), 4.24 (s, 2H, CH_2); ^{13}C NMR (100 MHz, $CDCl_3$) δ 47.4 (*C*H_2), 47.6 (*C*H_2), 47.8 (*C*H_2), 48.0 (*C*H_2), 49.7 (*C*H_2). ^{19}F NMR (376 MHz, MeOD) δ 77.2 (TFA salt). HRMS (ESI) required

for $C_{14}H_{27}N_4O_6^+$ 347.1886 observed MH^+ 347.1902. HRMS (ESI) required for $C_{14}H_{25}N_4O_6^-$ 345.1780 observed MH^-345.1751.

Synthesis of Gd^{III}-DO3A[144]

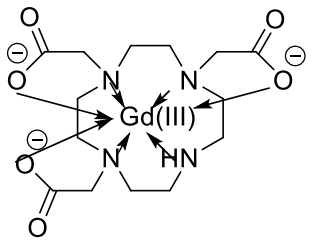

A solution of DO3A tri-acid (100 mg, 2.88 mmol, 1.0 eq.) in water (8 mL) was adjusted to pH 6.0 using potassium hydroxide (1 M, aqueous). Gadolinium (III) chloride (80 mg, 3.04 mmol, 1.0 eq.) in water (2 mL) was then added, and the solution adjusted to pH 6.0 using potassium hydroxide (1 M aqueous). The mixture was then stirred for 2 hours at ambient temperature. A final check to ensure that the solution was pH 6.0 was carried out, followed by lyophilisation. Ethanol (5 mL) was then added to the white solid and centrifuged, the supernatant was removed and the process repeated 3 times. The ethanol supernatants were then combined and concentrated *in vacuo* yielding the *gadolinium salt* as a white solid (80 mg, 53%). Decomposing at 245 ˚C. IR V_{max} (KBr solid)/cm^{-1} 1612 (C=O), 1329 (C-O). HRMS (ESI) required for $C_{14}H_{22}GdN_4O_6^-$ 500.0797 observed MH^-500.0833.

Synthesis of Eu(III)-DO3A

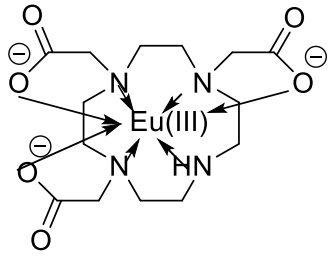

The title compound was synthesised using a procedure adapted from the literature.[144] A solution of DO3A tri-acid (25 mg, 72 µmol, 1.0 eq.) in water (2 mL) was adjusted to pH 6.0 using potassium hydroxide (1 M, aqueous). Europium (III) chloride hexahydrate (31 mg, 85 µmol, 1.0 eq.) in water (1 mL) was then added, and the solution adjusted to pH 6.0 using potassium hydroxide (1 M aqueous) and stirred for 2 hours at ambient temperature. A final check to ensure that the solution was pH 6.0 was carried out, followed by lyophilisation. Ethanol (5 mL) was then added to the white solid and centrifuged, the supernatant was removed and the process repeated 3 times. The ethanol supernatants were combined and concentrated *in vacuo* yielding the *europium salt* as a white solid (18 mg, 48%). Decomposing at 295 ˚C. IR V_{max} (Nujol)/cm^{-1} 1573 (C=O), 1376 (C-O).

Synthesis of di-*tert*-butyl 2,2'-(1,4,7,10-tetraazacyclododecane-1,7-diyl)diacetate

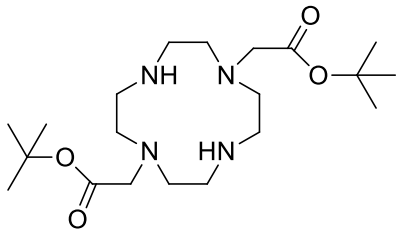

The title compound was synthesized using an adapted literature method.[123] To a solution of cyclen **111** (350 mg, 2.00 mmol, 1.0 eq.) in acetonitrile (250 mL), sodium carbonate (440 mg, 4.10 mmol, 2.0 eq.) was added and stirred for 15 minutes under a nitrogen atmosphere. A solution of *tert*-butyl bromoacetate (780 mg, 4.02 mmol, 2.0 eq.) in acetonitrile (100 mL) was added drop wise and then stirred for 30 minutes followed by a 16 hour reflux at 80 ˚C. The resulting white suspension was then filtered, the filtrate collected and concentrated *in vacuo* to yield the *di-tert butyl ester* as a sticky yellow wax. IR V_{max} (Nujol)/cm^{-1} 1728s (C=O); ^{1}H NMR (400 MHz, $CDCl_3$) δ 1.41 (s, 18H, 2 -C(CH_3)$_3$), 2.22-3.49 (m, 20H, 10 CH_2); ^{13}C NMR (100 MHz, $CDCl_3$) δ 28.0 (-C(*C*H_3)$_3$), 28.1 (-C(*C*H_3)$_3$), 42.9 (*C*H_2), 45.1 (*C*H_2), 46.0 (*C*H_2), 46.6 (*C*H_2), 49.8 (*C*H_2), 50.4 (*C*H_2), 50.8 (*C*H_2), 52.8 (*C*H_2), 53.2 (*C*H_2), 82.6 (2 x -*C*(CH_3)$_3$), 172.4 (*C*=O), 173.0 (*C*=O) HRMS (ESI) required for $C_{20}H_{41}N_4O_4^+$ 401.3083 observed MH^+ 401.3118.

Synthesis of di-*tert*-butyl 2,2'-(4-(2-(benzyloxy)-2-oxoethyl)-1,4,7,10-tetraazacyclododecane-1,7-diyl)diacetate

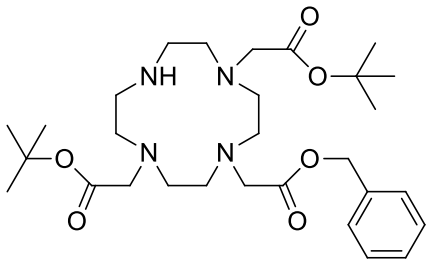

The title compound was synthesized using an adapted literature method.[123] To a solution of DO2A di-*tert*butyl ester (800 mg, 2.00 mmol, 1.0 eq.) in acetonitrile (20 mL), sodium carbonate (230 mg, 2.20 mmol, 1.1 eq.) was added and stirred for 15 minutes under a nitrogen atmosphere. A solution of benzyl bromoacetate (460 mg, 2.02 mmol, 1.0 eq.) in acetonitrile (10 mL) was added and stirred at ambient temperature for 16 hours. The white suspension was then filtered and concentrated *in vacuo*, resulting in the title *benzyl ester* (700 mg, 76%) as an orange-brown gum. IR V_{max} (Nujol)/cm^{-1} 1729b (C=O); ^{1}H NMR (400 MHz, $CDCl_3$) δ 1.48 (s, 18H, 2 -C(C*H*$_3$)$_3$), 2.01-3.83 (m, 20H, 10 -C*H*$_2$), 5.24 (s, 2H, C*H*$_2$-Ph), 7.32-7.44 (m, 5H, 5 Ar-C*H*); ^{13}C NMR (100 MHz, $CDCl_3$) δ 27.9 (-C(*C*H$_3$)$_3$), 28.1 (-C(*C*H$_3$)$_3$), 47.3 (CH_2), 47.4 (CH_2), 49.3 (CH_2), 49.4 (CH_2), 51.2 (CH_2), 51.2 (CH_2), 57.1 (CH_2), 57.9 (CH_2), 66.4 (CH_2), 66.9 (CH_2), 81.4 (-*C*(CH$_3$)$_3$), 82.1 (-*C*(CH$_3$)$_3$), 128.3 (2 x Ar-*C*H), 128.4 (Ar-*C*H), 128.6 (2 x Ar-*C*H), 135.5 (Ar-*C*q), 169.7 (C=O), 173.0 (C=O), 173.6 (C=O). HRMS (ESI) required for $C_{29}H_{49}N_4O_6^+$ 549.3607 observed MH^+ 549.3656.

Synthesis of 2-(4,10-bis(2-(*tert*-butoxy)-2-oxoethyl)-1,4,7,10-tetraazacyclododecan-1-yl)acetic acid

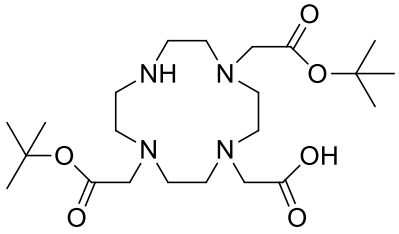

The title compound was synthesized using an adapted literature method.[123] To a solution of the above benzyl ester (700 mg, 1.28 mmol, 1.0 eq.) in methanol (40 mL), Pd/C (40 mg) in water (10 mL) was added. The system atmosphere was then evacuated, flushed with nitrogen three times; and the evacuation process repeated with hydrogen three times. The resulting black suspension was stirred for 24 hours at ambient temperature. The suspension was filtered, concentrated *in vacuo* and then lyophilised. The residue was then dissolved in chloroform (15 mL) and extracted with potassium hydroxide (1 M aqueous 10 mL x 3). The aqueous phase was then re-acidified with hydrochloric acid (1 M aqueous 10 mL x 3) and concentrated *in vacuo*. The resultant white solid was then washed with methanol, and the filtrate concentrated *in vacuo* to yield the title compound (600 mg, 95%) as a clear yellow wax. IR V_{max} (Nujol)/cm^{-1} 1729w (C=O); ^{1}H NMR (400 MHz, $CDCl_3$) δ 1.48 (s, 18H, 2 -C(CH_3)$_3$), 1.62-3.98 (m, 22H, 11 x -CH_2);); ^{1}H NMR (400 MHz, $CDCl_3$) δ 1.41 (s, 18H, 2 -C(CH_3)$_3$), 2.22-3.49 (m, 20H, 10 CH_2); ^{13}C NMR (100 MHz, $CDCl_3$) δ 28.1 (-C(CH_3)$_3$), 28.3 (-C(CH_3)$_3$), 39.57 (CH_2), 50.0 (CH_2), 52.2 (CH_2), 54.3 (CH_2), 54.9 (CH_2), 82.6 (2 x -C(CH_3)$_3$), 84.9 (2 x -C(CH_3)$_3$),170.4 (C=O), 170.6 (C=O); HRMS (ESI) required for $C_{22}H_{43}N_4O_6^+$ 459.3138 observed MH^+ 459.3179.

Synthesis of tri-*tert*-butyl 2,2',2''-(10-(2-methoxy-2-oxoethyl)-1,4,7,10-tetraazacyclododecane-1,4,7-triyl)triacetate

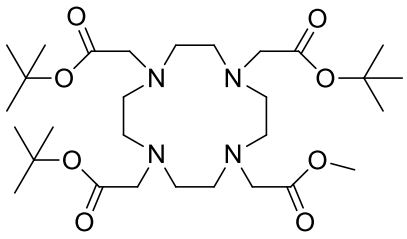

To a solution of compound **115** (220 mg, 0.430 mmol, 1.0 eq.) in acetonitrile (3 mL), potassium carbonate (90 mg, 0.65 mmol, 1.5 eq.) was added to give a white suspension that was stirred for 15 minutes under a nitrogen atmosphere. A solution of methyl bromoacetate (100 mg, 0.650 mmol, 1.5 eq.) in acetonitrile (2 mL) was added and the mixture stirred at ambient temperature for 16 hours. The white precipitate was then filtered and the filtrate concentrated *in vacuo*. The residue was then dissolved dichloromethane (10 mL) and successively washed with water (3 x 10 mL). The organic phase was dried over sodium sulphate, filtered and concentrated *in vacuo* to give the *methyl ester* (210 mg, 84%) as an orange-yellow viscous oil. IR V_{max} ($CHCl_3$)/cm^{-1} 1728 bs (C=O); ^{1}H NMR (400 MHz, $CDCl_3$) δ 1.43 (s, 27H, -C(CH_3)$_3$), 2.02-3.61 (m, 24H, CH_2), 3.67 (s, 3H, CH_3); ^{13}C NMR(100 MHz, $CDCl_3$) δ 27.9 (-C(*C*H_3)$_3$), 51.9 (C*H*$_3$), 54.7 (*C*H_2), 55.6 (*C*H_2), 55.6 (*C*H_2), 55.7 (*C*H_2), 81.9 (-*C*(CH_3)$_3$), 82.0 (-*C*(CH_3)$_3$), 82.1 (-*C*(CH_3)$_3$), 172.9 (C=O), 173.0 (C=O), 174.0 (C=O). HRMS (ESI) required for $C_{29}H_{55}N_4O_8^+$ 587.3975 observed MH^+ 587.4015. HRMS (ESI) required for $C_{29}H_{55}N_4O_8Na^+$ 609.3839 observed MNa^+ 609.3841. HRMS (ESI) required for $C_{25}H_{45}N_4O_8^-$ 529.3243 observed MH^- 529.4692.

ChemPubSoc Europe
DOI: 10.1002/cphc.201500367
CHEMPHYSCHEM Communications

Molecular Sensing with Hyperpolarized ^{129}Xe Using Switchable Chemical Exchange Relaxation Transfer

Francesco Zamberlan,[a] Clémentine Lesbats,[b] Nicola J. Rogers,[b, c] James L. Krupa,[a] Galina E. Pavlovskaya,[b] Neil R. Thomas,*[a] Henryk M. Faas,*[b, d] and Thomas Meersmann*[b]

An approach for hyperpolarized ^{129}Xe molecular sensors is explored using paramagnetic relaxation agents that can be deactivated upon chemical or enzymatic reaction with an analyte. Cryptophane encapsulated ^{129}Xe within the vicinity of the paramagnetic center experiences fast relaxation that, through chemical exchange of xenon atoms between cage and solvent pool, causes accelerated hyperpolarized ^{129}Xe signal decay in the dissolved phase. In this proof-of-concept work, the relaxivity of **Gadolinium^{III}**-DOTA on ^{129}Xe in the solvent was increased eightfold through tethering of the paramagnetic molecule to a cryptophane cage. This potent relaxation agent can be 'turned off' specifically for ^{129}Xe through chemical reactions that spatially separate the **Gd^{III}** centre from the attached cryptophane cage. Unlike ^{129}Xe chemical shift based sensors, the new concept does not require high spectral resolution and may lead to a new generation of responsive contrast agents for molecular MRI.

Molecular imaging enables the in vivo detection of the spatial distribution of specific target molecules that serve as 'biomarkers' for organ physiology. Imaging of biomarkers allows for the early detection of disease, for better monitoring of treatment, and for drug development. Among the strategies to enable molecular MRI,[1] the hyperpolarized (hp) ^{129}Xe biosensor concept pioneered by Pines, Wemmer, and co-workers[2] is a promising candidate due to xenon's non-toxicity, the simplicity of the corresponding NMR spectra, and its solubility in blood plasma and tissue.[3] Hp ^{129}Xe biosensors utilize an encapsulating agent, such as cryptophane cages, that can reversibly bind Xe atoms with fast rates of exchange. The large chemical shift range of ^{129}Xe leads to a distinguishable signal separation between encapsulated xenon atoms in the hydrophobic cavity and xenon in the solvent (signal from encapsulated ^{129}Xe not visible in Figure 1 b due to line broadening, see Figure S2 in the Supporting Information, SI). Furthermore, cryptophanes can be functionalized with suitable bioactive ligands to serve as biosensor molecules that interact with a particular biomarker, typically a protein. The biosensor–biomarker interaction further alters the environment of the encapsulated ^{129}Xe, giving rise to a different chemical shift that can be observed by NMR spectroscopy. This was originally shown with biotin-functionalized cryptophane as a sensor for the protein avidin[2a] for which biotin has a very high affinity.

Hyperpolarized ^{129}Xe Chemical Exchange Saturation Transfer (HyperCEST)[2c] improves the hp ^{129}Xe biosensor detection limit by orders of magnitude.[4] HyperCEST is achieved by selective irradiation (i.e. saturation) at the NMR frequency of the encapsulated ^{129}Xe signal that depolarizes its hp spin state. Chemical exchange continuously transfers depolarized ^{129}Xe from the cage to the dissolved phase and accelerates the decay of the dissolved phase signal.

Molecular sensing with HyperCEST usually relies on the small ^{129}Xe chemical shift differences created by biosensor-biomarker interactions that are typically in the 2–3 ppm range, with exceptional cases up to 8 ppm.[6] Although hp ^{129}Xe biosensors enable a host of biomolecular NMR applications,[3a,b,6–7] including in vitro MRI for cell tracking[8] and in vivo organ uptake of functionalized nanoparticles,[9] in vivo MRI usage in complex organisms such as vertebrates is generally limited by the low spectral resolution achievable. This is a limitation wherever chemical shift is required to distinguish between a binding (or cleaving) event and unspecific interaction (i.e. typically non-reacted sensors that are still present to a significant extent). A promising advancement has been reported very recently that does not require high spectral resolution because the unspecific background was very small. HyperCEST enabled imaging of cell-surface glycans at nanomolar concentrations in live-cell bioreactors.[5] However, wherever the biosensor molecules interacting with biomarker molecules need to be distinguished from a significant amount of biosensors that have not been

[a] Dr. F. Zamberlan,[+] J. L. Krupa, Prof. Dr. N. R. Thomas
Centre for Biomolecular Sciences
School of Chemistry, University of Nottingham
Nottingham, NG7 2RD (United Kingdom)
E-mail: Neil.Thomas@Nottingham.ac.uk

[b] C. Lesbats,[+] Dr. N. J. Rogers, Dr. G. E. Pavlovskaya, Dr. H. M. Faas, Prof. Dr. T. Meersmann
Sir Peter Mansfield Imaging Centre
Division of Respiratory Medicine, School of Medicine
University of Nottingham
Nottingham, NG7 2RD (United Kingdom)
E-mail: Thomas.Meersmann@Nottingham.ac.uk

[c] Dr. N. J. Rogers
Current address:
Department of Chemistry, Durham University
South Road, Durham, DH1 3LE, United Kingdom

[d] Dr. H. M. Faas
Sir Peter Mansfield Imaging Centre
Division of Clinical Neuroscience, School of Medicine, University of Nottingham
Nottingham, NG7 2UH (United Kingdom)
E-mail: Henryk.Faas@Nottingham.ac.uk

[+] These authors contributed equally.

Supporting Information for this article is available on the WWW under http://dx.doi.org/10.1002/cphc.201500367.

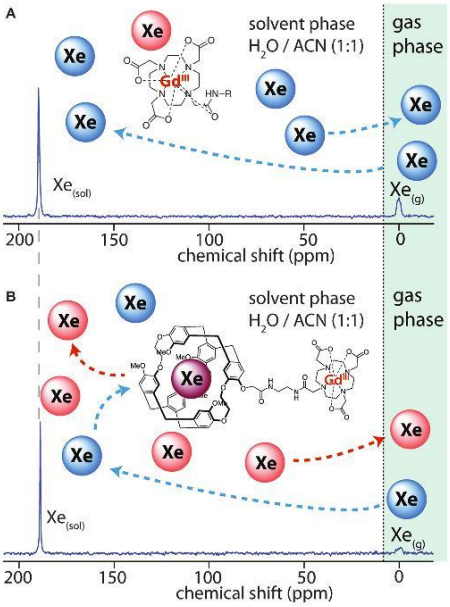

Figure 1. A) Hp ^{129}Xe NMR spectrum of a 1:1 v/v water/acetonitrile (H_2O/ACN) solution containing 0.33 mM **Gd**DOTA. The hp ^{129}Xe signal intensity of the dissolved phase (189.6 ppm)—and through exchange, the intensity of the gas phase (0 ppm)—is only moderately affected by the relaxation agent because the exposure time of the xenon atoms to the paramagnetic center is very limited. Note that blue and red color symbolizes ^{129}Xe atoms in the hyperpolarized and depolarized states, respectively. B) Hp ^{129}Xe NMR spectrum of 0.035 mM cryptophane-A tethered to **Gd**DOTA in H_2O/ACN solution. Encapsulated ^{129}Xe is not detected because of severe line broadening. This molecule serves as a strong relaxation agent, specifically for ^{129}Xe, due to prolonged duration of ^{129}Xe encapsulation in the close vicinity to the paramagnetic relaxation center. The effect of fast relaxation (or depolarization) of encapsulated hp ^{129}Xe is transferred via chemical exchange to the dissolved phase (189.3 ppm) where an accelerated decay of the $^{129}Xe_{(sol)}$ signal is observed.

bound, cleaved, or otherwise specifically reacted with a biomarker, imaging will likely have to cope with small chemical shift differences between the two biosensor moieties.

This proof-of-concept study presents a different approach for hp ^{129}Xe biosensors, sketched in Figure 1b, using paramagnetic relaxation instead of the chemical shift. Paramagnetic relaxation causes rapid decay of the hp signal. Paramagnetic metal centers are therefore usually avoided for hp MRI probes, except for the generation of negative contrast through shortened T_1, T_2, or T_2* times.[10] Subsequent to the submission of this manuscript, the authors learned that a paramagnetic relaxation based hp^{129}Xe biosensor concept has also been reported by Wemmer, Pines, and co-workers.[11] The new hp ^{129}Xe biosensor concept in this communication utilizes 'switchable' paramagnetic relaxation. Chemical sensing will be based on chemical changes brought about by target molecules that 'deactivate' the responsive relaxation agent. Hp ^{129}Xe will be administered after sufficient time has passed to allow for any deactivation to occur that causes positive MRI contrasts. NMR relaxation studies with the model sensor CrA-**Gd**DOTA were used to gain insights into the magnitude of the relaxivity change and hence to explore the concept feasibility.

Results and Discussion

A 1:1 v/v mixture of water with acetonitrile (H_2O/ACN) was found to be a suitable solvent for the model sensor, DOTA, Gd^{3+}, and xenon. As shown in Figure 2, the ^{129}Xe relaxation rates, $R_1 = 1/T_1$, were measured as a function of the concentration of the various relaxation agents, [**Rx**], to determine the relaxivity of the respective agents. The relaxivity of **Gd**DOTA for $^{129}Xe_{(sol)}$ was determined as $R_1/[\mathbf{Rx}] = 0.0515\ s^{-1}\,mM^{-1}$ (see Figure 3). The approximately 150 fold reduced relaxivity of gadolinium for $^{129}Xe_{(sol)}$ compared to that for H_2O protons ($7.66\ s^{-1}\,mM^{-1}$—see Figure 3) is caused in part by xenon's lower gyromagnetic ratio γ that contributes to an approximately 13 fold reduced relaxivity due to the γ^2 dependence of paramagnetic relaxation.[12,13] In addition, H_2O protons experience further accelerated relaxation because of direct coordination of water with the $\mathbf{Gd^{III}}$ center in DOTA complexes.[1]

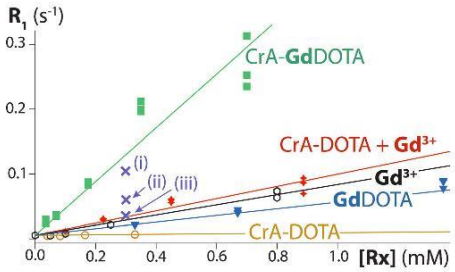

Figure 2. Relaxation rates, R_1, of dissolved phase $^{129}Xe_{(sol)}$ in 1:1 v/v H_2O/ACN solution as a function of the concentration of various agents, [**Rx**], at 293 K and 9.4 T field strength. Note that CrA-DOTA + $\mathbf{Gd^{3+}}$ (red '+' data points and red line) shows the relaxation data obtained more than 24 h after adding HCl to the solution with CrA-**Gd**DOTA, causing $\mathbf{Gd^{3+}}$ to be expelled from the molecule. Data point i) shows effect of CrA-**Gd**DOTA approximately 1 h after addition of HCl. ii) After 24 h the reaction to CrA-DOTA + $\mathbf{Gd^{3+}}_{(sol)}$ was 86% complete as determined by HPLC (see SI). iii) Reaction is 96% complete after 96 h. Data points (i)–(iii) (i.e. crosses) are averages from three measurements—all other data are from single measurements. Relaxivity values are reported in Figure 3.

A 1 mM **Gd**DOTA solution causes only slow hp $^{129}Xe_{(sol)}$ relaxation, with $T_1 = 19$ s, that will have little effect on the overall ^{129}Xe relaxation behavior in vivo. For example, typical relaxation times for hp $^{129}Xe_{(aq)}$ in blood range from approximately 2.7 to 7.9 s, depending on blood oxygenation.[14] In lung tissue and blood, rapid exchange with the gas phase prolongs the $^{129}Xe_{(aq)}$ relaxation times up to 20 s.[13]

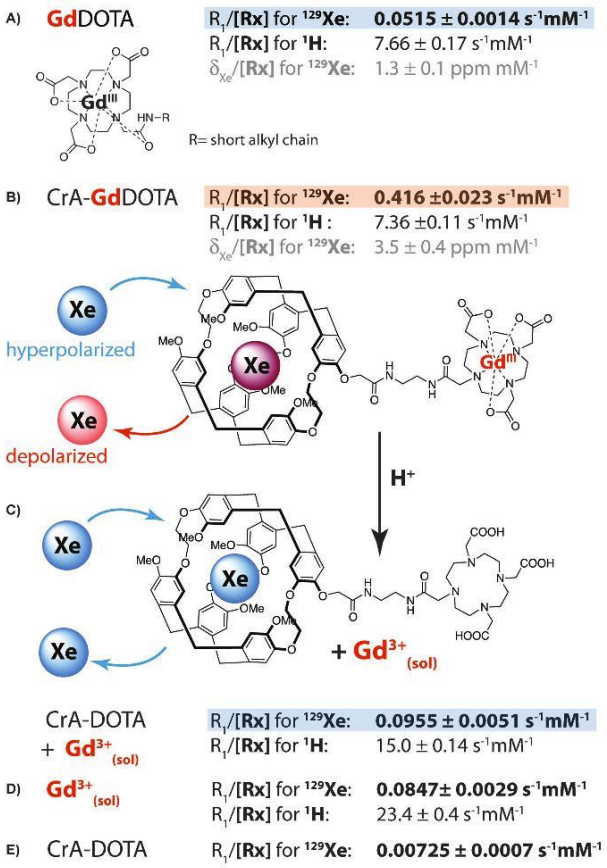

Figure 3. Relaxivity, R_1/[**Rx**], of various substances, **Rx**, for dissolved phase $^{129}Xe_{(sol)}$ and ^1H (of H_2O) at 293 K and 9.4 T in H_2O/ACN (1:1 v/v) solution. The relaxivity was determined from linear fitting of the data in Figure 2 with 0.0053 $s^{-1}mM^{-1}$ offset (i.e. experimental relaxivity of solvent). The dissolved phase $^{129}Xe_{(sol)}$ chemical shift δ_{Xe} dependence on [**Rx**] is obtained from linear fitting of the $^{129}Xe_{(sol)}$ peak position using a 189.3 ppm (solvent) offset. A) Relaxivity of **Gd**DOTA. B) Relaxivity model sensor molecule, that is, a cryptophane-A linked to **Gd**DOTA (**Rx** = CrA-**Gd**DOTA). C) DOTA protonation at pH 0 causing dissociation of Gd^{III} from the molecule. (**Rx** = CrA-DOTA + $Gd^{3+}_{(sol)}$). D) **Rx** = $Gd^{3+}_{(sol)}$ in H_2O/ACN solution at pH 7 and E) **Rx** = precursor of the sensor molecule without Gd^{III}.

For CrA-**Gd**DOTA, where **Gd**DOTA is tethered to the cryptophane cage, the Gd^{III} relaxivity for $^{129}Xe_{(sol)}$ increased more than eightfold to R_1/[**Rx**] = 0.416 $s^{-1}mM^{-1}$. The large relaxivity enhancement is likely caused by fast relaxation of encapsulated ^{129}Xe in close proximity to the paramagnetic **Gd**DOTA. Paramagnetic relaxation follows an r^{-6} dependence,[12] where r is the distance between the nuclear spin (here, of encapsulated ^{129}Xe) and the paramagnetic center. Chemical exchange between Xe in the cages and in solution transfers the relaxation effect and leads to accelerated R_1 rates for the dissolved phase $^{129}Xe_{(sol)}$. The relatively small $^{129}Xe_{(sol)}$ chemical shift dependence on [**Rx**] is listed in Figure 3A and Figure 3B for comparison.

The relaxivity of CrA-**Gd**DOTA for ^1H was very similar to that of **Gd**DOTA. This was expected from Solomon-Bloembergen-Morgan theory[12b] since the addition of the CrA group should have little effect on the number (q) of water molecules coordinated to Gd^{III} or their residence time. Furthermore, the rotational correlation time associated with the relatively small CrA-**Gd**DOTA molecule is too short to significantly alter the relaxation behavior.

A 1 mM CrA-**Gd**DOTA solution corresponds to a $^{129}Xe_{(sol)}$ relaxation time of T_1 = 2.4 s that is sufficiently short to affect the overall relaxation in vivo. Unlike HyperCEST, this effect does not require radiofrequency irradiation for saturation to accomplish depolarization. Rather, depolarization occurs as a consequence of the combined effect of relaxation in the bound phase (i.e. ^{129}Xe in the cage) followed by chemical exchange leading to the fast decay of the dissolved phase signal. To deactivate the depolarization, the relaxation agent will need to be 'turned off' through selective chemical or biochemical cleavage of the paramagnetic center from the encapsulating cage.

To demonstrate the deactivation concept, but also to further prove that accelerated ^{129}Xe relaxation was indeed caused by the close vicinity of the paramagnetic metal to the encapsulated ^{129}Xe, HCl (37% v/v) was added to protonate DOTA and leach the Gd^{III} ion out of the chelator moiety to form CrA-DOTA + $Gd^{3+}_{(sol)}$. This process, led to a 4.3 fold drop in the relaxivity for ^{129}Xe to 0.0955 ± 0.0051 $s^{-1}mM^{-1}$ shown in Figure 3C. This value is still 2 times higher than that found for **Gd**DOTA in Figure 3A, most likely because of increased contact of $^{129}Xe_{(sol)}$ with the unchelated paramagnetic metal ion (similarly effecting the ^1H relaxation in Figure 3C). In a control ex-

periment the relaxivity of **Gd**Cl_3 for ^{129}Xe in H_2O/ACN solution (Figure 3D, pH 7) was found to be $R_1/[\mathbf{Rx}] = 0.0847\ s^{-1}\,mM^{-1}$, close to the value in Figure 3C at pH 0.

Figure 2 also shows the time behavior (i–iii) of the DOTA protonation and the associated change in relaxivity that took several days for completion. This time behavior was verified through HPLC and mass spectrometry (see Supporting Information). It demonstrates that the change in relaxivity was indeed caused by the separation of the **Gd^{III}** center from the cryptophane cage and not by a pH dependence of the xenon in-out exchange rate with the cryptophane cage, in agreement with previous literature studying pH effects.[15]

Conclusions

The relaxation data generated in this study demonstrates a dramatic increase in relaxivity of a **Gd**DOTA for ^{129}Xe when the complex is tethered to a cryptophane cage. This increase is the consequence of the prolonged duration of cage bound ^{129}Xe in close vicinity to the paramagnetic metal center. The strong relaxation experienced by cage bound xenon is transferred through chemical exchange to the solvent phase ^{129}Xe. The dissolved phase ^{129}Xe signal decays at a rate that is the average of the relaxation rate in the cage and the relaxation rate in the solvent, scaled by the duration that the xenon atoms remain in the two respective phases.

As this hp ^{129}Xe chemical exchange relaxation transfer mechanism can be disrupted by the separation of CrA cage from the paramagnetic metal, a specifically designed responsive contrast agent can give rise to a new switchable ^{129}Xe depolarization based biosensor concept. Although this method may lack some of the intrinsic versatility of the HyperCEST concept, the presented responsive MRI contrast agent concept would not require high spectral resolution. In addition, switchable relaxation does not entail high power radiofrequency saturation that can be problematic for in vivo studies due to heat adsorption in tissue. Furthermore, the relaxation agent deactivation is ^{129}Xe specific and does not affect proton T_1 relaxation (compare Figure 3A and Figure 3B) and standard ^{1}H T_1 relaxation maps should allow to probe for the presence of biosensors independent of the activation state. This is important for the differentiation of regions with higher concentration of deactivated biosensor from regions with lower concentration of still active biosensor. Although both regions may result in similar ^{129}Xe relaxation rates, the very different ^{1}H relaxation behavior would enable correct interpretation.

The design of future responsive hp ^{129}Xe depolarization agents as potential biosensors deserves some consideration: In analogy to the r^{-6} dependence utilized in intramolecular Förster resonance energy transfer (FRET),[16] the r^{-6} dependence of paramagnetic relaxation on distance r between the cage and the paramagnetic metal center could be exploited for sensors that operate through conformational changes or through a cleavable linker between the two groups. Enzymatic cleavage of the linker between paramagnetic **Gd**DOTA and a ^{19}F containing reporter group was previously utilized to deactivate paramagnetic T_2 relaxation, thereby reducing line broadening in thermally polarized ^{19}F NMR.[17] Furthermore, enzymatic cleavage has been detected through a chemical shift based hp ^{129}Xe biosensor.[18] Similarly, cleavable linkers between a paramagnetic group and cryptophane cage may provide a usable responsive hp ^{129}Xe relaxation agents. The molecular design of the hp ^{129}Xe depolarization based biosensors can be advanced through an increase in the number of captured xenon atoms, for example through the usage of multiple cryptophane cages or through capsides[19] that would also increase rotational correlation times. Both effects will likely increase the relaxivity of the activated state but not of the deactivated state. Finally, **Gd^{III}** can be substituted by other paramagnetic groups with stronger relaxation properties such as **Mn^{II}** nanoparticles.[20]

Experimental Section

As described in detail in the SI, the model sensor CrA-**Gd**DOTA was synthesized from a DOTA chelator, modified with a short linker, and cryptophanol. Cryptophanol was synthesized as previously reported by Bertault and co-workers,[7d] while the DOTA-linker was simply obtained by reacting an appropriately protected DO3A with one of the α-bromoacetyl termini of a short bisamide linker. The cryptophanol was then reacted with the other α-bromoacetyl group. After deprotection of the DOTA carboxylic groups, the **Gd^{III}** cation was successfully chelated, yielding the desired compound CrA-**Gd**DOTA.

All NMR relaxation measurements were obtained at a temperature of 293 K at 9.4 T field strength. Hp ^{129}Xe was produced through spin exchange optical pumping (SEOP) using a custom-built instrument described elsewhere.[21] Prior to hp ^{129}Xe delivery in each experiment the solution was purged with N_2 for 2 min to ensure the removal of any residual O_2. The hp gas mixture was then delivered under continuous flow SEOP conditions for 45 s at 40 mL min^{-1} into the relaxation agent containing solution. After flow stoppage, the dissolved phase hp ^{129}Xe T_1 relaxation was measured through a sequence of 16 constant flip angle (12°) experiments.[22] A standard inversion recovery sequence was used to obtain the ^{1}H T_1 relaxation of H_2O.

Acknowledgements

This work was supported in parts by the Medical Research Council under Grant No. G0900785, by the Royal Society through the Paul Instrument Fund, through the EPSRC Research Development Fund—Bridging the Gaps, and a BBSRC Sparking Impact Award.

Keywords: cryptophane · hyperCEST · hyperpolarized xenon biosensor · molecular imaging · MRI contrast agent

[1] E. Terreno, D. Delli Castelli, A. Viale, S. Aime, *Chem. Rev.* **2010**, *110*, 3019–3042.
[2] a) M. M. Spence, S. M. Rubin, I. E. Dimitrov, E. J. Ruiz, D. E. Wemmer, A. Pines, S. Q. Yao, F. Tian, P. G. Schultz, *Proc. Natl. Acad. Sci. USA* **2001**, *98*, 10654–10657; b) M. M. Spence, E. J. Ruiz, S. M. Rubin, T. J. Lowery, N. Winssinger, P. G. Schultz, D. E. Wemmer, A. Pines, *J. Am. Chem. Soc.* **2004**, *126*, 15287–15294; c) L. Schroder, T. J. Lowery, C. Hilty, D. E. Wemmer, A. Pines, *Science* **2006**, *314*, 446–449.
[3] a) P. Berthault, G. Huber, H. Desvaux, *Prog. Nucl. Magn. Reson. Spectrosc.* **2009**, *55*, 35–60; b) O. Taratula, I. J. Dmochowski, *Curr. Opin. Chem. Biol.*

2010, *14*, 97 – 104; c) D. M. L. Lilburn, G. E. Pavlovskaya, T. Meersmann, *J. Magn. Reson.* **2012**, *229*, 173 – 186.
[4] Y. B. Bai, Y. F. Wang, M. Goulian, A. Driks, I. J. Dmochowski, *Chem. Sci.* **2014**, *5*, 3197 – 3203.
[5] C. Witte, V. Martos, H. M. Rose, S. Reinke, S. Klippel, L. Schroder, C. P. R. Hackenberger, *Angew. Chem. Int. Ed.* **2015**, *54*, 2806 – 2810; *Angew. Chem.* **2015**, *127*, 2848 – 2852.
[6] J. M. Chambers, P. A. Hill, J. A. Aaron, Z. H. Han, D. W. Christianson, N. N. Kuzma, I. J. Dmochowski, *J. Am. Chem. Soc.* **2009**, *131*, 563 – 569.
[7] a) V. Roy, T. Brotin, J. P. Dutasta, M. H. Charles, T. Delair, F. Mallet, G. Huber, H. Desvaux, Y. Boulard, P. Berthault, *ChemPhysChem* **2007**, *8*, 2082 – 2085; b) G. K. Seward, Q. Wei, I. J. Dmochowski, *Bioconjugate Chem.* **2008**, *19*, 2129 – 2135; c) A. Schlundt, W. Kilian, M. Beyermann, J. Sticht, S. Gunther, S. Hopner, K. Falk, O. Roetzschke, L. Mitschang, C. Freund, *Angew. Chem. Int. Ed.* **2009**, *48*, 4142 – 4145; *Angew. Chem.* **2009**, *121*, 4206 – 4209; d) C. Boutin, A. Stopin, F. Lenda, T. Brotin, J. P. Dutasta, N. Jamin, A. Sanson, Y. Boulard, F. Leteurtre, G. Huber, A. Bogaer *t*Buchmann, N. Tassali, H. Desvaux, M. Carriere, P. Berthault, *Bioorg. Med. Chem.* **2011**, 19, 4135 – 4143; e) K. K. Palaniappan, R. M. Ramirez, V. S. Bajaj, D. E. Wemmer, A. Pines, M. B. Francis, *Angew. Chem. Int. Ed.* **2013**, *52*, 4849 – 4853; *Angew. Chem.* **2013**, *125*, 4949 – 4953.
[8] H. M. Rose, C. Witte, F. Rossellaa, S. Klippel, C. Freund, L. Schroder, *Proc. Natl. Acad. Sci. USA* **2014**, *111*, 11697 – 11702.
[9] F. Lerouge, O. Melnyk, J. O. Durand, L. Raehm, P. Berthault, G. Huber, H. Desvaux, A. Constantinesco, P. Choquet, J. Detour, M. Smaihi, *J. Mater. Chem.* **2009**, *19*, 379 – 386.
[10] a) E. Terreno, M. Botta, P. Boniforte, C. Bracco, L. Milone, B. Mondino, F. Uggeri, S. Aime, *Chem—Eur J.* **2005**, *11*, 5531 – 5537; b) R. B. van Heeswijk, S. Laus, F. D. Morgenthaler, R. Gruetter, *Magn. Reson. Imaging* **2007**, *25*, 821 – 825; c) C. Gabellieri, M. O. Leach, T. R. Eykyn, *Contrast Media Mol. I* **2009**, *4*, 143 – 147; d) R. B. van Heeswijk, K. Uffmann, A. Comment, F. Kurdzesau, C. Perazzolo, C. Cudalbu, S. Jannin, J. A. Konter, P. Hautle, B. van den Brandt, G. Navon, J. J. van der Klink, R. Gruetter, *Magn. Reson. Med.* **2009**, *61*, 1489 – 1493; e) R. T. Branca, Z. I. Cleveland, B. Fubara, C. S. S. R. Kumar, R. R. Maronpot, C. Leuschner, W. S. Warren, B. Driehuys, *Proc. Natl. Acad. Sci. USA* **2010**, *107*, 3693 – 3697.
[11] M. Gomes, P. Dao, C. Slack, C. Vassiliou, A. Truxal, K. Jeong, D. E. Wemmer, M. B. Francis, A. Pines *56th Experimental NMR Conference, April 19 – 24*, Asilomar, **2015**.
[12] a) A. Abragam, *The Principles of Nuclear Magnetism*, Oxford University Press, Oxford, UK, **1961**; b) N. Bloembergen, L. O. Morgan, *J. Chem. Phys.* **1961**, *34*, 842.
[13] J. P. Mugler, T. A. Altes, *J. Magn. Reson. Imaging* **2013**, *37*, 313 – 331.
[14] a) M. S. Albert, D. F. Kacher, D. Balamore, A. K. Venkatesh, F. A. Jolesz, *J. Magn. Reson.* **1999**, *140*, 264 – 273; b) J. Wolber, A. Cherubini, A. S. K. Dzik-Jurasz, M. O. Leach, A. Bifone, *Proc. Natl. Acad. Sci. USA* **1999**, *96*, 3664 – 3669; c) G. Norquay, G. Leung, N. J. Stewart, G. M. Tozer, J. Wolber, J. M. Wild, *Magn. Reson. Med.* **2014**, DOI: 10.1002/mrm.25417.
[15] P. Berthault, H. Desvaux, T. Wendlinger, M. Gyejacquot, A. Stopin, T. Brotin, J. P. Dutasta, Y. Boulard, *Chem. Eur. J.* **2010**, *16*, 12941 – 12946.
[16] J. Zhang, R. E. Campbell, A. Y. Ting, R. Y. Tsien, *Nat. Rev. Mol. Cell Biol.* **2002**, *3*, 906 – 918.
[17] a) A. Y. Louie, M. M. Huber, E. T. Ahrens, U. Rothbacher, R. Moats, R. E. Jacobs, S. E. Fraser, T. J. Meade, *Nat. Biotechnol.* **2000**, *18*, 321 – 325; b) S. Mizukami, R. Takikawa, F. Sugihara, Y. Hori, H. Tochio, M. Walchli, M. Shirakawa, K. Kikuchi, *J. Am. Chem. Soc.* **2008**, *130*, 794 – 795; c) U. Himmelreich, S. Aime, T. Hieronymus, C. Justicia, F. Uggeri, M. Zenke, M. Hoehn, *Neuroimage* **2006**, *32*, 1142 – 1149; d) W. Cui, P. Otten, Y. Li, K. S. Koeneman, J. Yu, R. P. Mason, *Magn. Reson. Med.* **2004**, *51*, 616 – 620; e) Y. Takaoka, T. Sakamoto, S. Tsukiji, M. Narazaki, T. Matsuda, H. Tochio, M. Shirakawa, I. Hamachi, *Nat. Chem.* **2009**, *1*, 557 – 561; f) X. Y. Yue, Z. Wang, L. Zhu, Y. Wang, C. Q. Qian, Y. Ma, D. O. Kiesewetter, G. Niu, X. Y. Chen, *Mol. Pharm.* **2014**, *11*, 4208 – 4217.
[18] Q. Wei, G. K. Seward, P. A. Hill, B. Patton, I. E. Dimitrov, N. N. Kuzma, I. J. Dmochowski, *J. Am. Chem. Soc.* **2006**, *128*, 13274 – 13283.
[19] a) T. Meldrum, K. L. Seim, V. S. Bajaj, K. K. Palaniappan, W. Wu, M. B. Francis, D. E. Wemmer, A. Pines, *J. Am. Chem. Soc.* **2010**, *132*, 5936 – 5937; b) T. Stevens, K. Palaniappan, R. Ramirez, M. Francis, D. Wemmer, A. Pines, *Magn. Reson. Med.* **2013**, *69*, 1245 – 1252.
[20] J. M. Shin, R. M. Anisur, M. K. Ko, G. H. Im, J. H. Lee, I. S. Lee, *Angew. Chem. Int. Ed.* **2009**, *48*, 321 – 324; *Angew. Chem.* **2009**, *121*, 327 – 330.
[21] a) J. S. Six, T. Hughes-Riley, K. F. Stupic, G. E. Pavlovskaya, T. Meersmann, *Plos One* **2012**, *7*, e49927; b) K. F. Stupic, J. S. Six, M. D. Olsen, G. E. Pavlovskaya, T. Meersmann, *Phys Chem. Chem. Phys.* **2013**, *15*, 94 – 97; c) T. Hughes-Riley, J. S. Six, D. M. L. Lilburn, K. F. Stupic, A. C. Dorkes, D. E. Shaw, G. E. Pavlovskaya, T. Meersmann, *J. Magn. Reson.* **2013**, *237*, 23 – 33.
[22] K. F. Stupic, N. D. Elkins, G. E. Pavlovskaya, J. E. Repine, T. Meersmann, *Phys. Med. Biol.* **2011**, *56*, 3731 – 3748.

Received: May 7, 2015
Published online on ■■ ■■, 0000

F. Zamberlan, C. Lesbats, N. J. Rogers, J. L. Krupa, G. E. Pavlovskaya, N. R. Thomas, H. M. Faas,* T. Meersmann**

■■ – ■■

Molecular Sensing with Hyperpolarized ^{129}Xe Using Switchable Chemical Exchange Relaxation Transfer

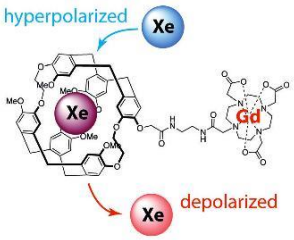

The relaxivity of paramagnetic GdDOTA for ^{129}Xe is dramatically increased through tethering to a cryptophane cage, providing the path for a responsive depolarization agent.

CHEMPHYSCHEM

Supporting Information

Molecular Sensing with Hyperpolarized ^{129}Xe Using Switchable Chemical Exchange Relaxation Transfer

Francesco Zamberlan,[a] Clémentine Lesbats,[b] Nicola J. Rogers,[b, c] James L. Krupa,[a] Galina E. Pavlovskaya,[b] Neil R. Thomas,*[a] Henryk M. Faas,*[b, d] and Thomas Meersmann*[b]

cphc_201500367_sm_miscellaneous_information.pdf

Supporting Information

Chemical Sensing with Hyperpolarized ^{129}Xe using Chemical Exchange Relaxation Transfer.

Francesco Zamberlan,[+[a]] Clémentine Lesbats,[+[b]] Nicola J. Rogers,[[b]] James L. Krupa,[[a]] Galina Pavlovskaya,[[b]] Neil R. Thomas,*[[a]] Henryk Faas,*[[b]] and Thomas Meersmann*[[b]]

Synthetic Methods

Unless otherwise noted, reagents were obtained from commercial sources and used without further purification. TLC analysis of reaction mixtures was performed using Merck Kieselgel 60 F_{254} plates; visualization was carried out by irradiation with a UV lamp (254 nm) and staining with phosphomolybdic acid. Compounds were purified via flash column chromatography on Sigma-Aldrich silica gel technical grade, pore size 60 Å, 230-400 mesh particle size, 40-63 nm particle size.

^{1}H and ^{13}C NMR spectra were recorded at ambient temperature with Bruker DPX 300, Bruker AV 400, Bruker AV(III) 400, Bruker DPX 400 or Bruker AV(III) 500 spectrometers and were referenced to residual ^{1}H and ^{13}C signals of the deuterated solvents respectively (δ H 7.26, δ C 77.00 for chloroform; δ H 3.31, δ C 49.0 for methanol; δ H 2.50, δ C 39.5 for DMSO; δ H 1.96, δ C 1.79 for acetonitrile).

High resolution mass spectra (HRMS) were recorded on a Bruker microTOF with ESI source or on a Micro-Mass LCT with ESI source. Values of mass to charge ratio (*m/z*) are given to four decimal places.

MALDI-ToF mass data were recorded on a Bruker Ultraflex III single analyzer dedicated Matrix Assisted Laser Desorption Ionization Time of Flight mass spectrometer. Details on the procedure for the recording of the accurate mass of the final products are also given.

All HPLC purifications were carried out on an Agilent 1200 series system equipped with a single channel wavelength detector at 215 nm and an automated fraction collector. Analytical HPLC was performed at 1.0 ml/min using an Agilent Eclipse XDB-C18 analytical column 4.6 x 150 mm, 5 µm pore size; semi-preparative HPLC was performed at 2.5 ml/min using an Agilent Eclipse XDB-C18 semi-preparative column 9.4 x 250 mm, 5 µm pore size. Solvent A was 0.1% formic acid in milli Q water, and solvent B was 0.1% formic acid in HPLC grade acetonitrile. The gradient used is as follows: solvent B 0% to 95% over 30 minutes.

Synthetic Strategy

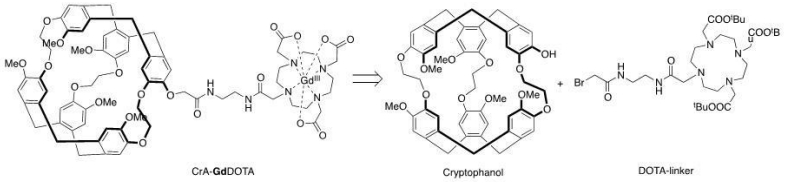

Scheme 1 Retrosynthesis for CrA-**Gd**DOTA

As shown in Scheme 1, the model sensor CrA-**Gd**DOTA is composed of three parts: a cryptophane cage, a DOTA-based chelator for a Gd^{III} ion and a linker to tether the two together.

Cryptophane-A (**1**, scheme 2) was easily and quickly synthesized following the procedure of Canceill *et al.*[1] Demethylation of a single methyl ether was achieved using TMSI,

yielding the cryptophanol cage (**2**). The only phenolic group of (**2**) was then used as the nucleophile in the alkylation reaction to link it to DO3A via a *bis*-amide under basic conditions.[2]

The symmetric linker (**3**) was obtained via double alkylation of ethylene diamine (**4**) with bromoacetyl bromide (**5**). The symmetrical linker was then used to alkylate the secondary amine of the cyclen ring of protected DO3A (**6**) that had been previously synthesized, affording the protected DOTA-linker adduct (**7**). This compound was used in an etherification reaction with the cryptophanol cage to yield (**8**). After deprotection of the macrocycle's carboxylic groups, the Gd^{III} cation was successfully chelated at neutral pH, giving the desired compound CrA-**Gd**DOTA (**9**). This was purified via HPLC and freeze-dried to yield a white and fluffy powder. Compound (**9**) was also found to be soluble in a 1:1 v/v solution of acetonitrile/water (H_2O/ACN).

Furthermore, it was observed that, upon storage at 2-8 °C for an extended period of time (three weeks), the powdered compound CrA-**Gd**DOTA (**9**) would change consistence and become less soluble.

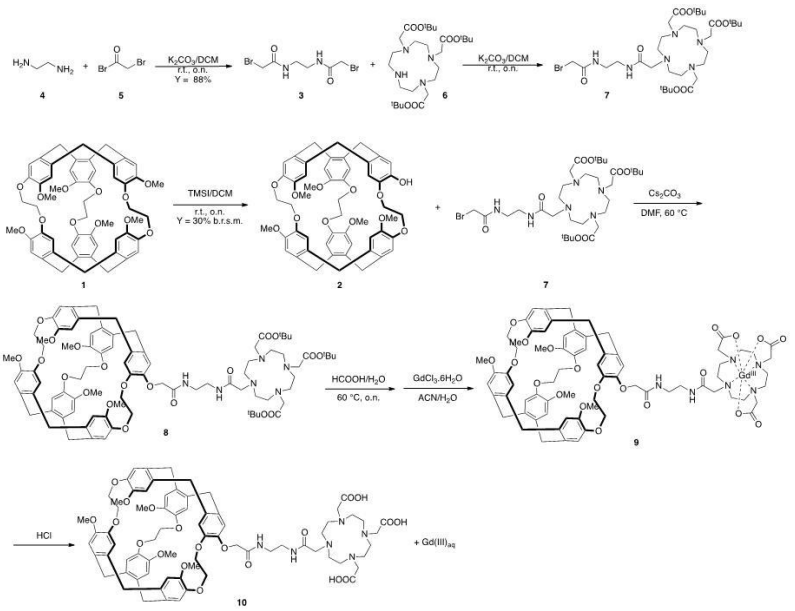

Scheme 2 Synthesis of CrA-**Gd**DOTA starting from Cryptophane-A and reaction back to CrA-DOTA.

After data collection for CrA-**Gd**DOTA (**9**), in a 1:1 v/v H_2O/ACN solution, concentrated HCl (37% v/v) was added to change the pH to 1 in order to leach the Gd^{III} ion out of the

protonated chelator, yielding CrA-DOTA (**10**) and free Gd^{III} ions. This was undertaken to measure the relaxivity of CrA-DOTA in the presence of free Gd^{III} ions and to prove a simple switch off mechanism for hp ^{129}Xe. This process was followed via MS and HPLC.

Synthesis of Cryptophanol-A

Cryptophanol-A (**2**) was synthesized from Cryptophane-A (**1**) according to a previously reported procedure. The obtained product matched the reported physical constants and NMR spectra.[2]

Synthesis of DO3A-Linker

*Synthesis of N,N'-(ethane-1,2-diyl)bis(2-bromoacetamide) (**3**)*

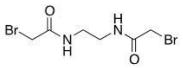

Ethylenediamine (**4**) (0.8 ml, 12 mmol) was dissolved in DCM (50 ml) and cooled to 0 °C. Potassium carbonate (10 g, 72 mmol, 6 eq.) was added in one portion under stirring. Bromoacetyl bromide (**5**) (3.13 ml, 36 mmol, 3 eq.) in DCM (10 ml) was added dropwise at 0 °C. The reaction was then allowed to reach room temperature and stirred for 16 hours.
The reaction was followed via MS and TLC. Upon reaction completion, water was cautiously added dropwise. The aqueous layer was extracted three times with DCM (50 ml). The combined organic layers were washed with 1M HCl (70 ml) and then brine (50 ml). The aqueous phase was furthermore extracted ethyl acetate (4x 100 ml). The combined organic phases were dried over anhydrous magnesium sulfate, filtered and concentrated *in vacuo* to yield 3.15 g (88%) of (**3**) as a white powder.
^{1}H-NMR (300 MHz; MeOD): δ 3.83 (s, 4H), 3.35 (s, 2H), 3.35 (s, 4H).
^{13}C-NMR (75 MHz; MeOD): δ 169.8, 40.3, 28.7.
HRMS (ESI): $C_6H_{10}Br_2N_2O_2$ calculated [M+Na^+]: 322.9000; found [M+Na^+]: 322.8983.

*Synthesis of DO3A(OtBu)$_3$ (**6**)[3]*

Cyclen (200 mg, 1.16 mmol) was dissolved in ACN (200 ml) and sodium carbonate (350 mg, 3.30 mmol, 3.0 eq.) was added in one portion under stirring. The resulting white suspension was stirred for 15 minutes under a nitrogen atmosphere. A solution of *tert*-butyl bromoacetate (660 mg, 3.40 mmol, 3.0 eq.) in ACN (50 ml) was slowly added over 15 minutes and the resulting suspension stirred for 30 minutes at ambient temperature, followed by a 16 hour reflux at 80 °C, as reported by Waengler *et al.*[3] The white precipitate was then

filtered and the filtrate recrystallised from the minimum amount of boiling toluene and washed with ice cold diethyl ether (20 mL) to quantitatively yield DO3A (**6**) (590 mg) as a fine white powder.
^{1}H-NMR (400 MHz, $CDCl_3$): δ 1.46 (s, 27H), 2.85-2.95 (m, 12H), 3.11 (s, 4H), 3.29 (s, 2H), 3.37 (s, 4H).
^{13}C-NMR (100 MHz, $CDCl_3$): δ 170.5, 169.6, 81.9, 81.9, 81.7, 58.2, 51.1, 49.1, 47.6, 28.3, 28.2.
HRMS (ESI): $C_{26}H_{51}N_4O_6^+$ calculated 515.3803; found [M+H$^+$] 515.3819.

Synthesis of DOTA(OtBu)$_3$-Linker (7):

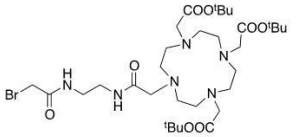

DO3A(O*t*Bu)$_3$ (**6**) (100 mg, 0.19 mmol) was dissolved in ACN (5 ml) and stirred in the presence of potassium carbonate (65 mg, 0.475 mmol, 2.5 eq.). After stirring for 5 minutes at room temperature, the *bis*-amide linker (**3**) (0.174 g, 0.58 mmol, 3 eq.) and five drops of DMF were added. The suspension was stirred for 16 hours at room temperature. The reaction was followed via MS, and it was filtered and concentrated *in vacuo* upon completion. The residue was then taken up in ethyl acetate (10 ml) and washed with brine (3x 15 ml). The organic layer was dried over anhydrous sodium sulfate, filtered and concentrated *in vacuo* to give the desired compound in quantitative crude yield (191 mg) as a sticky, white solid, which was carried forward without further purification.
^{1}H-NMR (400 MHz; MeOD): δ 4.06-4.04 (m, 1H), 3.83 (m, 3H), 3.37-2.01 (m, 24H), 1.57-1.45 (m, 12H).
^{13}C-NMR (100 MHz; MeOD): δ 173.0, 172.8, 172.4, 168.4, 168.3, 81.4, 81.4, 55.9, 55.4, 41.7, 39.2, 38.9, 38.8, 38.5, 35.5, 27.4, 27.3, 27.0, 27.0.
HRMS (ESI): $C_{32}H_{59}BrN_6O_8$ calculated [M+H$^+$] 735.3651; found [M+H$^+$] 735.3693.

Assembly of CrA-GdDOTA

*Synthesis of CrA-DOTA(OtBu)$_3$ (**8**)*

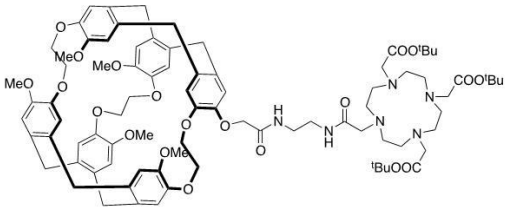

Cryptophanol-A (**2**) (43 mg, 49 µmol) was stirred in DMF (2 ml) in the presence of caesium carbonate (40 mg, 120 µmol, 2.5 eq.). To this solution, DOTA(O*t*Bu)$_3$-Linker (**7**) (72 mg, 99 µmol, 2 eq.) in 2 ml of ACN was added and the reaction was stirred at room temperature for 16 hours. The reaction was monitored via MS and upon completion, the pearl-white suspension was filtered and the solvents concentrated *in vacuo*. The residue was taken up in ethyl acetate and washed with brine (3x 10 ml). The organic layer was dried over anhydrous sodium sulfate, filtered and concentrated *in vacuo* to yield the crude target material in quantitative yield (92 mg) as yellowish oil, which was used as is in the next step.

^{1}H-NMR (500 MHz; MeOD): δ 4.82 (d, *J* = 6.6 Hz, 1H), 4.77 (d, *J* = 5.1 Hz, 1H), 4.65-4.29 (m, 15H), 4.07-4.00 (m, 5H), 3.91-3.82 (m, 11H), 3.51 (s, 8H), 3.42-3.38 (m, 6H), 3.02-2.03 (m, 43H), 1.53-1.52 (m, 27H).

^{13}C NMR (126 MHz; MeOD): δ 173.2, 173.0, 172.8, 172.6, 171.7, 171.6, 163.4, 149.4, 149.3, 149.3, 149.2, 146.8, 146.6, 146.4, 146.2,146.1, 134.6, 133.6, 133.4, 132.9, 132.1, 131.8, 131.7, 131.6, 120.5, 118.9, 118.8, 118.7, 116.8, 114.6, 114.54, 114.3, 114.0, 81.4, 81.3, 68.7, 68.6, 68.5, 68.4, 60.1, 57.9, 56.1, 55.9, 55.8, 55.7, 55.6, 55.4, 53.4, 35.5, 35.1, 34.9, 34.8, 30.2, 29.5, 29.3, 27.1, 27.0, 26.9, 19.4, 13.0

HRMS (ESI): $C_{85}H_{110}N_6O_{20}$ calculated [M+2H$^+$]: 768.3960; found [M+2H$^+$]: 768.3944.

*Synthesis of CrA-DOTA (**10**)*

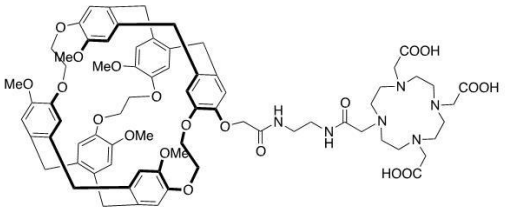

Cry-DOTA(O*t*Bu)$_3$ (**8**) obtained previously (92 mg) was heated at 60 °C for 16 hours in a mixture of formic acid/water (15 ml, 4:1 v/v). The reaction was monitored via MS and

upon completion the solvents were removed *in vacuo* to yield 80 mg of crude product as an off yellow oil. The obtained oil was dissolved in 3 ml of a 1:1:1:0.2 mixture of ACN/MeOH/water/DMSO, filtered on a Nalgene syringe filter (25 mm x 0.45 mm) and purified via semipreparative HPLC with the method reported in the Synthetic Methods. The observed retention time for this compound was 17.2 min. Freeze-drying of the collected fractions yielded 5 mg of target compound.
^{1}H-NMR (500 MHz; CD_3CN): δ 6.83-6.71 (m, 12H), 4.55-4.45 (m, 8H), 4.35 (dd, *J* = 8.1, 0.4 Hz, 2H), 4.26 (d, *J* = 7.9 Hz, 6H), 4.06-4.02 (m, 4H), 3.78-3.75 (m, 13H), 3.71-3.61 (m, 80H), 3.39-3.29 (m, 21H), 3.00 (s, 7H).
^{13}C NMR (126 MHz; CD_3CN): δ 175.3, 171.4, 170.6, 168.8, 149.0, 148.9, 148.7, 146.7, 145.5, 145.4, 145.3, 134.1, 133.9, 133.6, 133.4, 133.3, 132.3, 131.7, 131.6, 131.5, 68.5, 68.4, 68.3, 68.1, 67.8, 56.7, 55.9, 55.2, 54.4, 51.7, 51.6, 50.9, 48.3, 48.2, 48.2, 38.3, 35.2, 35.2, 35.1, 35.1
MALDI-ToF MS: $C_{73}H_{86}N_6O_{20}$ calculated [M+H$^+$]: 1367.5970; found [M+H$^+$]: 1367.6023.

*Synthesis of CrA-GdDOTA (**9**)*

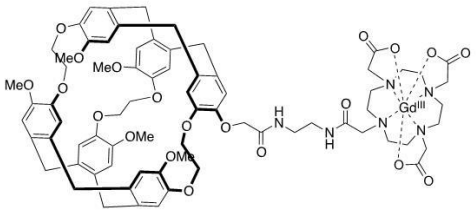

Crude CrA-DOTA (**10**) (57 mg) was dissolved in H_2O/ACN (0.5 ml, 1:1 v/v) and the pH was adjusted to 6 with 0.1M KOH. $GdCl_3.6H_2O$ (15 mg, 40 µmol, 1.05 eq) was added in one portion. The suspension was stirred at r.t. for 16 hours and monitored via MS. After depletion of the starting material, the solution solvents were evaporated under nitrogen flow. The solid residue was dissolved in 1 ml of water with 1% DMSO, filtered on a Nalgene syringe filter (25 mm x 0.45 mm) and purified via semipreparative HPLC with the method reported in the Synthetic Methods. The observed retention time for this compound was 18.4 min. Freeze-drying of the collected fractions yielded 4.3 mg of target compound.
MALDI-ToF MS: $C_{73}H_{83}GdN_6O_{20}$ calculated [M+H$^+$]: 1520.4838; found [M+H$^+$]: 1520.4768.

Sample preparation for NMR experiments

CrA-**Gd**DOTA (3.1 mg) was dissolved in H_2O/ACN (2 ml, 1:1 v/v) to make a 1 mM stock solution. From this, appropriate dilutions were obtained.

Addition of an appropriate quantity (see below) of a solution of ACN/HCl 37% 1:1 v/v caused the leaching of the Gd^{III} ion from the DOTA chelator over 48 to 96 hours, forming

a solution containing CrA-DOTA and Gd^{III} ions; this fact was confirmed by HPLC analyses and subsequent MS data of the collected fractions.
A time course experiment was set up. To a 0.4 mM solution of CrA-**Gd**DOTA in 2 ml H_2O/ACN 1:1 v/v, 0.66 ml of ACN/HCl 37% 1:1 v/v were added, giving a 0.3 mM solution of CrA-**Gd**DOTA. Initial acquisition of ^{129}Xe and ^{1}H relaxation data points gave point (i) in Fig. 2. The strongly acidic media gradually caused the leaching of the Gd^{III} ions from the DOTA-based chelator. ^{129}Xe and ^{1}H relaxation data were acquired after 1, 24 and 96 hours. Analytical HPLC was also used to quantify the conversion between the two species – see Figs. S4 and S5 respectively.

Hp ^{129}Xe Experimental setup

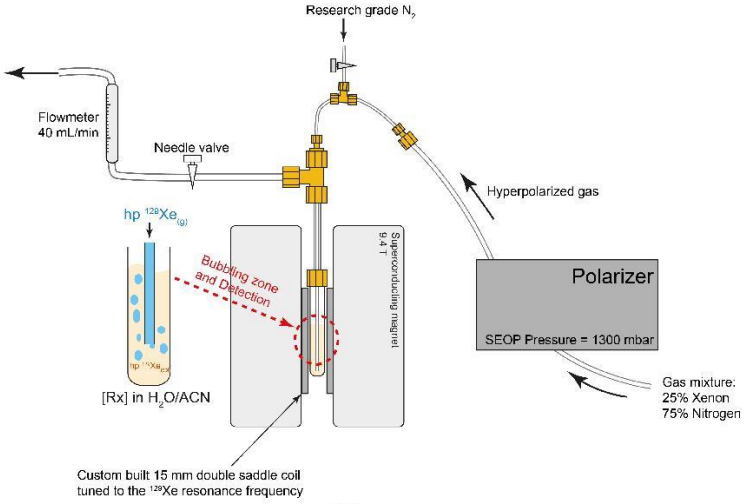

Figure S1 Experimental setup of hp ^{129}Xe relaxation measurements with various relaxation agents (**Rx**) and various concentrations [**Rx**] thereof. The polarizer set up had been previously described in Six *et al.*[4] and Hughes-Riley *et al.*[5] The solution was initially purged with nitrogen to remove any trace amounts of oxygen, as described in the manuscript. Hp ^{129}Xe flow was stopped before the actual relaxation measurement took place.

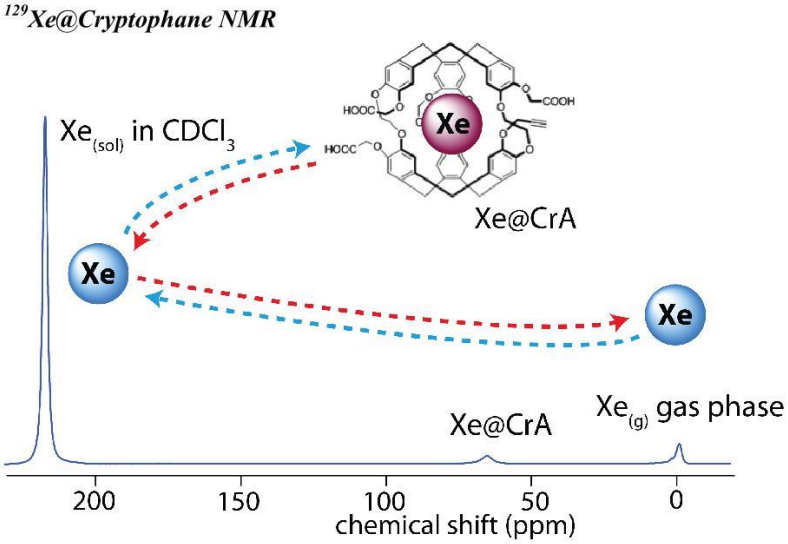

Figure S2. Hp ^{129}Xe NMR spectrum of synthesized cryptophane-A (CrA) cage dissolved in $CDCl_3$ using the setup of Fig. S1.